

**Self-assembly of 1,3,5-benzenetricarboxamides  
with tertiary amino substituents and  
preparation of hierarchical superstructures**

DISSERTATION

zur Erlangung des akademischen Grades  
eines Doktors der Naturwissenschaften (Dr. rer. nat.)  
in der Bayreuther Graduiertenschule für Mathematik und  
Naturwissenschaften (BayNAT)  
der Universität Bayreuth

vorgelegt von

**Andreas Frank**

geboren in Wolsk, Kasachstan

Bayreuth, 2023









Der experimentelle Teil der vorliegenden Arbeit wurde in der Zeit von Mai 2017 bis April 2022 in Bayreuth am Lehrstuhl für Makromolekulare Chemie I unter der Betreuung von Herrn Professor Dr. Hans-Werner Schmidt angefertigt.

Vollständiger Abdruck der von der Bayreuther Graduiertenschule für Mathematik und Naturwissenschaften (BayNAT) der Universität Bayreuth genehmigten Dissertation zur Erlangung des akademischen Grades eines Doktors der Naturwissenschaften (Dr. rer. nat.).

Form der Dissertation: Kumulative Dissertation

Dissertation eingereicht am: 16.06.2023

Zulassung durch das Leitungsgremium: 18.07.2023

Wissenschaftliches Kolloquium: 05.12.2023

Amtierender Direktor: Prof. Dr. Jürgen Köhler

Prüfungsausschuss:

Prof. Dr. Hans-Werner Schmidt (Gutachter)

Prof. Dr. Andreas Greiner (Gutachter)

Prof. Dr. Georg Papastavrou (Vorsitz)

Prof. Dr. Leonid Ionov



*Für meine Familie*



## Abbreviations

1D	One-dimensional
2D	Two-dimensional
3D	Three-dimensional
A	Adenine
AFM	Atomic force microscopy
ATR	Attenuated total reflection
AuNPs	Gold nanoparticles
BTA	1,3,5-benzenetricarboxamide
BTA-Methyl	<i>N</i> <sup>1</sup> , <i>N</i> <sup>3</sup> , <i>N</i> <sup>5</sup> -tris[2-(dimethylamino)-ethyl]-1,3,5-benzenetricarboxamide
<sup>13</sup> C NMR	Carbon nuclear magnetic resonance
C	Cytosine
CBS	Concentric back scattered
CDCl <sub>3</sub>	Deuterated chloroform
CDSA	Crystallization-driven self-assembly
CNTs	Carbon nanotubes
DCTB	Trans-2-[3-(4-tert-butylphenyl)-2-methyl-2-propenylidene]malononitrile
DMAP	4-Dimethylaminopyridine
DMDBS	1,3:2,4-di(3,4-dimethylbenzylidene) sorbitol
DMF	<i>N,N</i> -Dimethylformamide
DMSO	Dimethyl sulfoxide
DSC	Differential scanning calorimetry
μDSC	Micro-differential scanning calorimetry
e. g.	For example

## II | Abbreviations

---

EI	Spray ionization
ESEM	Environmental scanning electron microscopy
ESI	Electronic supplementary information
et al.	Et alli (and others)
EtOH	Ethanol
FIB	Focused ion beam
FluidFM	Combination of atomic force microscopy and nanofluidics
FT-IR	Fourier-transformation infrared
G	Guanine
GdL	Glucono-delta-lactone
$^1\text{H}$ NMR	Proton nuclear magnetic resonance
$\text{HAuCl}_4 \cdot 3\text{H}_2\text{O}$	Tetrachloroauric (III) acid trihydrate
HCl	Hydrochloric acid
$\text{H}_2\text{SO}_4$	Sulfuric acid
iPP	Isotactic polypropylene
<i>i</i> Pr-BTA	$N^1, N^3, N^5$ -tris[2-(diisopropylamino)-ethyl]-1,3,5-benzenetricarboxamide
LFD	Large-field (gaseous secondary electron) detector
MALDI-ToF MS	Matrix-assisted laser desorption/ionization time-of-flight mass spectrometry
MeOH	Methanol
MS	Mass spectrometry
$\text{NaBH}_4$	Sodium borohydride
$\text{Na}_2\text{PdCl}_4$	Sodium tetrachloropalladate(II)
PA-6	Polyamide-6
PAN	Polyacrylonitrile
PCL	Poly(lactide acid)



---

PDiPA	Poly( <i>N,N</i> -diisopropylaminoethyl methacrylamide)
PDMA	Poly( <i>N,N</i> -dimethylaminoethyl methacrylamide)
PdNPs	Palladium nanoparticles
PE	Polyethylene
PFDMS	Poly(ferrocenyldimethylsilane)
PMMA	Poly(methyl methacrylate)
POM	Polarizing optical microscopy
PS	Polystyrene
PS <sub>core</sub> /SEDiPA	Supporting polystyrene fibers/nonwovens with patchy worm-like micelles composed of polystyrene- <i>block</i> -polyethylene- <i>block</i> -poly( <i>N,N</i> -diisopropylaminoethyl methacrylamide)
PS <sub>core</sub> /SEDMA	Supporting polystyrene fibers with patchy worm-like micelles composed of polystyrene- <i>block</i> -polyethylene- <i>block</i> -poly( <i>N,N</i> -dimethylaminoethyl methacrylamide)
PSU	Polysulfone
RuO <sub>4</sub>	Ruthenium tetroxide
SEDiPA	Polystyrene- <i>block</i> -polyethylene- <i>block</i> -poly( <i>N,N</i> -diisopropylaminoethyl methacrylamide)
SEDMA	Polystyrene- <i>block</i> -polyethylene- <i>block</i> -poly( <i>N,N</i> -dimethylaminoethyl methacrylamide)
SEM	Scanning electron microscopy
SEM	Polystyrene- <i>block</i> -polyethylene- <i>block</i> -poly(methyl methacrylate)
T	Thymine
TEM	Transmission electron microscopy
THF	Tetrahydrofuran
XRD	X-ray powder diffraction



## Symbols and units

c	Concentration
°C	Degree Celsius
cm	Centimeter
d	Diameter
Đ	Dispersity
eV	Electron volt
g	Gram
h	Hour
K	Kelvin
kg	Kilogram
kV	Kilovolt
l	Length
L	Liter
M	Molar
M <sup>•+</sup>	Molecular ion peak
mg	Milligram
MHz	Megahertz
min	Minute
mL	Milliliter
mm	Millimeter
mM	Millimolar
M <sub>n</sub>	Number average molecular weight
mW	Milliwatt
m/z	Mass-to-charge ratio

## VI | Symbols and units

---

MΩ	Megaohm
nm	Nanometer
Pa	Pascal
pA	Picoampere
pm	Picometer
rpm	Revolutions per minute
s	Second
T	Temperature
T <sub>c</sub>	Crystallization temperature
T <sub>m</sub>	Melting temperature
V	Volume
wt.%	Weight percent
δ	Chemical shift
λ	Wavelength
μL	Microliter
μm	Micrometer
$\tilde{\nu}$	Wavenumber

## List of publications

The following publications are presented within this thesis:

- [I] **A. Frank**, A. Bernet, K. Kreger, H.-W. Schmidt.  
*Supramolecular microtubes based on 1,3,5-benzenetricarboxamides prepared by self-assembly upon heating*,  
Soft Matter **2020**, 16, 4564–4568.
- [II] **A. Frank**, C. Hils, M. Weber, K. Kreger, H. Schmalz, H.-W. Schmidt.  
*Hierarchical Superstructures by Combining Crystallization-Driven and Molecular Self-Assembly*,  
Angew. Chem. Int. Ed. **2021**, 60, 21767–21771,  
(German edition: Angew. Chem. **2021**, 133, 21935–21939).
- [III] **A. Frank**, M. Weber, C. Hils, U. Mansfeld, K. Kreger, H. Schmalz, H.-W. Schmidt.  
*Functional Mesostructured Electrospun Polymer Nonwovens with Supramolecular Nanofibers*,  
Macromol. Rapid Commun. **2022**, 43, 2200052, 1–8.

An additional publication [IV] evolved in collaboration with Macromolecular Chemistry II at the University of Bayreuth. This publication is related to the publications [II] and [III] by using triblock terpolymers of the patchy worm-like micelles prepared by crystallization-driven self-assembly.

- [IV] C. Hils, M. Dulle, G. Sitaru, S. Gekle, J. Schöbel, **A. Frank**, M. Drechsler, A. Greiner, H. Schmalz.  
*Influence of patch size and chemistry on the catalytic activity of patchy hybrid nonwovens*,  
Nanoscale Adv. **2020**, 2, 438–452.

Publications (V) to (IX) arose from further collaborations during the thesis. They are outside the focus of this thesis.

- [V] D. Nahm, F. Weigl, N. Schaefer, A. Sancho, **A. Frank**, J. Groll, C. Villmann, H.-W. Schmidt, P. D. Dalton, R. Luxenhofer.  
*A versatile biomaterial ink platform for the melt electrowriting of chemically-crosslinked hydrogels,*  
Mater. Horiz. **2020**, 7, 928–933.
- [VI] C. F. Dai, X. N. Zhang, C. Du, **A. Frank**, H.-W. Schmidt, Q. Zheng, Z. L. Wu.  
*Photoregulated Gradient Structure and Programmable Mechanical Performances of Tough Hydrogels with a Hydrogen-Bond Network,*  
ACS Appl. Mater. Interfaces **2020**, 12, 53376–53384.
- [VII] J. Mechau, **A. Frank**, E. Bakirci, S. Gumbel, T. Jungst, R. Giesa, J. Groll, P. D. Dalton, H.-W. Schmidt.  
*Hydrophilic (AB)<sub>n</sub> Segmented Copolymers for Melt Extrusion-Based Additive Manufacturing,*  
Macromol. Chem. Phys. **2021**, 222, 2000265, 1–10.
- [VIII] E. Bakirci, **A. Frank**, S. Gumbel, P. F. Otto, E. Fürsattel, I. Tessmer, H.-W. Schmidt, P. D. Dalton.  
*Melt Electrowriting of Amphiphilic Physically Crosslinked Segmented Copolymers,*  
Macromol. Chem. Phys. **2021**, 222, 2100259, 1–9.
- [IX] E. Karakaya, F. Bider, **A. Frank**, J. Teßmar, L. Schöbel L. Forster, S. Schrüfer, H.-W. Schmidt, D. W. Schubert, A. Blaeser, A. R. Boccaccini, R. Detsch.  
*Targeted Printing of Cells: Evaluation of ADA-PEG Bioinks for Drop on Demand Approaches,*  
Gels **2022**, 8, 206, 1–24.

## Table of contents

<b>Summary</b> .....	<b>1</b>
<b>Zusammenfassung</b> .....	<b>3</b>
<b>1. Introduction</b> .....	<b>7</b>
1.1. Supramolecular chemistry .....	7
1.2. Supramolecular class of 1,3,5-benzenetricarboxamides .....	13
1.3. Influence of the peripheral substituents of 1,3,5-benzenetricarboxamides on the structure formation .....	21
1.4. Hierarchical superstructures composed of fibers .....	31
1.5. References.....	39
<b>2. Objective of this thesis</b> .....	<b>57</b>
<b>3. Synopsis</b> .....	<b>59</b>
3.1. Synthesis and characterization of BTAs with tertiary amino substituents .....	59
3.2. Solubility and self-assembly behavior of BTAs with tertiary amino substituents ...	62
3.3. Supramolecular microtubes based on 1,3,5-benzenetricarboxamides prepared by self-assembly upon heating.....	65
3.4. Hierarchical superstructures .....	69
3.4.1 Crystallization-driven self-assembly of triblock terpolymers towards patchy worm-like micelles .....	69
3.4.2 Patchy micelles immobilized on supporting polymer fibers.....	70
3.4.3 Hierarchical superstructures by combining crystallization-driven and molecular self-assembly.....	72
3.5. Functional mesostructured electrospun polymer nonwovens with supramolecular nanofibers .....	76
3.6. Overview of the publications of this thesis.....	79

<b>4. Publications .....</b>	<b>81</b>
4.1. Individual contributions to joint publications .....	81
4.2. Supramolecular microtubes based on 1,3,5-benzenetricarboxamides prepared by self-assembly upon heating.....	85
4.3. Hierarchical superstructures by combining crystallization-driven and molecular self-assembly.....	117
4.4. Functional mesostructured electrospun polymer nonwovens with supramolecular nanofibers .....	147
<b>5. Extended summary.....</b>	<b>187</b>
<b>6. Danksagung.....</b>	<b>193</b>



## Summary

1,3,5-benzenetricarboxamides (BTAs) are one of the most prominent classes in supramolecular chemistry. Whereas the self-assembly process for common BTAs is widely understood, less is known about the role and influence of functional groups in their periphery as well as on the resulting surface properties of the corresponding supramolecular objects. Such functional BTAs can be processed from polar solvents to prepare hierarchical superstructures with different levels of complexity. The surface of the functional supramolecular objects allows, for example, the immobilization of specific metal nanoparticles.

In this context, the focus of this thesis is on the synthesis, characterization and self-assembly of *a new class of 1,3,5-benzenetricarboxamides with functional tertiary amino substituents*. For this purpose, a series of BTAs with an ethyl spacer and tertiary amino substituents with different alkyl groups ranging from *N,N*-dimethyl, *N,N*-diethyl, *N,N*-di-*n*-propyl to *N,N*-di-isopropyl groups were synthesized to systematically alter the hydrophilicity of the molecule and identify structure-property relationships. It was found that these moderate structural variations lead to *pronounced differences in the solubility of the BTAs in water*. The BTA with *N,N*-dimethyl groups shows an extremely high water solubility of more than 150 g L<sup>-1</sup>. In contrast, the BTA with *N,N*-di-*n*-propyl or *N,N*-di-isopropyl groups possess a solubility of less than 0.01 g L<sup>-1</sup> in water. The BTA with *N,N*-diethyl groups shows a water solubility of up to 100 g L<sup>-1</sup> at room temperature. None of these BTAs shows the typical self-assembly behavior in solution upon cooling. Surprisingly, the BTA with *N,N*-diethyl groups exhibits a reversible, unique two-step *self-assembly behavior upon heating* the aqueous solutions. With increasing temperature, first, a clouding of the entire sample is observed, resulting from a liquid-liquid phase separation followed by the formation of supramolecular fiber-like structures of the BTAs. These supramolecular structures can be isolated without damage and feature a well-defined *microtube morphology*. These microtubes are several hundred micrometers long and have an outer average diameter of about 4.7 μm.

To prepare more *complex supramolecular structures*, two self-assembly concepts, namely crystallization-driven self-assembly and molecular self-assembly, were combined for the first time. Here, patchy worm-like micelles consisting of the triblock terpolymer polystyrene-*block*-polyethylene-*block*-poly(*N,N*-dimethylaminoethyl methacrylamide), prepared by crystallization-driven self-assembly were immobilized on the surface of a supporting

polystyrene fiber by coaxial electrospinning. These patchy worm-like micelles exhibit a crystalline core with pendant alternating nanometer-sized polystyrene and amino patches in the corona. The polystyrene patches guarantee adhesion to the supporting polystyrene fiber. The amino patches enable the initiation of supramolecular BTA fiber growth. This allows the preparation of *hierarchical superstructures* with a higher level of complexity. A *chemical matching* of the functional amino patches with the substituents of the BTA was found to be important. Thus, using patchy worm-like micelles with *N,N*-dimethyl groups in combination with the BTA with *N,N*-dimethyl groups it was possible to prepare such hierarchical superstructures from water. Immersion of the polymer fibers with patchy worm-like micelles in an aqueous BTA solution induced the patch-mediated molecular self-assembly due to the local increase in the concentration of the BTA with *N,N*-dimethyl groups. After solvent evaporation, complex structures resembling a *fir-tree-like morphology* are obtained where defined supramolecular functional BTA nanofibers have grown away as short fibers.

Complex hierarchical fiber morphologies with a functional surface are promising carriers, for example, for catalysts and reactions in water as a medium. In order to utilize such a *complex hierarchical superstructure* with supramolecular BTA fibers, the use of *electrospun polystyrene nonwovens as support* is beneficial. In addition, the water stability of the supramolecular fibers is a prerequisite. Different combinations of amino-containing BTAs and suitable patchy worm-like micelles immobilized on electrospun nonwovens were investigated. Detailed solubility and self-assembly investigations revealed that only the BTA with *N,N*-di-isopropyl groups is suitable for this purpose due to its negligible water solubility. At room temperature, the BTA with *N,N*-di-isopropyl groups is soluble at low concentrations in isopropanol without dissolving the supporting polystyrene nonwoven. This allows the immersion in the BTA solution and uptake within the nonwoven. The chemical matching of the patchy worm-like micelles with the peripheral groups of the BTA initiates the self-assembly of the BTA into nanofibers due to local enrichment of the BTA and results in a fixation on the surface of the nonwoven fibers. The *hierarchically mesostructured nonwovens* are stable in water and feature off-standing short supramolecular BTA nanofibers on top of the supporting polystyrene fibers of the nonwoven, resembling a *barbed wire-like morphology*. This allows the selective adsorption of single palladium nanoparticles on the surface of the functional supramolecular nanofibers from aqueous media while the complex morphology of the composite stays intact. Such mesostructured nonwovens are attractive systems for potential use in catalytic applications.

## Zusammenfassung

1,3,5-Benzoltricarboxamide (BTAs) sind eine der bekanntesten Klassen in der supramolekularen Chemie. Während der Selbstassemblierungsprozess für herkömmliche BTAs weitestgehend verstanden ist, ist weniger über die Rolle und den Einfluss funktioneller Gruppen in der Peripherie, sowie den resultierenden Oberflächeneigenschaften der entsprechenden supramolekularen Objekte bekannt. Solch funktionelle BTAs können in polaren Lösungsmitteln zur Herstellung von hierarchischen Überstrukturen mit unterschiedlichen Komplexitätsgraden prozessiert werden. Die Oberfläche der funktionellen supramolekularen Objekte ermöglicht zum Beispiel die Immobilisierung spezifischer Metallnanopartikel.

In diesem Zusammenhang liegt der Schwerpunkt dieser Arbeit auf der Synthese, Charakterisierung und Selbstassemblierung *einer neuen Klasse von 1,3,5-Benzoltricarboxamiden mit funktionellen tertiären Aminosubstituenten*. Hierfür wurde eine Reihe von BTAs mit einer Ethyl-Einheit und tertiären Aminosubstituenten mit verschiedenen Alkylgruppen synthetisiert, die von *N,N*-Dimethyl-, *N,N*-Diethyl-, *N,N*-Di-*n*-propyl- bis hin zu *N,N*-Di-isopropylgruppen reichen, um die Hydrophilie des Moleküls systematisch zu variieren und somit Struktur-Eigenschaftsbeziehungen zu identifizieren. Es wurde gefunden, dass diese moderaten Strukturvariationen zu *ausgeprägten Unterschieden in der Löslichkeit der BTAs in Wasser führen*. Das BTA mit *N,N*-Dimethylgruppen weist eine extrem hohe Wasserlöslichkeit von mehr als  $150 \text{ g L}^{-1}$  auf. Hingegen besitzen die BTAs mit *N,N*-Di-*n*-propyl- oder *N,N*-Di-isopropylgruppen eine Löslichkeit von weniger als  $0,01 \text{ g L}^{-1}$  in Wasser. Das BTA mit *N,N*-Diethylgruppen besitzt eine Wasserlöslichkeit von bis zu  $100 \text{ g L}^{-1}$  bei Raumtemperatur. Keines dieser BTAs zeigt in Lösung das typisch zu erwartende Selbstassemblierungsverhalten beim Abkühlen. Überraschenderweise zeigt das BTA mit *N,N*-Diethylgruppen ein reversibles, neuartiges *zweistufiges Selbstassemblierungsverhalten beim Erhitzen* der wässrigen Lösungen. Mit zunehmender Temperatur wird zunächst eine Trübung der gesamten Probe beobachtet, die aus einer flüssig-flüssig-Phasentrennung resultiert, gefolgt von der Assemblierung der BTAs zu supramolekularen faserartigen Strukturen. Diese supramolekularen Strukturen können zerstörungsfrei isoliert werden und weisen eine wohldefinierte *Mikroröhrenmorphologie* auf. Diese Mikroröhrchen sind mehrere hundert Mikrometer lang und haben einen durchschnittlichen Außendurchmesser von etwa  $4,7 \text{ }\mu\text{m}$ .

Zur Herstellung von *komplexeren supramolekularen Strukturen* wurden erstmals zwei Selbstassemblierungskonzepte, nämlich die kristallisationsinduzierte Selbstassemblierung und die molekulare Selbstassemblierung, kombiniert. Hierzu wurden Patch-artige Zylindermizellen, die aus dem Triblockterpolymer Polystyrol-*block*-Polyethylen-*block*-Poly(*N,N*-dimethylaminoethylmethacrylamid) bestehen, durch kristallisationsinduzierte Selbstassemblierung hergestellt und durch koaxiales Elektrosponnen auf der Oberfläche einer Polystyrol-Trägerfaser immobilisiert. Diese Patch-artigen Zylindermizellen weisen einen kristallinen Kern mit alternierend angeordneten nanometergroßen Polystyrol- und Amino-Patches in der Korona auf. Die Polystyrol-Patches gewährleisten die Haftung an der Polystyrol-Trägerfaser. Die Amino-Patches erlauben die Initiierung des supramolekularen BTA-Faserwachstums. Dies ermöglicht die Herstellung von *hierarchischen Überstrukturen* mit einem höheren Komplexitätsgrad. Es hat sich gezeigt, dass die *chemische Übereinstimmung* der funktionellen Amino-Patches mit den Substituenten des BTAs wichtig ist. So gelang es mit den Patch-artigen Zylindermizellen mit *N,N*-Dimethylgruppen in Kombination mit dem BTA mit *N,N*-Dimethylgruppen solche hierarchischen Überstrukturen aus Wasser herzustellen. Das Eintauchen der Polymerfasern mit Patch-artigen Zylindermizellen in eine wässrige BTA-Lösung, induziert die Patch-vermittelte molekulare Selbstassemblierung aufgrund der lokalen Konzentrationserhöhung des BTAs mit *N,N*-Dimethylgruppen. Nach dem Verdampfen des Lösungsmittels erhält man komplexe Strukturen, die einer *Tannenzweig-artigen Morphologie* ähneln. Hierbei sind definierte supramolekulare funktionelle BTA-Nanofasern als kurze Fasern gewachsen.

Komplexe hierarchische Fasermorphologien mit einer funktionellen Oberfläche sind vielversprechende Träger, beispielsweise für Katalysatoren und Reaktionen in Wasser als Medium. Um eine solche *komplexe hierarchische Superstruktur* mit supramolekularen BTA-Fasern nutzen zu können, ist die Verwendung von *elektrogesponnenen Polystyrol-vliesstoffen als Träger* von Vorteil. Darüber hinaus ist die Stabilität der supramolekularen Fasern in Wasser eine Voraussetzung. Es wurden verschiedene Kombinationen von BTAs mit Aminogruppen und geeigneten Patch-artigen Zylindermizellen, die auf elektrogesponnenen Vliesstoffen immobilisiert sind, untersucht. Detaillierte Untersuchungen zur Löslichkeit und Selbstassemblierung ergaben, dass nur das BTA mit *N,N*-Diisopropylgruppen aufgrund der vernachlässigbaren Wasserlöslichkeit für diesen Zweck geeignet ist. Das BTA mit *N,N*-Diisopropylgruppen ist bei geringen Konzentrationen bei Raumtemperatur in

Isopropanol löslich und der Polystyrol-Trägervliesstoff wird nicht aufgelöst. Dies ermöglicht das Eintauchen in die BTA-Lösung und die Aufnahme innerhalb des Vliesstoffes. Die chemische Übereinstimmung der Patch-artigen Zylindermizellen mit den peripheren Gruppen des BTAs initiiert die Selbstassemblierung des BTAs zu Nanofasern aufgrund der lokalen Anreicherung des BTAs und führt zu einer Fixierung auf der Oberfläche der Vliesstofffasern. Die *hierarchisch mesostrukturierten Vliesstoffe* sind beständig in Wasser und zeichnen sich durch abstehende kurze supramolekulare BTA-Nanofasern aus, die auf den Polystyrol-Trägerfasern des Vliesstoffes eine *Stacheldraht-artige Morphologie* bilden. Dies ermöglicht die selektive Adsorption einzelner Palladium-Nanopartikel auf der Oberfläche der funktionellen supramolekularen Nanofasern aus wässrigen Medien, während die komplexe Morphologie des Verbundstoffes intakt bleibt. Solche mesostrukturierten Vliesstoffe sind attraktive Systeme für den potenziellen Einsatz in katalytischen Anwendungen.



# 1. Introduction

## 1.1. Supramolecular chemistry

Nature uses supramolecular chemistry to create multiscale hierarchical superstructures. These structures are of great scientific interest as they may have, for example, a high degree of order, a complex architecture, or functionality that has unique properties for their respective field of application.<sup>[1]</sup>

Supramolecular chemistry<sup>[2,3]</sup> uses molecular building blocks to create objects in the form of fibers and sheets via a bottom-up self-assembly approach. Self-assembly is described as a spontaneous and reversible arrangement of building blocks towards well-defined structures via directed non-covalent interactions.<sup>[4]</sup> Common described non-covalent secondary interactions with their binding energies are, for example, van-der-Waals forces ( $< 5 \text{ kJ}\cdot\text{mol}^{-1}$ ),  $\pi$ - $\pi$  interactions ( $2 - 50 \text{ kJ}\cdot\text{mol}^{-1}$ ), hydrogen bonds ( $4 - 120 \text{ kJ}\cdot\text{mol}^{-1}$ ), dipole-dipole interactions ( $5 - 50 \text{ kJ}\cdot\text{mol}^{-1}$ ), ion-dipole interactions ( $50 - 200 \text{ kJ}\cdot\text{mol}^{-1}$ ), ion-ion interactions ( $100 - 350 \text{ kJ}\cdot\text{mol}^{-1}$ ) and coordination bonds of complex transition-metal ions with ligands ( $100 - 300 \text{ kJ}\cdot\text{mol}^{-1}$ ).<sup>[5]</sup> Secondary interactions are weaker compared to covalent bonds, for example, such as covalent single carbon-carbon bonds ( $\sim 350 \text{ kJ}\cdot\text{mol}^{-1}$ ).<sup>[6]</sup> However, non-covalent interactions allow reversibility of the formed dynamic structures.

The complexity or level in the hierarchy of supramolecular structures can vary and be either very low or very high. The double-stranded DNA is a prominent example of self-assembly toward complex hierarchical structures. The DNA is built by nucleotides. A nucleotide consists of a sugar molecule (deoxyribose for DNA), a phosphate group and a nucleobase. The nucleobases are adenine (A), cytosine (C), guanine (G) and thymine (T).<sup>[7]</sup> The DNA possess a sugar-phosphate backbone and multivalent hydrogen bonds of the complementary nucleic base pairs (A-T and C-G), forming the double helix of two antiparallel strands.<sup>[7]</sup> Hydrogen bonds are used in nature and also in supramolecular chemistry to create supramolecular structures. A hydrogen bond is formed between a hydrogen atom attached to a more electronegative atom compared to hydrogen (hydrogen-bond donor) and a second electronegative atom with free or polarizable electrons (hydrogen-bond acceptor).<sup>[5,7]</sup> Donor groups can be O-H or N-H with the electropositive hydrogen atom and the electronegative atom in the acceptor groups are, for example, O, N and F. Particularly, in the important amide unit, the C=O is the acceptor and N-H is the donor group, representing the hydrogen bonds of

amide units. The geometry, length (short- or long-range) and strength of hydrogen bonds can differ.<sup>[5]</sup> Furthermore, hydrogen bonds are directed and can be intramolecular or intermolecular.<sup>[7]</sup>

Another prominent example of non-covalent interactions and self-assembly in nature are proteins. They can assemble into complex structures with different hierarchical levels (**Figure 1.1.1**). In a simplified way, the primary structure of proteins consists of multiple covalently linked peptide groups of amino acids representing a polypeptide. Intramolecular hydrogen bonds between N-H and C=O stabilize the  $\alpha$ -helix and intermolecular hydrogen bonds between several  $\beta$ -strands leads to  $\beta$ -sheets, representing the secondary structure of proteins. Further increase in hierarchical level and complexity towards three-dimensional structures is the formation of the tertiary structure of proteins. Here, the distribution and the interactions (hydrogen bonds, hydrophobic and ionic interactions) of the subunits of  $\alpha$ -helices and  $\beta$ -sheets play an important role. The quaternary structure of proteins is built up by the interaction of the previously formed polypeptide chains. However, the primary structure and the sequence of amino acids and thus the position of the functional groups, determines the resulting hierarchical structure.<sup>[7]</sup>

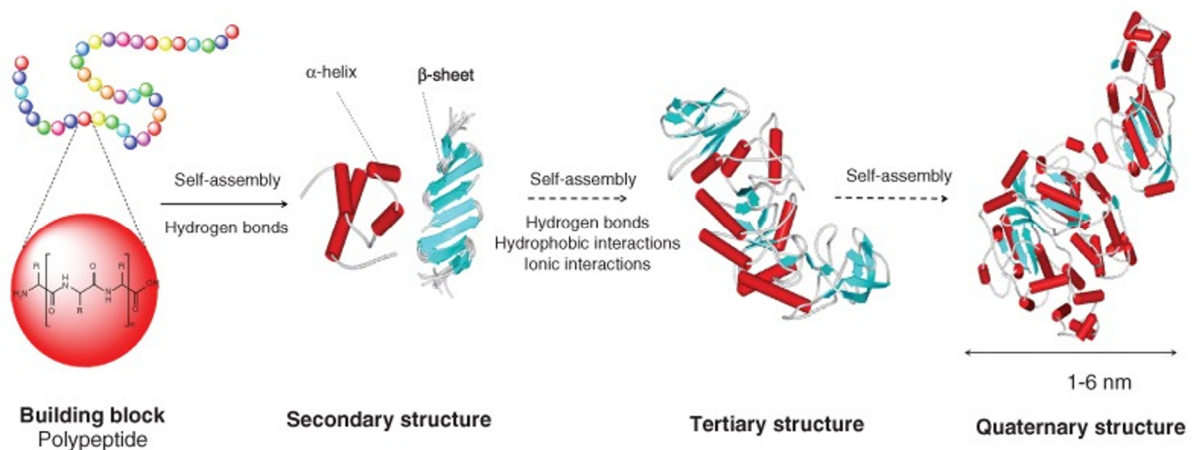


**Figure 1.1.1.** Self-assembly of proteins towards different hierarchical levels. A) The primary structure of a polypeptide chain B) the secondary structure, C) the tertiary and D) the quaternary structure. Adapted and reproduced with permission from Ref. <sup>[7]</sup> (© 2013 Wiley Periodicals, Inc.).

The hierarchical self-assembly towards complex hierarchical structures is predominantly governed by non-covalent interactions on different length scales (**Figure 1.1.2**).<sup>[1,7,8]</sup> The different levels of hierarchical structures from short- to long-range order are built by the self-assembly of molecular building blocks to twisted chains ( $\alpha$ -helix) or folded chains



( $\beta$ -sheets), then fiber bundles or even highly ordered crystalline sheets. Each kind of interaction has a certain task during the self-assembly process and such supramolecular structures are built by the combination of secondary interactions. Often, two or more secondary interactions are present in the supramolecular structure and the interactions need to be balanced.<sup>[1]</sup>

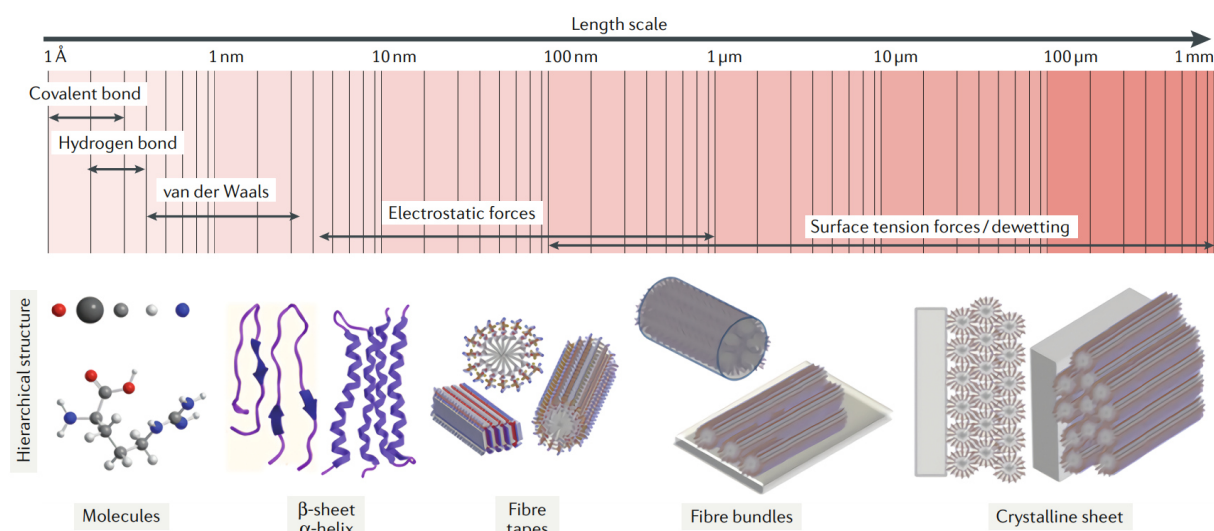


**Figure 1.1.2.** Different intermolecular interactions participating in the self-assembly and structures on different hierarchical levels created by peptide self-assembly. Adapted and reproduced with permission from Ref. <sup>[1,7,8]</sup> (© 2007 WILEY-VCH Verlag GmbH & Co. KGaA, Weinheim, © 2013 Wiley Periodicals, Inc and © 2019 Springer Nature Limited).

Since the preparation of hierarchical superstructures is achieved by secondary interactions, the understanding of the non-covalent interactions and designing of the molecular building block to create functional supramolecular structures is a major challenge in supramolecular chemistry. In this context, nature shows important aspects which can be adapted regarding the molecular building blocks in size and functional groups. Hence, the molecular structure, the physical properties of the molecular building block, the orientation and strength of the interactions, the processing parameters (e.g., temperature, solvent, concentration) determine the self-assembly behavior and the resulting structure.<sup>[1,8]</sup>

Another approach to create artificial complex structures is the self-assembly of block copolymers. First self-assembly studies of amorphous block copolymers in solution were reported in the 1960s.<sup>[9,10]</sup> Different morphologies like helical, cylindrical or spherical micelles and vesicles were achieved from amorphous block copolymers.<sup>[11,12]</sup> However, the preparation of well-defined micelles regarding the control over the length and length distribution is still challenging. Control over size and shape can be achieved by using semi-crystalline block copolymers by the crystallization-driven self-assembly (CDSA), which was pioneered by the work of Manners and Winnik in the late 1990s.<sup>[13]</sup> They investigated the self-assembly of diblock copolymers with a crystallizable poly(ferrocenyldimethylsilane) (PFDMS) block.<sup>[13,14]</sup> The driving force for the formation of anisotropic micellar structures is the crystallization of the PFDMS block.<sup>[14]</sup> The CDSA can be performed in a living manner by using small micellar seeds allowing the control over growth.<sup>[15,16]</sup> A detailed insight into living CDSA is provided by the excellent review recently published by the group of Manners.<sup>[17]</sup> At the seeds, molecularly dissolved block copolymers with a crystallizable block so-called unimers were added over time.<sup>[15,16]</sup> This seeded-growth mechanism allows the preparation of cylindrical micelles with control over the micelle length and paves the way to prepare different architectures, for example, platelet-shaped micelles,<sup>[18–21]</sup> branched micelles,<sup>[22–24]</sup> windmill micelles,<sup>[25–27]</sup> block co-micelles and patchy micelles.<sup>[28,29]</sup> Patchy micelles consist of defined patches in the corona, leading to different surface and interaction properties.<sup>[30]</sup> Other block copolymers with a crystallizable semi-crystalline block are able to undergo CDSA, for example, poly(3-hexylthiophene),<sup>[31]</sup> poly( $\epsilon$ -caprolactone),<sup>[32–34]</sup> poly(L-lactide),<sup>[35,36]</sup> polycarbonates<sup>[37]</sup> and polyethylene (PE)<sup>[38–42]</sup> or a double-crystalline core of PE and poly(ethylene oxide).<sup>[43]</sup>

For example, the triblock terpolymer composed of polystyrene-*block*-polyethylene-*block*-poly(methyl methacrylate) (SEM) with the semi-crystalline PE middle block can be prepared as spherical or patchy worm-like micelles under appropriate conditions (**Figure 1.1.3**).<sup>[38,40]</sup> The middle position of the PE block is important since the crystallizable PE block is the driving force for CDSA.<sup>[38]</sup> The triblock terpolymer is dissolved in a good solvent for PE at elevated temperatures above the melting temperature of the PE block. Upon cooling, a small number of micelles with a crystalline PE core are obtained. The self-assembly process occurs by cooling to the crystallization temperature ( $T_c$ ) of the PE block. The unimers are deposited onto these crystalline micelles resulting in patchy worm-like micelles with increasing time. The two outer

blocks of the triblock terpolymer are composed of different amorphous polymers. The resulting corona of the patchy worm-like micelles consists of alternating nanometer-sized patches of these two polymer types. In contrast, using a bad solvent for PE results in the formation of spherical micelles with a crystalline PE core.<sup>[38]</sup>

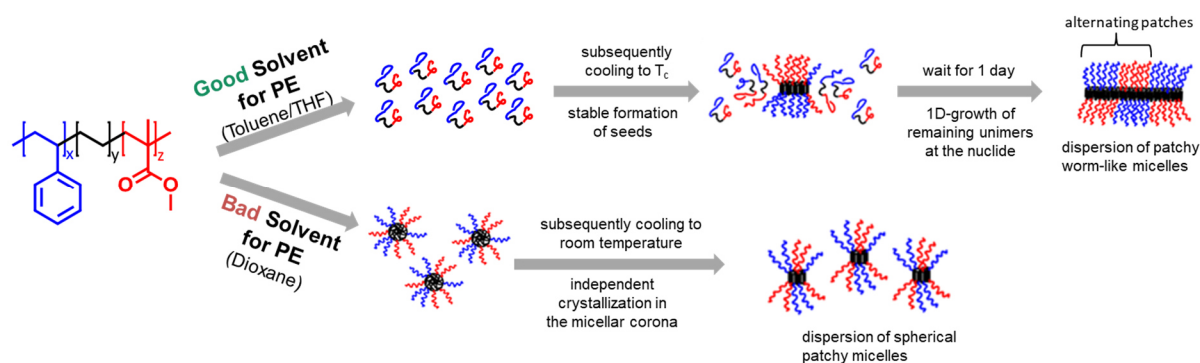


**Figure 1.1.3.** Schematic preparation of patchy worm-like micelles or spherical patchy micelles by crystallization-driven self-assembly exemplary for the triblock terpolymer polystyrene-*block*-polyethylene-*block*-poly(methyl methacrylate). The triblock terpolymer is composed of a crystallizable PE middle block (black) and two outer polymer blocks of polystyrene (blue) and poly(methyl methacrylate) (red). The solvent for the PE block and the self-assembly conditions determines the resulting structure of the micelles. Adapted with permission from Ref. <sup>[38]</sup>. © 2011 American Chemical Society.

Patchy worm-like micelles were investigated regarding their interfacial activity.<sup>[44]</sup> Furthermore, post-polymerization modification of the poly(methyl methacrylate) (PMMA) block of the SEM triblock terpolymer with different *N,N*-dialkylethylenediamines leads to polystyrene-*block*-polyethylene-*block*-poly(*N,N*-dialkylaminoethyl methacrylamide) allowing the preparation of patchy micelles with a functional block.<sup>[45,46]</sup> Patchy micelles with a functionality allow, for example, the in situ synthesis or the immobilization of nanoparticles.<sup>[45,46]</sup>

Another prominent self-assembly motif in supramolecular chemistry are 1,3,5-benzene-tricarboxamides (BTAs). BTAs can self-assemble into complex supramolecular objects via directed hydrogen bonds. This thesis is focused on the controlled self-assembly of BTAs and the preparation of hierarchical superstructures. Therefore, this class will be described in the following in more detail.



## 1.2. Supramolecular class of 1,3,5-benzenetricarboxamides

One of the best studied molecular building blocks to prepare supramolecular structures via a bottom-up approach is the class of 1,3,5-benzenetricarboxamides (BTAs). The general molecular structure of BTAs is depicted in **Figure 1.2.1**.

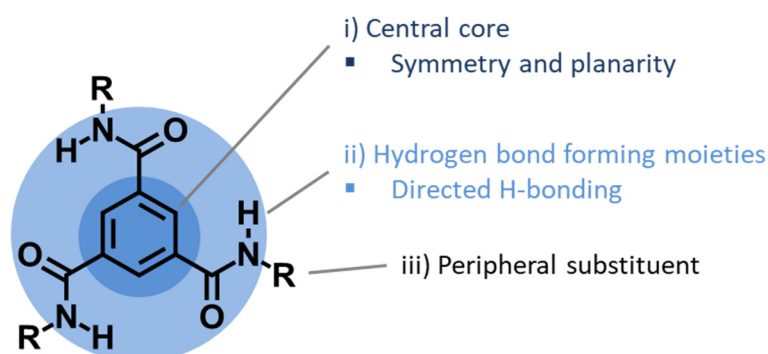


**Figure 1.2.1.** General structure of 1,3,5-benzenetricarboxamides, including the benzene core as central unit, three hydrogen forming amide units and peripheral substituents R.

Three important aspects need to be considered in the molecular design of BTAs: i) the central core, ii) the hydrogen forming moieties and iii) the peripheral substituents. BTAs consist of a benzene ring as central core unit with three symmetrically substituted amide units at the 1<sup>st</sup>, 3<sup>rd</sup> and 5<sup>th</sup> positions leading to a C<sub>3</sub>-symmetry and planarity of the molecule.<sup>[47]</sup> Besides the benzene ring as central core unit, a structural similar material class are 1,3,5-cyclohexanetricarboxamides.<sup>[48–53]</sup> Here, cyclohexane is used as central core instead of benzene. The amide groups are responsible for intermolecular interactions due to directed threefold hydrogen bonds and, thus, the preferable formation of one-dimensional supramolecular structures.<sup>[47,54,55]</sup> The amide groups can be either attached with the carbon atom (C-centered) or the nitrogen atom (N-centered) to the benzene or cyclohexane core and a mixed attachment is also possible (**Figure 1.2.2**).<sup>[47,56–66]</sup> Mostly, three identical peripheral substituents R are attached to the core leading to a C<sub>3</sub>-symmetry. However, unsymmetrical BTA derivatives with different substituents at the amide groups were also reported. The choice of the peripheral substituents R connected to the amide groups can influence the thermal properties, the solubility and self-assembly behavior. Especially the influence of peripheral functional groups is described in detail in **Chapter 1.3**.

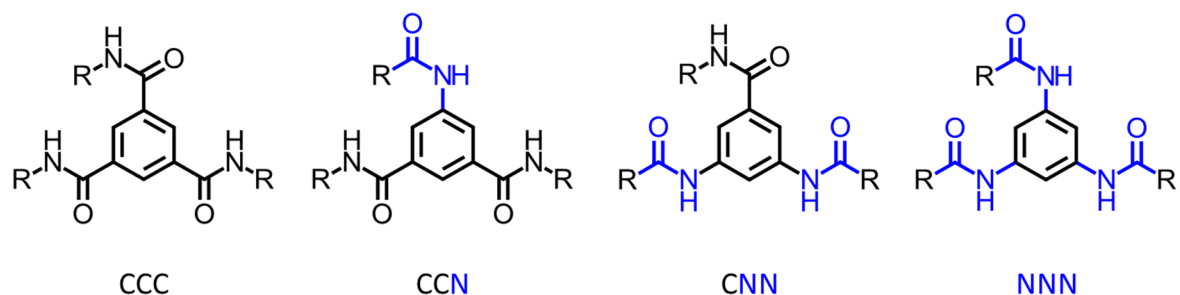


**Figure 1.2.2.** Chemical structures of 1,3,5-benzenetrisamides derivatives with different C- and N-centered amide linkage. Based on 1,3,5-benzenetricarboxylic acid core all amide units are C-centered (CCC). Based on 5-aminoisophthalic acid core one amide linkage is inverted (CCN). Based on 3,5-diaminobenzoic acid core two amide linkages are inverted (CNN). Based on 1,3,5-triaminobenzene core all amide groups are N-centered (NNN).

### *Self-assembly of BTA derivatives in solid state*

BTAs can form supramolecular columns in bulk or solution. The peripheral substituents not only influence the solubility behavior or thermal properties but also the packing behavior and crystal structure in solid state. For example, Lightfoot et al.<sup>[55]</sup> investigated the crystal structure of the BTA with methoxyethyl peripheral groups. These findings revealed that this BTA forms a helical columnar structure in solid state due to the formation of triple hydrogen bonds between the molecular building blocks along the columnar axis. All amide groups of one BTA are orientated in the same direction. The benzene rings of the molecular building blocks are stacked parallel to each other with a 60° twist leading to a helical arrangement (**Figure 1.2.3**).<sup>[47,55,58]</sup>

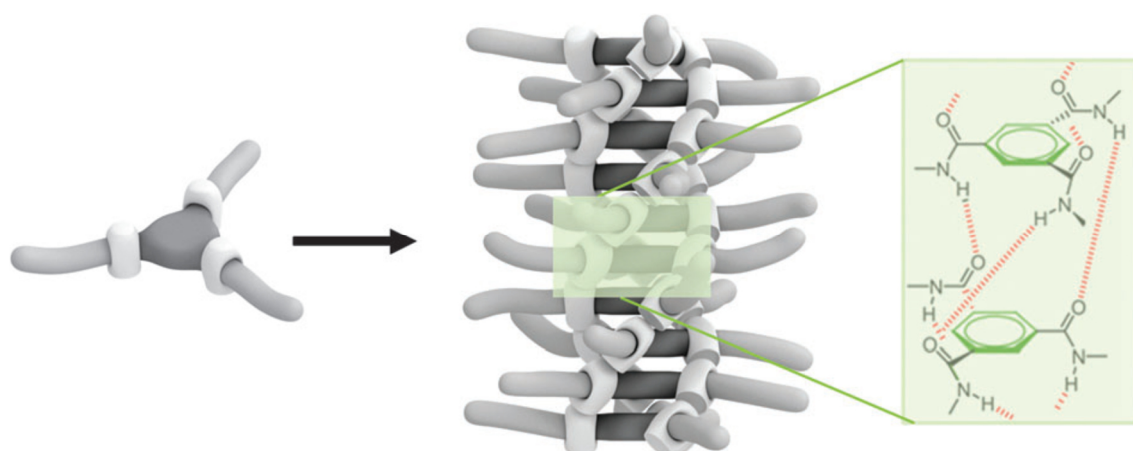


**Figure 1.2.3.** Schematic illustration of the self-assembly of a BTA into a helical columnar structure. The structure is observed by the formation of three-folded intermolecular hydrogen bonds. Reproduced from Ref. <sup>[47]</sup> with permission from the Royal Society of Chemistry (© 2012).

Due to the orientation of the hydrogen bonds  $N-H\cdots O=C$  of one BTA in the same direction, the formation of individual dipole moments resulting in a macrodipole directed along the supramolecular column axis was observed (**Figure 1.2.4**).<sup>[52,67–69]</sup> Each molecule of the supramolecular column contributes with its individual dipole moment to the strength of the macrodipole. The dipole moment arises due to the alignment of the polar  $C=O$  and  $N-H$  bonds. The molecular structure influences the strength of the macrodipole.<sup>[52,68]</sup> The presence of the macrodipole allows polar switching and recently, ferroelectric and piezoelectric properties of BTA derivatives were investigated.<sup>[69–72]</sup> The BTAs are not limited to the formation of directed threefold hydrogen bonds. This was observed, for example, for small peripheral substituents and fluorine-containing substituents.<sup>[67,73]</sup>

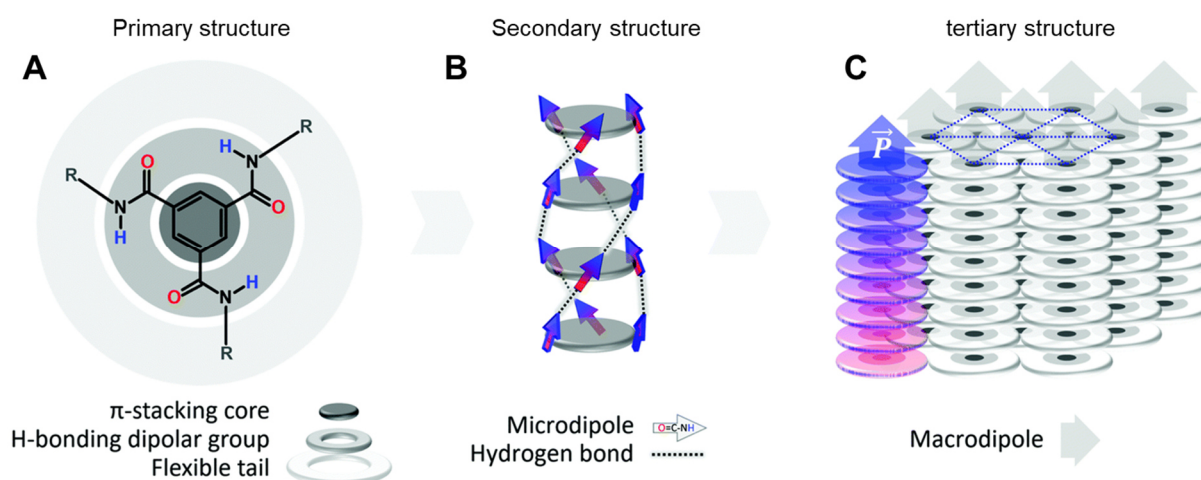


**Figure 1.2.4.** A) Chemical structure of a BTA derivative with a central benzene core and three amide groups displays the primary structure. B) Self-assembly of the BTA into a column with a triple-helix with intermolecular hydrogen bonds represents the secondary structure. The stacking of the disk-shaped BTA is shown in a simplified way and the dotted lines indicate the hydrogen bonds. C) The tertiary structure is the arrangement of the single columns in a columnar-hexagonal packing and results in a macrodipole. The arrows upwards indicate the macrodipole of the supramolecular structure. Reproduced from Ref. <sup>[71]</sup> with permission from the PCCP Owner Societies (© 2019).

*Self-assembly of BTA derivatives in solution or polymer melt*

The self-assembly process of BTAs to form one-dimensional supramolecular objects can be promoted under certain conditions by external triggers such as the change in temperature, concentration, solubility or pH value. In particular, the respective BTA has to be molecularly dissolved in a medium (e.g., polymer, solvent) (**Figure 1.2.5**). The self-assembly process is initiated by an external trigger. This leads to the aggregation of the individual molecular building blocks to columns and further self-assembly leads to supramolecular objects.<sup>[55,74,75]</sup> This process is fully reversible due to the non-covalent interactions.

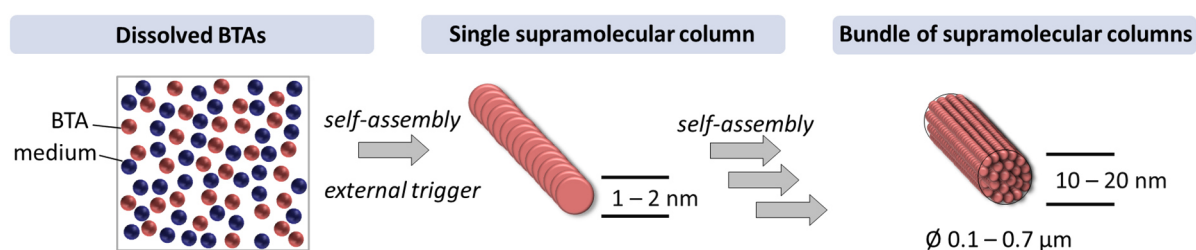


**Figure 1.2.5.** Schematic representation of the general self-assembly process of BTAs. The self-assembly of the molecularly dissolved BTA molecules is initiated by external triggers. This leads to aggregation into supramolecular columns consisting of single BTA molecules. Further self-assembly results in the formation of supramolecular objects. Source: University of Bayreuth; Macromolecular Chemistry I.

The self-assembly process of BTAs towards supramolecular structures is influenced by several factors (**Figure 1.2.6**). One important factor is the molecular structure of the BTA itself. This includes the size/length and the kind of functional peripheral substituents. Furthermore, the used BTA concentration within the medium can influence the resulting supramolecular structure or the morphology of the formed structures. Besides this, the process parameters (temperature, heating and cooling rates) determine the self-assembly behavior and, thus, the diameter of the resulting supramolecular structures. As well, the used medium/solvent to molecularly dissolve the BTA needs to be considered in the self-assembly process. Using different solvents can also change the resulting morphology. All these parameters influence the formation of supramolecular objects.<sup>[75]</sup>



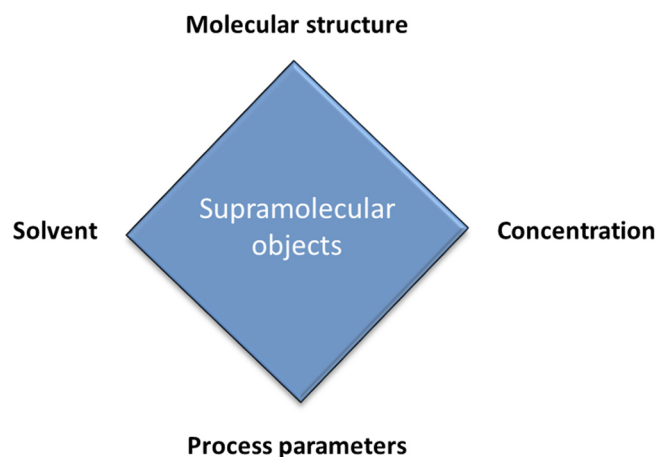


**Figure 1.2.6.** Important influence factors for the self-assembly of BTAs. Source: University of Bayreuth; Macromolecular Chemistry I.

#### *Self-assembly processes for BTA derivatives from solution*

One typical method to promote the self-assembly process of BTAs to form supramolecular objects is upon cooling at constant concentration using the temperature change as trigger (**Figure 1.2.7A**).<sup>[75]</sup> For this, the respective BTA is molecularly dissolved in a solvent at elevated temperatures. Upon cooling at constant concentration, the solubility of the BTA is decreased and the self-assembly process occurs. The formation of supramolecular objects from the molecular building blocks typically occurs within the time range of seconds. This is attributed to the temperature-dependent solubility of the BTA in the solvent. Heating dissolves the formed supramolecular objects and upon cooling, the self-assembled objects are formed again. The formed supramolecular objects can be isolated by completely removing of the solvent or by filtration.<sup>[75]</sup>

Depending on the concentration, BTAs are capable of forming gels in organic solvents consisting of a self-assembled supramolecular fiber network.<sup>[53,54,66,76–80]</sup> The BTAs are capable to immobilize the used solvent. Typically, the gels are obtained when the BTA is molecularly dissolved in the solvent upon heating and subsequent cooling, leading to the gelation due to self-assembly to supramolecular structures. The gelation process can occur within seconds or aging for several days can be necessary.

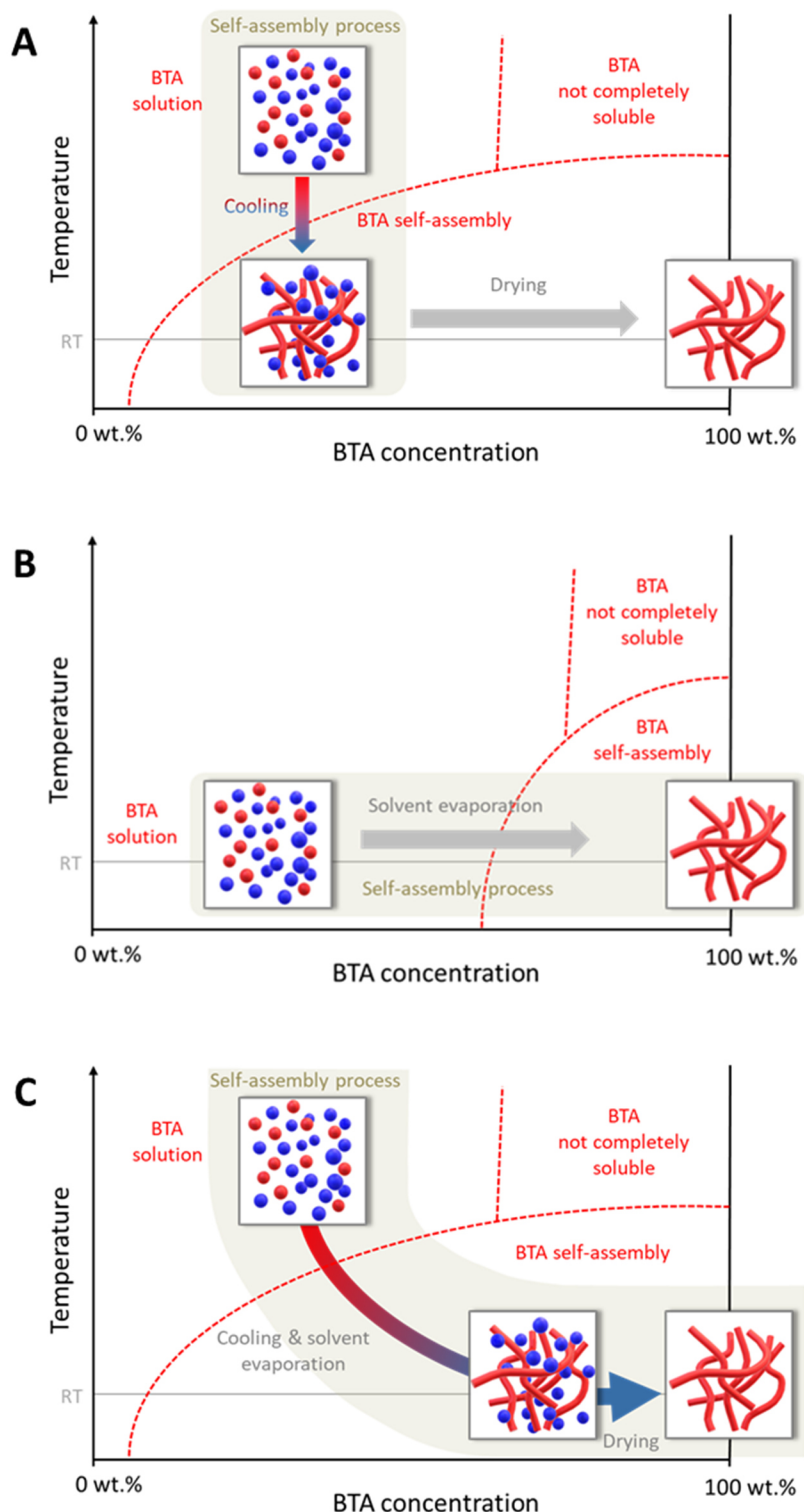


**Figure 1.2.7.** Schematic representation of typical self-assembly processes from solution A) upon cooling at constant BTA concentration, B) upon solvent evaporation at room temperature and C) simultaneous cooling and evaporation of the solvent from elevated temperatures. For all three processes, the BTA (red dots) is molecularly dissolved in the solvent (blue dots). A) Upon cooling at constant BTA concentration, supramolecular structures are formed, and a dispersion is present. The supramolecular structures can be isolated by removing of the solvent. B) A molecularly dissolved solution is present at room temperature. Supramolecular structure formation can be initiated by increase in BTA concentration during solvent evaporation at room temperature. C) Simultaneous cooling and solvent evaporation induce supramolecular structure formation after complete solvent evaporation. Source: University of Bayreuth; Macromolecular Chemistry I.

Another method to promote the self-assembly process of BTAs towards supramolecular structures is upon solvent evaporation at constant temperature (**Figure 1.2.7B**). A molecularly dissolved solution is present at room temperature. The self-assembly process can be initiated by solvent evaporation at constant temperature. This leads to an increase in BTA concentration and, thus, to the formation of supramolecular objects when a certain threshold BTA concentration is reached. Complete drying of the solvent leads to isolated supramolecular objects.

The last self-assembly process is initiated by simultaneous cooling and solvent evaporation of a BTA solution from elevated temperatures (**Figure 1.2.7C**). The respective BTA is molecularly dissolved in a solvent at elevated temperatures. Due to the complex process of simultaneous cooling and solvent evaporation, supramolecular objects are created. This process was, for example, used to create in situ supramolecular nanofibers to achieve microfiber-nanofiber composites for filtration applications.<sup>[81,82]</sup>

Further possibilities to initiate or accelerate the self-assembly process by changing the solubility is the addition of an anti-solvent to the molecularly dissolved BTA solution. For example, Cao et al.<sup>[83]</sup> showed for a BTA derivative with L-glutamic acid diethyl ester peripheral groups that gelation took place immediately within seconds at room temperature after adding small amounts of the anti-solvent water to the BTA solution in organic solvent. In pure organic solvents, the gelation is obtained within two hours upon cooling the solution. The resulting structures were investigated after solvent removal and revealed tubular superstructures with a hexagonal cross-section. Another example was shown by Nagarajan et al.<sup>[84]</sup> where the gelation of a series of BTAs with peripheral para-alkyl phenyl groups with different lengths of the alkyl group was accelerated from around four days in pure dimethyl sulfoxide towards seconds after addition of some droplets of water to the dimethyl sulfoxide BTA solution. A fibrous morphology was observed after solvent removal.<sup>[84]</sup>



### 1.3. Influence of the peripheral substituents of 1,3,5-benzenetricarboxamides on the structure formation

The general molecular structure of BTAs is depicted in **Figure 1.3.1**. However, in this section, special attention is given to the peripheral substituents R. As described before, the central core unit is a benzene ring with three symmetrically substituted amide groups at the 1<sup>st</sup>, 3<sup>rd</sup> and 5<sup>th</sup> positions. Also, the amide groups are responsible for intermolecular interactions due to directed threefold hydrogen bonds and, thus, the formation of supramolecular objects.<sup>[47]</sup> Variations in the design of the molecular building blocks, especially with respect to the peripheral substituents, can lead to a different self-assembly behavior. The peripheral substituents R and the amide forming units can be separated by different spacers to avoid intramolecular interactions and shield the core from the solvent. This can be important when the peripheral group provides functionality and contain, for example, O, S and N atoms, which also have the potential for secondary interactions. The choice of the peripheral substituents R can influence the thermal properties, the solubility and the nature of the self-assembly behavior. Thus, a smart choice in the peripheral groups can tailor these properties.

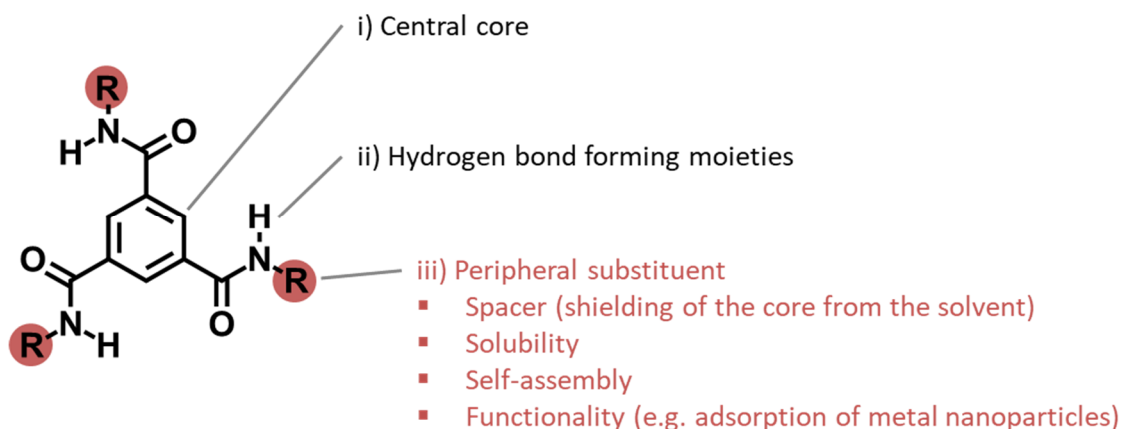


**Figure 1.3.1.** General structure of 1,3,5-benzenetricarboxamides, including the central benzene core unit, three hydrogen forming amide units and peripheral substituents R.

A huge number of BTAs with different peripheral substituents were synthesized over the last decades and investigated in detail regarding their crystal structure, solubility and self-assembly behavior. The nature of the peripheral substituents can be, for example, aliphatic (linear, branched, cyclic), aromatic, with chiral center groups or achiral, neutral or charged, non-polar to protic polar groups.<sup>[47]</sup>

### *BTAs with aliphatic side groups*

BTAs with aliphatic groups in the periphery and their self-assembly into supramolecular structures is mainly conducted in organic solvents. The variety of peripheral substituents leads to different applications due to the well-defined morphology of the supramolecular BTA structures. For example, Matsunaga et al.<sup>[85,86]</sup> described the liquid crystalline behavior of several alkyl-substituted BTAs. Furthermore, Timme et al.<sup>[87]</sup> investigated BTAs with linear and branched alkyl chains with respect to the phase behavior. Already small changes in the molecular design led to strong differences in the thermal properties. Further investigations on alkyl-substituted BTAs were carried out by Stals et al.<sup>[88]</sup> The nature of the peripheral groups is important regarding potential applications. BTAs with bulky, aliphatic peripheral groups are high melting crystalline solids which can assemble in supramolecular needle-shaped crystals.<sup>[89]</sup> This attribute allows BTAs to be used as effective nucleation and clarification agents in various polymers like isotactic polypropylene (iPP),<sup>[56,62,89–91]</sup> poly(vinylidene fluoride),<sup>[63]</sup> poly(butylene terephthalate),<sup>[64]</sup> poly(lactide acid),<sup>[92–96]</sup> or as cell nucleation agent for iPP<sup>[97]</sup> and polystyrene foams.<sup>[98,99]</sup> BTAs with short aliphatic or cyclohexyl substituents were used in PP to improve the electret properties.<sup>[74]</sup> In contrast, a thermotropic liquid crystalline behavior is achieved by long alkyl side chains and long branched alkyl side chains leading to the formation of orangogels.<sup>[47,54,77]</sup>

### *BTAs with functional side groups*

The thesis is focused on BTAs with peripheral functional groups and the self-assembly in polar solvents. The self-assembly of BTAs in organic solvents via directed hydrogen bonds is well understood. However, the self-assembly of BTAs in the presence of water can influence hydrogen bond formation. Adding a functional peripheral group to the BTA could increase the property profile of the supramolecular objects and be beneficial for superior applications. For example, BTAs with peripheral groups like ethers,<sup>[100–106]</sup> benzo-crown ethers,<sup>[107–109]</sup> pillar[5]arene,<sup>[110,111]</sup> saccharides,<sup>[112–115]</sup> acids like carboxylic acid,<sup>[116–126]</sup> glutamic acid,<sup>[127,128]</sup> sulfuric acid,<sup>[129–131]</sup> sulfur containing groups,<sup>[132]</sup> azobenzene units<sup>[133–137]</sup> and pyridyl groups<sup>[138–147]</sup> were described in the literature. Beyond small peripheral groups, the attachment of functional poly(ethylene glycol) blocks onto BTAs is shown.<sup>[148]</sup> The lateral substituents can differ in symmetry, size and functionality. However, introducing a functional

group make BTA derivatives as molecular building block interesting for various research fields such as biomaterials or hydrogels.

Several functional BTA derivatives were studied by the group of Meijer. For example, they investigated BTA derivatives bearing hydrophilic linear ethylene glycol-based side chains, dendritic oligoglycerol-based side chains, different lengths of aliphatic spacers and number of hydrophobic side chains.<sup>[100–105]</sup> The hydrophilic part results in water solubility, while a sufficient hydrophobic part is necessary to shield the core and the hydrogen forming amide units for the self-assembly in water.<sup>[100,101,103]</sup> A interference of the intermolecular amide hydrogen bonding with the intramolecular hydrogen interactions due to the back folding of the ethylene glycol side chains is assumed.<sup>[100,103]</sup> Already moderate changes in the molecular design drastically affect the columnar packing. Upon cooling, the BTA derivative with an aliphatic hydrophobic dodecyl spacer and a hydrophilic tetraethylene glycol tail with alcohol end groups in the periphery self-assembles into micrometer long supramolecular nanofibers with a diameter of around 5 nm (**Figure 1.3.2**).<sup>[101,106]</sup> A higher BTA concentration results in the formation of hydrogels.<sup>[102]</sup> Furthermore, computational and experimental studies were conducted to investigate the role of hydrogen bond formation to understand the molecular design principles, especially in water.<sup>[106,149–151]</sup> The structural motif of BTAs allows for further modification and functionalization. Recently, symmetrical and unsymmetrical BTAs with undecyl and dodecyl aliphatic spacers and tetraethylene glycol tails with C- and inverted N-centered amide bond connectivity were co-assembled, showing the potential as biomaterials.<sup>[60]</sup>

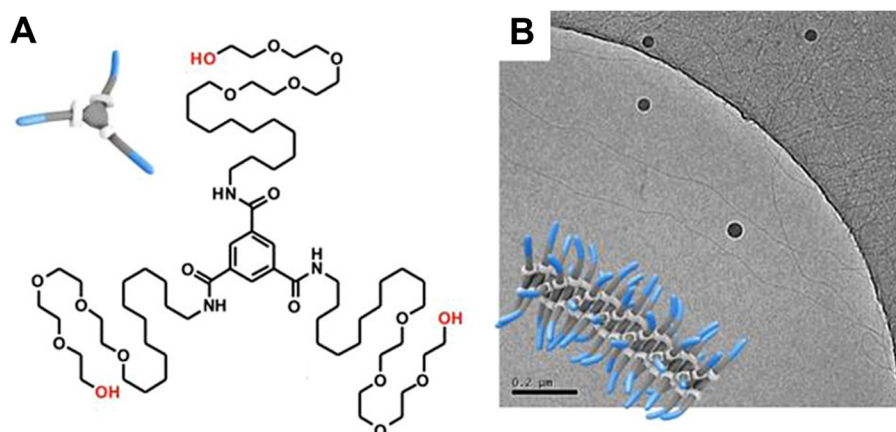


**Figure 1.3.2.** A) Chemical structure of a BTA with a hydrophobic dodecyl spacer and tetraethylene glycol tail groups. B) Upon cooling, the BTA self-assembles into long supramolecular BTA nanofibers from aqueous solutions. Adapted with permission from Ref. <sup>[106]</sup>. © 2016 American Chemical Society.

Further examples are benzo-crown ether groups in the periphery of BTAs. For example, Lee and Qi et al.<sup>[107,109]</sup> utilized the temperature-dependent phase separation of BTA derivatives with peripheral benzo-crown ether groups upon heating aqueous solutions or mixtures of water and organic solvents. The solubility is dependent on the size of the crown ether. Heating the solutions lead to separation of the water molecules from the molecular building blocks and, thus, the formation of supramolecular structures.<sup>[107,109]</sup> Furthermore, Dong et al.<sup>[108]</sup> investigated different BTA derivatives containing benzo-crown substituents of different sizes and cores. Especially the BTA with benzo-21-crown-7 substituents (**Figure 1.3.3A**) shows an increase in viscosity with the addition of water. Depending on the concentration of the BTA in water, it can be used as adhesive material between hydrophilic surfaces and can withstand weights up to 10 kg (**Figure 1.3.3B**).<sup>[108]</sup> The adhesive behavior decreases with increasing temperature, which makes the material reusable without a loss in performance.<sup>[108]</sup>

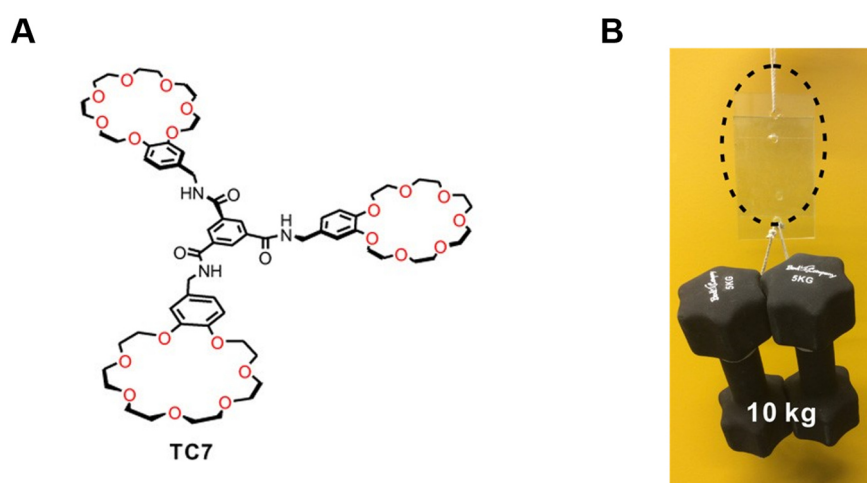


**Figure 1.3.3.** A) Chemical structure of a BTA with benzo-21-crown-7 substituents. B) The BTA can be used as adhesive material between two hydrophilic glass slides and was weighted with two dumbbells. Adapted and reproduced from Ref. <sup>[108]</sup>. Published in Science Advances under the terms of the Creative Commons Attribution 4.0 International License (© 2017 The Authors).



Leenders et al.<sup>[112]</sup> synthesized various BTAs with peripheral monosaccharide groups (glucose, galactose and mannose) and investigated the self-assembly behavior in water by varying the length of the alkyl spacer between the BTA core and the functional groups. A dodecyl spacer is necessary to obtain one-dimensional long supramolecular nanofibers, while the type of monosaccharide showed no noticeable impact on the self-assembly behavior. Furthermore, the group of Meijer investigated BTA derivatives with an aliphatic dodecyl spacer with and without tetraethylene glycol groups and different monosaccharides end groups regarding their self-assembly behavior in water.<sup>[113,114]</sup> In contrast, Wang et al.<sup>[115]</sup> investigated the self-assembly behavior of monosaccharide-containing BTAs with glucose, galactose and mannose as peripheral substituents without any aliphatic spacer (**Figure 1.3.4**). The used monosaccharides differ only in the orientation of the hydroxyl group. The BTA with glucose self-assembled into spherical vesicles, the BTA with galactose into nanorings and the BTA with mannose into long twisted fibers in aqueous solution. Already moderate changes in the structure result in different supramolecular morphologies. It was proposed that the orientation of the hydroxyl group plays an essential role in the resulting supramolecular structures. Here, the kind of monosaccharide has an impact on the self-assembly behavior.<sup>[115]</sup>

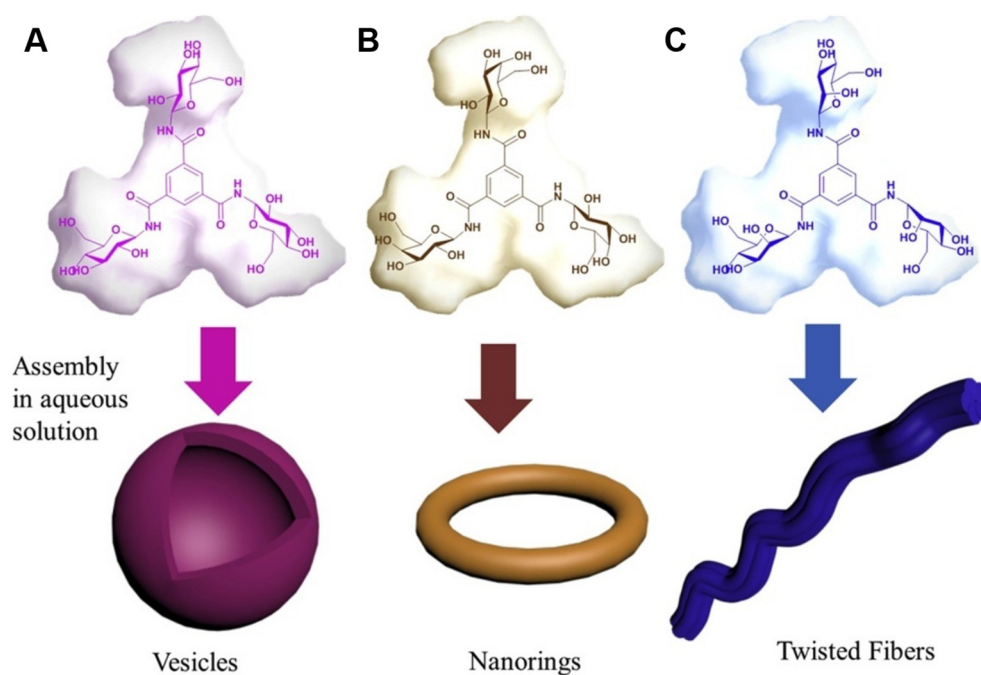


**Figure 1.3.4.** Self-assembly of BTAs with different monosaccharides resulting in different morphologies. The BTAs contain A) glucose (pink), B) galactose (brown) and C) mannose (blue) as peripheral substituents. Reprinted from Ref. <sup>[115]</sup> with permission from Elsevier (© 2018).

Introducing carboxylic acid peripheral groups to BTAs allows the preparation of hydrogels. However, the formation of supramolecular structures of the BTAs is triggered by the pH change. Bernet et al.<sup>[116]</sup> showed the successful preparation of hydrogels of a BTA with aromatic carboxylic acid side groups by reducing the pH value. The chemical structure is depicted in **Figure 1.3.5A**. Howe et al.<sup>[117]</sup> synthesized a similar series of BTAs with aromatic carboxylic acid periphery acting as pH-sensitive hydrogelators.<sup>[117]</sup> Furthermore, Lynes et al.<sup>[118]</sup> synthesized five BTAs derivatives with different lengths of aliphatic spacers between the core and the carboxylic acid group and showed the influence on the self-assembly behavior. The pH sensitivity allows the investigation of the self-assembly kinetics in a microfluidic device.<sup>[119]</sup> This kind of BTA was used for the controlled preparation of hydrogel films by electrogelation (**Figure 1.3.5B**).<sup>[120]</sup> The BTA is deprotonated under basic conditions. This leads to water solubility due to electrostatic repulsion and can be achieved by adding an aqueous NaOH solution. By acidification, the BTA is protonated and the solubility of the BTA in water is reduced, which induces self-assembly.<sup>[116]</sup> The reduction in pH value can be achieved via electrolysis of water and results in the growth of a supramolecular hydrogel film.<sup>[120]</sup> With the combination of atomic force microscopy (AFM) and nanofluidics (FluidFM), the hydrogel film can be selectively structured by an alkaline solution stream, ejected through a hollow AFM-cantilever with micrometer precision (**Figure 1.3.5C**).<sup>[120]</sup>

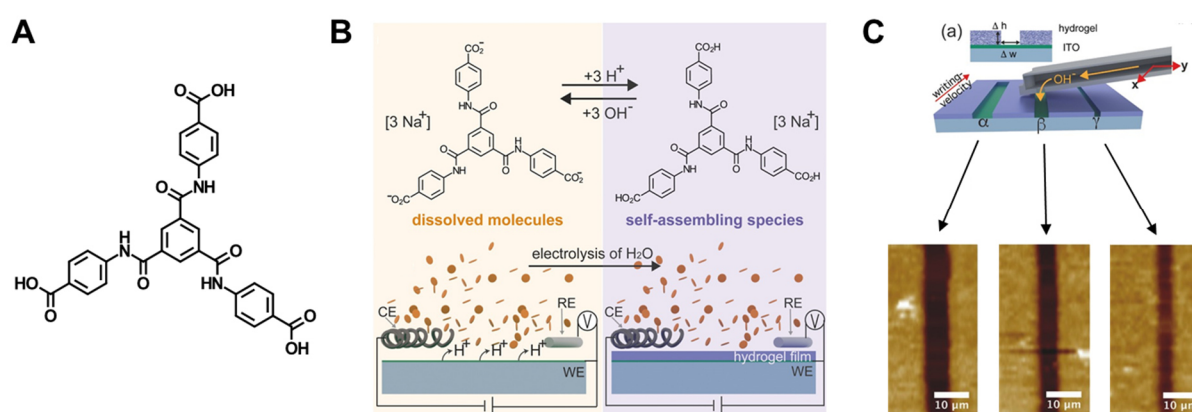


**Figure 1.3.5.** A) Chemical structure of *N,N',N''*-tris(4-carboxyphenylene)-1,3,5-benzenetricarboxamide. B) As sodium salt, the BTA is deprotonated and soluble in water. By reducing the pH value via electrolysis of water by local production of  $\text{H}^+$ -ions, the BTA forms a supramolecular hydrogel film and is insoluble in water in its protonated state. The schematic electrogelation setup is shown with a three-electrode electrochemical cell (CE = counter-, RE = reference- and WE = working electrode). C) Schematic writing setup with FluidFM. By ejection of an alkaline solution, the BTA hydrogel changes the solubility in water and can be selectively structured. Depending on the writing velocity, different widths of the lines are observed. Adapted with permission from Ref. <sup>[120]</sup> (© 2017 WILEY-VCH Verlag GmbH & Co. KGaA, Weinheim).

Furthermore, the reduction in pH value and, thus, the protonation of the BTA with carboxylic acid peripheral groups can be achieved by adding glucono-delta-lactone (GdL), which release protons due to hydrolysis.<sup>[116,121]</sup> Huang et al.<sup>[121]</sup> investigated the self-assembly depending on the concentration of GdL in view of lyotropic chromonic liquid crystals behavior. Matsumoto et al.<sup>[122]</sup> synthesized unsymmetrical BTA derivatives where one of the three side chains bears carboxylic acid end groups and the length of the spacer between the core and the end group was varied. It was shown that different morphologies in form of fibers, membranes and hollow tubes can be achieved by using, in this case, the temperature change as an external self-assembly trigger.<sup>[122]</sup>

Another example reported in the literature to prepare hydrogels is the use of glutamic acid as peripheral groups (**Figure 1.3.6A**).<sup>[127]</sup> VandenBerg et al.<sup>[127]</sup> investigated the self-assembly of this BTA to prepare hierarchically complex structures by controlling the self-assembly kinetics using the pH change as an external trigger. For a slow pH change, GdL was used and for a fast pH change, HCl was added. After 1h after the addition of HCl, a turbid gel composed of a dense network of thick fibers is observed (**Figure 1.3.6B**). In comparison, 24h after the addition of GdL, a transparent gel composed of a mesh of thinner fibers is obtained. A variation in the kinetic of the pH change results in different supramolecular structures.

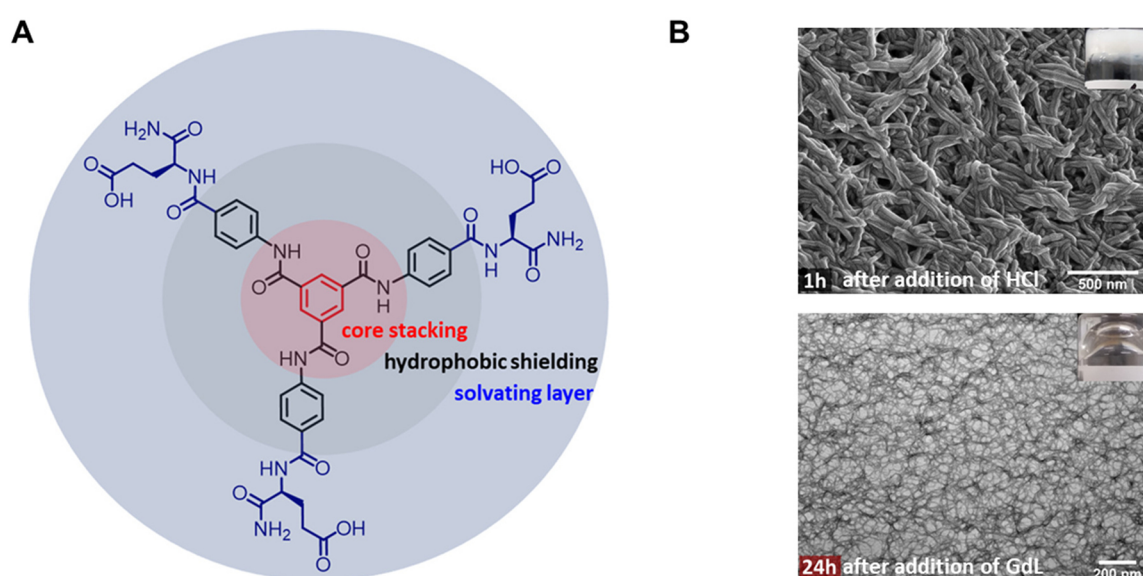


**Figure 1.3.6.** A) Chemical structure of a BTA with peripheral glutamic acid groups. B) The self-assembly can be triggered by the change in pH value. By the addition of HCl, the reduction in pH is fast, leading to a turbid gel (see inset picture after 1h) composed of a dense network of thick fibers. By the addition of GdL, the reduction in pH value is slow, leading to transparent gel (see inset picture after 24h) composed of thin fibrillar structures. Adapted with permission from Ref. <sup>[127]</sup>. © 2020 American Chemical Society.

Furthermore, Spitzer et al.<sup>[128]</sup> reported a multi stimuli-responsive behavior in water for a dendritic BTA containing the pH-switchable glutamic acid, redox-responsive methionine groups and thermoresponsive triethylene glycol groups in the periphery.

Another functional group described in the literature to prepare water-soluble BTAs is the introduction of sulfonic acid groups.<sup>[129–131]</sup> For example, Wang et al.<sup>[131]</sup> investigated rigid BTAs with sulfonic acid groups (**Figure 1.3.7A**). The liquid crystalline behavior in water at room temperature was studied for different BTA concentrations by polarized optical microscopy. At low concentrations, a solution is present. Increasing the concentration to 7 wt.% leads to a liquid-crystal behavior (**Figure 1.3.7B**). Further increase in concentration to 13 wt.% shows a gel-like state. The texture of the gel can be aligned by shearing, which is promising for anisotropic ionic conductivity.<sup>[131]</sup>

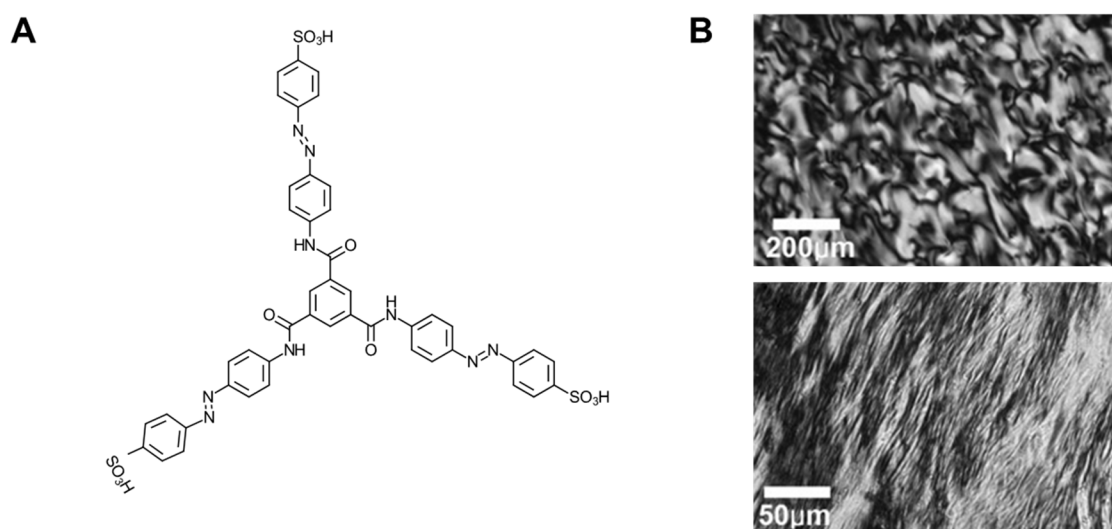
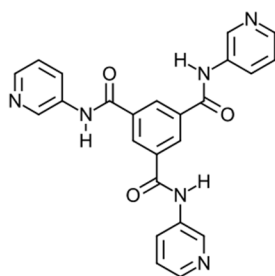


**Figure 1.3.7.** A) Chemical structure of *N*<sup>1</sup>,*N*<sup>3</sup>,*N*<sup>5</sup>-tris[4-(azobenzene-4-sulphonic acid)phenyl]benzene-1,3,5-tricarboxamide. B) Polarizing optical micrographs of the liquid-crystalline behavior of the BTA in water at a concentration of 7 wt.% (top) and resulting gel at a higher concentration of 13 wt.% (bottom). The gel is aligned by shearing the sample. Adapted with permission from Ref. <sup>[131]</sup> (© 2013 WILEY-VCH Verlag GmbH & Co. KGaA, Weinheim).

Recently, the preparation of functional supramolecular fibers of BTAs containing sulfur in the periphery was investigated in our group.<sup>[132]</sup> Besides the investigation of the self-assembly behavior, the preparation of functional supramolecular fibers comprising a core-shell structure and the preparation of supramolecular nanofiber composites for the filtration of bacteria from water was demonstrated.<sup>[132]</sup>

Apart from the mentioned examples, several BTAs with peripheral pyridyl groups can form hydrogen bonds and coordinate metal ions. For example, Palmans et al.<sup>[138]</sup> synthesized and investigated the crystal structure of *N,N',N''*-tri(pyridine-3-yl)benzene-1,3,5-tricarboxamide (**Figure 1.3.8A**). Kumar et al.<sup>[139]</sup> showed with this BTA and the *N,N',N''*-tri(pyridine-4-yl)benzene-1,3,5-tricarboxamide analogues with a different position of the N in the pyridine ring the preparation of hydrogels upon cooling mixtures of water and organic co-solvents. The co-solvent is necessary since both BTAs are insoluble in water. The dried hydrogels exhibit a fibrous structure.<sup>[139]</sup> Shi et al.<sup>[140]</sup> prepared fibrous hydrogels from the 3-pyridyl substituted BTA and used it as a matrix for biomineralization. In a further study by Shi et al.<sup>[141]</sup> the use of a co-solvent was also reported to improve the solubility of 3-methylpyridyl substituted BTA derivative in water to prepare hydrogels. The BTA derivate self-assembled into hexagonal microtubes upon cooling the heated aqueous mixtures. Increasing the BTA concentration lead to larger microtubes.<sup>[141]</sup> Tzeng et al.<sup>[142]</sup> showed that the 3- and 4-pyridyl substituted BTA are capable of acting as bridging ligands for the preparation of molecular cages. The preparation of hydrogen-bonded organic frameworks was reported by Luo et al.<sup>[143]</sup> with the 4-pyridyl substituted BTA derivative, which is stable in organic solvents and water and shows a selective absorption for gases. This attribute is promising for potential application for gas purification.<sup>[143]</sup>

A



B

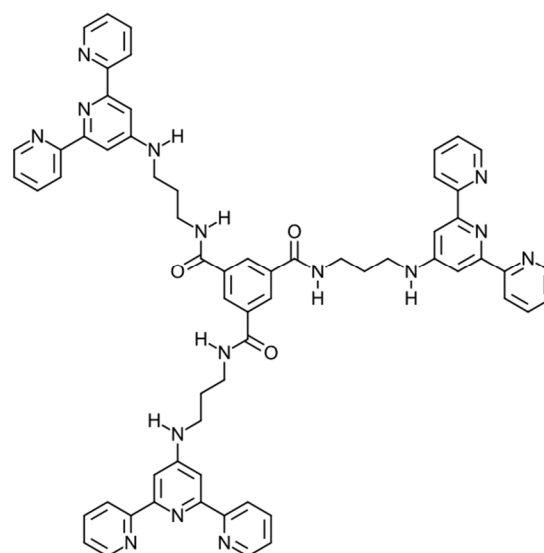


**Figure 1.3.8.** A) Chemical structure *N,N',N''*-tri(pyridine-3-yl)benzene-1,3,5-tricarboxamide. B) Chemical structure of benzene-1,3,5-tricarboxylic acid tris-{[3-([2,2';6',2'']terpyridin-4'-ylamino)-propyl]-amide}.

Increasing the peripheral substituent to terpyridyl substituents allows the coordination of metal ions. For example, Kotova et al.<sup>[144]</sup> used  $\text{Eu}^{\text{III}}$  ions to prepare luminescent gels with a fibrous structure of a terpyridyl-containing BTA. The chemical structure is depicted in **Figure 1.3.8B**. Furthermore, Jung et al.<sup>[145]</sup> prepared gels of supramolecular fibers of the same terpyridyl-containing BTA with a defined helical order by adding chiral compounds allowing incorporation of gold nanoparticles in a defined manner in the hierarchical structure. For a deeper insight into the preparation of functional supramolecular nanofibers with various symmetrical and unsymmetrical substituted pyridine- and terpyridine-containing BTAs with different C- or N-centered amide connection it is referred to the recent investigations from our group.<sup>[146]</sup>

#### *Concluding remarks*

As shown in the examples from the literature, the self-assembly behavior in water for BTAs with functional groups can be triggered, for example, upon cooling, pH change and adding a co-solvent depending on the peripheral groups. Crucial for self-assembly are the process conditions. Already small deviations can lead to different self-assembly morphologies. Therefore, exact self-assembly protocols are necessary. Furthermore, as described above, already moderate structural variations have a significant impact on the self-assembly behavior and the resulting supramolecular structures. Therefore, considerations of the molecular design are very important.

The focus of this thesis is the investigation of BTAs with tertiary amino groups in der periphery. In literature, BTAs with positively charged tertiary amino groups were investigated regarding their affinity to selectively binds in grooves of DNA or RNA.<sup>[152]</sup> Furthermore, the BTA with positively charged tertiary *N,N*-dimethylamino groups in the presence of polyoxometalate trianion resulted in an insoluble inorganic-organic hybrid material.<sup>[153]</sup> Camerel et al.<sup>[154]</sup> described a BTA with an aromatic spacer between the core and the peripheral charged tertiary amino groups (with iodide counterions), which is able to form an organogel complexed with sodium n-hexadecyl sulfate or dihexadecyl phosphate. Robison et al.<sup>[155]</sup> synthesized different compounds resembling the structure of peptides and described, among others, a synthesis route for amino-containing BTAs and investigated the different compounds regarding the ability for enhanced calcium release from cardiac sarcoplasmic reticulum vesicles.

#### 1.4. Hierarchical superstructures composed of fibers

Polymer fibers of different lengths and diameters in the micro- or nanometer range can be prepared by conventional top-down methods. For example, typical well-established methods for polymer fiber preparation are melt blowing,<sup>[156–158]</sup> centrifugal spinning,<sup>[159–161]</sup> solution blow spinning,<sup>[162–167]</sup> and electrospinning.<sup>[168–171]</sup> Electrospinning allows the preparation of fibers, free-standing nonwovens, or fibers/nonwovens deposited on a support. A modified version of electrospinning, the coaxial electrospinning, allows the fabrication of complex fiber geometries by using dual instead of single nozzles.<sup>[172]</sup>

The combination of electrospun nanofibers with nanoparticles and the preparation of multilayer composites are beneficial to enhance the performance of electrospun fibers or nonwovens for different filtration applications for various pollutants or biomedical applications.<sup>[173–177]</sup> The multilayer approach leads to an increase in complexity and hierarchy and can be described in different ways. For example, the combination of electrospun poly(lactide acid) (PCL) nanofibers with porous PCL fibers showed an improved filtration performance due to the hierarchically structured composite and the pores on the fiber surface.<sup>[178]</sup> Another approach is the combination of different electrospun polymer fiber types and polymer fibers, which differ in the fiber diameter resulting in different hierarchical levels of pore size and packing density, leading to improved filtration properties.<sup>[179–181]</sup> In this context, Zhang et al.<sup>[180]</sup> prepared a nonwoven composed of three different electrospun layers of polysulfone (PSU) microfibers, polyacrylonitrile (PAN) nanofibers and polyamide-6 (PA-6) nanonets with controlled fiber diameters resulting in a gradually changing pore structure with improved filtration performance (**Figure 1.4.1**).

Composites with fibers with a small size in diameter combined with very small pore sizes are beneficial for high filtration efficiencies for fine particles. This can be realized by the electronetting technology. Electronetting is a combination of electrospinning with charged droplets leading to structures with a nanofiber network, described as nanonet.<sup>[182–185]</sup> The preparation of a nanonet of poly(*m*-phenylene isophthalamide) / polyurethane or polyacrylonitrile within a nonwoven fabric leads to highly efficient filters due to the small pore size.<sup>[183,184]</sup>

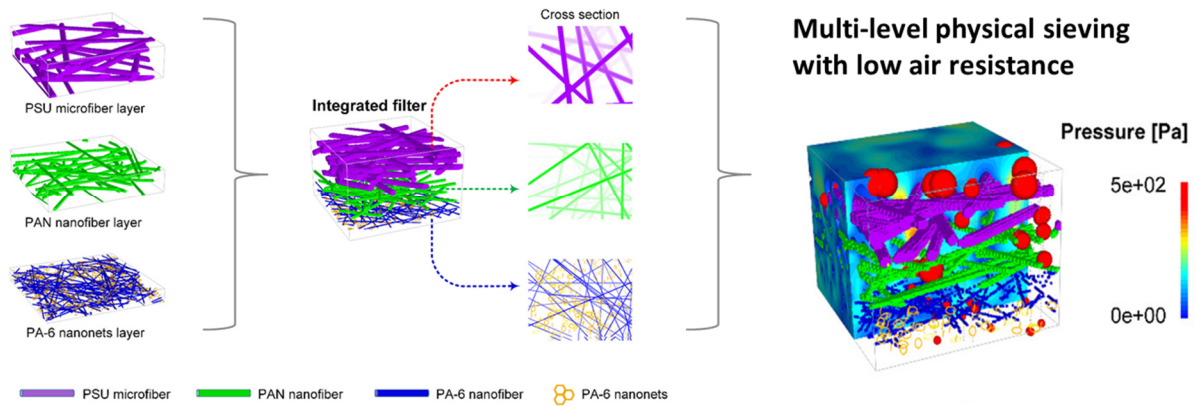


**Figure 1.4.1.** Schematic concept of an integrated multilayer filter composed of three electrospun polymer layers with different sizes in fiber diameter. The filter is composed of a polysulfone (PSU) microfiber layer, a polyacrylonitrile (PAN) nanofiber layer and a polyamide-6 (PA-6) nanonet layer. This filter allows multi-level physical sieving of particles with a low air resistance as simulated by particles of various sizes in each layer. Adapted with permission from Ref. <sup>[180]</sup>. © 2016 American Chemical Society.

The self-assembly of BTAs is an bottom-up approach and can be used to incorporate self-assembled nanofibers within nonwovens. This approach allows, for example, the in situ formation of supramolecular fibers within a nonwoven. In this context, Misslitz et al.<sup>[81]</sup> prepared a composite nonwoven consisting of a commercial polymer nonwoven based on polyester microfibers with supramolecular nanofibers of a BTA with branched alkyl groups in the periphery (**Figure 1.4.2**). For the preparation of the composite, the nonwoven was immersed in a molecularly dissolved supramolecular BTA solution at an elevated temperature. During the immersion, the nonwoven is soaked with the solvent and the BTA building blocks. Upon cooling and simultaneously solvent evaporation, the formation of supramolecular fibers within the nonwoven occurs.<sup>[81]</sup>



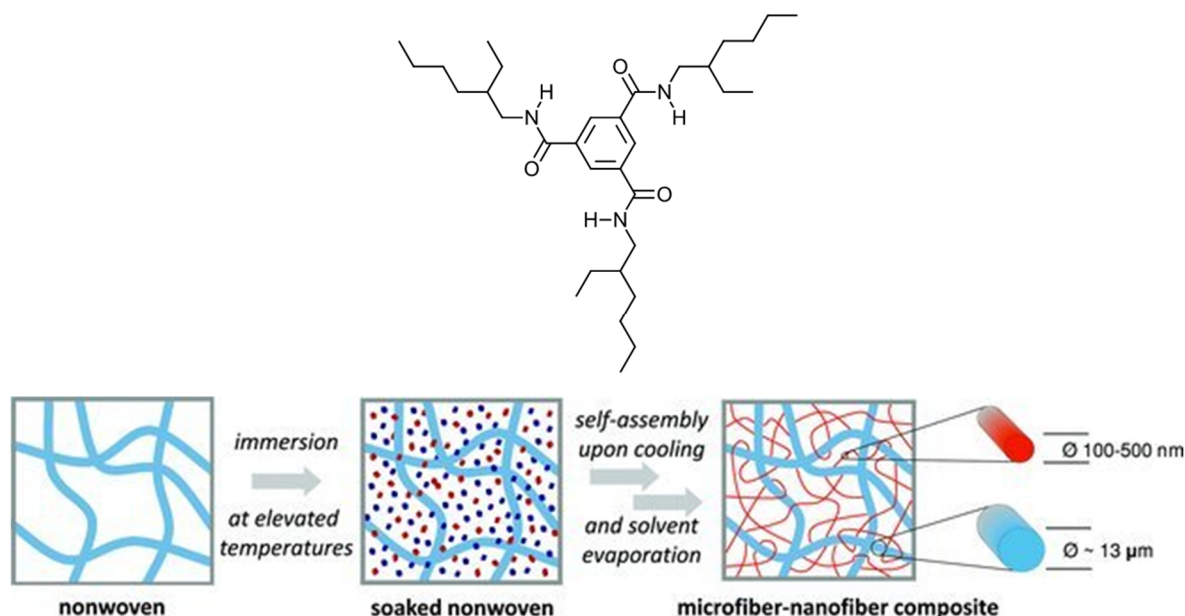


**Figure 1.4.2.** Chemical structure of *N,N,N'*-tris(2-ethylhexyl)-1,3,5-benzenetricarboxamide and the schematic illustration of the in situ preparation process of a microfiber-nanofiber composite composed of supramolecular BTA nanofibers (red fibers) within a nonwoven (blue fibers). For this, the nonwoven was immersed in a molecularly dissolved BTA solution (blue dots: solvent, red dots: molecular BTA units). Upon cooling and solvent evaporation, the microfiber-nanofiber composite was obtained. Reproduced with permission from Ref. <sup>[81]</sup> (© 2013 WILEY-VCH Verlag GmbH & Co. KGaA, Weinheim).

Weiss et al.<sup>[82]</sup> described the influence of the solvent on the resulting supramolecular fibers within a polymer-based nonwoven for two different BTAs with peripheral branched alkyl groups with different lengths (**Figure 1.4.3**). For this, the nonwoven based on viscose polyester was clamped into a holder and immersed in the molecularly dissolved BTA solution (**Figure 1.4.3A and B**). After drying, a microfiber/nanofiber composite composed of polymer microfibers and supramolecular BTA nanofibers is obtained (**Figure 1.4.3C**). Important requirements for the preparation of the microfiber/nanofiber composites are: i) a molecularly dissolved BTA solution allowing the immersion of the nonwoven, ii) the temperature of the solution and iii) the used solvent should not destroy or dissolve the polymer-based nonwoven. The resulting microfiber/nanofiber composites were tested for air filtration applications.<sup>[82]</sup>

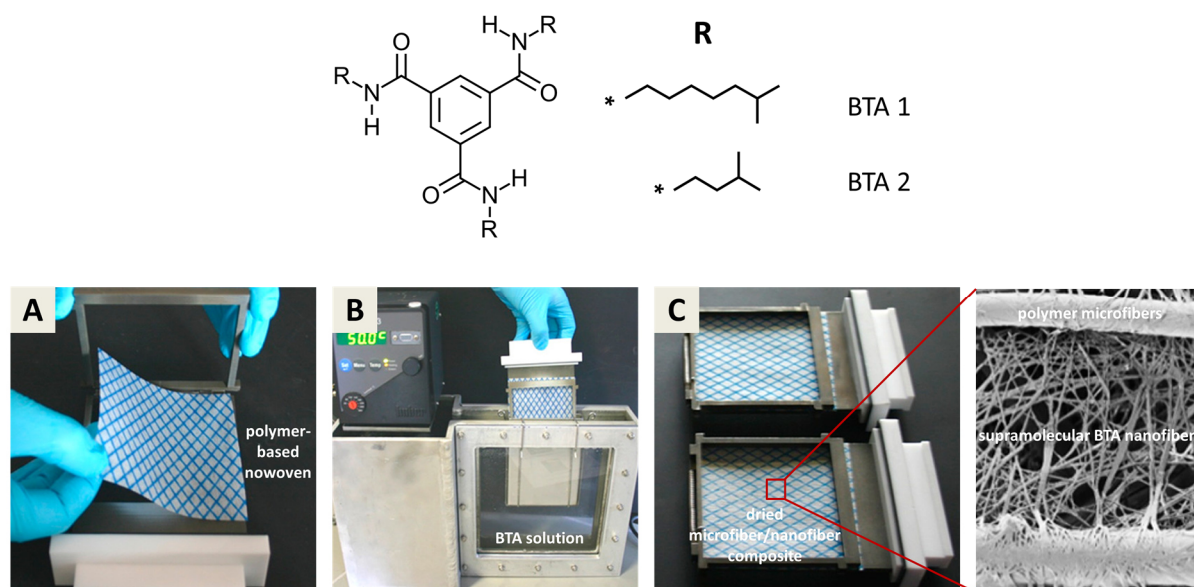


**Figure 1.4.3.** Chemical structures of *N,N,N'*-tris(6-methylheptyl)-1,3,5-benzenetricarboxamide (BTA 1) and *N,N,N'*-tris(3-methylbutyl)-1,3,5-benzenetricarboxamide (BTA 2). Preparation of microfiber/nanofiber composite based on the in situ self-assembly of BTA nanofibers within a polymer nonwoven upon simultaneous cooling and solvent evaporation. A) The polymer-based nonwoven is placed into a holder. B) The nonwoven is immersed in a molecularly dissolved BTA solution at 50 °C. C) After removing the nonwoven from the hot solution, the nonwoven is allowed to dry. Upon cooling and simultaneously solvent evaporation, the BTA self-assembles into supramolecular nanofibers within the nonwoven. Adapted with permission from Ref. [82]. © 2016 American Chemical Society.

The integration of self-assembled structures within a nonwoven was also realized by using other molecular building blocks. For example, a hierarchical dual-nanonet was prepared by the combination of polyacrylonitrile (PAN) nanofibers and sorbitol derivatives.<sup>[186,187]</sup> For this, Hu et al.<sup>[186]</sup> prepared PAN nanofiber nonwovens by solution blowing and immersed the prepared nonwovens into a hot sorbitol solution (DMDBS) (**Figure 1.4.4**). Upon cooling, the in situ self-assembly is initiated and after solvent evaporation, the hierarchical dual-nanonet was investigated by scanning electron microscopy. The resulting morphology of the DMDBS nanofibers is concentration dependent. A low concentration results in a fragile web. A certain concentration is necessary to achieve void free webs. Compared to the PAN nonwoven without DMDBS, the hierarchical dual-nanonet showed improved filtration efficiencies.<sup>[186]</sup> Further reported examples of creating self-assembled structures within or on top of nonwovens are based on cellulose<sup>[188]</sup> or perylene diimide derivative.<sup>[189]</sup>

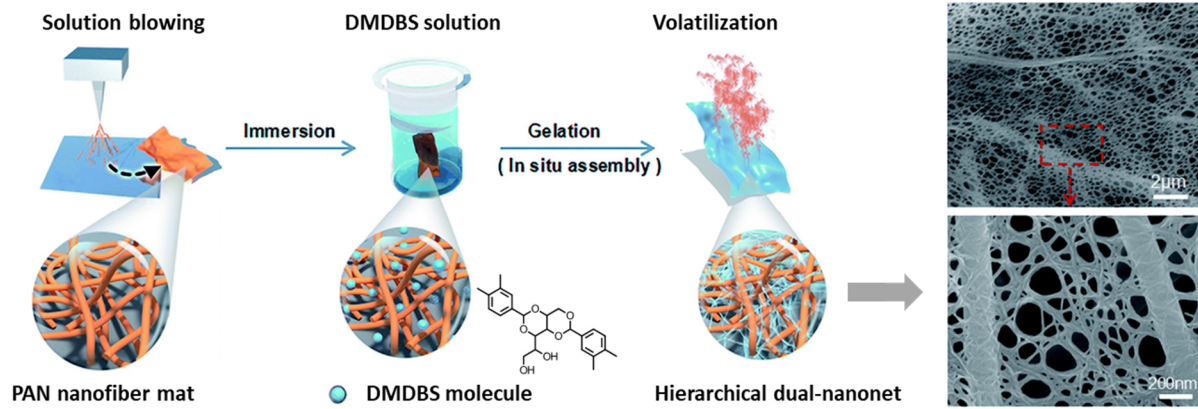


**Figure 1.4.4.** Schematic preparation of a hierarchical dual-nanonet composed of solution-blown polyacrylonitrile (PAN) nanofibers (yellow) and supramolecular 1,3:2,4-di(3,4-dimethylbenzylidene) sorbitol (DMBDS) nanofibrils (blue) after immersion, self-assembly and subsequent solvent evaporation. The resulting hierarchical dual-nanonet is shown by scanning electron micrographs at different magnifications. Reproduced from Ref. <sup>[186]</sup> with permission from the Royal Society of Chemistry (© 2021).

In the mentioned examples, the resulting morphologies arise from the combination of the various fiber types and supramolecular motifs. A defined morphology can enhance the property profile. For example, Burgard et al.<sup>[190]</sup> prepared mesostructured nonwovens by combining electrospinning of polymer fibers with the self-assembly of a BTA with alkoxy peripheral groups (**Figure 1.4.5**). The prepared nonwovens feature a special structure of electrospun polymer fibers with off-standing supramolecular fibers, resembling a penguin downy feather-like morphology.<sup>[190]</sup> To achieve the defined structure, BTA seeds were deposited on supporting polystyrene (PS) fibers by coaxial electrospinning followed by the in situ self-assembly of BTA fibers. Here, the electrospun polymer fibers comprise the middle strand with off-standing fibers composed of supramolecular BTA nanofibers of the mesostructured nonwoven. This morphology was shown to be efficient in the removal of particles in air filtration with a low pressure drop.<sup>[190]</sup>

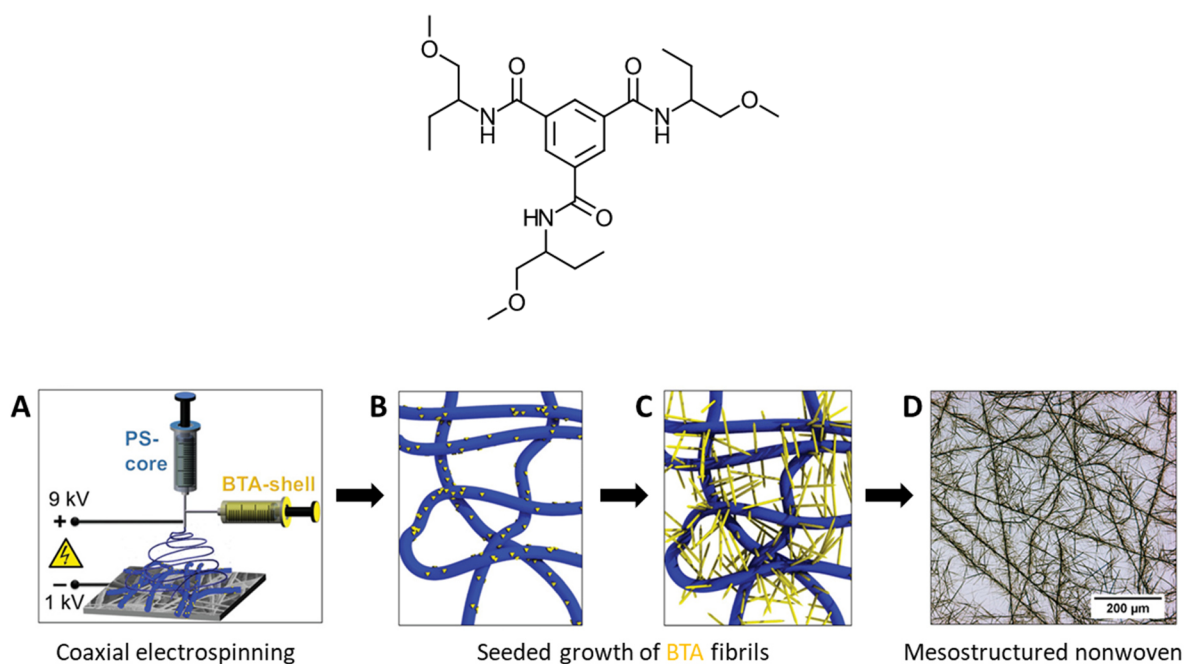


**Figure 1.4.5.** Chemical structure of *N,N',N''*-tris(1-(methoxymethyl)propyl)benzene-1,3,5-tricarboxamide. Schematic illustration to prepare mesostructured nonwovens with a special morphology. A) Coaxial electrospinning of polystyrene (PS) fibers (colored in blue) with BTA seeds (colored in yellow). B) Resulting BTA seeds on top of the PS fibers. C) Mesostructured nonwoven composed of polymer and supramolecular BTA fibers after seeded growth of the BTA fibers. D) The corresponding optical micrograph of the mesostructured nonwoven. Adapted and reproduced with permission from Ref. <sup>[190]</sup> (© 2019 WILEY-VCH Verlag GmbH & Co. KGaA, Weinheim).

Using a BTA with peripheral functional groups can add functionality leading to an increase in hierarchical level and complexity. Recently, Drummer et al.<sup>[147]</sup> prepared a functional mesoscale nonwoven with a wet-laid<sup>[191]</sup> procedure using a mixture of short electrospun polyacrylonitrile (PAN) fibers and a functional terpyridine-based BTA as a supramolecular motif (**Figure 1.4.6**).<sup>[147]</sup> These functional nonwovens are capable of immobilizing gold nanoparticles (AuNPs) without agglomeration. The functionality was demonstrated by the catalytic reduction of 4-nitrophenol to 4-aminophenol.<sup>[147]</sup>

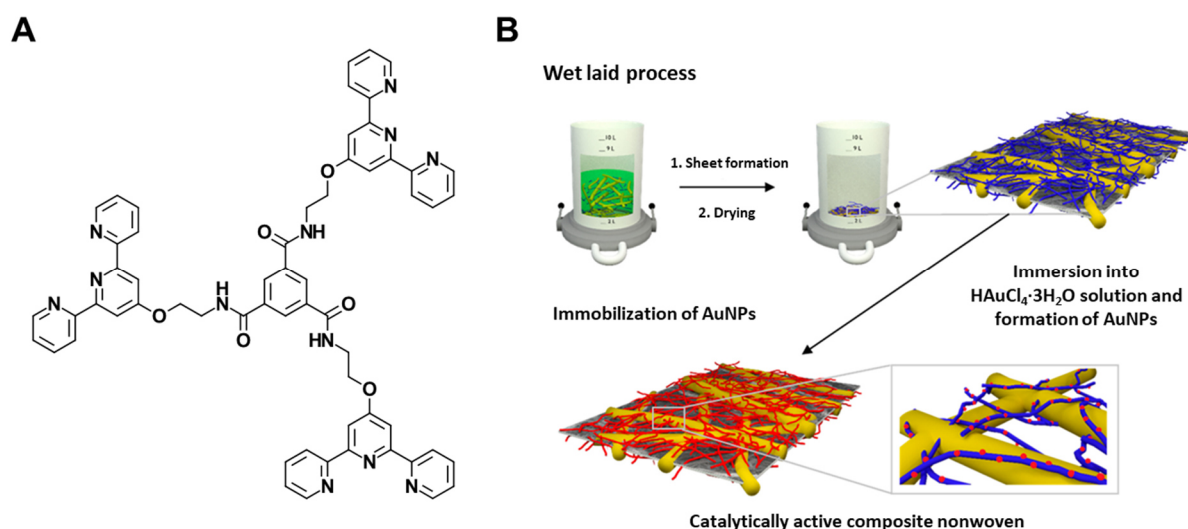


**Figure 1.4.6.** A) Chemical structure of  $N^1, N^3, N^5$ -tris(2-([2,2':6',2''-terpyridin]-4'-yloxy)ethyl)benzene-1,3,5-tricarboxamide. B) Schematic representation to prepare catalytically active composite nonwoven. Short electrospun polyacrylonitrile (PAN) fibers (yellow fibers) were mixed with a functional terpyridine-based BTA as supramolecular motif (blue nanofibers) and prepared with the wet-laid process. After immersion into a  $\text{HAuCl}_4 \cdot 3\text{H}_2\text{O}$  solution and formation of AuNPs (red dots), a stable catalytically active composite nonwoven is observed. Adapted with permission from Ref. <sup>[147]</sup>. © 2021 American Chemical Society.

The preparation of hierarchical structures in combination with peripheral functional groups increases the application possibilities. However, the use of functional groups in the periphery of BTAs is challenging in terms of a controlled self-assembly process. Since small deviations in the self-assembly conditions for BTAs with hydrophilic groups could result in different morphologies. Furthermore, the preparation of defined and the same time, complex hierarchical structures can be promising for superior applications. The investigation of a completely new class of BTAs with functional groups and the preparation of hierarchical superstructures is challenging.



## 1.5. References

- [1] C. Yuan, W. Ji, R. Xing, J. Li, E. Gazit, X. Yan. *Hierarchically oriented organization in supramolecular peptide crystals*, Nat. Rev. Chem. **2019**, 3, 567–588.
- [2] J.-M. Lehn. *Supramolecular Chemistry-Scope and Perspectives Molecules, Supermolecules, and Molecular Devices (Nobel Lecture)*, Angew. Chem. Int. Ed. Engl. **1988**, 27, 89–112.
- [3] J. W. Steed, J. L. Atwood. *Supramolecular chemistry*, Wiley, Chichester, UK **2009**.
- [4] G. M. Whitesides, J. P. Mathias, C. T. Seto. *Molecular Self-Assembly and Nanochemistry: A Chemical Strategy for the Synthesis of Nanostructures*, Science **1991**, 254, 1312–1319.
- [5] D. B. Varshey, J. R. G. Sander, T. Friščić, L. R. MacGillivray, in *Supramolecular Chemistry: From Molecules to Nanomaterials* (Eds.: J. W. Steed, P. A. Gale), Wiley. Hoboken, NJ **2012**.
- [6] Y.-R. Luo. *Comprehensive Handbook of Chemical Bond Energies*, CRC Press, Boca Raton, FL **2007**.
- [7] A. C. Mendes, E. T. Baran, R. L. Reis, H. S. Azevedo. *Self-assembly in nature: using the principles of nature to create complex nanobiomaterials*, WIREs Nanomed. Nanobiotechnol. **2013**, 5, 582–612.
- [8] V. Palermo, P. Samorì. *Molecular Self-Assembly across Multiple Length Scales*, Angew. Chem. Int. Ed. **2007**, 46, 4428–4432.
- [9] S. Krause. *Dilute Solution Properties of a Styrene-Methyl Methacrylate Block Copolymer*, J. Phys. Chem. **1964**, 68, 1948–1955.
- [10] S. Newman. *Note on Colloidal Dispersions from Block Copolymers*, J. Appl. Polym. Sci. **1962**, 6, 15–16.
- [11] F. H. Schacher, P. A. Rugar, I. Manners. *Functional Block Copolymers: Nanostructured Materials with Emerging Applications*, Angew. Chem. Int. Ed. **2012**, 51, 7898–7921.
- [12] U. Tritschler, S. Pearce, J. Gwyther, G. R. Whittell, I. Manners. *50th Anniversary Perspective: Functional Nanoparticles from the Solution Self-Assembly of Block Copolymers*, Macromolecules **2017**, 50, 3439–3463.
- [13] J. Massey, K. N. Power, I. Manners, M. A. Winnik. *Self-Assembly of a Novel Organometallic-Inorganic Block Copolymer in Solution and the Solid State: Nonintrusive Observation of Novel Wormlike Poly(ferrocenyldimethylsilane)-b-Poly(dimethylsiloxane) Micelles*, J. Am. Chem. Soc. **1998**, 120, 9533–9540.



- [14] J. A. Massey, K. Temple, L. Cao, Y. Rharbi, J. Raez, M. A. Winnik, I. Manners. *Self-Assembly of Organometallic Block Copolymers: The Role of Crystallinity of the Core-Forming Polyferrocene Block in the Micellar Morphologies Formed by Poly(ferrocenyldimethylsilane-*b*-dimethylsiloxane) in *n*-Alkane Solvents*, *J. Am. Chem. Soc.* **2000**, 122, 11577–11584.
- [15] J. B. Gilroy, T. Gädt, G. R. Whittell, L. Chabanne, J. M. Mitchels, R. M. Richardson, M. A. Winnik, I. Manners. *Monodisperse cylindrical micelles by crystallization-driven living self-assembly*, *Nat. Chem.* **2010**, 2, 566–570.
- [16] R. L. N. Hailes, A. M. Oliver, J. Gwyther, G. R. Whittell, I. Manners. *Polyferrocenyldimethylsilanes: synthesis, properties, and applications*, *Chem. Soc. Rev.* **2016**, 45, 5358–5407.
- [17] L. MacFarlane, C. Zhao, J. Cai, H. Qiu, I. Manners. *Emerging applications for living crystallization-driven self-assembly*, *Chem. Sci.* **2021**, 12, 4661–4682.
- [18] H. Qiu, Y. Gao, C. E. Boott, O. E. C. Gould, R. L. Harniman, M. J. Miles, S. E. D. Webb, M. A. Winnik, I. Manners. *Uniform patchy and hollow rectangular platelet micelles from crystallizable polymer blends*, *Science* **2016**, 352, 697–701.
- [19] A. Nazemi, X. He, L. R. MacFarlane, R. L. Harniman, M.-S. Hsiao, M. A. Winnik, C. F. J. Faul, I. Manners. *Uniform "Patchy" Platelets by Seeded Heteroepitaxial Growth of Crystallizable Polymer Blends in Two Dimensions*, *J. Am. Chem. Soc.* **2017**, 139, 4409–4417.
- [20] X. He, M.-S. Hsiao, C. E. Boott, R. L. Harniman, A. Nazemi, X. Li, M. A. Winnik, I. Manners. *Two-dimensional assemblies from crystallizable homopolymers with charged termini*, *Nat. Mater.* **2017**, 16, 481–489.
- [21] S. Pearce, X. He, M.-S. Hsiao, R. L. Harniman, L. R. MacFarlane, I. Manners. *Uniform, High-Aspect-Ratio, and Patchy 2D Platelets by Living Crystallization-Driven Self-Assembly of Crystallizable Poly(ferrocenyldimethylsilane)-Based Homopolymers with Hydrophilic Charged Termini*, *Macromolecules* **2019**, 52, 6068–6079.
- [22] H. Qiu, V. A. Du, M. A. Winnik, I. Manners. *Branched Cylindrical Micelles via Crystallization-Driven Self-Assembly*, *J. Am. Chem. Soc.* **2013**, 135, 17739–17742.
- [23] H. Qiu, Y. Gao, V. A. Du, R. Harniman, M. A. Winnik, I. Manners. *Branched Micelles by Living Crystallization-Driven Block Copolymer Self-Assembly under Kinetic Control*, *J. Am. Chem. Soc.* **2015**, 137, 2375–2385.



- [24] Y. Gao, H. Qiu, H. Zhou, X. Li, R. Harniman, M. A. Winnik, I. Manners. *Crystallization-Driven Solution Self-Assembly of Block Copolymers with a Photocleavable Junction*, J. Am. Chem. Soc. **2015**, 137, 2203–2206.
- [25] P. A. Rugar, L. Chabanne, M. A. Winnik, I. Manner. *Non-Centrosymmetric Cylindrical Micelles by Unidirectional Growth*, Science **2012**, 337, 559–562.
- [26] X. Li, Y. Gao, C. E. Boott, M. A. Winnik, I. Manners. *Non-covalent synthesis of supermicelles with complex architectures using spatially confined hydrogen-bonding interactions*, Nat. Commun. **2015**, 6, 8127, 1-8.
- [27] X. Li, Y. Gao, C. E. Boott, D. W. Hayward, R. Harniman, G. R. Whittell, R. M. Richardson, M. A. Winnik, I. Manners. *"Cross" Supermicelles via the Hierarchical Assembly of Amphiphilic Cylindrical Triblock Comicelles*, J. Am. Chem. Soc. **2016**, 138, 4087–4095.
- [28] A. M. Oliver, R. J. Spontak, I. Manners. *Solution self-assembly of ABC triblock terpolymers with a central crystallizable poly(ferrocenyldimethylsilane) core-forming segment*, Polym. Chem. **2019**, 10, 2559–2569.
- [29] J. Xu, H. Zhou, Q. Yu, G. Guerin, I. Manners, M. A. Winnik. *Synergistic self-seeding in one-dimension: a route to patchy and block comicelles with uniform and controllable length*, Chem. Sci. **2019**, 10, 2280–2284.
- [30] J. Du, R. K. O'Reilly. *Anisotropic particles with patchy, multicompartiment and Janus architectures: preparation and application*, Chem. Soc. Rev. **2011**, 40, 2402–2416.
- [31] X. Li, P. J. Wolanin, L. R. MacFarlane, R. L. Harniman, J. Qian, O. E. C. Gould, T. G. Dane, J. Rudin, M. J. Cryan, T. Schmaltz, H. Frauenrath, M. A. Winnik, C. F. J. Faul, I. Manners. *Uniform electroactive fibre-like micelle nanowires for organic electronics*, Nat. Commun. **2017**, 8, 15909, 1-8.
- [32] M. C. Arno, M. Inam, Z. Coe, G. Cambridge, L. J. Macdougall, R. Keogh, A. P. Dove, R. K. O'Reilly. *Precision Epitaxy for Aqueous 1D and 2D Poly( $\epsilon$ -caprolactone) Assemblies*, J. Am. Chem. Soc. **2017**, 139, 16980–16985.
- [33] W. Yu, J. C. Foster, A. P. Dove, R. K. O'Reilly. *Length Control of Biodegradable Fiber-Like Micelles via Tuning Solubility: A Self-Seeding Crystallization-Driven Self-Assembly of Poly( $\epsilon$ -caprolactone)-Containing Triblock Copolymers*, Macromolecules **2020**, 53, 1514–1521.

- [34] G. Rizis, T. G. M. van de Ven, A. Eisenberg. *Crystallinity-driven morphological ripening processes for poly(ethylene oxide)-block-polycaprolactone micelles in water*, *Soft Matter* **2014**, 10, 2825–2835.
- [35] W. Yu, M. Inam, J. R. Jones, A. P. Dove, R. K. O'Reilly. *Understanding the CDSA of poly(lactide) containing triblock copolymers*, *Polym. Chem.* **2017**, 8, 5504–5512.
- [36] M. Inam, G. Cambridge, A. Pitto-Barry, Z. P. L. Laker, N. R. Wilson, R. T. Mathers, A. P. Dove, R. K. O'Reilly. *1D vs. 2D shape selectivity in the crystallization-driven self-assembly of polylactide block copolymers*, *Chem. Sci.* **2017**, 8, 4223–4230.
- [37] J. R. Finnegan, X. He, S. T. G. Street, J. D. Garcia-Hernandez, D. W. Hayward, R. L. Harniman, R. M. Richardson, G. R. Whittell, I. Manners. *Extending the Scope of “Living” Crystallization-Driven Self-Assembly: Well-Defined 1D Micelles and Block Comicelles from Crystallizable Polycarbonate Block Copolymers*, *J. Am. Chem. Soc.* **2018**, 140, 17127–17140.
- [38] J. Schmelz, M. Karg, T. Hellweg, H. Schmalz. *General Pathway toward Crystalline-Core Micelles with Tunable Morphology and Corona Segregation*, *ACS Nano* **2011**, 5, 9523–9534.
- [39] B. Fan, L. Liu, J.-H. Li, X.-X. Ke, J.-T. Xu, B.-Y. Du, Z.-Q. Fan. *Crystallization-driven one-dimensional self-assembly of polyethylene-*b*-poly(tert-butylacrylate) diblock copolymers in DMF: effects of crystallization temperature and the corona-forming block*, *Soft Matter* **2016**, 12, 67–76.
- [40] H. Schmalz, J. Schmelz, M. Drechsler, J. Yuan, A. Walther, K. Schweimer, A. M. Mihut. *Thermo-Reversible Formation of Wormlike Micelles with a Microphase-Separated Corona from a Semicrystalline Triblock Terpolymer*, *Macromolecules* **2008**, 41, 3235–3242.
- [41] S. Xu, C. Zhang, L. Li, S. Zheng. *Polystyrene-block-polyethylene-block-polystyrene triblock copolymers: Synthesis and crystallization-driven self-assembly behavior*, *Polymer* **2017**, 128, 1–11.
- [42] J. Schmelz, A. E. Schedl, C. Steinlein, I. Manners, H. Schmalz. *Length Control and Block-Type Architectures in Worm-like Micelles with Polyethylene Cores*, *J. Am. Chem. Soc.* **2012**, 134, 14217–14225.

- [43] C. Hils, J. Schmelz, M. Drechsler, H. Schmalz. *Janus Micelles by Crystallization-Driven Self-Assembly of an Amphiphilic, Double-Crystalline Triblock Terpolymer*, *J. Am. Chem. Soc.* **2021**, 143, 15582–15586.
- [44] J. Schmelz, D. Pirner, M. Krekhova, T. M. Ruhland, H. Schmalz. *Interfacial activity of patchy worm-like micelles*, *Soft Matter* **2013**, 9, 11173–11177.
- [45] J. Schöbel, M. Karg, D. Rosenbach, G. Krauss, A. Greiner, H. Schmalz. *Patchy Wormlike Micelles with Tailored Functionality by Crystallization-Driven Self-Assembly: A Versatile Platform for Mesostuctured Hybrid Materials*, *Macromolecules* **2016**, 49, 2761–2771.
- [46] J. Schöbel, C. Hils, A. Weckwerth, M. Schlenk, C. Bojer, M. C. A. Stuart, J. Breu, S. Förster, A. Greiner, M. Karg, S. Holger. *Strategies for the selective loading of patchy worm-like micelles with functional nanoparticles*, *Nanoscale* **2018**, 10, 18257–18268.
- [47] S. Cantekin, T. F. A. de Greef, A. R. A. Palmans. *Benzene-1,3,5-tricarboxamide: a versatile ordering moiety for supramolecular chemistry*, *Chem. Soc. Rev.* **2012**, 41, 6125–6137.
- [48] E. Fan, J. Yang, S. J. Geib, T. C. Stoner, M. D. Hopkins, A. D. Hamilton. *Hydrogen-bonding Control of Molecular Aggregation: Self-complementary Subunits lead to Rod-shaped Structures in the Solid State*, *J. Chem. Soc., Chem. Commun.* **1995**, 12, 1251–1252.
- [49] K. Hanabusa, A. Kawakami, M. Kimura, H. Shirai. *Small Molecular Gelling Agents to Harden Organic Liquids: Trialkyl cis-1,3,5-Cyclohexanetricarboxamides*, *Chem. Lett.* **1997**, 26, 191–192.
- [50] K. J. C. van Bommel, C. van der Pol, I. Muizebelt, A. Friggeri, A. Heeres, A. Meetsma, B. L. Feringa, J. van Esch. *Responsive Cyclohexane-Based Low-Molecular-Weight Hydrogelators with Modular Architecture*, *Angew. Chem. Int. Ed.* **2004**, 43, 1663–1667.
- [51] I. Tomatsu, C. F. C. Fitié, D. Byelov, W. H. de Jeu, P. C. M. M. Magusin, M. Wübbenhorst, R. P. Sijbesma. *Thermotropic Phase Behavior of Trialkyl Cyclohexanetriamides*, *J. Phys. Chem. B* **2009**, 113, 14158–14164.
- [52] R. Q. Albuquerque, A. Timme, R. Kress, J. Senker, H.-W. Schmidt. *Theoretical Investigation of Macrodipoles in Supramolecular Columnar Stackings*, *Chem. Eur. J.* **2013**, 19, 1647–1657.
- [53] M. de Loos, J. H. van Esch, R. M. Kellogg, B. L. Feringa. *C<sub>3</sub>-Symmetric, amino acid based organogelators and thickeners: a systematic study of structure–property relations*, *Tetrahedron* **2007**, 63, 7285–7301.

- [54] K. Hanabusa, C. Koto, M. Kimura, H. Shirai, A. Kakehi. *Remarkable Viscoelasticity of Organic Solvents Containing Trialkyl-1,3,5-benzenetricarboxamides and Their Intermolecular Hydrogen Bonding*, Chem. Lett. **1997**, 26, 429–430.
- [55] M. P. Lightfoot, F. S. Mair, R. G. Pritchard, J. E. Warren. *New supramolecular packing motifs:  $\pi$ -stacked rods encased in triply-helical hydrogen bonded amide strands*, Chem. Commun. **1999**, 19, 1945–1946.
- [56] M. Blomenhofer, S. Ganzleben, D. Hanft, H.-W. Schmidt, M. Kristiansen, P. Smith, K. Stoll, D. Mäder, K. Hoffmann. *“Designer” Nucleating Agents for Polypropylene*, Macromolecules **2005**, 38, 3688–3695.
- [57] D. Kluge, F. Abraham, S. Schmidt, H.-W. Schmidt, A. Fery. *Nanomechanical Properties of Supramolecular Self-Assembled Whiskers Determined by AFM Force Mapping*, Langmuir **2010**, 26, 3020–3023.
- [58] M. Wegner, D. Dudenko, D. Sebastiani, A. R. A. Palmans, T. F. A. de Greef, R. Graf, H. W. Spiess. *The impact of the amide connectivity on the assembly and dynamics of benzene-1,3,5-tricarboxamides in the solid state*, Chem. Sci. **2011**, 2, 2040–2049.
- [59] D. Kluge, J. C. Singer, J. W. Neubauer, F. Abraham, H.-W. Schmidt, A. Fery. *Influence of the Molecular Structure and Morphology of Self-Assembled 1,3,5-Benzenetrisamide Nanofibers on their Mechanical Properties*, Small **2012**, 8, 2563–2570.
- [60] S. M. C. Schoenmakers, B. W. L. van den Berselaar, S. Dhiman, L. Su, A. R. A. Palmans. *Facilitating functionalization of benzene-1,3,5-tricarboxamides by switching amide connectivity*, Org. Biomol. Chem. **2021**, 19, 8281–8294.
- [61] L. N. J. de Windt, Z. Fernández, M. Fernández-Míguez, F. Freire, A. R. A. Palmans. *Elucidating the Supramolecular Copolymerization of N- and C-Centered Benzene-1,3,5-Tricarboxamides: The Role of Parallel and Antiparallel Packing of Amide Groups in the Copolymer Microstructure*, Chem. Eur. J. **2022**, 28, e202103691, 1-12.
- [62] F. Abraham, S. Ganzleben, D. Hanft, P. Smith, H.-W. Schmidt. *Synthesis and Structure-Efficiency Relations of 1,3,5-Benzenetrisamides as Nucleating Agents and Clarifiers for Isotactic Poly(propylene)*, Macromol. Chem. Phys. **2010**, 211, 171–181.
- [63] F. Abraham, H.-W. Schmidt. *1,3,5-Benzenetrisamide based nucleating agents for poly(vinylidene fluoride)*, Polymer **2010**, 51, 913–921.

- [64] F. Richter, H.-W. Schmidt. *Supramolecular Nucleating Agents for Poly(butylene terephthalate) Based on 1,3,5-Benzenetrisamides*, *Macromol. Mater. Eng.* **2013**, 298, 190–200.
- [65] P. J. M. Stals, J. C. Everts, R. de Bruijn, I. A. W. Filot, M. M. J. Smulders, R. Martín-Rapún, E. A. Pidko, T. F. A. de Greef, A. R. A. Palmans, E. W. Meijer. *Dynamic Supramolecular Polymers Based on Benzene-1,3,5-tricarboxamides: The Influence of Amide Connectivity on Aggregate Stability and Amplification of Chirality*, *Chem. Eur. J.* **2010**, 16, 810–821.
- [66] S. Kumar, S. Bera, S. K. Nandi, D. Haldar. *The effect of amide bond orientation and symmetry on the self-assembly and gelation of discotic tripeptides*, *Soft Matter* **2021**, 17, 113–119.
- [67] C. S. Zehe, J. A. Hill, N. P. Funnell, K. Kreger, K. P. van der Zwan, A. L. Goodwin, H.-W. Schmidt, J. Senker. *Mesoscale Polarization by Geometric Frustration in Columnar Supramolecular Crystals*, *Angew. Chem. Int. Ed.* **2017**, 56, 4432–4437.
- [68] A. Sakamoto, D. Ogata, T. Shikata, O. Urakawa, K. Hanabusa. *Large macro-dipoles generated in a supramolecular polymer of N,N',N''-tris(3,7-dimethyloctyl)benzene-1,3,5-tricarboxamide in n-decane*, *Polymer* **2006**, 47, 956–960.
- [69] C. F. C. Fitié, W. S. C. Roelofs, P. C. M. M. Magusin, M. Wübbenhorst, M. Kemerink, R. P. Sijbesma. *Polar Switching in Trialkylbenzene-1,3,5-tricarboxamides*, *J. Phys. Chem. B* **2012**, 116, 3928–3937.
- [70] I. Urbanaviciute, X. Meng, T. D. Cornelissen, A. V. Gorbunov, S. Bhattacharjee, R. P. Sijbesma, M. Kemerink. *Tuning the Ferroelectric Properties of Trialkylbenzene-1,3,5-tricarboxamide (BTA)*, *Adv. Electron. Mater.* **2017**, 3, 1600530, 1–7.
- [71] I. Urbanaviciute, S. Bhattacharjee, M. Biler, J. A. M. Lugger, T. D. Cornelissen, P. Norman, M. Linares, R. P. Sijbesma, M. Kemerink. *Suppressing depolarization by tail substitution in an organic supramolecular ferroelectric*, *Phys. Chem. Chem. Phys.* **2019**, 21, 2069–2079.
- [72] I. Urbanaviciute, X. Meng, M. Biler, Y. Wei, T. D. Cornelissen, S. Bhattacharjee, M. Linares, M. Kemerink. *Negative piezoelectric effect in an organic supramolecular ferroelectric*, *Mater. Horiz.* **2019**, 6, 1688–1698.
- [73] C. Zehe, M. Schmidt, R. Siegel, K. Kreger, V. Daebel, S. Ganzleben, H.-W. Schmidt, J. Senker. *Influence of fluorine side-group substitution on the crystal structure formation of benzene-1,3,5-trisamides*, *CrystEngComm* **2014**, 16, 9273–9283.

- [74] N. Mohmeyer, N. Behrendt, X. Zhang, P. Smith, V. Altstädt, G. M. Sessler, H.-W. Schmidt. *Additives to improve the electret properties of isotactic polypropylene*, *Polymer* **2007**, 48, 1612–1619.
- [75] D. Weiss, K. Kreger, H.-W. Schmidt. *Self-Assembly of Alkoxy-Substituted 1,3,5-Benzenetricarboxamides Under Controlled Conditions*, *Macromol. Mater. Eng.* **2017**, 302, 1600390, 1-8.
- [76] J. J. van Gorp, J. A. J. M. Vekemans, E. W. Meijer. *C<sub>3</sub>-Symmetrical Supramolecular Architectures: Fibers and Organic Gels from Discotic Trisamides and Trisureas*, *J. Am. Chem. Soc.* **2002**, 124, 14759–14769.
- [77] Y. Yasuda, E. Iishi, H. Inada, Y. Shirota. *Novel Low-molecular-weight Organic Gels: N,N',N''-Tristearyltrimesamide/Organic Solvent System*, *Chem. Lett.* **1996**, 25, 575–576.
- [78] A. Paikar, A. Pramanik, D. Haldar. *Influence of side-chain interactions on the self-assembly of discotic tricarboxyamides: a crystallographic insight*, *RSC Adv.* **2015**, 5, 31845–31851.
- [79] S. J. Lee, C. R. Park, J. Y. Chang. *Molecular Aggregation of Disklike Benzenetricarboxamides Containing Diacetylenic Groups in Bulk and Organic Solvents*, *Langmuir* **2004**, 20, 9513–9519.
- [80] S. Y. Ryu, S. Kim, J. Seo, Y.-W. Kim, O.-H. Kwon, D.-J. Jang, S. Y. Park. *Strong fluorescence emission induced by supramolecular assembly and gelation: luminescent organogel from nonemissive oxadiazole-based benzene-1,3,5-tricarboxamide gelator*, *Chem. Commun.* **2004**, 1, 70–71.
- [81] H. Misslitz, K. Kreger, H.-W. Schmidt. *Supramolecular Nanofiber Webs in Nonwoven Scaffolds as Potential Filter Media*, *Small* **2013**, 9, 2053-2058.
- [82] D. Weiss, D. Skrybeck, H. Misslitz, D. Nardini, A. Kern, K. Kreger, H.-W. Schmidt. *Tailoring Supramolecular Nanofibers for Air Filtration Applications*, *ACS Appl. Mater. Interfaces* **2016**, 8, 14885–14892.
- [83] H. Cao, P. Duan, X. Zhu, J. Jiang, M. Liu. *Self-Assembled Organic Nanotubes through Instant Gelation and Universal Capacity for Guest Molecule Encapsulation*, *Chem. Eur. J.* **2012**, 18, 5546–5550.
- [84] V. Nagarajan, V. R. Pedireddi. *Gelation and Structural Transformation Study of Some 1,3,5-Benzenetricarboxamide Derivatives*, *Cryst. Growth Des.* **2014**, 14, 1895–1901.

- [85] Y. Matsunaga, Y. Nakayasu, S. Sakai, M. Yonenaga. *Liquid Crystal Phases Exhibited by N,N',N''-Trialkyl-1,3,5-Benzenetricarboxamides*, Mol. Cryst. Liq. Cryst. **1986**, 141, 327–333.
- [86] Y. Matsunaga, N. Miyajima, Y. Nakayasu, S. Sakai, M. Yonenaga. *Design of Novel Mesomorphic Compounds: N,N',N''-Trialkyl-1,3,5-benzenetricarboxamides*, Bull. Chem. Soc. Jpn. **1988**, 61, 207–210.
- [87] A. Timme, R. Kress, R. Q. Albuquerque, H.-W. Schmidt. *Phase Behavior and Mesophase Structures of 1,3,5-Benzene- and 1,3,5-Cyclohexanetricarboxamides: Towards an Understanding of the Losing Order at the Transition into the Isotropic Phase*, Chem. Eur. J. **2012**, 18, 8329–8339.
- [88] P. J. M. Stals, M. M. J. Smulders, R. Martín-Rapún, A. R. A. Palmans, E. W. Meijer. *Asymmetrically Substituted Benzene-1,3,5-tricarboxamides: Self-Assembly and Odd-Even Effects in the Solid State and in Dilute Solution*, Chem. Eur. J. **2009**, 15, 2071–2080.
- [89] M. Kristiansen, P. Smith, H. Chanzy, C. Baerlocher, V. Gramlich, L. McCusker, T. Weber, P. Pattison, M. Blomenhofer, H.-W. Schmidt. *Structural Aspects of 1,3,5-Benzenetrisamides—A New Family of Nucleating Agents*, Cryst. Growth Des. **2009**, 9, 2556–2558.
- [90] P. M. Kristiansen, A. Gress, P. Smith, D. Hanft, H.-W. Schmidt. *Phase behavior, nucleation and optical properties of the binary system isotactic polypropylene/N,N',N''-tris-isopentyl-1,3,5-benzene-tricarboxamide*, Polymer **2006**, 47, 249–253.
- [91] M. Kersch, L. Pischke, H.-W. Schmidt, V. Altstädt. *Influence of trisamide-based additives on the morphological and mechanical properties of isotactic polypropylene*, Polymer **2014**, 55, 3227–3233.
- [92] Y.-H. Cai, Y. Tang, L.-S. Zhao. *Poly(L-lactic acid) with the organic nucleating agent N,N,N'-tris(1H-benzotriazole) trimesinic acid acethydrazide: Crystallization and melting behavior*, J. Appl. Polym. Sci. **2015**, 132, 42402, 1–7.
- [93] X. Zhang, L. Meng, G. Li, N. Liang, J. Zhang, Z. Zhu, R. Wang. *Effect of nucleating agents on the crystallization behavior and heat resistance of poly(L-lactide)*, J. Appl. Polym. Sci. **2016**, 133, 42999, 1–7.
- [94] T. Wang, Y. Yang, C. Zhang, Z. Tang, H. Na, J. Zhu. *Effect of 1,3,5-Trialkyl-Benzenetricarboxylamide on the Crystallization of Poly(lactic acid)*, J. Appl. Polym. Sci. **2013**, 130, 1328–1336.

- [95] H. Bai, W. Zhang, H. Deng, Q. Zhang, Q. Fu. *Control of Crystal Morphology in Poly(L-lactide) by Adding Nucleating Agent*, *Macromolecules* **2011**, 44, 1233–1237.
- [96] H. Nakajima, M. Takahashi, Y. Kimura. *Induced Crystallization of PLLA in the Presence of 1,3,5-Benzenetricarboxylamide Derivatives as Nucleators: Preparation of Haze-Free Crystalline PLLA Materials*, *Macromol. Mater. Eng.* **2010**, 295, 460–468.
- [97] M. Stumpf, A. Spörrer, H.-W. Schmidt, V. Altstädt. *Influence of supramolecular additives on foam morphology of injection-molded i-PP*, *J. Cell. Plast.* **2011**, 47, 519–534.
- [98] M. Aksit, B. Klose, C. Zhao, K. Kreger, H.-W. Schmidt, V. Altstädt. *Morphology control of extruded polystyrene foams with benzene-trisamide-based nucleating agents*, *J. Cell. Plast.* **2019**, 55, 249–261.
- [99] M. Aksit, C. Zhao, B. Klose, K. Kreger, H.-W. Schmidt, V. Altstädt. *Extruded Polystyrene Foams with Enhanced Insulation and Mechanical Properties by a Benzene-Trisamide-Based Additive*, *Polymers* **2019**, 11, 268, 1-10.
- [100] P. J. M. Stals, J. F. Haveman, R. Martín-Rapún, C. F. C. Fitié, A. R. A. Palmans, E. W. Meijer. *The influence of oligo(ethylene glycol) side chains on the self-assembly of benzene-1,3,5-tricarboxamides in the solid state and in solution*, *J. Mater. Chem.* **2009**, 19, 124–130.
- [101] C. M. A. Leenders, L. Albertazzi, T. Mes, M. M. E. Koenigs, A. R. A. Palmans, E. W. Meijer. *Supramolecular polymerization in water harnessing both hydrophobic effects and hydrogen bond formation*, *Chem. Commun.* **2013**, 49, 1963–1965.
- [102] C. M. A. Leenders, T. Mes, M. B. Baker, M. M. E. Koenigs, P. Besenius, A. R. A. Palmans, E. W. Meijer. *From supramolecular polymers to hydrogel materials*, *Mater. Horiz.* **2014**, 1, 116–120.
- [103] C. M. A. Leenders, M. B. Baker, I. A. B. Pijpers, R. P. M. Lafleur, L. Albertazzi, A. R. A. Palmans, E. W. Meijer. *Supramolecular polymerisation in water; elucidating the role of hydrophobic and hydrogen-bond interactions*, *Soft Matter* **2016**, 12, 2887–2893.
- [104] B. N. S. Thota, X. Lou, D. Bochicchio, T. F. E. Paffen, R. P. M. Lafleur, J. L. J. van Dongen, S. Ehrmann, R. Haag, G. M. Pavan, A. R. A. Palmans, E. W. Meijer. *Supramolecular Copolymerization as a Strategy to Control the Stability of Self-Assembled Nanofibers*, *Angew. Chem. Int. Ed.* **2018**, 57, 6843–6847.
- [105] R. P. M. Lafleur, S. Herziger, S. M. C. Schoenmakers, A. D. A. Keizer, J. Jahzerah, B. N. S. Thota, L. Su, P. H. H. Bomans, N. A. J. M. Sommerdijk, A. R. A. Palmans, R. Haag,



- H. Friedrich, C. Böttcher, E. W. Meijer. *Supramolecular Double Helices from Small C<sub>3</sub>-Symmetrical Molecules Aggregated in Water*, J. Am. Chem. Soc. **2020**, 142, 17644–17652.
- [106] M. Garzoni, M. B. Baker, C. M. A. Leenders, I. K. Voets, L. Albertazzi, A. R. A. Palmans, E. W. Meijer, G. M. Pavan. *Effect of H-Bonding on Order Amplification in the Growth of a Supramolecular Polymer in Water*, J. Am. Chem. Soc. **2016**, 138, 13985–13995.
- [107] S. Lee, J.-S. Lee, C. H. Lee, Y.-S. Jung, J.-M. Kim. *Nonpolymeric Thermosensitive Benzenetricarboxamides*, Langmuir **2011**, 27, 1560–1564.
- [108] S. Dong, J. Leng, Y. Feng, M. Liu, C. J. Stackhouse, A. Schönhals, L. Chiappisi, L. Gao, W. Chen, J. Shang, L. Jin, Z. Qi, C. A. Schalley. *Structural water as an essential comonomer in supramolecular polymerization*, Sci. Adv. **2017**, 3, eaao0900, 1–8.
- [109] Z. Qi, L. Chiappisi, H. Gong, R. Pan, N. Cui, Y. Ge, C. Böttcher, S. Dong. *Ion Selectivity in Nonpolymeric Thermosensitive Systems Induced by Water-Attenuated Supramolecular Recognition*, Chem. Eur. J. **2018**, 24, 3854–3861.
- [110] X.-J. Kuang, A. Wajahat, W.-T. Gong, M. K. Dhinakaran, X.-H. Li, G.-L. Ning. *Supramolecular gel from self-assembly of a C<sub>3</sub>-symmetrical discotic molecular bearing pillar[5]arene*, Soft Matter **2017**, 13, 4074–4079.
- [111] W. Ali, W. Gong, M. Hassan, W. Qu, L. Liu, G. Ning. *Guest induced morphology transitions of star shaped pillar[5]arene trimer via endo host-guest and “exo-wall” electron-transfer interactions*, Chin. Chem. Lett. **2021**, 32, 371–374.
- [112] C. M. A. Leenders, G. Jansen, M. M. M. Frissen, R. P. M. Lafleur, I. K. Voets, A. R. A. Palmans, E. W. Meijer. *Monosaccharides as Versatile Units for Water-Soluble Supramolecular Polymers*, Chem. Eur. J. **2016**, 22, 4608–4615.
- [113] S. I. S. Hendrikse, L. Su, T. P. Hogervorst, R. P. M. Lafleur, X. Lou, G. A. van der Marel, J. D. C. Codee, E. W. Meijer. *Elucidating the Ordering in Self-Assembled Glycocalyx Mimicking Supramolecular Copolymers in Water*, J. Am. Chem. Soc. **2019**, 141, 13877–13886.
- [114] S. Varela-Aramburu, G. Morgese, L. Su, S. M. C. Schoenmakers, M. Perrone, L. Leanza, C. Perego, G. M. Pavan, A. R. A. Palmans, E. W. Meijer. *Exploring the Potential of Benzene-1,3,5-tricarboxamide Supramolecular Polymers as Biomaterials*, Biomacromolecules **2020**, 21, 4105–4115.

- [115] J. Wang, W. Qi, G. Chen. *The effect of monosaccharides on self-assembly of benzenetricarboxamides*, *Chin. Chem. Lett.* **2019**, 30, 587–591.
- [116] A. Bernet, R. Q. Albuquerque, M. Behr, S. T. Hoffmann, H.-W. Schmidt. *Formation of a supramolecular chromophore: a spectroscopic and theoretical study*, *Soft Matter* **2012**, 8, 66–69.
- [117] R. C. T. Howe, A. P. Smalley, A. P. M. Guttenplan, M. W. R. Doggett, M. D. Eddleston, J. C. Tan, G. O. Lloyd. *A family of simple benzene 1,3,5-tricarboxamide (BTA) aromatic carboxylic acid hydrogels*, *Chem. Commun.* **2013**, 49, 4268–4270.
- [118] A. D. Lynes, C. S. Hawes, E. N. Ward, B. Haffner, M. E. Möbius, K. Byrne, W. Schmitt, R. Pal, T. Gunnlaugsson. *Benzene-1,3,5-tricarboxamide n-alkyl ester and carboxylic acid derivatives: tuneable structural, morphological and thermal properties*, *CrystEngComm* **2017**, 19, 1427–1438.
- [119] S. Seibt, S. With, A. Bernet, H.-W. Schmidt, S. Förster. *Hydrogelation Kinetics Measured in a Microfluidic Device with in Situ X-ray and Fluorescence Detection*, *Langmuir* **2018**, 34, 5535–5544.
- [120] N. Helfricht, A. Mark, M. Behr, A. Bernet, H.-W. Schmidt, G. Papastavrou. *Writing with Fluid: Structuring Hydrogels with Micrometer Precision by AFM in Combination with Nanofluidics*, *Small* **2017**, 13, 1700962, 1-7.
- [121] N. Huang, J. Tao, S. Wei, W. Huang, D. Wang. *Positional Order in the Columnar Phase of Lyotropic Chromonic Liquid Crystals Mediated by Ionic Additives*, *ACS Omega* **2020**, 5, 9937–9943.
- [122] N. M. Matsumoto, R. P. M. Lafleur, X. Lou, K.-C. Shih, S. P. W. Wijnands, C. Guibert, J. W. A. M. van Rosendaal, I. K. Voets, A. R. A. Palmans, Y. Lin, E. W. Meijer. *Polymorphism in Benzene-1,3,5-tricarboxamide Supramolecular Assemblies in Water: A Subtle Trade-off between Structure and Dynamics*, *J. Am. Chem. Soc.* **2018**, 140, 13308–13316.
- [123] J. Li, N. Huang, D. Wang, L. Xu, Y. Huang, M. Chen, J. Tao, G. Pan, Z. Wu, L. Li. *Highly ordered, ultra long nanofibrils via the hierarchical self-assembly of ionic aromatic oligoamides*, *Soft Matter* **2013**, 9, 4642–4647.
- [124] Z. Shen, Y. Sang, T. Wang, J. Jiang, Y. Meng, Y. Jiang, K. Okuro, T. Aida, M. Liu. *Asymmetric catalysis mediated by a mirror symmetry-broken helical nanoribbon*, *Nat. Commun.* **2019**, 10, 3976, 1-8.

- [125] W. Huang, S. Wei, D. Frenkel, N. Huang. *The pathway and kinetics of hierarchical assembly of ionic oligomers into a lyotropic columnar phase*, *Soft Matter* **2019**, *15*, 4460–4466.
- [126] Y. Sang, D. Yang, Z. Shen, P. Duan, M. Liu. *Mechanically Controlled and Consecutively Boosted Circularly Polarized Luminescence of Nanoassemblies from Achiral Molecules*, *J. Phys. Chem. C* **2020**, *124*, 17274–17281.
- [127] M. A. VandenBerg, J. K. Sahoo, L. Zou, W. McCarthy, M. J. Webber. *Divergent Self-Assembly Pathways to Hierarchically Organized Networks of Isopeptide-Modified Discotics under Kinetic Control*, *ACS Nano* **2020**, *14*, 5491–5505.
- [128] D. Spitzer, L. L. Rodrigues, D. Straßburger, M. Mezger, P. Besenius. *Tuneable Transient Thermogels Mediated by a pH- and Redox-Regulated Supramolecular Polymerization*, *Angew. Chem. Int. Ed.* **2017**, *56*, 15461–15465.
- [129] Y. Huang, Y. Cong, J. Li, D. Wang, J. Zhang, L. Xu, W. Li, L. Li, G. Pan, C. Yang. *Anisotropic ionic conductivities in lyotropic supramolecular liquid crystals*, *Chem. Commun.* **2009**, *48*, 7560–7562.
- [130] Y. Huang, D. Wang, L. Xu, Y. Cong, J. Li, L. Li. *Multiscale fibers via supramolecular self-assembly of a fully rigid, discotic aromatic aramid molecule*, *Eur. Polym. J.* **2013**, *49*, 1682–1687.
- [131] D. Wang, Y. Huang, J. Li, L. Xu, M. Chen, J. Tao, L. Li. *Lyotropic Supramolecular Helical Columnar Phases Formed by  $C_3$ -Symmetric and Unsymmetric Rigid Molecules*, *Chem. Eur. J.* **2013**, *19*, 685–690.
- [132] D. Nardini. *Sulfur-Containing Functional Supramolecular Fibers for Filtration Applications*, Dissertation, Universität Bayreuth **2022**.
- [133] Y. Zhou, M. Xu, T. Yi, S. Xiao, Z. Zhou, F. Li, C. Huang. *Morphology-Tunable and Photoresponsive Properties in a Self-Assembled Two-Component Gel System*, *Langmuir* **2007**, *23*, 202–208.
- [134] K. Kreger, P. Wolfer, H. Audorff, L. Kador, N. Stingelin-Stutzmann, P. Smith, H.-W. Schmidt. *Stable Holographic Gratings with Small-Molecular Trisazobenzene Derivatives*, *J. Am. Chem. Soc.* **2010**, *132*, 509–516.
- [135] S. Lee, S. Oh, J. Lee, Y. Malpani, Y.-S. Jung, B. Kang, J. Y. Lee, K. Ozasa, T. Isoshima, S. Y. Lee, M. Hara, D. Hashizume, J.-M. Kim. *Stimulus-Responsive Azobenzene Supramolecules: Fibers, Gels, and Hollow Spheres*, *Langmuir* **2013**, *29*, 5869–5877.

- [136] J. Lee, S. Oh, J. Pyo, J.-M. Kim, J. H. Je. *A light-driven supramolecular nanowire actuator*, *Nanoscale* **2015**, 7, 6457–6461.
- [137] Y.-J. Choi, D.-Y. Kim, M. Park, W.-J. Yoon, Y. Lee, J.-K. Hwang, Y.-W. Chiang, S.-W. Kuo, C.-H. Hsu, K.-U. Jeong. *Self-Assembled Hierarchical Superstructures from the Benzene-1,3,5-Tricarboxamide Supramolecules for the Fabrication of Remote-Controllable Actuating and Rewritable Films*, *ACS Appl. Mater. Interfaces* **2016**, 8, 9490–9498.
- [138] A. R. A. Palmans, J. A. J. M. Vekemans, H. Kooijman, A. L. Spek, E. W. Meijer. *Hydrogen-bonded porous solid derived from trimesic amide*, *Chem. Commun.* **1997**, 22, 2247–2248.
- [139] D. K. Kumar, D. A. Jose, P. Dastidar, A. Das. *Nonpolymeric Hydrogelators Derived from Trimesic Amides*, *Chem. Mater.* **2004**, 16, 2332–2335.
- [140] N. Shi, G. Yin, M. Han, Z. Xu. *Anions bonded on the supramolecular hydrogel surface as the growth center of biominerals*, *Colloids Surf., B* **2008**, 66, 84–89.
- [141] N. Shi, G. Yin, H. Li, M. Han, Z. Xu. *Uncommon hexagonal microtubule based gel from a simple trimesic amide*, *New J. Chem.* **2008**, 32, 2011–2015.
- [142] B.-C. Tzeng, B.-S. Chen, H.-T. Yeh, G.-H. Lee, S.-M. Peng. *Self-assembly of  $N,N',N''$ -tris(4-pyridyl)trimesic amide and  $N,N',N''$ -tris(3-pyridyl)trimesic amide with  $Ag^I$  or  $Cd^{II}$  ions*, *New J. Chem.* **2006**, 30, 1087–1092.
- [143] X.-Z. Luo, X.-J. Jia, J.-H. Deng, J.-L. Zhong, H.-J. Liu, K.-J. Wang, D.-C. Zhong. *A Microporous Hydrogen-Bonded Organic Framework: Exceptional Stability and Highly Selective Adsorption of Gas and Liquid*, *J. Am. Chem. Soc.* **2013**, 135, 11684–11687.
- [144] O. Kotova, R. Daly, C. M. G. dos Santos, M. Boese, P. E. Kruger, J. J. Boland, T. Gunnlaugsson. *Europium-Directed Self-Assembly of a Luminescent Supramolecular Gel from a Tripodal Terpyridine-Based Ligand*, *Angew. Chem. Int. Ed.* **2012**, 51, 7208–7212.
- [145] S. H. Jung, J. Jeon, H. Kim, J. Jaworski, J. H. Jung. *Chiral Arrangement of Achiral Au Nanoparticles by Supramolecular Assembly of Helical Nanofiber Templates*, *J. Am. Chem. Soc.* **2014**, 136, 6446–6452.
- [146] M. Drummer. *Functional supramolecular nanofibers and their applications in nanoparticle immobilization and catalysis*, Dissertation, Universität Bayreuth **2022**.
- [147] M. Drummer, C. Liang, K. Kreger, S. Rosenfeldt, A. Greiner, H.-W. Schmidt. *Stable Mesoscale Nonwovens of Electrospun Polyacrylonitrile and Interpenetrating*

- Supramolecular 1,3,5-Benzenetrisamide Fibers as Efficient Carriers for Gold Nanoparticles*, ACS Appl. Mater. Interfaces **2021**, 13, 34818–34828.
- [148] T. Klein, F. V. Gruschwitz, S. Rogers, S. Hoepfener, I. Nischang, J. C. Brendel. *The influence of directed hydrogen bonds on the self-assembly of amphiphilic polymers in water*, J. Colloid Interface Sci. **2019**, 557, 488–497.
- [149] M. B. Baker, L. Albertazzi, I. K. Voets, C. M. A. Leenders, A. R. A. Palmans, G. M. Pavan, E. W. Meijer. *Consequences of chirality on the dynamics of a water-soluble supramolecular polymer*, Nat. Commun. **2015**, 6, 6234, 1-12.
- [150] D. Bochicchio, G. M. Pavan. *From Cooperative Self-Assembly to Water-Soluble Supramolecular Polymers Using Coarse-Grained Simulations*, ACS Nano **2017**, 11, 1000–1011.
- [151] D. Bochicchio, G. M. Pavan. *Effect of Concentration on the Supramolecular Polymerization Mechanism via Implicit-Solvent Coarse-Grained Simulations of Water-Soluble 1,3,5-Benzenetricarboxamide*, J. Phys. Chem. Lett. **2017**, 8, 3813–3819.
- [152] N. Lomadze, H.-J. Schneider. *Reversal of polyamine selectivity for DNA and RNA by steric hindrance*, Tetrahedron Lett. **2002**, 43, 4403–4405.
- [153] M. Vasylyev, R. Popovitz-Biro, L. J. W. Shimon, R. Neumann. *Inorganic–organic hybrid materials based on keggin type polyoxometalates and organic polyammonium cations*, J. Mol. Struct. **2003**, 656, 27–35.
- [154] F. Camerel, C. F. J. Faul. *Combination of ionic self-assembly and hydrogen bonding as a tool for the synthesis of liquid-crystalline materials and organogelators from a simple building block*, Chem. Commun. **2003**, 15, 1958–1959.
- [155] K. Robinson, C. J. Easton, A. F. Dulhunty, M. G. Casarotto. *Exploiting Peptidomimetics to Synthesize Compounds That Activate Ryanodine Receptor Calcium Release Channels*, ChemMedChem **2018**, 13, 1957–1971.
- [156] R. Uppal, G. Bhat, C. Eash, K. Akato. *Meltblown Nanofiber Media for Enhanced Quality Factor*, Fibers Polym. **2013**, 14, 660–668.
- [157] X. Hao, Y. Zeng. *A Review on the Studies of Air Flow Field and Fiber Formation Process during Melt Blowing*, Ind. Eng. Chem. Res. **2019**, 58, 11624–11637.
- [158] Y. Kara, K. Molnár. *A review of processing strategies to generate melt-blown nano/microfiber mats for high-efficiency filtration applications*, J. Ind. Text. **2022**, 51, 137S-180S.

- [159] X. Zhang, Y. Lu. *Centrifugal Spinning: An Alternative Approach to Fabricate Nanofibers at High Speed and Low Cost*, Polym. Rev. **2014**, 54, 677–701.
- [160] Z.-M. Zhang, Y.-S. Duan, Q. Xu, B. Zhang. *A review on nanofiber fabrication with the effect of high-speed centrifugal force field*, J. Eng. Fibers Fabr. **2019**, 14, 1–11.
- [161] B. Atıcı, C. H. Ünlü, M. Yanılmaz. *A Review on Centrifugally Spun Fibers and Their Applications*, Polym. Rev. **2022**, 62, 1–64.
- [162] E. S. Medeiros, G. M. Glenn, A. P. Klamczynski, W. J. Orts, L. H. C. Mattoso. *Solution Blow Spinning: A New Method to Produce Micro- and Nanofibers from Polymer Solutions*, J. Appl. Polym. Sci. **2009**, 113, 2322–2330.
- [163] J. L. Daristotle, A. M. Behrens, A. D. Sandler, P. Kofinas. *A Review of the Fundamental Principles and Applications of Solution Blow Spinning*, ACS Appl. Mater. Interfaces **2016**, 8, 34951–34963.
- [164] B. Khalid, X. Bai, H. Wei, Y. Huang, H. Wu, Y. Cui. *Direct Blow-Spinning of Nanofibers on a Window Screen for Highly Efficient PM<sub>2.5</sub> Removal*, Nano Lett. **2017**, 17, 1140–1148.
- [165] Y. Gao, J. Zhang, Y. Su, H. Wang, X.-X. Wang, L.-P. Huang, M. Yu, S. Ramakrishna, Y.-Z. Long. *Recent progress and challenges in solution blow spinning*, Mater. Horiz. **2021**, 8, 426–446.
- [166] Z. Li, J. Song, Y. Long, C. Jia, Z. Liu, L. Li, C. Yang, J. Liu, S. Lin, H. Wang, Y. Liu, M. Fang, H. Wu. *Large-scale blow spinning of heat-resistant nanofibrous air filters*, Nano Res. **2020**, 13, 861–867.
- [167] K. G. d. C. Monsores, A. O. d. Silva, S. d. S. A. Oliveira, R. P. Weber, M. L. Dias. *Production of nanofibers from solution blow spinning (SBS)*, J. Mater. Res. Technol. **2022**, 16, 1824–1831.
- [168] D. Li, Y. Xia. *Electrospinning of Nanofibers: Reinventing the Wheel?*, Adv. Mater. **2004**, 16, 1151–1170.
- [169] A. Greiner, J. H. Wendorff. *Electrospinning: A Fascinating Method for the Preparation of Ultrathin Fibers*, Angew. Chem. Int. Ed. **2007**, 46, 5670–5703.
- [170] S. Agarwal, A. Greiner, J. H. Wendorff. *Electrospinning of Manmade and Biopolymer Nanofibers-Progress in Techniques, Materials, and Applications*, Adv. Funct. Mater. **2009**, 19, 2863–2879.
- [171] J. Xue, T. Wu, Y. Dai, Y. Xia. *Electrospinning and Electrospun Nanofibers: Methods, Materials, and Applications*, Chem. Rev. **2019**, 119, 5298–5415.

- [172] P. Rathore, J. D. Schiffman. *Beyond the Single-Nozzle: Coaxial Electrospinning Enables Innovative Nanofiber Chemistries, Geometries, and Applications*, ACS Appl. Mater. Interfaces **2021**, 13, 48–66.
- [173] M. Zhu, J. Han, F. Wang, W. Shao, R. Xiong, Q. Zhang, H. Pan, Y. Yang, S. K. Samal, F. Zhang, C. Huang. *Electrospun Nanofibers Membranes for Effective Air Filtration*, Macromol. Mater. Eng. **2017**, 302, 1600353, 1-27.
- [174] S. Jung, J. Kim. *Advanced Design of Fiber-Based Particulate Filters: Materials, Morphology, and Construction of Fibrous Assembly*, Polymers **2020**, 12, 1714, 1-23.
- [175] D. M. dos Santos, D. S. Correa, E. S. Medeiros, J. E. Oliveira, L. H. C. Mattoso. *Advances in Functional Polymer Nanofibers: From Spinning Fabrication Techniques to Recent Biomedical Applications*, ACS Appl. Mater. Interfaces **2020**, 12, 45673–45701.
- [176] L. de Sio, B. Ding, M. Focsan, K. Kogermann, P. Pascoal-Faria, F. Petronela, G. Mitchell, E. Zussman, F. Pierini. *Personalized Reusable Face Masks with Smart Nano-Assisted Destruction of Pathogens for COVID-19: A Visionary Road*, Chem. Eur. J. **2021**, 27, 6112–6130.
- [177] Y. Li, X. Yin, J. Yu, B. Ding. *Electrospun nanofibers for high-performance air filtration*, Compos. Commun. **2019**, 15, 6–19.
- [178] Z. Wang, Z. Pan. *Preparation of hierarchical structured nano-sized/porous poly(lactic acid) composite fibrous membranes for air filtration*, Appl. Surf. Sci. **2015**, 356, 1168–1179.
- [179] S. Zhang, H. Liu, X. Yin, J. Yu, B. Ding. *Anti-deformed Polyacrylonitrile/Polysulfone Composite Membrane with Binary Structures for Effective Air Filtration*, ACS Appl. Mater. Interfaces **2016**, 8, 8086–8095.
- [180] S. Zhang, N. Tang, L. Cao, X. Yin, J. Yu, B. Ding. *Highly Integrated Polysulfone/Polyacrylonitrile/Polyamide-6 Air Filter for Multilevel Physical Sieving Airborne Particles*, ACS Appl. Mater. Interfaces **2016**, 8, 29062–29072.
- [181] K. Xu, J. Deng, R. Lin, H. Zhang, Q. Ke, C. Huang. *Surface fibrillation of para-aramid nonwoven as a multi-functional air filter with ultralow pressure drop*, J. Mater. Chem. A **2020**, 8, 22269–22279.
- [182] S. Zhang, H. Liu, N. Tang, J. Ge, J. Yu, B. Ding. *Direct electrospinning of high-performance membranes based on self-assembled 2D nanoarchitected networks*, Nat. Commun. **2019**, 10, 1458, 1-11.

- [183] S. Zhang, H. Liu, N. Tang, N. Ali, J. Yu, B. Ding. *Highly Efficient, Transparent, and Multifunctional Air Filters Using Self-Assembled 2D Nanoarchitected Fibrous Networks*, ACS Nano **2019**, 13, 13501–13512.
- [184] H. Liu, L. Liu, J. Yu, X. Yin, B. Ding. *High-efficiency and super-breathable air filters based on biomimetic ultrathin nanofiber networks*, Compos. Commun. **2020**, 22, 100493, 1-6.
- [185] S. Zhang, H. Liu, N. Tang, S. Zhou, J. Yu, B. Ding. *Spider-Web-Inspired PM<sub>0.3</sub> Filters Based on Self-Sustained Electrostatic Nanostructured Networks*, Adv. Mater. **2020**, 32, 2002361, 1-8.
- [186] M. Hu, Y. Wang, Z. Yan, G. Zhao, Y. Zhao, L. Xia, B. Cheng, Y. Di, X. Zhuang. *Hierarchical dual-nanonet of polymer nanofibers and supramolecular nanofibrils for air filtration with a high filtration efficiency, low air resistance and high moisture permeation*, J. Mater. Chem. A **2021**, 9, 14093–14100.
- [187] Y. Wang, G. Chao, X. Li, F. Dong, X. Zhuang, L. Shi, B. Cheng, X. Xu. *Hierarchical fibrous microfiltration membranes by self-assembling DBS nanofibrils in solution-blown nanofibers*, Soft Matter **2018**, 14, 8879–8882.
- [188] N. Tang, S. Zhang, Y. Si, J. Yu, B. Ding. *An ultrathin bacterial cellulose membrane with a Voronoi-net structure for low pressure and high flux microfiltration*, Nanoscale **2019**, 11, 17851–17859.
- [189] E. Krieg, H. Weissman, E. Shirman, E. Shimoni, B. Rybtchinski. *A recyclable supramolecular membrane for size-selective separation of nanoparticles*, Nat. Nanotechnol. **2011**, 6, 141–146.
- [190] M. Burgard, D. Weiss, K. Kreger, H. Schmalz, S. Agarwal, H.-W. Schmidt, A. Greiner. *Mesostructured Nonwovens with Penguin Downy Feather-Like Morphology—Top-Down Combined with Bottom-Up*, Adv. Funct. Mater. **2019**, 29, 1903166, 1-7.
- [191] M. Langner, A. Greiner. *Wet-Laid Meets Electrospinning: Nonwovens for Filtration Applications from Short Electrospun Polymer Nanofiber Dispersions*, Macromol. Rapid Commun. **2016**, 37, 351–355.



## 2. Objective of this thesis

1,3,5-benzenetricarboxamides (BTAs) are a well-investigated class to obtain supramolecular nanofibers by the self-assembly into columnar structures driven by three directed hydrogen bonds. The use of BTAs with functional groups in the molecules' periphery is challenging during the nanofiber preparation and promising in terms of application. On the one hand, the functional groups of the molecular dissolved building block may be prone to interact with the solvent molecules or with interfaces featuring similar chemical matching groups. On the other hand, supramolecular nanofibers based on such BTAs exhibit functional surfaces, which can be beneficially used for the immobilization of metal nanoparticles.

Therefore, the aim of this thesis is the synthesis and characterization of *a new class of BTAs with functional peripheral tertiary amino substituents*. These functional BTAs will be investigated regarding their solubility and self-assembly behavior in polar solvents such as aqueous media and alcohols. To prepare complex hierarchical supramolecular structures with dimensions on the mesoscale, special focus is given to the combination of two self-assembly concepts in which the self-assembled nanostructures feature peripheral similar chemical matching groups. To use this approach, the findings will be transferred to nonwovens and their potential for nanoparticle immobilization by the functional surface of the BTA nanofibers will be investigated.

To reveal structure-property relationships, a series of BTAs, which differ in the alky groups at the tertiary amino substituents, will be prepared. This systematic change will tailor the hydrophilicity of the molecule, whereas it is expected that the water solubility increases from *N,N*-di-isopropyl, *N,N*-di-*n*-propyl, *N,N*-diethyl to *N,N*-dimethyl substituents (**Figure 2.1**).

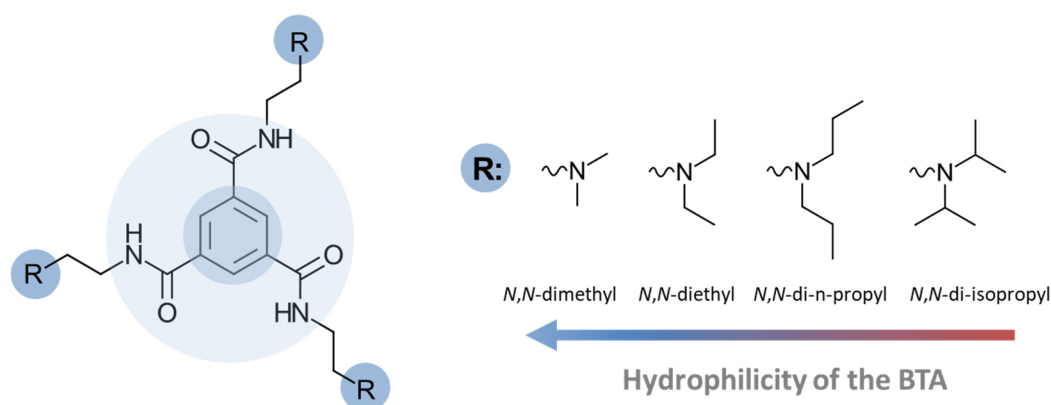


**Figure 2.1.** This thesis explores 1,3,5-benzenetricarboxamides with tertiary amino substituents in the periphery. The alkyl groups are systematically varied to change the hydrophilicity of the BTA.

In general, the self-assembly of BTAs in pure water is rarely observed. This may be related to a proper molecular design of the BTAs suitable to interact with water at a given set of conditions. This represents an interesting fundamental question of how these BTAs with peripheral tertiary amino substituents will self-assemble in water. Consequently, special attention is given to elaborated and detailed protocols in aqueous media to gain insight into the self-assembly process of the supramolecular nano- and microstructure formation.

To achieve more complex hierarchical superstructures, two self-assembly concepts shall be combined for the first time, namely the crystallization-driven self-assembly of triblock terpolymers and the molecular self-assembly of BTAs. Crystallization-driven self-assembly of triblock terpolymers under appropriate conditions can result in patchy worm-like micelles. To immobilize the patchy worm-like micelles, they will be deposited on electrospun polymer fibers. The patchy worm-like micelles will be designed to yield nanometer-sized patches with the same side groups as in the BTA. A very fundamental question is how chemical matching between different components can be used to control the self-assembly of these BTA building blocks. Thus, studies have to be performed to reveal the requirements and parameters necessary to initiate the self-assembly of the BTAs from those patches from solution.

Finally, to demonstrate the functionality of the surface of the supramolecular nanofibers of these BTAs, hierarchically mesostructured nonwovens should be prepared and their potential to immobilize metal nanoparticles from aqueous media should be investigated. Consequently, these composites have to be water stable. This requires adopting and selecting BTAs with lower hydrophilicity (**Figure 2.1**) while retaining their functionality. Moreover, patchy worm-like micelles with the same chemical matching have to be identified and selected. The patchy worm-like micelles will be deposited on the polymer fibers of the nonwovens in a similar manner as described above. Studies have to be performed to reveal the influencing parameters to initiate the molecular self-assembly of the BTAs from those patches on the surface of the supporting polymer fibers within the nonwoven to create hierarchically mesostructured nonwovens. Investigations on the immobilization of nanoparticles on the functional supramolecular surface of the BTAs from water need to be conducted to ensure the functionality and stability in water.

### 3. Synopsis

The main focus of this thesis is on the synthesis and characterization of *1,3,5-benzenetricarboxamides with tertiary amino substituents*. These functional BTAs were investigated regarding their solubility and self-assembly behavior at different concentrations in selected solvents. Basic self-assembly studies of these BTAs with functional tertiary amino substituents are explored in detail to reveal structure-property relationships. To prepare complex hierarchical superstructures, the combination of two-self-assembly concepts was investigated. The crystallization-driven self-assembly of triblock terpolymers was combined for the first time with the molecular self-assembly of benzenetricarboxamides. Special attention is given on peripheral similar chemical matching groups between the different building blocks. This concept should be transferred to electrospun nonwovens to show the potential of the functional surface of the BTA nanofibers to immobilize metal nanoparticles.

#### 3.1. Synthesis and characterization of BTAs with tertiary amino substituents

Fundamental considerations are required for the molecular design and the synthesis of BTAs with functional peripheral tertiary amino substituents. Typically, BTAs are synthesized by using an Einhorn-type of the Schotten-Baumann reaction. In this reaction, amines are reacted with trimesic trichloride in the presence of at least stoichiometric amounts of a base to give the corresponding amides. A base such as pyridine acts as hydrochloric acid scavenger resulting in salt formation. Here, the tertiary amino groups of the BTAs will also result in salt formation requiring elaborated work up. To avoid this, a straightforward two-step route was developed to synthesize BTAs with an aliphatic ethyl spacer and tertiary amino substituents (**Figure 3.1.1**). Starting with the esterification of trimesic acid to trimesic trimethyl ester and subsequent conversion of trimesic trimethyl ester with the *N,N*-alkylamine resulted in the respective BTA with peripheral *N,N*-dimethyl, *N,N*-diethyl, *N,N*-di-*n*-propyl and *N,N*-di-isopropyl groups. This systematic change in the alkyl groups at the tertiary amino substituent allows to tailor the molecule's hydrophilicity and to establish structure-property relationships. All BTAs were molecularly characterized by nuclear magnetic resonance spectroscopy ( $^1\text{H}$  NMR and  $^{13}\text{C}$  NMR), mass spectrometry, elemental analysis and FT-IR spectroscopy.

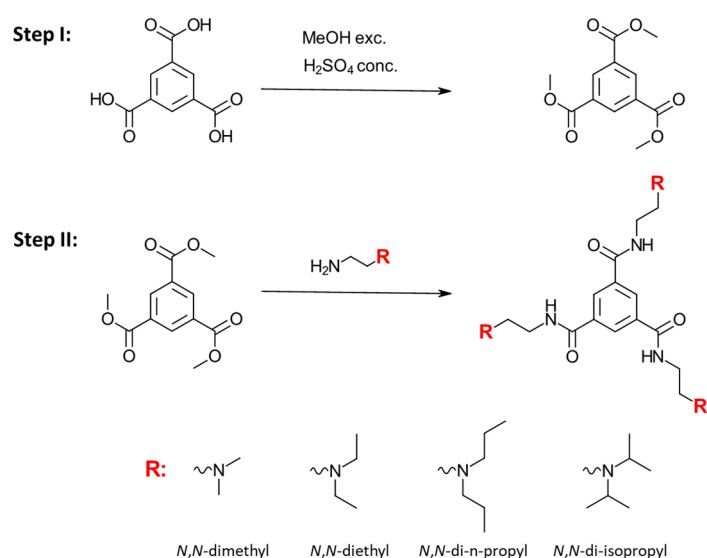


**Figure 3.1.1.** Two-step synthesis of 1,3,5-benzenetricarboxamides with tertiary amino substituents in the periphery with different alky groups and an aliphatic ethyl spacer between the BTA core and the amino substituent. First step is the esterification of trimesic acid to trimesic acid trimethyl ester and subsequent conversion to the respective BTA with *N,N*-dimethyl, *N,N*-diethyl, *N,N*-di-*n*-propyl and *N,N*-di-isopropyl groups.

The bulk thermal properties of the synthesized BTAs were investigated by differential scanning calorimetry. Upon heating, one pronounced phase transition occurs for all investigated BTAs. The phase transition occurs for the BTA with *N,N*-dimethyl, *N,N*-diethyl, *N,N*-di-*n*-propyl and *N,N*-di-isopropyl groups at 212 °C, 206 °C, 207 °C and 291 °C, respectively. Upon cooling, the phase transition occurs at 188 °C, 200 °C, 200 °C and 277 °C for the BTA with *N,N*-dimethyl, *N,N*-diethyl, *N,N*-di-*n*-propyl and *N,N*-di-isopropyl groups. To further investigate the nature of the phase transitions in bulk, temperature-dependent polarizing optical microscopy investigations with and without shearing the samples were conducted (**Figure 3.1.2**). Only the BTA with *N,N*-dimethyl groups shows a brittle behavior and fractures during shearing, confirming a crystalline phase. The other three BTAs show deformable structures, indicative for a mesophase.

BTAs are known to self-assemble into highly ordered columnar structures due to the formation of three directed strands of hydrogen bonds. Therefore, the synthesized BTAs were investigated with IR spectroscopy to reveal the most relevant amide vibrations (amide A, amide I and II) for columnar stacking in bulk. All four compounds show IR signals at around 3240 cm<sup>-1</sup> (amide A, N-H stretch vibrations), at around 1640 cm<sup>-1</sup> (amide I, C=O stretch vibrations) and at around 1560 cm<sup>-1</sup> (amide II, superposition of N-H bend and C-N stretch vibrations), providing evidence for a columnar arrangement.

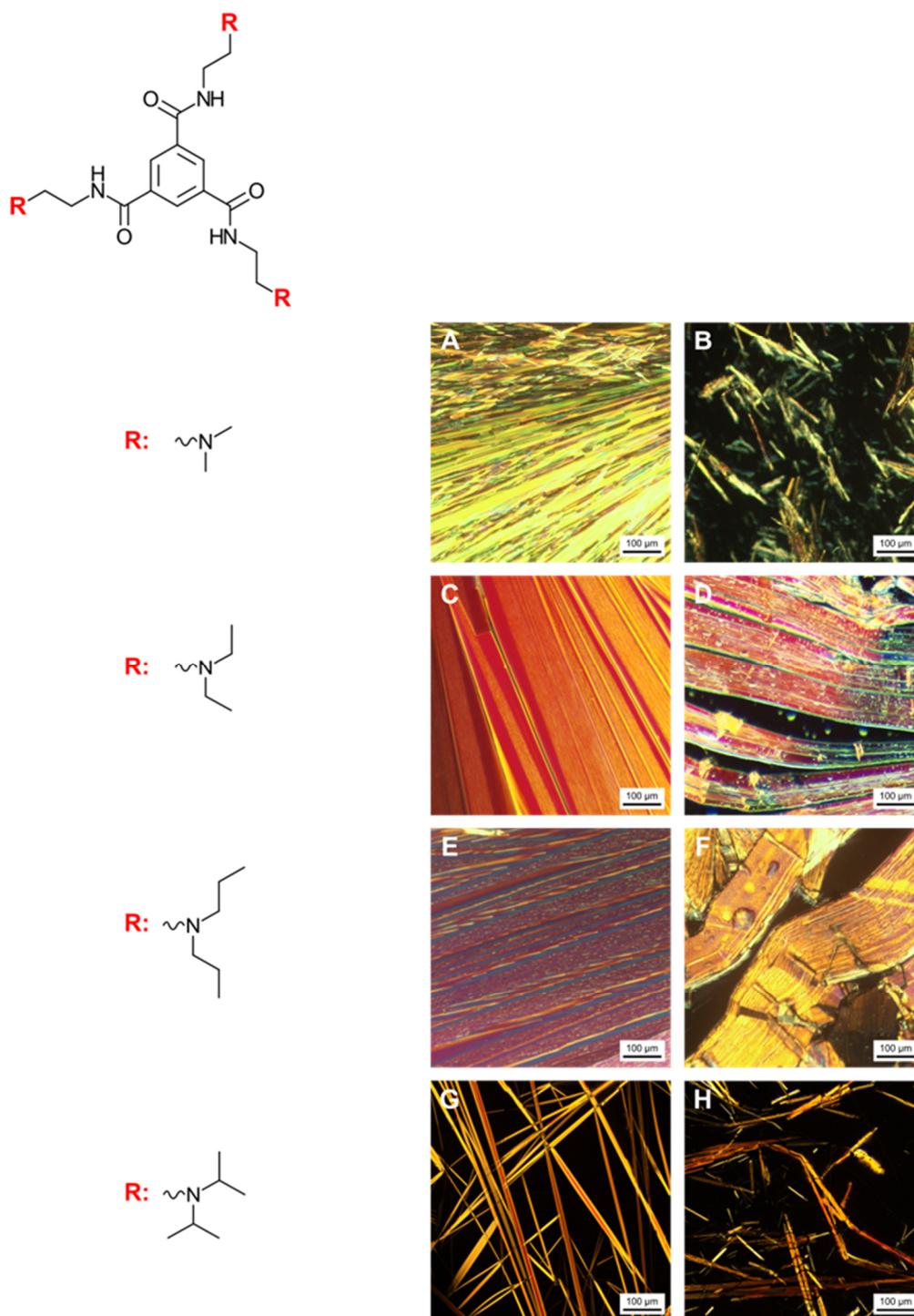


**Figure 3.1.2.** A – H: Temperature-dependent polarized optical micrographs of the 1,3,5-benzenetricarboxamides with tertiary amino substituents with different alkyl groups in bulk at 180 °C (A, C, E) and 210 °C (G), before and after (B, D, F and H) shearing the sample. All BTAs show birefringent textures. Only the BTA with *N,N*-dimethyl groups shows a brittle behavior and breaks upon shearing, which confirms a crystalline behavior (B). The other BTAs show a bending of the textures. This is indicative for a mesophase (D, F and H). Adapted and reproduced from Ref. <sup>[1]</sup> with permission from the Royal Society of Chemistry (© 2020).

<sup>[1]</sup> A. Frank, A. Bernet, K. Kreger, H.-W. Schmidt. *Supramolecular microtubes based on 1,3,5-benzenetricarboxamides prepared by self-assembly upon heating*, *Soft Matter* **2020**, 16, 4564–4568.

### 3.2. Solubility and self-assembly behavior of BTAs with tertiary amino substituents

Typically, supramolecular structures from BTAs are prepared from organic media. However, only a few known BTAs featuring hydrophilic substituents show self-assembly from water or water mixtures. Introducing such substituents impacts not only the solubility, but also the self-assembly process since functional groups have the potential for secondary interactions. Common methods to initiate the self-assembly of BTAs to supramolecular fibers are upon cooling a molecularly dissolved solution at an elevated temperature at a given concentration or upon solvent evaporation of a molecularly dissolved solution.

The synthesized series of BTAs with tertiary amino substituents with different alkyl groups were investigated regarding their solubility and self-assembly upon solvent evaporation in different organic solvents. Exemplary, the BTA with *N,N*-di-isopropyl groups was dissolved in polar solvents such as ethanol, isopropanol, dimethyl sulfoxide and dimethylformamide at an initial concentration of 2.00 wt.% at room temperature. Molecularly dissolved solutions containing the BTA with *N,N*-di-isopropyl groups were achieved by heating the solutions. Upon solvent evaporation, self-assembly towards supramolecular structures was investigated and the results of the BTA with *N,N*-di-isopropyl groups are given in **Figure 3.2.1**. In these solvents, supramolecular structures, which differ in size and shape, can be observed.

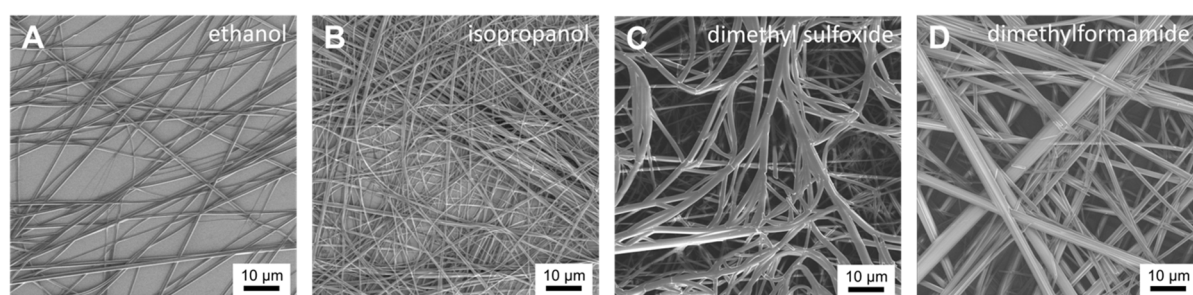


**Figure 3.2.1.** Self-assembly of the BTA with *N,N*-di-isopropyl groups upon solvent evaporation from different solvents. Scanning electron micrographs of the dried supramolecular structures from a 2.00 wt.% hot solution of the BTA with *N,N*-di-isopropyl in A) ethanol, B) isopropanol, C) dimethyl sulfoxide and D) dimethylformamide dropped on a silicon wafer.

The concentration limit for a molecularly dissolved BTA solution arises from the molecular structure of the used BTA, the used solvent and the boiling point of the solvent. For example, the BTA with *N,N*-di-isopropyl groups is not soluble at room temperature in dimethylformamide. However, the solubility can significantly be increased up to 12.5 wt.% at elevated temperatures. Several factors influence the self-assembly process of BTAs towards supramolecular structures. One crucial factor is the molecular structure of the BTA itself and the used BTA concentration. Besides this, the process parameters (temperature, heating and cooling rates) determine the self-assembly behavior. Additionally, the solvent used to dissolve the BTA impacts the self-assembly process. All these parameters need to be considered or optimized to create supramolecular objects.

Therefore, to investigate the solubility and self-assembly behavior of the BTAs with tertiary amino substituents, extensively temperature-dependent turbidity measurements were conducted. The BTAs were prepared in various solvents at different concentrations and the transmittance was recorded for a defined heating and cooling profile depending on the used solvent. Exemplarily, the resulting phase diagram for the BTA with *N,N*-di-isopropyl groups in isopropanol from temperature-dependent solubility measurements is shown in **Figure 3.2.2**. The BTA is not soluble in isopropanol at room temperature, but the solubility can be enhanced at elevated temperatures. After dissolution, the solutions were cooled down to identify if a stable solution was present at room temperature. Three regimes were determined. For concentrations below 0.75 wt.%, a stable and molecularly dissolved BTA solution is obtained at room temperature in regime I because no cloud and clearing points are observed. In regime II, between concentrations of 0.75 wt.% and 4.00 wt.%, the BTA forms a turbid gel upon cooling when passing the cloud points (see the inset picture). The temperature of the cloud points increases with increasing concentration. This process is fully reversible upon heating and the gel dissolves again when reaching the clearing points. A small hysteresis between the cloud and clearing points can be observed, which indicates a fast self-assembly and disassembly process. In regime III at concentrations above 4.00 wt.%, the BTA is not completely soluble anymore at elevated temperatures.



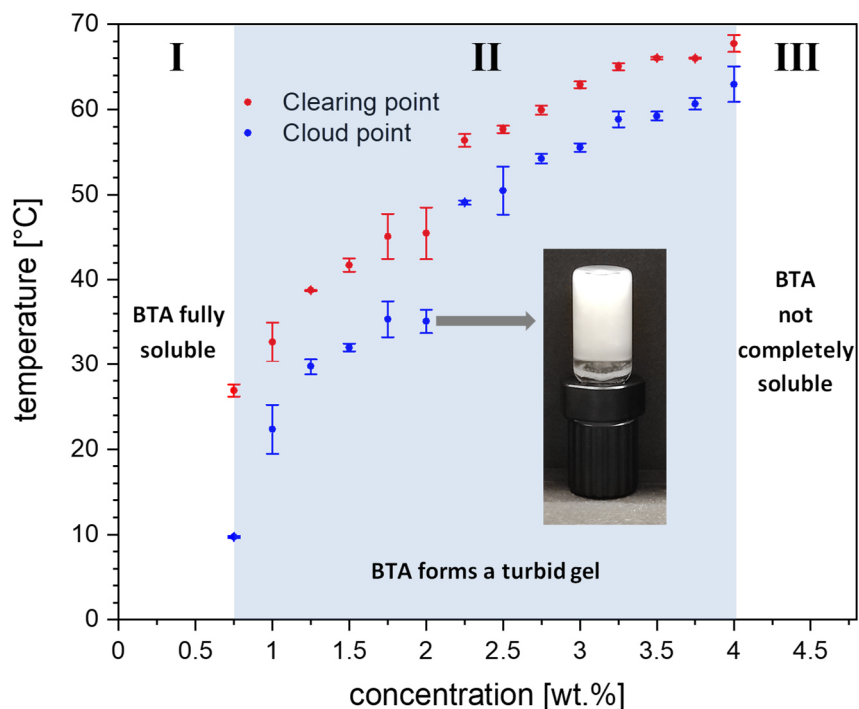


**Figure 3.2.2.** Phase diagram of the BTA with *N,N*-di-isopropyl groups in isopropanol. Three regimes (I-III) were determined. In regime I the BTA remains molecularly dissolved. Increasing the BTA concentration leads to the formation of a gel upon cooling within the regime II. Upon heating, this process is completely reversible. In regime III the BTA is not completely soluble. Adapted and reproduced from Ref. <sup>[111]</sup>. Published by Wiley-VCH GmbH under the terms of the Creative Commons Attribution 4.0 International License (© 2022 The Authors).

In summary, the results confirm that the solubility and self-assembly behavior of BTAs depends on the chemical structure of the BTA, the concentration, the used solvent, as well as on the cooling and evaporation conditions. Therefore, comprehensive investigations are necessary to optimize the self-assembly conditions for a given BTA. As mentioned, the self-assembly behavior in water is not widely explored. Therefore, the synthesized series of BTAs with tertiary amino substituents allows the investigation regarding solubility and self-assembly behavior in water.

<sup>[111]</sup> A. Frank, M. Weber, C. Hils, U. Mansfeld, K. Kreger, H. Schmalz, H.-W. Schmidt. *Functional Mesostructured Electrospun Polymer Nonwovens with Supramolecular Nanofibers*, *Macromol. Rapid Commun.* **2022**, 43, 2200052, 1–8.



### 3.3. Supramolecular microtubes based on 1,3,5-benzenetricarboxamides prepared by self-assembly upon heating<sup>[1]</sup>

Only a few BTAs are known that self-assemble from aqueous media. The goal was to investigate the solubility and self-assembly behavior in water of a series of BTAs with tertiary amino substituents with alkyl groups of different lengths.

The main achievement in this publication is the finding of a unique two-step self-assembly behavior of the tertiary amino-containing BTA with *N,N*-diethyl groups upon heating aqueous solutions resulting in supramolecular microtubes. The chemical structure is depicted in **Figure 3.3.1**.

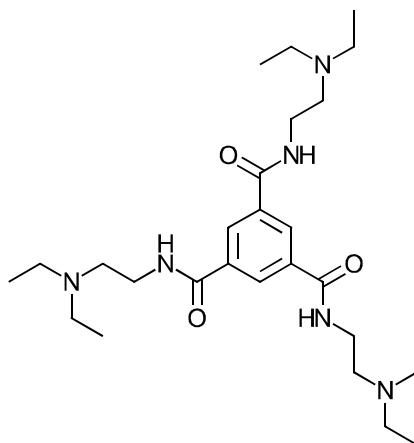


**Figure 3.3.1.** Chemical structure of *N*<sup>1</sup>,*N*<sup>3</sup>,*N*<sup>5</sup>-tris[2-(diethylamino)-ethyl]-1,3,5-benzenetricarboxamide.

Moderate changes in the structure of the molecule resulted in a pronounced difference in the solubility in aqueous media. The solubility in water decreases with increasing length of the alkyl groups from more than 150 g L<sup>-1</sup> to 100 g L<sup>-1</sup> and less than 0.01 g L<sup>-1</sup> for the BTA with *N,N*-dimethyl, *N,N*-diethyl and *N,N*-di-*n*-propyl groups, respectively. No self-assembly of all three BTAs was observed at room temperature or for the most common method upon cooling.

<sup>[1]</sup> A. Frank, A. Bernet, K. Kreger, H.-W. Schmidt. *Supramolecular microtubes based on 1,3,5-benzenetricarboxamides prepared by self-assembly upon heating*, *Soft Matter* **2020**, 16, 4564–4568. The full reprint of this publication can be found in **Chapter 4.2**.

Surprisingly, by heating aqueous solutions of the BTA with *N,N*-diethyl groups clouding of the entire sample was observed. This process is fully reversible upon cooling the solution. This phenomenon was not observed for the BTAs with *N,N*-dimethyl and *N,N*-di-*n*-propyl groups. Hence, this unique behavior of the BTA with *N,N*-diethyl groups was investigated in detail. Different concentrations between 1 and 100 g L<sup>-1</sup> of the BTA with *N,N*-diethyl groups were prepared in aqueous media at room temperature and the transmission during heating and cooling of the samples was recorded to investigate the cloud and clearing behavior of the solutions. **Figure 3.3.2A** shows the concentration-dependent development of the cloud and clearing points upon heating and upon cooling. With increasing concentration of the BTA, the cloud and clearing point temperatures decrease and level off above a concentration of 50 g L<sup>-1</sup>. A small hysteresis between the cloud and clearing points can be observed, which indicates a fast self-assembly and disassembly behavior.

Temperature-dependent polarizing optical microscopy studies, as shown in **Figure 3.3.2B–G**, reveal a two-step process. A clear aqueous solution of the BTA with *N,N*-diethyl groups with a concentration of 20 g L<sup>-1</sup> was heated from room temperature (B) to 80 °C. Upon heating, a liquid–liquid phase separation occurs at 33 °C (C). With increasing temperature, the phase separation is more visible and the self-assembly of fiber-like structures occurs (D). Further increasing in temperature lead to a depletion zone close to the fibers (E) and the fibers increase in length (several hundred μm) and thickness (a few μm) due to the consumption of the phase-separated droplets (G). Upon cooling, the supramolecular fibers disassemble and a clear solution is obtained again. This finding also holds for different BTA concentrations. Only the self-assembly temperature varies slightly.

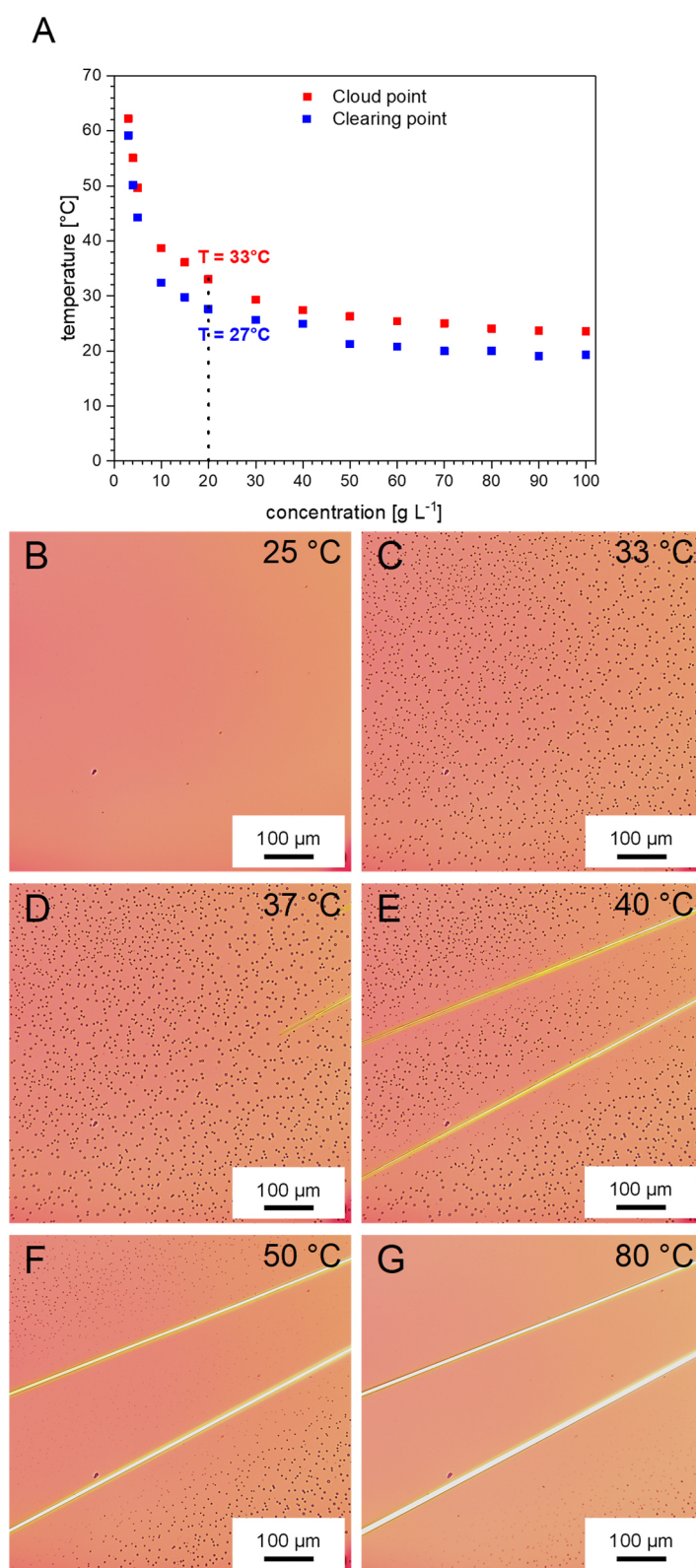


**Figure 3.3.2.** (A) The BTA with *N,N*-diethyl groups shows a concentration-dependent development of the cloud and clearing points upon heating/cooling aqueous solutions. (B)–(G) Sequence of polarized optical micrographs of the BTA with *N,N*-diethyl groups with a concentration of 20 g L<sup>-1</sup> in water. Heating the sample with a heating rate of 1 K min<sup>-1</sup> from 25 °C to 80 °C reveals a two-step process. First, a phase separation of the solution is observed, followed by self-assembly of the BTA into supramolecular fiber-like structures. Reproduced from Ref. <sup>[1]</sup> with permission from the Royal Society of Chemistry (© 2020).

Furthermore, by evaporation of the solvent at elevated temperatures, it is possible to isolate these supramolecular fiber-like structures. **Figure 3.3.3** shows an optical and a scanning electron micrograph of isolated supramolecular structures, which reveal a hexagonal shape and the microtubular morphology.

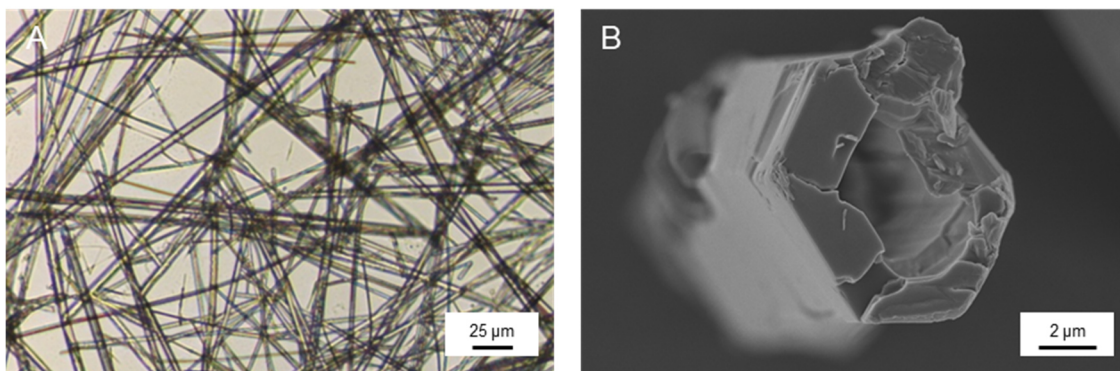


**Figure 3.3.3.** Isolated supramolecular structures. A) Optical image of isolated supramolecular structures and B) scanning electron image of an isolated supramolecular microtubule. Adapted and reproduced from Ref. <sup>[1]</sup> with permission from the Royal Society of Chemistry (© 2020).

In summary, the variation of the length of the alkyl groups at the tertiary amino substituents of this series of BTAs, the hydrophilicity of the molecule and thus the solubility is strongly affected. For the first time, a unique two-step self-assembly behavior upon heating aqueous solutions of the BTA with *N,N*-diethyl groups was found. Here, a liquid-liquid phase separation occurs, which is followed by the self-assembly towards supramolecular structures in the form of microtubes. This functional tertiary amino-containing BTA is promising for reversible application systems in aqueous media for catalysis.

### 3.4. Hierarchical superstructures

To prepare defined hierarchical superstructures, the combination of crystallization-driven self-assembly of triblock terpolymers to patchy worm-like micelles and the molecular self-assembly of functional BTAs with tertiary amino substituents to fiber-like supramolecular structures was investigated.

#### 3.4.1 Crystallization-driven self-assembly of triblock terpolymers towards patchy worm-like micelles

The crystallization-driven self-assembly (CDSA), which was introduced in **Chapter 1.1**, of triblock terpolymers allows, under appropriate conditions, the preparation of patchy worm-like micelles (**Figure 3.4.1**).

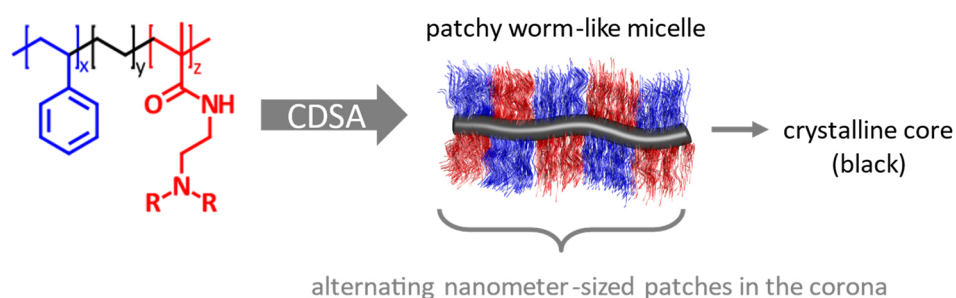


**Figure 3.4.1.** Schematic illustration of patchy worm-like micelles prepared by crystallization-driven self-assembly (CDSA) of triblock terpolymers. The triblock terpolymer is composed of a polyethylene middle block which is the driven force for the self-assembly process. The two outer polymer blocks are polystyrene and a functional tertiary amino-containing polymer. This composition of the triblock terpolymer results under appropriate self-assembly conditions in defined patchy worm-like micelles with a crystalline core and alternating nanometer-sized patches of polystyrene and tertiary amino groups in the corona.

To achieve defined patchy worm-like micelles with controlled size and size distribution in solution, a crystallizable polymer middle block like polyethylene (PE) is used. The middle position of the PE block is a prerequisite since this triggers the one-dimensional growth. Briefly, the triblock terpolymer is dissolved in a good solvent like tetrahydrofuran for PE at elevated temperatures. Upon cooling, a small number of micelles with a crystalline PE core are obtained. The self-assembly process occurs by cooling to the crystallization temperature of the PE block. The molecularly dissolved block copolymers with a crystallizable block (unimers) are deposited onto these crystalline micelles resulting in patchy worm-like micelles with

increasing time. The two outer blocks of the triblock terpolymer are composed of different polymers, whereas one block is polystyrene and the other block bears peripheral functional tertiary amino groups representing the patches in the corona.

### 3.4.2 Patchy micelles immobilized on supporting polymer fibers<sup>[II, III, IV]</sup>

Defined one-dimensional patchy nanostructures are interesting materials for applications as carriers for nanoparticles due to their excellent interfacial activity. To use these patchy nanostructures, the immobilization on a supporting polymer fiber or supporting polymer nonwoven is beneficial.

Within the thesis, the collaboration with the chair of Macromolecular Chemistry II at the University of Bayreuth led to a publication where triblock terpolymers were assembled into patchy micelles with different shapes by crystallization-driven self-assembly. The used triblock terpolymers consist of three blocks i) polystyrene (PS), ii) polyethylene (PE) and iii) functional poly(*N,N*-dialkylaminoethyl methacrylamide), where dialkyl groups of methyl or isopropyl were used. The shape of the patchy micelles depends on the solvent used for self-assembly. A bad solvent for the crystallizable PE middle block leads to the formation of patchy micelles with a spherical shape. A good solvent for the PE middle block leads to the formation of patchy worm-like micelles.

These patchy worm-like micelles can be immobilized on supporting polymer fibers via coaxial electrospinning to create patchy polymer fibers as nonwoven, as exemplary shown in **Figure 3.4.2**. The patchy worm-like micelles exhibit a crystalline PE core with pendant alternating nanometer-sized PS patches and patches containing tertiary amino groups in the corona. The PS patches guarantee adhesion to the supporting PS fibers and the amino patches enable functionalization. The patchy micelles on top of the supporting PS fibers could be identified by scanning electron microscopy without sputtering the samples by employing the special beam deceleration mode.<sup>[IV]</sup>

---

<sup>[II]</sup> A. Frank, C. Hils, M. Weber, K. Kreger, H. Schmalz, H.-W. Schmidt. *Hierarchical Superstructures by Combining Crystallization-Driven and Molecular Self-Assembly*, *Angew. Chem. Int. Ed.* **2021**, 60, 21767–21771.

<sup>[III]</sup> A. Frank, M. Weber, C. Hils, U. Mansfeld, K. Kreger, H. Schmalz, H.-W. Schmidt. *Functional Mesostructured Electrospun Polymer Nonwovens with Supramolecular Nanofibers*, *Macromol. Rapid Commun.* **2022**, 43, 2200052, 1–8.

<sup>[IV]</sup> C. Hils, M. Dulle, G. Sitaru, S. Gekle, J. Schöbel, A. Frank, M. Drechsler, A. Greiner, H. Schmalz. *Influence of patch size and chemistry on the catalytic activity of patchy hybrid nonwovens*, *Nanoscale Adv.* **2020**, 2, 438–452.

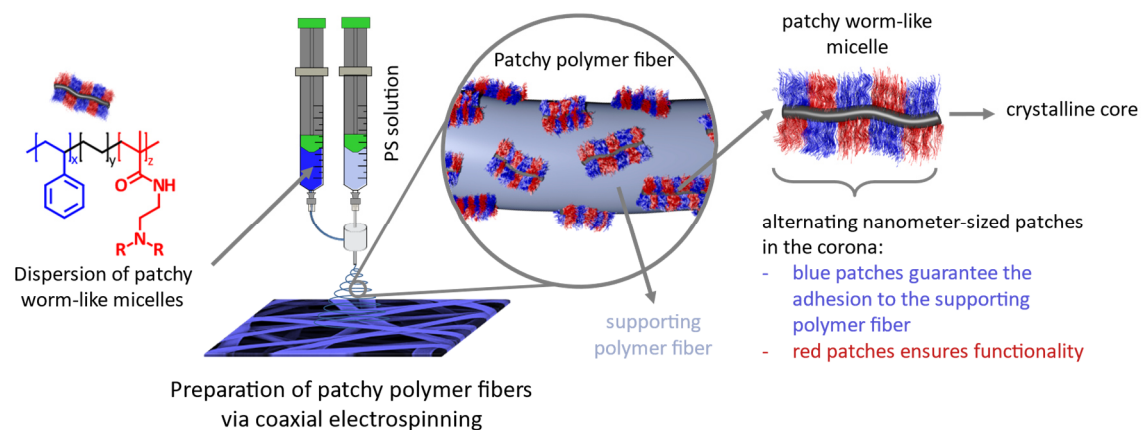


**Figure 3.4.2.** Schematic illustration of patchy polymer fibers and their preparation. The patchy polymer fibers consist of a supporting polymer fiber and patchy worm-like micelles. The patchy worm-like micelles are composed of a triblock terpolymer, comprising a semi-crystalline middle block and alternating nanometer-sized patches where one patch guarantees the adhesion to the supporting polymer fiber and the other one bearing functional tertiary amino groups. Adapted from Ref. <sup>[1]</sup>. Parts of this figure are published by Wiley-VCH GmbH under the terms of the Creative Commons Attribution 4.0 International License (© 2021 The Authors).

Furthermore, it was shown that the patchy polymer nonwovens could be functionalized with gold nanoparticles (AuNPs). The functional amino patches in the corona of the patchy micelles act as anchor groups for the AuNPs. The shape (spherical or worm-like) of these patchy micelles, the size of the patches and the chemistry (different tertiary amino groups) of the functional patches were investigated regarding the heterogeneous catalytic activity in the gold nanoparticle catalyzed alcoholics of dimethylphenylsilane in *n*-butanol.<sup>[IV]</sup>

<sup>[IV]</sup> C. Hils, M. Dulle, G. Sitaru, S. Gekle, J. Schöbel, A. Frank, M. Drechsler, A. Greiner, H. Schmalz. *Influence of patch size and chemistry on the catalytic activity of patchy hybrid nonwovens*, *Nanoscale Adv.* **2020**, *2*, 438–452.



### 3.4.3 Hierarchical superstructures by combining crystallization-driven and molecular self-assembly<sup>[1]</sup>

The aim was the preparation of defined hierarchical superstructures by combining two self-assembly concepts, namely the crystallization-driven self-assembly of triblock terpolymers to patchy worm-like micelles and the molecular self-assembly of functional BTAs to fiber-like structures. The chemical structure of the functional BTA with *N,N*-dimethyl substituents used in this study is shown in **Figure 3.4.3**.

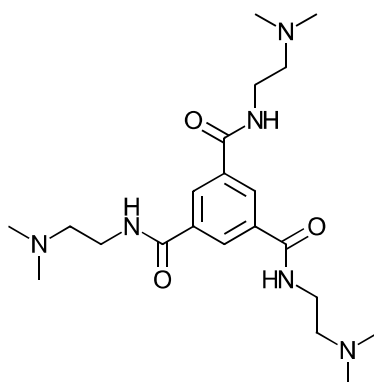


**Figure 3.4.3.** Chemical structure of *N*<sup>1</sup>,*N*<sup>3</sup>,*N*<sup>5</sup>-tris[2-(dimethylamino)-ethyl]-1,3,5-benzenetricarboxamide.

To prepare defined hierarchical superstructures, the molecular self-assembly of tertiary amino-containing BTAs from a polymer fiber surface decorated with functional chemical matching patchy worm-like micelles were investigated. For this, patchy worm-like micelles were prepared by crystallization-driven self-assembly and attached to a supporting polystyrene (PS) fiber via coaxial electrospinning (**Figure 3.4.4A**). The worm-like micelles consist of the triblock terpolymer of polystyrene-*block*-polyethylene-*block*-poly(*N,N*-dimethylaminoethyl methacrylamide) (SEDMA). The patchy worm-like micelles have a crystalline polyethylene core with pendant alternating nanometer-sized PS and functional poly(*N,N*-dimethylaminoethyl methacrylamide) (PDMA) patches in the corona. The PS patches guarantee a good adhesion to the supporting PS fibers and the functional amino patches represent the possibility for functionalization and, thus, the initiation of supramolecular BTA fiber growth.

<sup>[1]</sup> A. Frank, C. Hils, M. Weber, K. Kreger, H. Schmalz, H.-W. Schmidt. *Hierarchical Superstructures by Combining Crystallization-Driven and Molecular Self-Assembly*, *Angew. Chem. Int. Ed.* **2021**, 60, 21767–21771. The full reprint of this publication can be found in **Chapter 4.3**.



The BTA with peripheral *N,N*-dimethyl groups (**Figure 3.4.4B**) was selected for the combination with the polymer fibers with patchy worm-like micelles for several reasons. This BTA shows a very high solubility in water at room temperature. Furthermore, no self-assembly in solution, whether upon cooling, upon heating, or upon aging at room temperature the aqueous solution, can be induced under these conditions. This allows immersing of the polymer fibers with patchy worm-like micelles into stable aqueous BTA solutions at room temperature. The concentration of the BTA was chosen in a way that the molecular self-assembly of the BTA is only induced upon solvent evaporation, that is an increase in concentration. Most important, the used BTA with peripheral tertiary amino groups shows a chemical matching with the tertiary amino groups in the methacrylamide patches, which determines the swelling in water and the accessibility of the patches for the water-soluble molecular BTA building blocks.

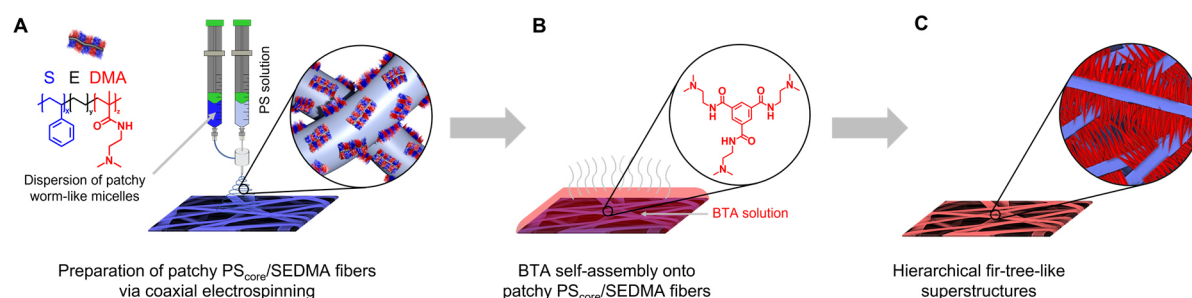


**Figure 3.4.4.** Schematically illustration for the preparation of hierarchical superstructures. A) The dispersion of patchy worm-like polystyrene-*block*-polyethylene-*block*-poly(*N,N*-dimethylaminoethyl methacrylamide) (SEDMA) triblock terpolymer micelles were coaxial electrospun on supporting polystyrene (PS) fibers to prepare patchy PS<sub>core</sub>/SEDMA fibers. B) The prepared patchy polymer fibers were immersed into an aqueous solution containing the BTA with *N,N*-dimethyl groups. Subsequent evaporation leads to the patch-mediated molecular self-assembly of the BTA onto the patchy polymer fibers and C) results in a hierarchical fir-tree-like superstructure. Reproduced from Ref. [11]. Published by Wiley-VCH GmbH under the terms of the Creative Commons Attribution 4.0 International License (© 2021 The Authors).

After immersion of the polymer fibers decorated with patchy worm-like micelles into the aqueous BTA solution and subsequent solvent evaporation, hierarchical fir-tree-like superstructures can be observed (**Figure 3.4.4C**). The self-assembly of the BTA is promoted by the patchy worm-like micelles. The formation of hierarchical superstructures is initiated by the local increase in BTA concentration close to the patches due to the chemical match and results in the molecular self-assembly after reaching a threshold concentration. A scanning

electron micrograph of the obtained hierarchical fir-tree-like superstructures is depicted in **Figure 3.4.5A**. It can be clearly seen that defined short supramolecular BTA fibers are grown away from the patchy polymer fiber in a controlled way. This is further confirmed in the respective Raman image in **Figure 3.4.5B**. The polymer fiber is colored in blue and the supramolecular BTA fibers are colored in red.

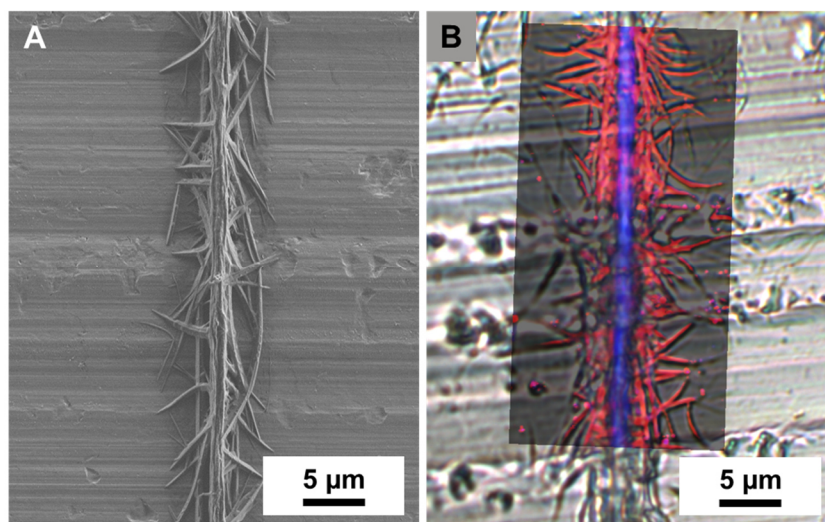


**Figure 3.4.5.** A) Scanning electron image of the hierarchical superstructure prepared by patch-mediated molecular self-assembly and B) the spatially resolved component distribution from Raman and optical microscopy imaging. The PS-rich regions are colored in blue and supramolecular BTA-rich regions are colored in red. Adapted and reproduced from Ref. [11]. Published by Wiley-VCH GmbH under the terms of the Creative Commons Attribution 4.0 International License (© 2021 The Authors).

The chemical match of the peripheral groups of the BTA with the tertiary amino substituents of the patchy worm-like micelles is essential to initiate the patch-mediated molecular self-assembly of the BTA towards hierarchical superstructures. Similar chemical groups also determine the solubility and accessibility of the patch for the molecular building blocks. The used BTA shows a very good solubility in water. This is also known for the homopolymer PDMA, which is the functional block of the patchy worm-like micelles. To prove that patches with a chemical match of the peripheral groups are necessary, reference experiments with the neat electrospun PS fibers and patchy polymer fibers with worm-like micelles composed of the triblock terpolymer polystyrene-*block*-polyethylene-*block*-poly(methyl methacrylate) (SEM) with hydrophobic poly(methyl methacrylate) patches are conducted. In both cases, no controlled molecular self-assembly of the BTA was observed and only an accumulation of

unstructured BTA assemblies near the polymer fibers was observed (**Figure 3.4.6**). Hence, defined hierarchical superstructures are only obtained by choosing the chemical match of the patches of the triblock terpolymer and the peripheral groups of the BTA.

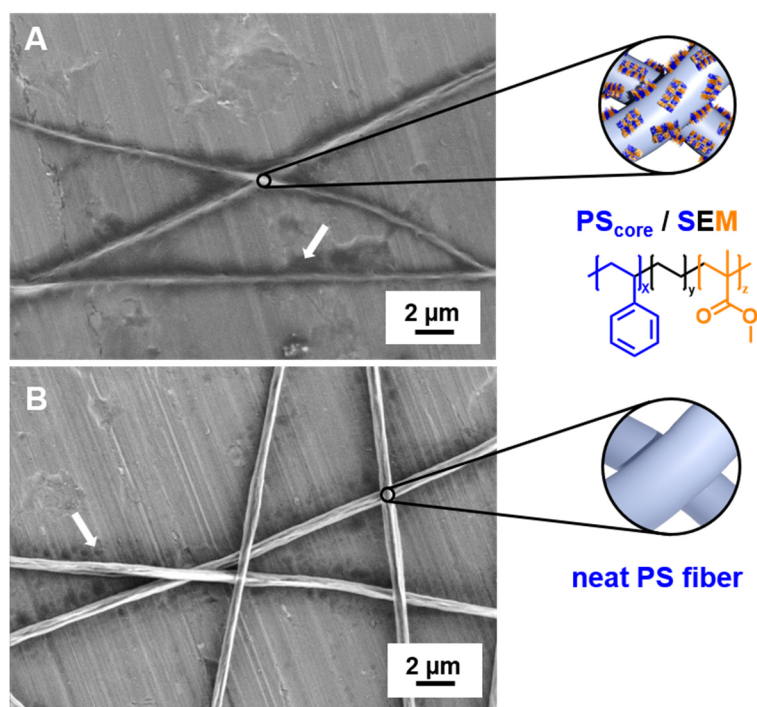


**Figure 3.4.6.** Reference experiments with A) hydrophobic micelles composed of the triblock terpolymer polystyrene-*block*-polyethylene-*block*-poly(methyl methacrylate) (SEM) and B) only with the supporting PS fibers without patchy worm-like micelles. Both scanning electron micrographs reveal the absence of hierarchical superstructures. Reproduced from Ref. [11]. Published by Wiley-VCH GmbH under the terms of the Creative Commons Attribution 4.0 International License (© 2021 The Authors).

### 3.5. Functional mesostructured electrospun polymer nonwovens with supramolecular nanofibers<sup>[iii]</sup>

Increasing the hierarchical level towards complex fiber morphologies with functionality widely expands the application possibilities. For example, complex fiber morphologies with a functional surface can be used as carriers for catalysis applications.

The goal was to create and utilize a complex hierarchical superstructure with functional supramolecular BTA fibers for the immobilization of metal nanoparticles from water. Using single polymer fibers featured with patchy worm-like micelles hinders the usability of applications. Therefore, polymer fibers with patchy worm-like micelles were prepared as nonwovens to transfer this approach to create three-dimensional hierarchically mesostructured nonwovens. For this, the concept of patch-mediated molecular self-assembly was investigated by different combinations of tertiary amino-containing BTA derivatives and appropriate patchy worm-like micelles immobilized on electrospun nonwovens. The BTA as molecular building block needs to be selected based on different criteria since the formed supramolecular structures should not disintegrate in aqueous media. For example, the BTA with *N,N*-dimethyl groups is not suited due to the very high water solubility. In contrast, the BTA with *N,N*-di-isopropyl groups shows no solubility in water. The chemical structure of the BTA with *N,N*-di-isopropyl groups is shown in **Figure 3.5.1**.

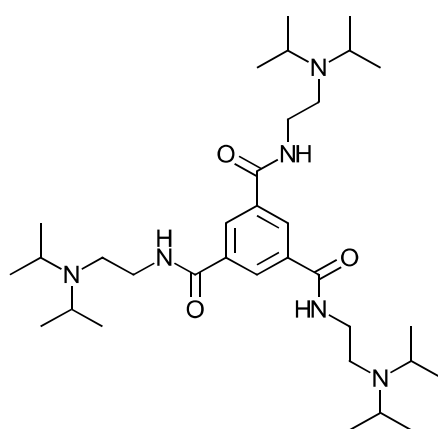


**Figure 3.5.1.** Chemical structure of  $N^1,N^3,N^5$ -tris[2-(diisopropylamino)-ethyl]-1,3,5-benzenetricarboxamide.

<sup>[iii]</sup> A. Frank, M. Weber, C. Hils, U. Mansfeld, K. Kreger, H. Schmalz, H.-W. Schmidt. *Functional Mesostructured Electrospun Polymer Nonwovens with Supramolecular Nanofibers*, *Macromol. Rapid Commun.* **2022**, 43, 2200052, 1–8. The full reprint of this publication can be found in **Chapter 4.4**.

Detailed solubility and self-assembly studies for the BTA with *N,N*-di-isopropyl groups at various concentrations in isopropanol were conducted. A phase diagram was developed from temperature-dependent solubility measurements (**Figure 3.2.2**). From the phase diagram, it can be concluded that a stable and molecularly dissolved BTA solution at room temperature is obtained only in regime I for BTA concentrations below 0.75 wt.%.

The supporting polymer nonwoven is composed of polystyrene fibers and is resistant to polar solvents such as isopropanol. The electrospun polystyrene nonwovens with the appropriate patchy worm-like micelles composed of the triblock terpolymer polystyrene-*block*-polyethylene-*block*-poly(*N,N*-diisopropylaminoethyl methacrylamide) were immersed at room temperature in the molecularly dissolved BTA solutions from regime I to prepare hierarchically mesostructured nonwovens. The polystyrene patches are responsible for the adhesion to the supporting polystyrene nonwoven. The patch with the tertiary amino groups matches the peripheral substituents of the BTA, which promote the local increase of the BTA concentration near the patches and initiate the molecular self-assembly. The patchy worm-like micelles are also responsible for the fixation of the supramolecular nanofibers on the polystyrene nonwoven fibers. The resulting hierarchically mesostructured nonwovens for two selected BTA concentrations are shown in **Figure 3.5.2**. In both cases, the nonwoven composites feature short supramolecular nanofibers. The supramolecular fibers are on top or off-standing from the supporting polystyrene fibers of the nonwovens. A higher BTA concentration leads to longer supramolecular fibers.

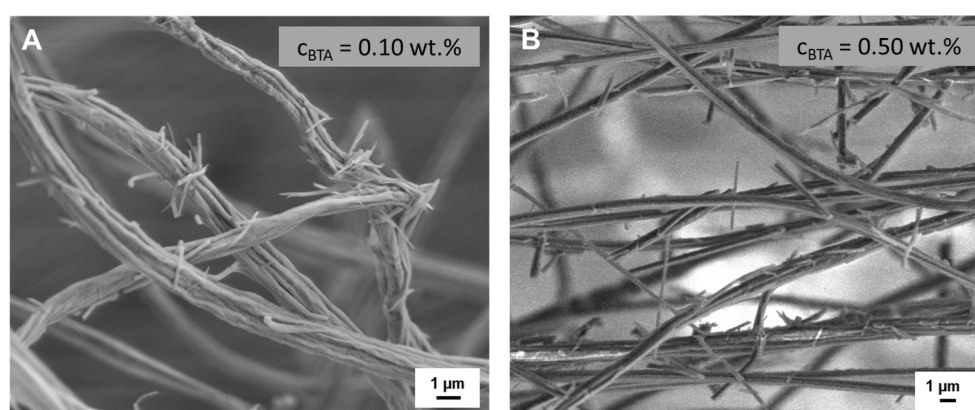


**Figure 3.5.2.** Scanning electron micrographs of hierarchically mesostructured nonwovens with functional supramolecular BTA nanofibers. Immersion of the patchy nonwovens at room temperature in BTA isopropanol solutions of different concentrations A) 0.10 wt.% and B) 0.50 wt.% and subsequent drying at ambient conditions lead to hierarchically mesostructured nonwovens. Adapted and reproduced from Ref. [10]. Published by Wiley-VCH GmbH under the terms of the Creative Commons Attribution 4.0 International License (© 2022 The Authors).

The prepared nonwovens were immersed in an aqueous palladium nanoparticle (PdNPs) dispersion to confirm the functionality of the hierarchically mesostructured nonwovens and, thus, the tertiary amino groups of the supramolecular nanofibers. The complex morphology of the hierarchical nonwoven keeps its shape after dipping into the aqueous nanoparticle dispersion. Successfully, single PdNPs can be observed on the surface of the functional supramolecular nanofibers proofing the functionality of the tertiary amino groups **(Figure 3.5.3)**.

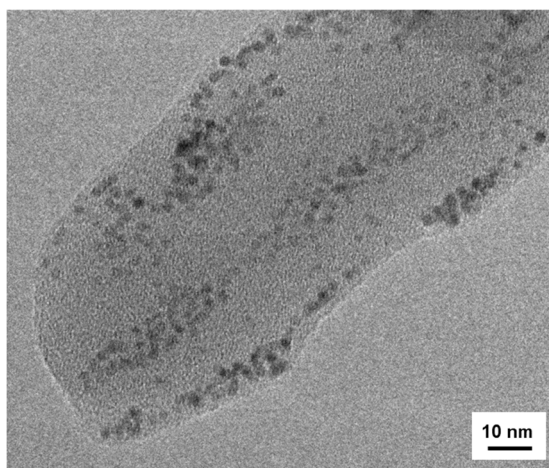


**Figure 3.5.3.** Transmission electron micrograph of immobilized palladium nanoparticles on the surface of a supramolecular BTA nanofiber. The hierarchically mesostructured nonwoven was mechanically broken for the sample preparation process. Adapted and reproduced from Ref. <sup>[111]</sup>. Published by Wiley-VCH GmbH under the terms of the Creative Commons Attribution 4.0 International License (© 2022 The Authors).

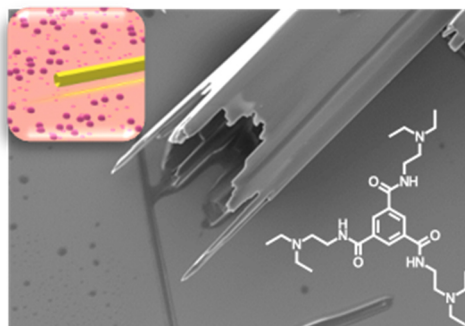
### 3.6. Overview of the publications of this thesis

This cumulative thesis is based on the following three publications.

**Publication 1: *Supramolecular microtubes based on 1,3,5-benzenetricarboxamides prepared by self-assembly upon heating***

A. Frank, A. Bernet, K. Kreger and H.-W. Schmidt.

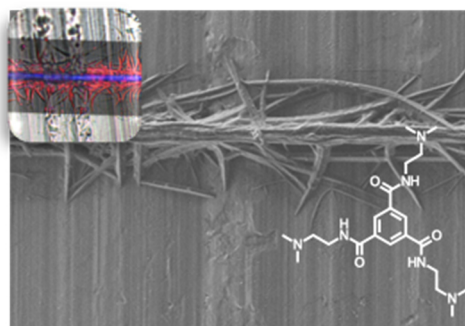
Soft Matter **2020**, 16, 4564–4568.



**Publication 2: *Hierarchical Superstructures by Combining Crystallization-Driven and Molecular Self-Assembly***

A. Frank, C. Hils, M. Weber, K. Kreger, H. Schmalz and H.-W. Schmidt.

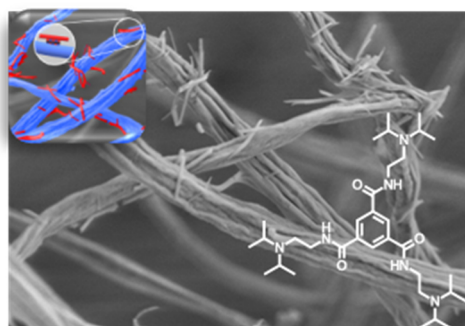
Angew. Chem. Int. Ed. **2021**, 60, 21767–21771.



**Publication 3: *Functional Mesostructured Electrospun Polymer Nonwovens with Supramolecular Nanofibers***

A. Frank, M. Weber, C. Hils, U. Mansfeld, K. Kreger, H. Schmalz and H.-W. Schmidt

Macromol. Rapid Commun. **2022**, 43, 2200052, 1–8.







## 4. Publications

### 4.1. Individual contributions to joint publications

The following section specifies the individual contributions of all authors. Work done by myself was carried out at the chair of Macromolecular Chemistry I of the University of Bayreuth and the Keylab Electron and Optical Microscopy of the Bavarian Polymer Institute under supervision of Prof. Dr. Hans-Werner Schmidt.

#### **Publication 1: Supramolecular microtubes based on 1,3,5-benzenetricarboxamides prepared by self-assembly upon heating**

Soft Matter **2020**, 16, 4564–4568.

A. Frank, A. Bernet, K. Kreger and H.-W. Schmidt.

This publication is published as communication article with detailed supplementary information. The focus is on the self-assembly behavior in water of a special 1,3,5-benzenetricarboxamide with tertiary amino substituents into supramolecular fiber-like structures in form of microtubes. Based on the preliminary experiments of one BTA with tertiary amino substituents by Andreas Bernet at the chair of Macromolecular Chemistry I, I further explored and extended his findings. I synthesized on a larger scale a series of 1,3,5-benzenetricarboxamides with tertiary amino substituents with alkyl groups of different lengths. I conducted the molecular and thermal characterization and the analysis of these compounds. I conducted all self-assembly experiments in various solvents. The cloud and clearing points of aqueous BTA solutions at different concentrations were determined by myself. In addition, I carried out temperature-dependent measurements with polarizing optical light microscopy and SEM measurements. I developed an experimental method to show for the first time the in situ disassembly of the supramolecular structures with the environmental scanning electron microscopy (ESEM) in water atmosphere at different temperatures. The first draft of the manuscript was written by me. Andreas Bernet contributed with the  $\mu$ DSC measurements and the figure of supramolecular microtubes by optical light microscopy. Klaus Kreger was involved in scientific discussions during the project. Hans-Werner Schmidt conceived the topic, supervised the project and contributed with helpful discussions. All authors were involved in finalizing the manuscript.

**Publication 2: Hierarchical Superstructures by Combining Crystallization-Driven and Molecular Self-Assembly**

Angew. Chem. Int. Ed. **2021**, 60, 21767–21771.

A. Frank, C. Hils, M. Weber, K. Kreger, H. Schmalz and H.-W. Schmidt.

This publication is a collaboration of the chairs Macromolecular Chemistry I and II. This work is published as communication article with detailed supplementary information. This publication utilizes for the first time the unique combination of two different self-assembly concepts, namely the crystallization-driven self-assembly of triblock terpolymers and the molecular self-assembly of BTAs. The aim was the preparation of defined hierarchical superstructures. Christian Hils and I contributed equally to this publication. We conceived the concept to combine these two self-assembly methods. Based on the results of numerous solubility and self-assembly experiments conducted by myself with various BTAs with tertiary amino substituents in different solvents and various concentrations, a suitable BTA to achieve the goal of this publication was identified. Melina Weber performed additional self-assembly studies. The characterization by SEM was conducted by me. Christian Hils prepared polymer fibers with patchy worm-like micelles on the surface via coaxial electrospinning. Holger Schmalz performed the RAMAN measurements. The first draft of the manuscript was written by me. Klaus Kreger was the whole time involved in scientific discussions of the experiments and the manuscript preparation. Holger Schmalz and Hans-Werner Schmidt supervised the project. They were involved in scientific discussions and contributed to the manuscript. All authors were involved in finalizing the manuscript.

This publication was also translated into German with the title *Hierarchische Überstrukturen durch Kombination von kristallisationsinduzierter und molekularer Selbstassemblierung*. The German edition is published in Angew. Chem. **2021**, 133, 21935-21939.

**Publication 3: Functional Mesostructured Electrospun Polymer Nonwovens with Supramolecular Nanofibers**

Macromol. Rapid Commun. **2022**, 43, 2200052, 1–8.

A. Frank, M. Weber, C. Hils, U. Mansfeld, K. Kreger, H. Schmalz and H.-W. Schmidt

The preparation of hierarchically functional mesostructured nonwovens is published as research article with more detailed supplementary information. The focus of this publication was to further expand the concept of combining the crystallization-driven self-assembly of triblock terpolymers and the molecular self-assembly of BTAs. Here, an electrospun nonwoven was used for the self-assembly in isopropanol to allow applications in aqueous media. Christian Hils prepared the polymer fibers and polymer nonwovens decorated with patchy worm-like micelles via coaxial electrospinning. For this, a special BTA was required to fulfill processing from non-aqueous solutions resulting in water stable supramolecular structures. I conducted various experiments with respect to the solubility and self-assembly of BTAs with tertiary amino substituents. Synthesis, molecular characterization and thermal analysis of the identified BTA was carried out by myself. The cloud and clearing points of this BTA at different concentrations was jointly measured with Melina Weber. All self-assembly experiments in solution and upon solvent evaporation as well as the preparation method for the functional hierarchically mesostructured nonwovens of this BTA, were mainly conducted by me and supported by Melina Weber. I performed all SEM measurements, including the analysis. Christian Hils synthesized the nanoparticles. Ulrich Mansfeld conducted the TEM measurements. The first draft of the manuscript was written by me. Klaus Kreger and Holger Schmalz were involved in several scientific discussions during this work and finalizing the manuscript. Hans-Werner Schmidt supervised the project and contributed with helpful scientific discussions and the preparation of the manuscript.



4.2. Supramolecular microtubes based on 1,3,5-benzenetricarboxamides prepared by self-assembly upon heating



***Supramolecular microtubes based on 1,3,5-benzenetricarboxamides prepared by self-assembly upon heating***

Andreas Frank, Andreas Bernet, Klaus Kreger and Hans-Werner Schmidt\*

Macromolecular Chemistry, Bavarian Polymer Institute (BPI), University of Bayreuth, Universitätsstraße 30, 95447 Bayreuth, Germany.

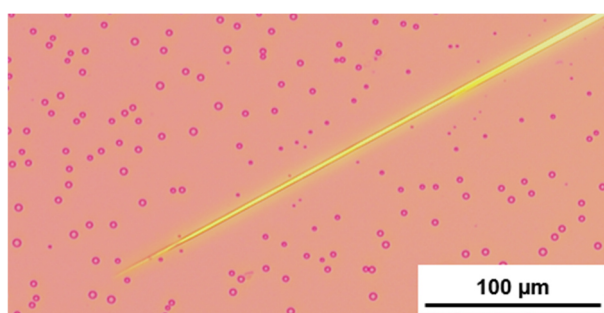
\*E-mail: hans-werner.schmidt@uni-bayreuth.de

The results of this chapter have been published as a communication article in *Soft Matter* **2020**, 16, 4564–4568. DOI: 10.1039/d0sm00268b.

Reproduced with permission from the Royal Society of Chemistry (© 2020).

Electronic supplementary information (ESI) available: Experimental details, characterization by FT-IR, DSC,  $\mu$ DSC, X-ray, SEM and additional figures. See DOI: 10.1039/d0sm00268b.

**Graphical abstract**



1,3,5-Benzenetricarboxamides with peripheral tertiary *N,N*-diethyl-ethylamino substituents shows a unique self-assembly behavior upon heating aqueous solutions to supramolecular microtubes.

A series of three 1,3,5-benzenetricarboxamides with peripheral tertiary *N,N*-dialkyl-ethylamino substituents with different length of the alkyl groups is reported. In particular, the *N*<sup>1</sup>,*N*<sup>3</sup>,*N*<sup>5</sup>-tris[2-(diethylamino)-ethyl]-1,3,5-benzenetricarboxamide exhibits phase separation followed by self-assembly upon heating from aqueous solution into well-defined supramolecular fiber-like structures in the form of microtubes.

Supramolecular chemistry utilizes noncovalent interactions between the constituent molecular building blocks to form well-defined supramolecular nano and microstructures. The preparation of supramolecular structures *via* a bottom-up approach holds great potential in view of applications. In this context, 1,3,5-benzenetrisamides (BTAs) are one of the most prominent supramolecular building blocks to prepare self-assembled micro and nanostructures.<sup>1</sup> This includes for example thickeners or gelators,<sup>2,3</sup> nucleating and clarifying agents for semi-crystalline polymers<sup>4-8</sup> and supramolecular nanofibers for air filtration applications.<sup>9,10</sup>

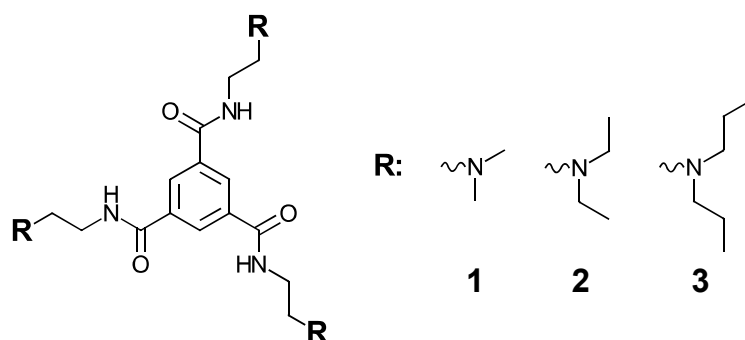
Whereas typically organic media are used to achieve supramolecular structures, only a few 1,3,5-benzenetrisamide systems are known, which allows for a structure formation from water and water mixtures upon cooling, solvent evaporation or pH change. For example, Palmans *et al.* synthesized 1,3,5-benzenetricarboxamides with pyridyl substituents and investigated the crystal structure.<sup>11</sup> With this compound, hydrogels can be prepared from a mixture of water with MeOH, EtOH, DMSO or DMF upon cooling.<sup>12</sup> Shi *et al.* expanded this system to use the hydrogels as a matrix for biomineralization.<sup>13</sup> Terpyridyl substituents with Eu<sup>III</sup> ions were used by Kotova *et al.* to prepare luminescent gels from water/MeOH mixtures.<sup>14</sup> Meijer and co-workers have demonstrated that BTAs with hydrophobic aliphatic spacers and hydrophilic ethylene glycol units in the periphery can assemble into micrometer long thin nanofibers from water upon cooling.<sup>15-17</sup> Moreover, Huang *et al.* has shown that hexasulfonato-substituted BTAs can be used to realize ion-conducting membranes from aqueous solution.<sup>18</sup> Another approach for supramolecular nanostructure formation based on BTAs in aqueous media uses pH changes as an external trigger. In this context, we have shown that 1,3,5-benzenetricarboxamides with aromatic carboxylic acid side groups can be successfully used to prepare hydrogels by reducing the pH value.<sup>19</sup> This concept was extended by Howe *et al.* yielding a set of pH-sensitive hydrogelators.<sup>20</sup> Due to this pH-sensitivity, it is possible to reveal the self-assembly kinetics *via* microfluidics.<sup>21</sup> This type of molecules allows

also structuring of hydrogels with micrometer precision by AFM in combination with nanofluidics.<sup>22</sup>

The group of Besenius have developed amphiphilic dendritic BTAs, which are characterized by a multistimuli-responsive behavior in water. These BTAs forms hydrogels not only upon changing the pH, but also upon heating the aqueous solution.<sup>23</sup> Such thermo-responsive BTAs, which self-assemble upon heating, are very rare. Lee and Qi *et al.* demonstrated an another example of a thermo-responsive self-assembly by utilizing BTAs with peripheral crown ether or ethylene glycol units in water or mixtures of DMSO/water and MeOH/water depending on the crown ether size.<sup>24,25</sup> Upon heating, the quality of the solvent decreases with respect to the peripheral groups resulting in a separation of the water from the supramolecular building blocks. This approach makes use of the temperature-dependent phase separation of ethylene glycols or crown ether upon heating in water.<sup>26,27</sup> Another class of compounds featuring phase separation from water upon heating are low molecular weight amine derivatives.<sup>28</sup> Higher substitution of the amine increases the temperature sensitivity. A more pronounced phase separation is observed for branched secondary or tertiary amines containing five or six carbon atoms.<sup>29</sup>

Here we report on a study based on a series of three 1,3,5-benzenetrisamides with peripheral *N,N*-dialkyl-ethylamino substituents, namely with *N,N*-dimethyl **1**, *N,N*-diethyl **2** and *N,N*-dipropyl **3** moieties (**Scheme 1**). By varying these substituents, we found pronounced differences in the solubility behavior in water. We show that subtle structural variations of the periphery of these three benzenetricarboxamides have a strong impact on the self-assembly behavior in aqueous solution.





**Scheme 1** Chemical structures of the 1,3,5-benzenetricarboxamides, ( $N^1,N^3,N^5$ -tris[2-(dimethylamino)-ethyl]-1,3,5-benzenetricarboxamide) **1**, ( $N^1,N^3,N^5$ -tris[2-(diethylamino)-ethyl]-1,3,5-benzenetricarboxamide) **2**, and ( $N^1,N^3,N^5$ -tris[2-(dipropylamino)-ethyl]-1,3,5-benzenetricarboxamide) **3**.

To synthesize 1,3,5-benzenetricarboxamides with tertiary amine substituents, we selected a feasible and straightforward route in a similar manner as recently described by Robinson *et al.*<sup>30</sup> Conversion of trimesic trimethyl ester with *N,N*-dimethyl-ethylenediamine, *N,N*-diethyl-ethylenediamine or *N,N*-dipropyl-ethylenediamine resulted in the respective 1,3,5-benzenetricarboxamides **1–3**. Beneficially, this approach avoids hydrochloric acid formation, as it is typically formed if trimesic acid trichloride is used. Hydrochloric acid will result in ammoniumhydrochlorides of the peripheral side groups complicating the isolation of the product. Detailed information on the synthetic procedure and molecular characterization is given in **S1**, ESI.†

1,3,5-Benzenetrisamides are known to self-assemble due to the formation of three directed strands of hydrogen bonds into highly ordered columnar structures. Depending on the lengths and branching of the peripheral substituents high melting transitions are present and columnar mesophases can occur.<sup>4,31</sup> In this context, IR spectroscopy is a beneficial method to reveal a columnar stacking in bulk. We found for all three compounds IR signals at around  $3240\text{ cm}^{-1}$  (Amide A, N–H stretch vibrations), at around  $1640\text{ cm}^{-1}$  (Amide I, C=O stretch vibrations) and at around  $1560\text{ cm}^{-1}$  (Amide II, N–H bend and C–N stretch vibrations) (**Fig. S2**, ESI<sup>†</sup>), which are indicative for a columnar arrangement.<sup>32</sup> Differential scanning calorimetry (**Fig. S3**, ESI<sup>†</sup>) reveal for **1** upon heating one pronounced phase transition at  $212\text{ }^\circ\text{C}$ . Upon cooling, the transition occurs supercooled at  $188\text{ }^\circ\text{C}$ . This is indicative for a crystallization process. **2** and **3** also exhibit upon heating a pronounced phase transition at  $206\text{ }^\circ\text{C}$  and  $207\text{ }^\circ\text{C}$ , respectively. Upon cooling, the phase transition is for both at higher temperatures around  $200\text{ }^\circ\text{C}$  and less supercooling occurs. To distinguish between a crystalline

phase and a plastic crystalline phase, we performed temperature-dependent polarizing optical microscopy (POM) and investigated the phase behavior of compound **1–3** in bulk at 180 °C with and without shearing the sample (**Fig. S4.1**, ESI<sup>†</sup>). Whereas **1** has a brittle behaviour and fractures during shearing, thus confirming a crystalline phase, **2** show deformable structures, indicating a plastic crystalline phase. The findings for **2** is supported by XRD measurements (**Fig. S5.1**, ESI<sup>†</sup>). A similar behavior is found for **3** (**Fig. S4.1**, ESI<sup>†</sup>).

By varying the peripheral *N,N*-dialkyl-ethylamino substituents, we found a significant difference in the solubility behavior in water at ambient conditions. **1** with the *N,N*-dimethyl substituents features a very pronounced solubility in water at room temperature of more than 150 g L<sup>-1</sup>. **2** with the *N,N*-diethyl substituents has a solubility of up to 100 g L<sup>-1</sup>, whereas **3** with the *N,N*-dipropyl substituents has a very low solubility of less than 0.01 g L<sup>-1</sup>. At room temperature, no indication of self-assembly of all three compounds was observed. When heating aqueous solutions of **2** we found clouding of the entire sample. We attribute this to a decrease in solubility of the substituents with increasing temperature. Upon cooling, this process is fully reversible. This phenomenon is not observed for aqueous solutions of **1**. The solubility of **3** is not sufficiently increased at higher temperatures. Therefore, **2** was investigated in detail with respect to the clouding and clearing behavior at different concentrations. The concentration and temperature dependence of the cloud and clearing point of **2** was determined optically and parallel for 16 concentrations by means of a crystallization system. Concentrations between 1 and 100 g L<sup>-1</sup> of **2** in water were prepared at room temperature. Transmission of each sample was recorded for two heating and cooling cycles with a rate of 0.5 K min<sup>-1</sup> in the range from 5 to 80 °C. An example of the cloud and clearing point determination is described in **S6**, ESI.<sup>†</sup> Here, we determined cloud and clearing point at transmissions of 0% and 100%, respectively.

The concentration-dependent development of the cloud and clearing points of **2** in water is shown in **Fig. 1A**. The samples with a concentration of 1 and 2 g L<sup>-1</sup> of **2** did not show clouding under the applied conditions. At a concentration of 3 g L<sup>-1</sup> of **2** clouding was observed at around 62 °C upon heating. Upon cooling, a clear solution was obtained again at 59 °C, showing a small hysteresis between the cloud and clearing point. With increasing concentration of **2** upon heating the cloud point temperatures of the samples decrease rapidly and level off above a concentration of 50 g L<sup>-1</sup>. Here, the cloud points are around 25 °C. Upon

cooling, a similar progression was found for the development of the clearing points, at slightly lower temperatures.

Micro-differential scanning calorimetry ( $\mu$ DSC) measurements of an aqueous solution of **2** with a concentration of  $20 \text{ g L}^{-1}$  were conducted. **Fig. S7**, ESI<sup>+</sup> depicts the respective heating and cooling curves of the  $\mu$ DSC measurements determined at a very slow rate of  $0.1 \text{ K min}^{-1}$ . Upon heating, a smaller peak with an onset at about  $29 \text{ }^\circ\text{C}$  and a stronger peak with a maximum at  $36 \text{ }^\circ\text{C}$  are present revealing a two-step process. Two peaks are also visible upon cooling, demonstrating the reversibility. We note that the cloud and clearing points are in the same temperature range, but do not clearly correlate with one of these phase transitions upon heating and cooling, respectively.

To gain more insight into this two-step process, we performed temperature-dependent polarizing optical microscopy studies as shown in **Fig. 1B-G**. A clear aqueous solution of **2** with a concentration of  $20 \text{ g L}^{-1}$  was heated from  $25 \text{ }^\circ\text{C}$  (**B**) with a heating rate of  $1 \text{ K min}^{-1}$  to  $80 \text{ }^\circ\text{C}$ . While heating, a liquid–liquid phase separation occurs. At  $33 \text{ }^\circ\text{C}$  (**C**) this phase separation is clearly visible. At  $37 \text{ }^\circ\text{C}$  (**D**) this becomes increasingly pronounced and the formation of self-assembled fiber-like structures evolves. These fibers grow at the expense of the phase separated droplets resulting in a growing depletion zone close to the fibers (**E**). By further increasing the temperature, the supramolecular fibers become thicker due to consumption of the droplets (**G**). At this temperature, supramolecular fibers with a length of several hundred  $\mu\text{m}$  and diameters of a few  $\mu\text{m}$  are present. Independently of the heating rate ( $1, 5$  and  $10 \text{ K min}^{-1}$ ), the same behavior and morphology of the supramolecular fibers is observed (see **Fig. S4.2 – S4.4**, ESI<sup>+</sup>). Upon cooling, the fibers disassemble in all cases and a clear solution is obtained again. A similar behavior was found when performing the self-assembly experiments at different concentrations in the range from  $3$  to  $60 \text{ g L}^{-1}$ . Although the temperature at which self-assembly and disassembly occurs varies slightly, the morphology of the supramolecular structures are very comparable.

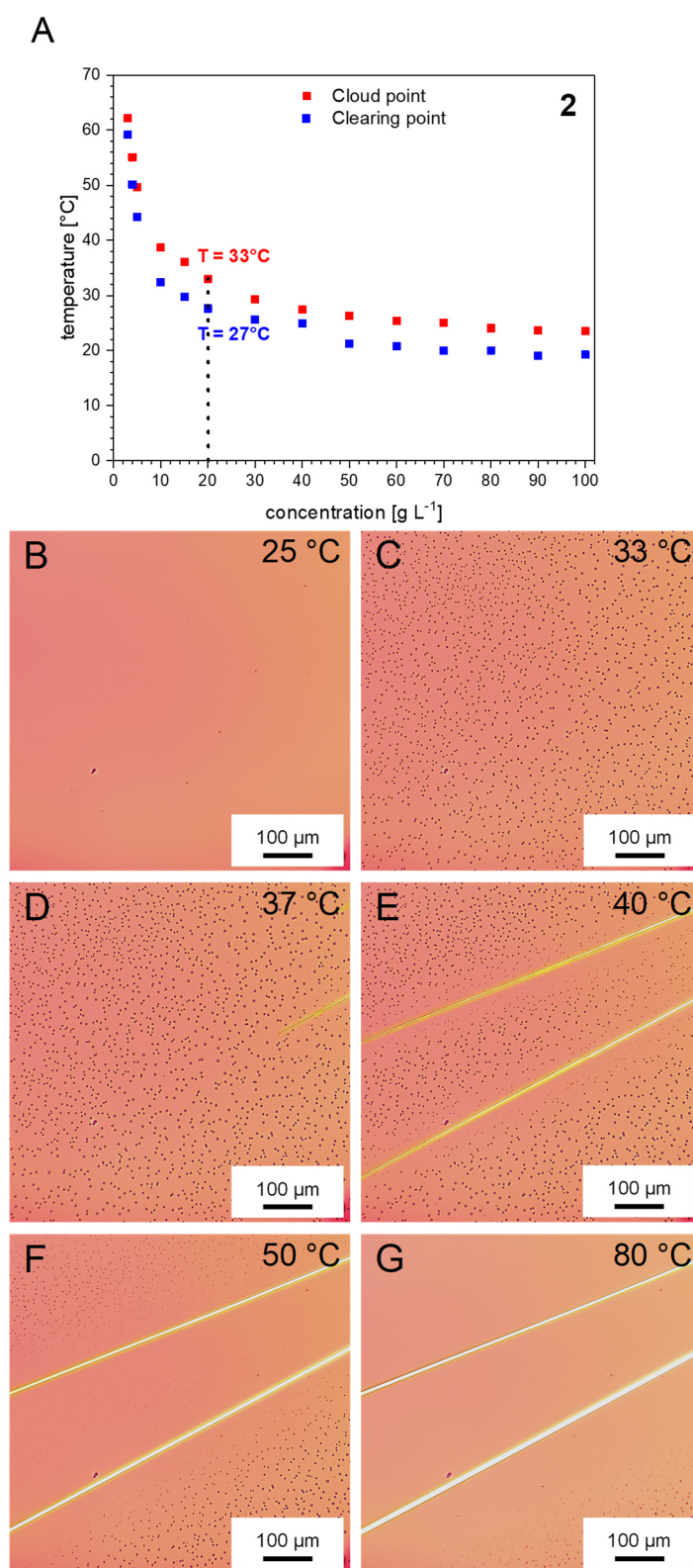


**Fig. 1** (A) Concentration-dependent development of the cloud and clearing point of **2** in water at heating and cooling rates of 0.5 K min<sup>-1</sup>. (B)–(G) Series of polarized optical micrographs with  $\lambda/4$  plate of 20 g L<sup>-1</sup> of **2** in water. Heating from 25 °C to 80 °C with a heating rate of 1 K min<sup>-1</sup> reveals phase separation of the solution followed by self-assembly of **2** into supramolecular fiber-like structures.

Moreover, X-ray powder diffraction (XRD) measurements of **2** in water with a concentration of  $20 \text{ g L}^{-1}$  were carried out at different temperatures, which are depicted in **Fig. S5.2**, ESI.† A sample of **2** at room temperature did not show any diffraction peaks, indicating a homogenous solution. Upon heating to  $40 \text{ }^\circ\text{C}$ , weak diffraction peaks were observed corresponding to the XRD peaks of the neat powder **2**. After subsequent cooling the sample to room temperature, no diffraction peaks are visible anymore, which also demonstrates the reversibility of the process.

In order to get a clearer picture of the *in situ* formation and disassembly of supramolecular structures, we additionally performed environmental scanning electron microscopy (ESEM). For this investigation,  $2 \text{ }\mu\text{L}$  of the clear solution of **2** in water with a concentration of  $20 \text{ g L}^{-1}$  was placed in the sample holder of a heating/cooling stage in the microscope at  $60 \text{ }^\circ\text{C}$ , shown in **Fig. S8A**, ESI.† The clear solution immediately turned turbid at this temperature, which is attributed to the formation of supramolecular fiber-like structures (**Fig. S8B** and **C**, ESI†). Subsequently, the sample holder was cooled stepwise from  $60 \text{ }^\circ\text{C}$  to  $1 \text{ }^\circ\text{C}$ . We found that the fiber-like structures are stable at  $60 \text{ }^\circ\text{C}$  (**Fig. 2A**) down to  $10 \text{ }^\circ\text{C}$  (**B**). The supramolecular structures started to disappear at around  $2 \text{ }^\circ\text{C}$  (**C**) and the structures are fully dissolved at  $1 \text{ }^\circ\text{C}$  (**D**). This behavior is also illustrated in a video in the ESI† (Video1\_BTA2-ESEM). Due to the different conditions in the ESEM chamber compared to ambient conditions, the transition temperatures are shifted to lower temperatures. Overall, all observations from the polarizing optical microscopy,  $\mu\text{DSC}$  and ESEM investigations confirm the reversibility of the self-assembly process.

An important point is that it is possible to isolate the supramolecular structures without damage by evaporation of the solvent at elevated temperatures. For isolating the structures, we dropped a small amount of a clear aqueous solution of **2** with a concentration of  $10 \text{ g L}^{-1}$  or  $20 \text{ g L}^{-1}$  on a glass slide or silicon wafer preheated to  $80 \text{ }^\circ\text{C}$  and evaporated the water completely at this temperature. The obtained isolated supramolecular structures and the fiber morphology were further investigated with optical microscopy and scanning electron microscopy (SEM). Uniform fiber-like structures with lengths of several hundreds of  $\mu\text{m}$  are visible, indicating a hollow nature (**Fig. 2E**). The isolated structures exhibit a mean diameter of  $4.7 \pm 1.6 \text{ }\mu\text{m}$  (**Fig. S9**, ESI†). Such supramolecular structures with a microtubular morphology based on BTAs, are very rare. One example was reported by Shi *et al.* with a BTA with pyridine substituents.<sup>33</sup> SEM micrographs of our isolated supramolecular structures reveal also a

hexagonal shape and clearly show the microtubular nature (**Fig. 2**). This is evident in the micrographs showing a respective end of supramolecular microtubes as grown (**F**), as fractured (**G**) and as cut by a focused ion beam (FIB) (**H**). It should be pointed out that these supramolecular microtubes are thermally stable up to the transition temperature to the isotropic melt at around 200 °C (**Fig. S3**, ESI<sup>†</sup>).

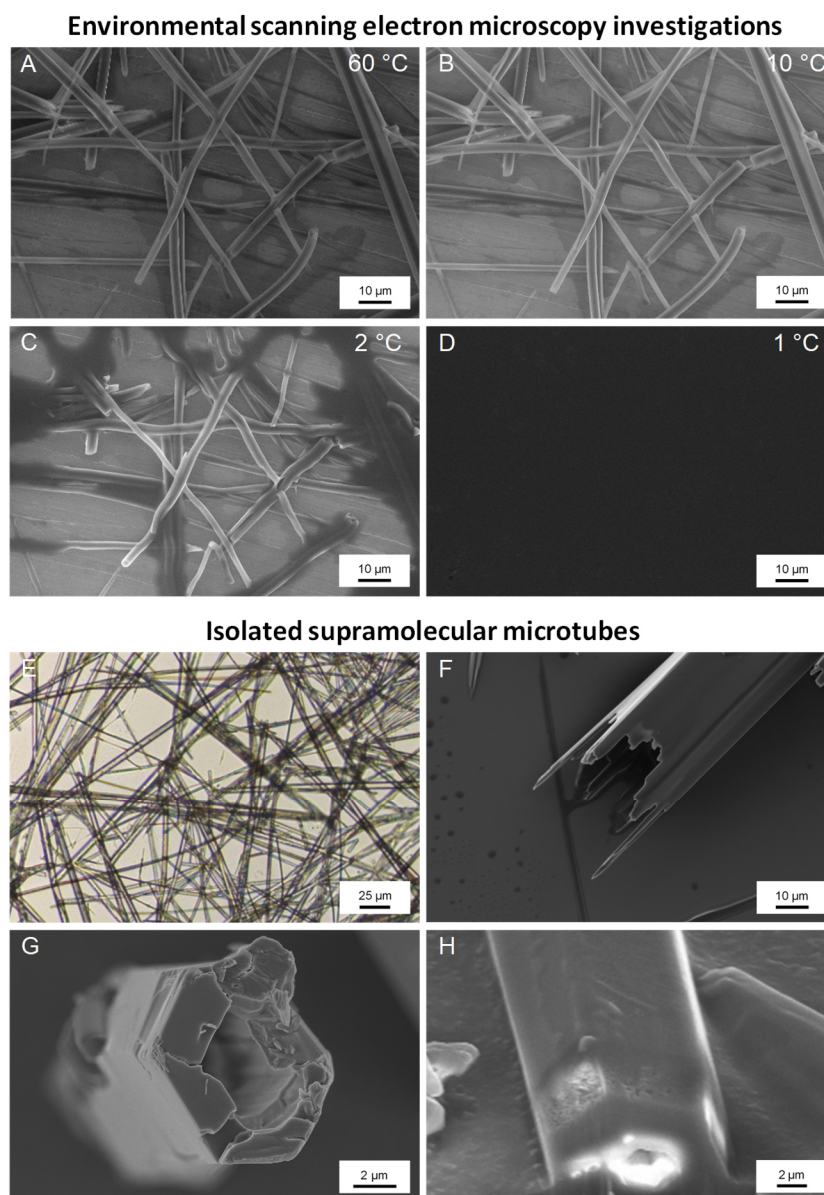


**Fig. 2** (A)–(D) Scanning electron micrographs of supramolecular structures of **2** at different temperatures measured in ESEM mode in water atmosphere, showing the disassembly of the fiber-like structures by reducing the temperature. (E) Optical micrograph of isolated supramolecular microtubes of **2** prepared by an aqueous solution of 10 g L<sup>-1</sup> on a glass substrate. (F)–(H) Scanning electron micrographs of supramolecular microtubes prepared from aqueous solution of **2** of 20 g L<sup>-1</sup> on silicon wafer. Magnifications of the respective end of supramolecular microtubes as grown (F), as fractured (G) and as cut by FIB (H).

## Conclusions

In conclusion, 1,3,5-benzenetricarboxamides with peripheral tertiary *N,N*-dialkyl-ethylamino substituents with different length of the alkyl groups allow to tune the solubility in water. We identified (*N*<sup>1</sup>,*N*<sup>3</sup>,*N*<sup>5</sup>-tris[2-(diethylamino)-ethyl]-1,3,5-benzenetricarboxamide) with a solubility up to 100 g L<sup>-1</sup> in water as most suitable system for a self-assembly process upon heating. We found that the quality of the solvent becomes increasingly worse when increasing the temperature and as consequence, a concentration-dependent clouding behavior is observed upon heating. This process was found to be reversible and clearing of the solution occurred upon cooling. Surprisingly, a two-step process, namely, a phase separation followed by a self-assembly process to fiber-like supramolecular structures was found. These structures can be isolated without damage during water evaporation at elevated temperatures, which we identified as well-defined microtubes. These findings may facilitate the development of reversible systems, which may be used as carriers for drug delivery in water or temperature-stable micro and nanocontainers and supports for catalysis.

## Conflicts of interest

There are no conflicts to declare.

## Acknowledgements

This work was financially supported by the German Research Foundation (DFG), Collaborative Research Center SFB840, project B8. AF thanks the Elite Study Program Macromolecular Science within the Elite Network of Bavaria (ENB) for support. The authors would like to thank Jutta Failner and Doris Hanft (Macromolecular Chemistry I, UBT) for their help with synthesis and characterization. Marina Behr and Steffen Czich are acknowledged for recording the XRD measurements. Hannah Kurz (Inorganic Chemistry IV, UBT) is acknowledged for carrying out the elemental analysis. The authors are indebted to Martina Heider and Werner Reichstein (Bavarian Polymer Institute) for their help with the SEM investigations.

**References\***

- [1] S. Cantekin, T. F. A. de Greef, A. R. A. Palmans.  
*Benzene-1,3,5-tricarboxamide: a versatile ordering moiety for supramolecular chemistry,*  
Chem. Soc. Rev. **2012**, 41, 6125–6137.
- [2] K. Hanabusa, C. Koto, M. Kimura, H. Shirai, A. Takehi.  
*Remarkable Viscoelasticity of Organic Solvents Containing Trialkyl-1,3,5-benzenetricarboxamides and Their Intermolecular Hydrogen Bonding,*  
Chem. Letters **1997**, 26, 429–430.
- [3] J. J. van Gorp, J. A. J. M. Vekemans, E. W. Meijer.  
*C<sub>3</sub>-Symmetrical Supramolecular Architectures: Fibers and Organic Gels from Discotic Trisamides and Trisureas,*  
J. Am. Chem. Soc. **2002**, 124, 14759–14769.
- [4] M. Blomenhofer, S. Ganzleben, D. Hanft, H.-W. Schmidt, M. Kristiansen, P. Smith, K. Stoll, D. Mäder, K. Hoffmann.  
*“Designer” Nucleating Agents for Polypropylene,*  
Macromolecules **2005**, 38, 3688–3695.
- [5] F. Abraham, H.-W. Schmidt.  
*1,3,5-Benzenetrisamide based nucleating agents for poly(vinylidene fluoride),*  
Polymer **2010**, 51, 913–921.
- [6] F. Richter, H.-W. Schmidt.  
*Supramolecular Nucleating Agents for Poly(butylene terephthalate) Based on 1,3,5-Benzenetrisamides,*  
Macromol. Mater. Eng. **2013**, 298, 190–200.
- [7] H. Nakajima, M. Takahashi, Y. Kimura.  
*Induced Crystallization of PLLA in the Presence of 1,3,5-Benzenetricarboxylamide Derivatives as Nucleators: Preparation of Haze-Free Crystalline PLLA Materials,*  
Macromol. Mater. Eng. **2010**, 295, 460-468.

---

\*The titles of the publications are included in this list of references.



- [8] H. Bai, W. Zhang, H. Deng, Q. Zhang, Q. Fu.  
*Control of Crystal Morphology in Poly(L-lactide) by Adding Nucleating Agent*,  
Macromolecules **2011**, 44, 1233–1237.
- [9] H. Misslitz, K. Kreger, H.-W. Schmidt.  
*Supramolecular Nanofiber Webs in Nonwoven Scaffolds as Potential Filter Media*,  
Small **2013**, 9, 2053–2058.
- [10] D. Weiss, D. Skrybeck, H. Misslitz, D. Nardini, A. Kern, K. Kreger, H.-W. Schmidt.  
*Tailoring Supramolecular Nanofibers for Air Filtration Applications*,  
ACS Appl. Mater. Interfaces **2016**, 8, 14885–14892.
- [11] A. R. A. Palmans, J. A. J. M. Vekemans, H. Kooijman, A. L. Spek, E. W. Meijer.  
*Hydrogen-bonded porous solid derived from trimesic amide*,  
Chem. Commun. **1997**, 22, 2247–2248.
- [12] D. K. Kumar, D. A. Jose, P. Dastidar, A. Das.  
*Nonpolymeric Hydrogelators Derived from Trimesic Amides*,  
Chem. Mater. **2004**, 16, 2332–2335.
- [13] N. Shi, G. Yin, M. Han, Z. Xu.  
*Anions bonded on the supramolecular hydrogel surface as the growth center of biominerals*,  
Colloids Surf., B **2008**, 66, 84–89.
- [14] O. Kotova, R. Daly, C. M. G. dos Santos, M. Boese, P. E. Kruger, J. J. Boland, T. Gunnlaugsson.  
*Europium-Directed Self-Assembly of a Luminescent Supramolecular Gel from a Tripodal Terpyridine-Based Ligand*,  
Angew. Chem., Int. Ed. **2012**, 51, 7208–7212.
- [15] C. M. A. Leenders, L. Albertazzi, T. Mes, M. M. E. Koenigs, A. R. A. Palmans, E. W. Meijer.  
*Supramolecular polymerization in water harnessing both hydrophobic effects and hydrogen bond formation*,  
Chem. Commun. **2013**, 49, 1963–1965.

- [16] C. M. A. Leenders, M. B. Baker, I. A. B. Pijpers, R. P. M. Lafleur, L. Albertazzi, A. R. A. Palmans, E. W. Meijer.  
*Supramolecular polymerisation in water; elucidating the role of hydrophobic and hydrogen-bond interactions,*  
Soft Matter **2016**, 12, 2887–2893.
- [17] N. M. Matsumoto, R. P. M. Lafleur, X. Lou, K.-C. Shih, S. P. W. Wijnands, C. Guibert, J. W. A. M. van Rosendaal, I. K. Voets, A. R. A. Palmans, Y. Lin, E. W. Meijer.  
*Polymorphism in Benzene-1,3,5-tricarboxamide Supramolecular Assemblies in Water: A Subtle Trade-off between Structure and Dynamics,*  
J. Am. Chem. Soc. **2018**, 140, 13308–13316.
- [18] Y. Huang, D. Wang, L. Xu, Y. Cong, J. Li, L. Li.  
*Multiscale fibers via supramolecular self-assembly of a fully rigid, discotic aromatic aramid molecule,*  
Eur. Polym. J. **2013**, 49, 1682–1687.
- [19] A. Bernet, R. Q. Albuquerque, M. Behr, S. T. Hoffmann, H.-W. Schmidt.  
*Formation of a supramolecular chromophore: a spectroscopic and theoretical study*  
Soft Matter **2012**, 8, 66–69.
- [20] R. C. T. Howe, A. P. Smalley, A. P. M. Guttenplan, M. W. R. Doggett, M. D. Eddleston, J. C. Tan, G. O. Lloyd.  
*A family of simple benzene 1,3,5-tricarboxamide (BTA) aromatic carboxylic acid hydrogels,*  
Chem. Commun. **2013**, 49, 4268–4270.
- [21] S. Seibt, S. With, A. Bernet, H.-W. Schmidt, S. Förster.  
*Hydrogelation Kinetics Measured in a Microfluidic Device with in Situ X-ray and Fluorescence Detection,*  
Langmuir, **2018**, 34, 5535–5544.
- [22] N. Helfricht, A. Mark, M. Behr, A. Bernet, H.-W. Schmidt, G. Papastavrou.  
*Writing with Fluid: Structuring Hydrogels with Micrometer Precision by AFM in Combination with Nanofluidics,*  
Small, **2017**, 13, 1700962.

- [23] D. Spitzer, L. L. Rodrigues, D. Straßburger, M. Mezger, P. Besenius.  
*Tuneable Transient Thermogels Mediated by a pH- and Redox-Regulated Supramolecular Polymerization*,  
Angew. Chem., Int. Ed., **2017**, 56, 15461-15465.
- [24] S. Lee, J.-S. Lee, C. H. Lee, Y.-S. Jung, J.-M. Kim.  
*Nonpolymeric Thermosensitive Benzenetricarboxamides*,  
Langmuir **2011**, 27, 1560–1564.
- [25] Z. Qi, L. Chiappisi, H. Gong, R. Pan, N. Cui, Y. Ge, C. Böttcher, S. Dong.  
*Ion Selectivity in Nonpolymeric Thermosensitive Systems Induced by Water-Attenuated Supramolecular Recognition*,  
Chem. – Eur. J. **2018**, 24, 3854–3861.
- [26] S. Dong, L. Wang, J. Wu, L. Jin, Y. Ge, Z. Qi, C. Wu.  
*Thermosensitive Phase Behavior of Benzo-21-crown-7 and Its Derivatives*,  
Langmuir **2017**, 33, 13861–13866.
- [27] E. E. Dormidontova.  
*Role of Competitive PEO-Water and Water-Water Hydrogen Bonding in Aqueous Solution PEO Behavior*,  
Macromolecules **2002**, 35, 987–1001.
- [28] M. Góral, D. G. Shaw, A. Mączyński, B. Wiśniewska-Goćłowska, P. Oracz.  
*IUPAC-NIST Solubility Data Series. 96. Amines with Water Part 1. C<sub>4</sub> - C<sub>6</sub> Aliphatic Amines*,  
J. Phys. Chem. Ref. Data **2012**, 41, 043106, 1–40.
- [29] R. R. Davidson, W. H. Smith Jr., D. W. Hood.  
*Structure and Amine-Water Solubility in Desalination by Solvent Extraction*,  
J. Chem. Eng. Data, **1960**, 5, 420-423.
- [30] K. Robinson, C. J. Easton, A. F. Dulhunty, M. G. Casarotto.  
*Exploiting Peptidomimetics to Synthesize Compounds That Activate Ryanodine Receptor Calcium Release Channels*,  
ChemMedChem **2018**, 13, 1957–1971.

- [31] A. Timme, R. Kress, R. Q. Albuquerque, H.-W. Schmidt.  
*Phase Behavior and Mesophase Structures of 1,3,5-Benzene- and 1,3,5-Cyclohexanetricarboxamides: Towards an Understanding of the Losing Order at the Transition into the Isotropic Phase,*  
Chem. – Eur. J. **2012**, 18, 8329–8339.
- [32] P. J. M. Stals, M. M. J. Smulders, R. Martín-Rapún, A. R. A. Palmans, E. W. Meijer.  
*Asymmetrically Substituted Benzene-1,3,5-tricarboxamides: Self-Assembly and Odd-Even Effects in the Solid State and in Dilute Solution,*  
Chem. – Eur. J. **2009**, 15, 2071–2080.
- [33] N. Shi, G. Yin, H. Li, M. Han and Z. Xu.  
*Uncommon hexagonal microtubule based gel from a simple trimesic amide,*  
New J. Chem., **2008**, 32, 2011-2015.

## Supporting Information

### ***Supramolecular microtubes based on 1,3,5-benzenetricarboxamides prepared by self-assembly upon heating***

Andreas Frank, Andreas Bernet, Klaus Kreger and Hans-Werner Schmidt\*

**S1:** Synthesis and characterization of 1,3,5-benzenetricarboxamides **1 – 3**

**S2:** FT-IR investigation of 1,3,5-benzenetricarboxamides **1 – 3**

**S3:** Differential scanning calorimetry of 1,3,5-benzenetricarboxamides **1 – 3**

**S4:** Polarizing optical microscopy of 1,3,5-benzenetricarboxamides **1 – 3**

**S5:** X-ray powder diffraction patterns of 1,3,5-benzenetricarboxamide **2**

**S6:** Cloud and clearing point determination of 1,3,5-benzenetricarboxamide **2** in water

**S7:** Micro-differential scanning calorimetry of 1,3,5-benzenetricarboxamide **2** in water

**S8:** Scanning electron microscopy of 1,3,5-benzenetricarboxamide **2**

**S9:** Optical micrograph and fiber diameter histogram of supramolecular microtubes of 1,3,5-benzenetricarboxamide **2**

## S1: Synthesis and characterization of 1,3,5-benzenetricarboxamides 1 – 3

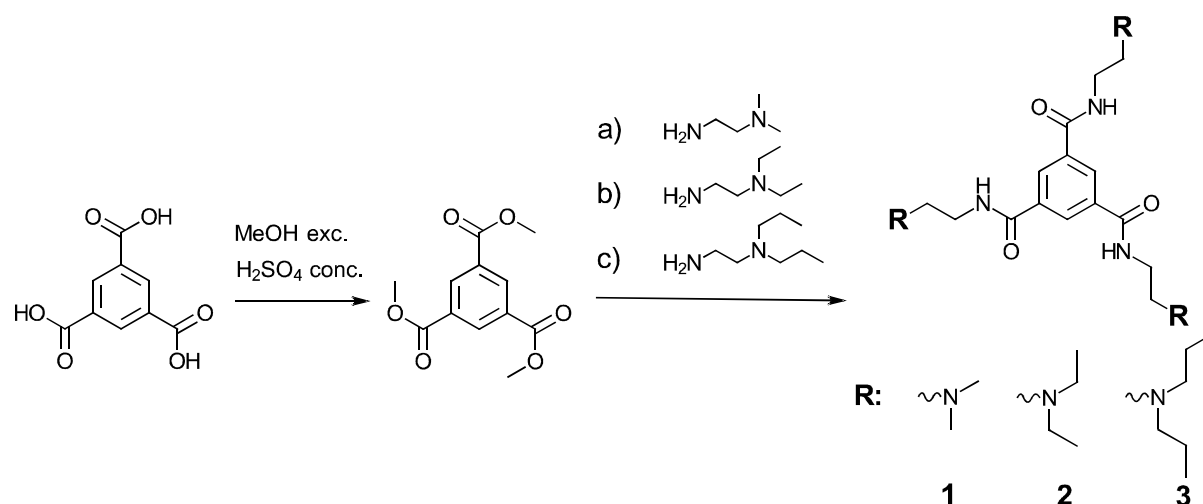


**Figure S1.** Two step synthesis of 1,3,5-benzenetricarboxamides 1–3: Esterification of trimesic acid to 1,3,5-benzenetricarboxylic acid trimethyl ester and subsequent synthesis of the respective 1,3,5-benzenetricarboxamides, (*N*<sup>1</sup>,*N*<sup>3</sup>,*N*<sup>5</sup>-tris[2-(dimethylamino)-ethyl]-1,3,5-benzenetricarboxamide) **1**, (*N*<sup>1</sup>,*N*<sup>3</sup>,*N*<sup>5</sup>-tris[2-(diethylamino)-ethyl]-1,3,5-benzenetricarboxamide) **2**, and (*N*<sup>1</sup>,*N*<sup>3</sup>,*N*<sup>5</sup>-tris[2-(dipropylamino)-ethyl]-1,3,5-benzenetricarboxamide) **3**.

#### Synthesis of trimesic acid trimethyl ester (1,3,5-benzenetricarboxylic acid trimethyl ester)

All chemicals were used as received without further purification. 100 g of trimesic acid (1,3,5-benzenetricarboxylic acid) (0.476 mol) were dissolved in 1.5 L of methanol. 7 mL of concentrated H<sub>2</sub>SO<sub>4</sub> were added, and the mixture was heated under reflux for two days. Complete conversion was determined by thin layer chromatography. After cooling to room temperature, the precipitated product was filtrated, washed with small amounts of methanol and dried under reduced pressure, yielding 108.0 g (0.465 mol, 90 %) of trimesic acid trimethyl ester as a white powder.

<sup>1</sup>H NMR (300 MHz, CDCl<sub>3</sub>) δ (ppm): 3.99 (s, 9H), 8.85 (s, 3H).

<sup>13</sup>C NMR (75 MHz, CDCl<sub>3</sub>) δ (ppm): 52.6, 131.2, 134.6, 165.4.

MS-EI (m/z): 252 (M<sup>+</sup>), 222, 221, 193.

*Synthesis of N<sup>1</sup>,N<sup>3</sup>,N<sup>5</sup>-tris[2-(dimethylamino)-ethyl]-1,3,5-benzenetricarboxamide 1*

10.0 g (0.04 mol) of trimesic acid trimethyl ester were dispersed in 22.0 mL (17.6 g, 0.2 mol) of *N,N*-dimethyl-ethylenediamine under argon atmosphere. The mixture was heated to 125 °C, stirred overnight and subsequently allowed to cool down to room temperature. The resulting mixture was dispersed in acetone and heated until an almost clear solution was obtained. The hot solution was filtrated using a sintered funnel. The solvent was removed and the product was dried in a vacuum oven at 50 °C over night resulting in 5.3 g (32 %) of **1** as a white powder.

<sup>1</sup>H NMR (300 MHz, CDCl<sub>3</sub>) δ (ppm): 2.30 (s, 18H), 2.56 (m, 6H), 3.57 (quartet, 6H), 7.21 (t(br), 3H), 8.48 (s, 3H).

<sup>13</sup>C NMR (75 MHz, CDCl<sub>3</sub>) δ (ppm): 37.3, 45.0, 57.7, 135.0, 165.6.

MS-EI (m/z): 420 (M<sup>+</sup>), 350, 72, 71, 58.

Anal. calcd. for C<sub>21</sub>H<sub>36</sub>N<sub>6</sub>O<sub>3</sub>: C 60.0, H 8.6, N 20.0; found: C 58.8, H 8.0, N 18.7.

*Synthesis of N<sup>1</sup>,N<sup>3</sup>,N<sup>5</sup>-tris[2-(diethylamino)-ethyl]-1,3,5-benzenetricarboxamide 2*

10.0 g (0.04 mol) of trimesic acid trimethyl ester were dispersed in 28.1 mL (23.2 g, 0.2 mol) of *N,N*-diethyl-ethylenediamine under argon atmosphere. The mixture was heated to 125 °C, stirred overnight and subsequently allowed to cool down to room temperature. The crude product was recrystallized from ca. 450 mL of acetic acid ethyl ester and washed with hexane, yielding after drying 8.98 g (45 %) of **2** as a white powder.

<sup>1</sup>H NMR (300 MHz, CDCl<sub>3</sub>) δ (ppm): 1.06 (t, 18H), 2.60 (quartet, 12H), 2.68 (m, 6H), 3.53 (quartet, 6H), 7.20 (t(br), 3H), 8.44 (s, 3H).

<sup>13</sup>C NMR (75 MHz, CDCl<sub>3</sub>) δ (ppm): 11.6, 37.4, 46.6, 51.3, 128.2, 135.2, 165.6.

MS-EI (m/z): 504 (M<sup>+</sup>), 99, 87, 86, 58.

Anal. calcd. for C<sub>27</sub>H<sub>48</sub>N<sub>6</sub>O<sub>3</sub>: C 64.3, H 9.6, N 16.7; found: C 64.4, H 9.1, N 16.6.

*Synthesis of N<sup>1</sup>,N<sup>3</sup>,N<sup>5</sup>-tris[2-(dipropylamino)-ethyl]-1,3,5-benzenetricarboxamide 3*

1.75 g (0.0069 mol) of trimesic acid trimethyl ester were dispersed in 6.25 mL (5.0 g, 0.03 mol) of *N,N*-dipropyl-ethylenediamine under nitrogen atmosphere. The mixture was heated to 125 °C, stirred overnight and subsequently allowed to cool down to room temperature. The crude product was recrystallized from DMF with some drops of water. The product was filtrated and dried under reduced pressure, yielding 2.1 g (52 %) of **3** as a light yellowish powder.

<sup>1</sup>H NMR (300 MHz, CDCl<sub>3</sub>) δ (ppm): 0.89 (t, 18H), 1.48 (sextet, 12H), 2.44 (m, 12H), 2.67 (t, 6H), 3.52 (quartet, 6H), 7.12 (t(br), 3H), 8.38 (s, 3H).

<sup>13</sup>C NMR (75 MHz, CDCl<sub>3</sub>) δ (ppm): 11.9, 20.1, 37.5, 52.4, 55.8, 128.0, 135.3, 165.6.

MS-EI (m/z): 588 (M<sup>+</sup>), 559, 286, 128, 115, 114, 86, 72.

Anal. calcd. for C<sub>33</sub>H<sub>60</sub>N<sub>6</sub>O<sub>3</sub>: C 67.3, H 10.3, N 14.3; found: C 67.3, H 9.8, N 14.0.

*Methods*

Nuclear magnetic resonance spectroscopy:

<sup>1</sup>H NMR (300 MHz) and <sup>13</sup>C NMR (75 MHz) experiments were carried out on a Bruker Avance AC 300 spectrometer at room temperature. The compounds were dissolved in CDCl<sub>3</sub>.

Mass spectroscopy:

Mass spectra were recorded on a Finnigan MAT 8500 spectrometer (Thermo Fisher Scientific) (EI, 70 eV) using direct injection mode. Only molecule peak (M<sup>+</sup>) and peaks with relative intensities ≥ 30 % are reported in the corresponding characterization data.

Elemental analysis:

Elemental analysis (C, H, N) was carried out with a Unicube from Elementar Analysen-Systeme with sulfanilamide as a standard. The samples were placed in tin boats and measured twice. The theoretical amount of all elements was calculated using Chemicalize. Values are given in weight %.



**S2: FT-IR investigation of 1,3,5-benzenetricarboxamides 1 – 3**

FT-IR spectra of bulk materials as obtained from synthesis were recorded with a Perkin-Elmer Spectrum 100 FT-IR spectrometer in ATR mode.

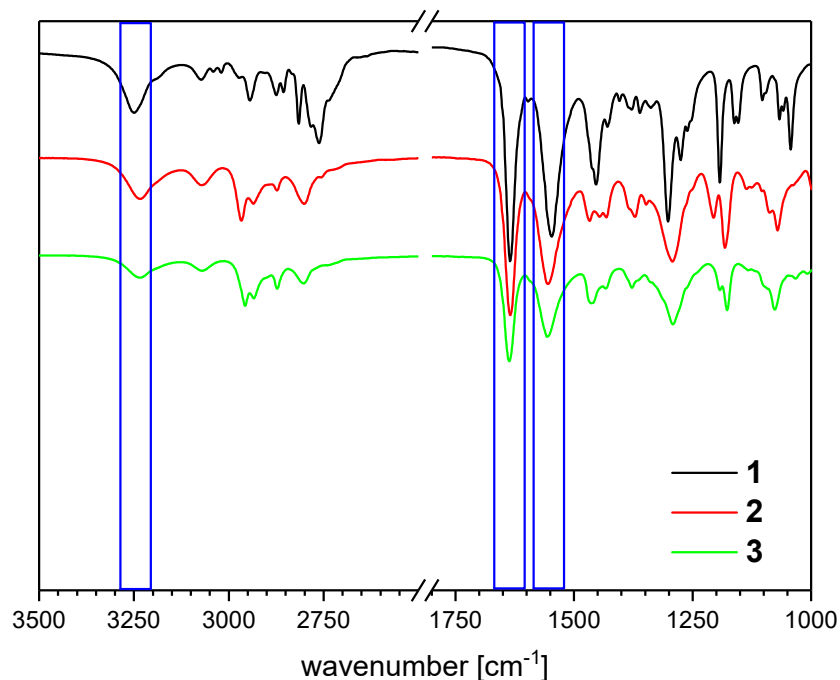


**Figure S2.** FT-IR spectra of **1 – 3** as obtained from synthesis. The BTAs show IR signals (see blue boxes) at around 3240 cm<sup>-1</sup> (Amide A, N-H stretch vibrations), at around 1640 cm<sup>-1</sup> (Amide I, C=O stretch vibrations) and at around 1560 cm<sup>-1</sup> (Amide II; superposition of N-H bend and C-N stretch vibrations). The position of the signals indicates a columnar stacking due to threefold hydrogen bonds between the BTA building blocks.<sup>1</sup>

<sup>1</sup> P. J. M. Stals, M. M. J. Smulders, R. Martín-Rapún, A. R. A. Palmans and E. W. Meijer, *Chem. Eur. J.*, 2009, **15**(9), 2071.

**S3: Differential scanning calorimetry of 1,3,5-benzenetricarboxamides 1 – 3**

DSC were performed on a Mettler Toledo DSC<sup>3+</sup> STAR<sup>e</sup> System. Typically, 10 mg of the compound were weighed in a crucible. Three heating and cooling curves were recorded from -50 °C to 250 °C with a rate of 10 K min<sup>-1</sup> under nitrogen atmosphere.

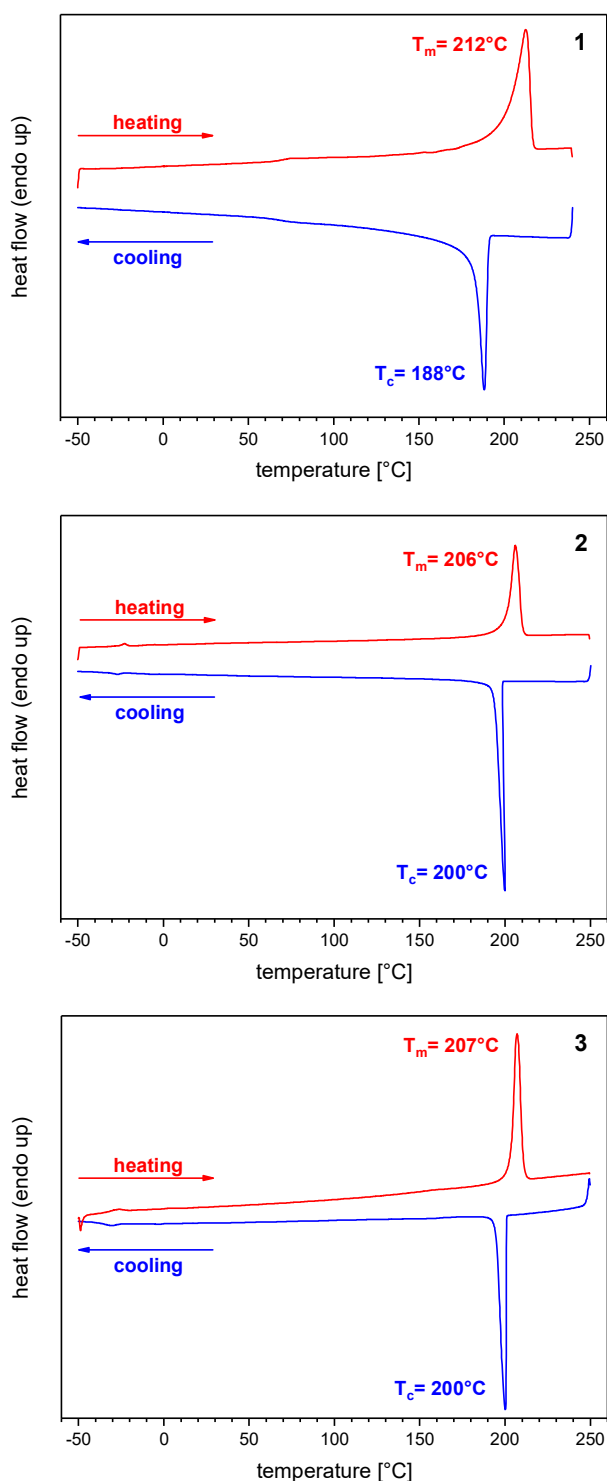


**Figure S3.** DSC 2<sup>nd</sup> heating and 2<sup>nd</sup> cooling curves of **1 – 3** at a rate of 10 K min<sup>-1</sup> under nitrogen atmosphere. The melting peak and the crystallization peak are labeled as  $T_m$  and  $T_c$ , respectively.

**S4: Polarizing optical microscopy of 1,3,5-benzenetricarboxamides 1 – 3*****Temperature-dependent polarizing optical microscopy of 1,3,5-benzenetricarboxamides 1 – 3 in bulk:***

small portion of the powder was placed on a glass slide (Menzel-Gläser), covered with a cover slide and heated to 250 °C. Images were recorded between crossed polarizers using a Nikon Diaphot 300 microscope equipped with a camera and a Mettler Toledo hotstage.

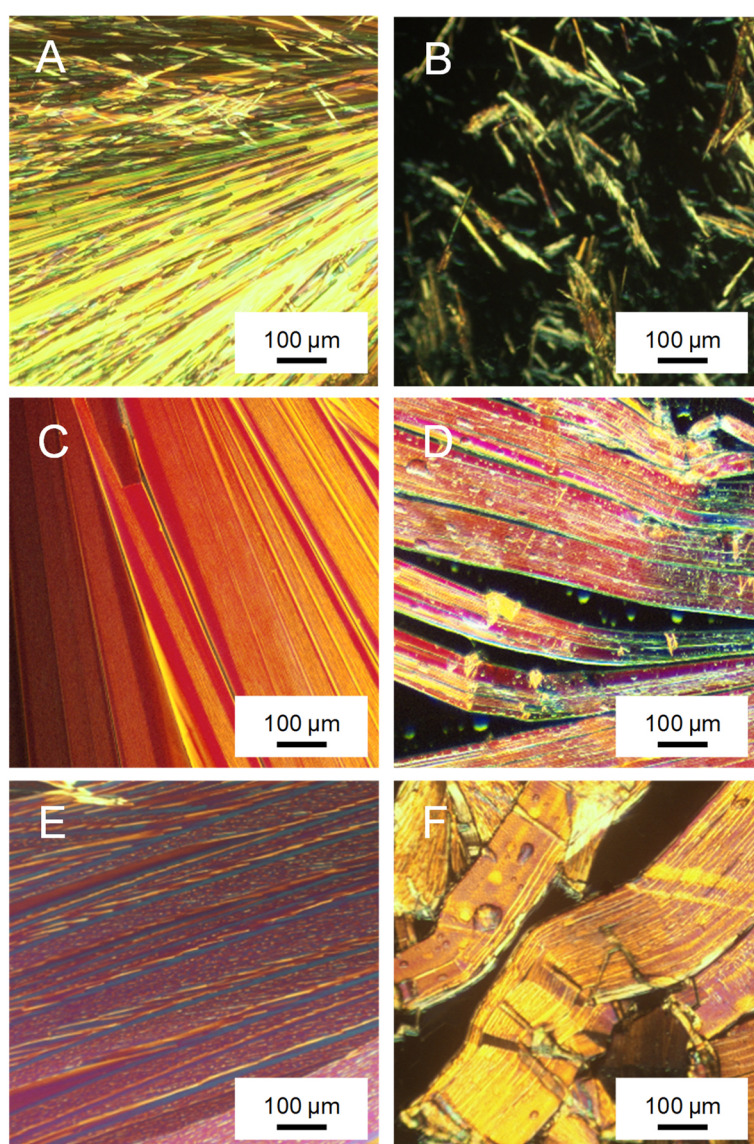


**Figure S4.1.** A – F: Temperature-dependent polarized optical micrographs in bulk of **1**, **2** and **3** at 180 °C, before (A, C and E) and after (B, D and F) shearing the sample. All three compounds show birefringent textures. **1** shows a brittle behavior and breaks upon shearing, confirming a crystalline structure (B). **2** and **3** show deformable textures and bending, which is indicative for a plastic crystalline behavior (D and F).

***Temperature-dependent polarizing optical microscopy of aqueous solution of 1,3,5-benzenetricarboxamides 2:***

An aqueous solution with a concentration of 20 g L<sup>-1</sup> of **2** was placed on a glass slide (Menzel-Gläser) and covered with a smaller cover slide. The liquid sample was then sealed with silicon high-vacuum grease to prevent evaporation. Images were taken between crossed polarizers in the presence of a  $\lambda/4$  plate using a Nikon Diaphot 300 microscope equipped with a camera and a Mettler Toledo hotstage.

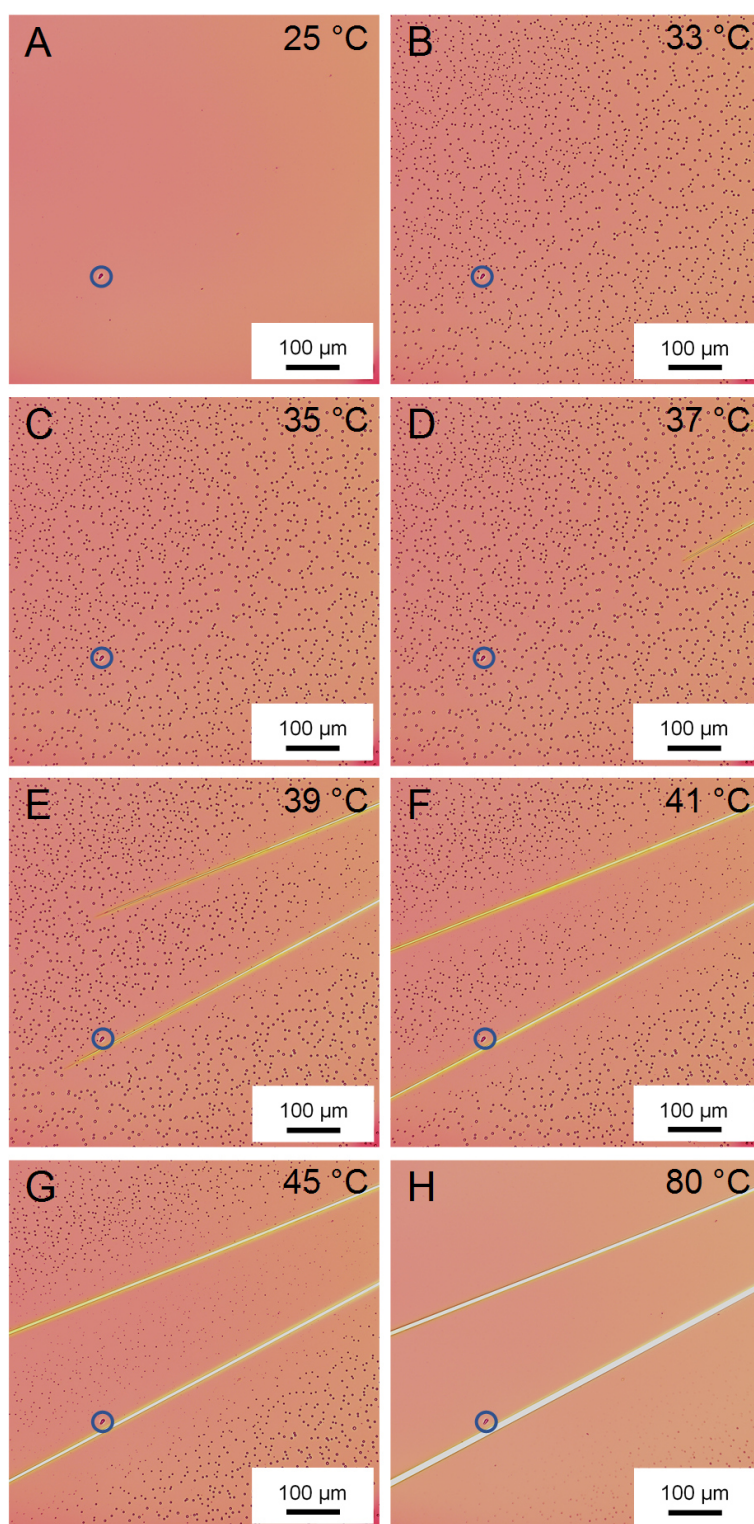


**Figure S4.2.** A – H: Series of polarized optical micrographs with  $\lambda/4$  plate of 20 g L<sup>-1</sup> of **2** in water. Heating the sample (blue circle indicates same position) from 25 °C to 80 °C with a heating rate of 1 K min<sup>-1</sup> reveals phase separation of the solution followed by self-assembly of **2** into supramolecular fiber-like structures.



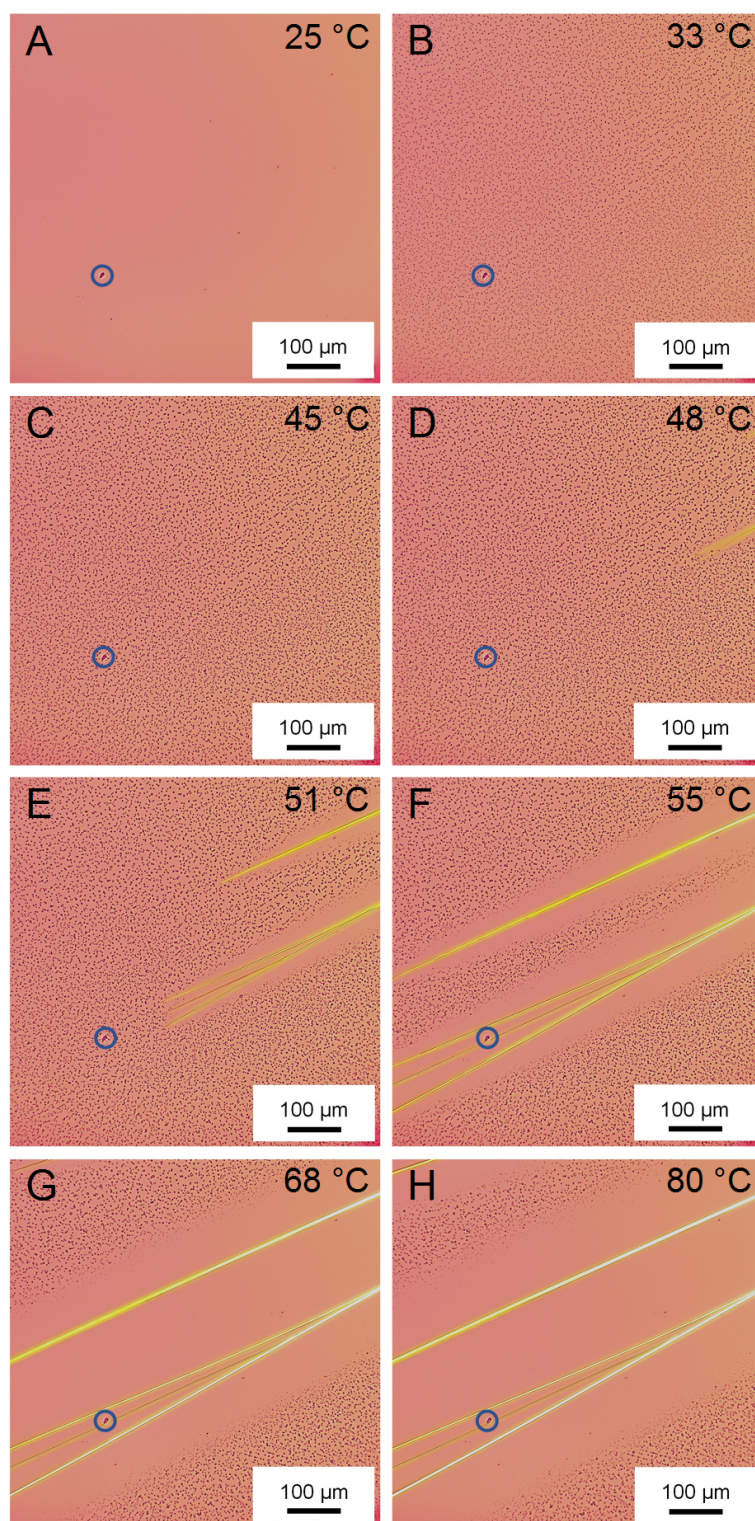


**Figure S4.3.** A – H: Series of polarized optical micrographs with  $\lambda/4$  plate of 20 g L<sup>-1</sup> of **2** in water. Heating the sample (blue circle indicates same position) from 25 °C to 80 °C with a heating rate of 5 K min<sup>-1</sup> reveals phase separation of the solution followed by self-assembly of **2** into supramolecular fiber-like structures.

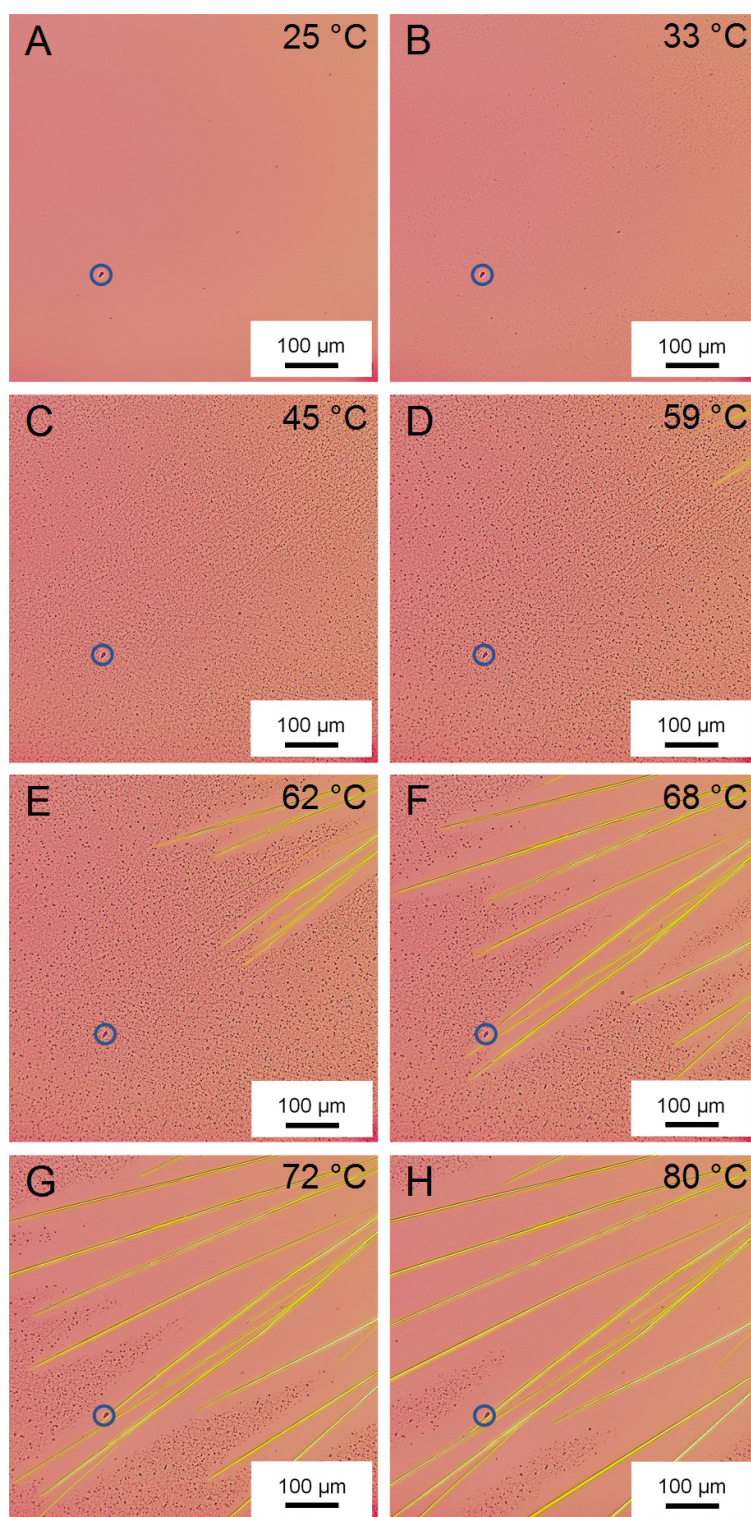


**Figure S4.4.** A – H: Series of polarized optical micrographs with  $\lambda/4$  plate of  $20 \text{ g L}^{-1}$  of **2** in water. Heating the sample (blue circle indicates same position) from  $25 \text{ }^\circ\text{C}$  to  $80 \text{ }^\circ\text{C}$  with a heating rate of  $10 \text{ K min}^{-1}$  reveals phase separation of the solution followed by self-assembly of **2** into supramolecular fiber-like structures.



**S5: X-ray powder diffraction patterns of 1,3,5-benzenetricarboxamide 2**

X-ray powder diffraction (XRD) measurements of the bulk material and of aqueous samples were performed on a Huber Guinier diffractometer 600, equipped with a Huber germanium monochromator 611 to receive a  $\text{Cu}_{\text{K}\alpha 1}$  radiation of  $\lambda = 154.051$  pm. A custom-made oven was installed into the diffractometer to investigate the samples at different temperatures. For the measurements, Mark tubes with an outer diameter of 1 mm were used for the bulk material and Mark tubes with an outer diameter of 2 mm for the aqueous samples, respectively. In all cases, the wall thickness of the Mark tubes was 0.01 mm.

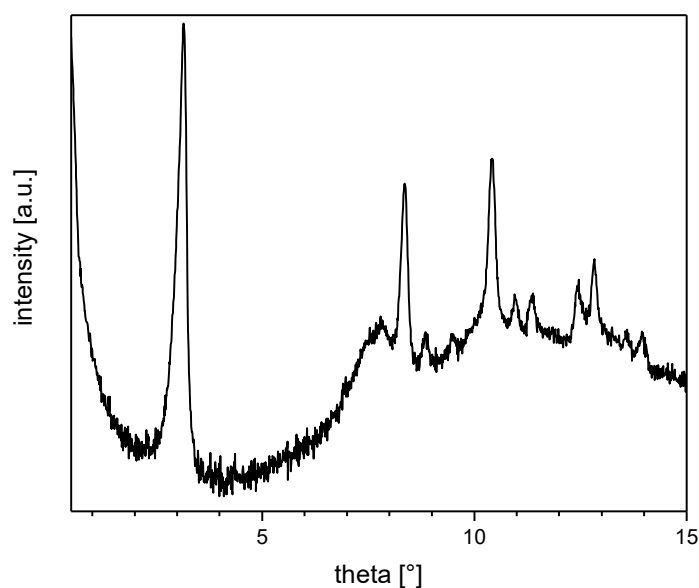


**Figure S5.1.** X-ray powder diffraction pattern of **2** at room temperature as obtained from synthesis.

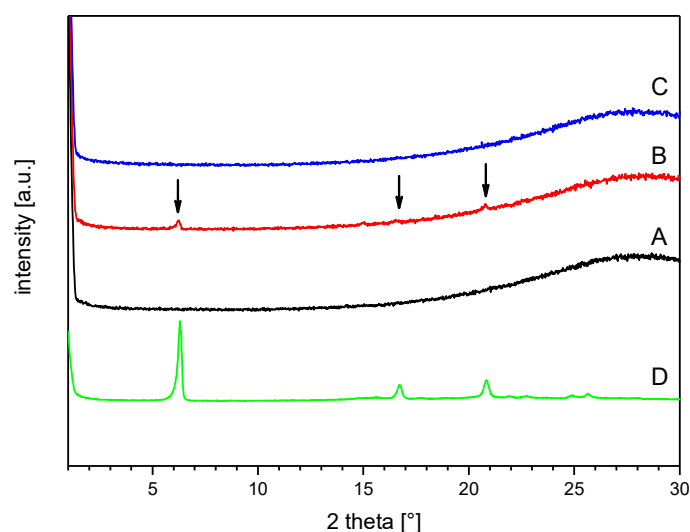


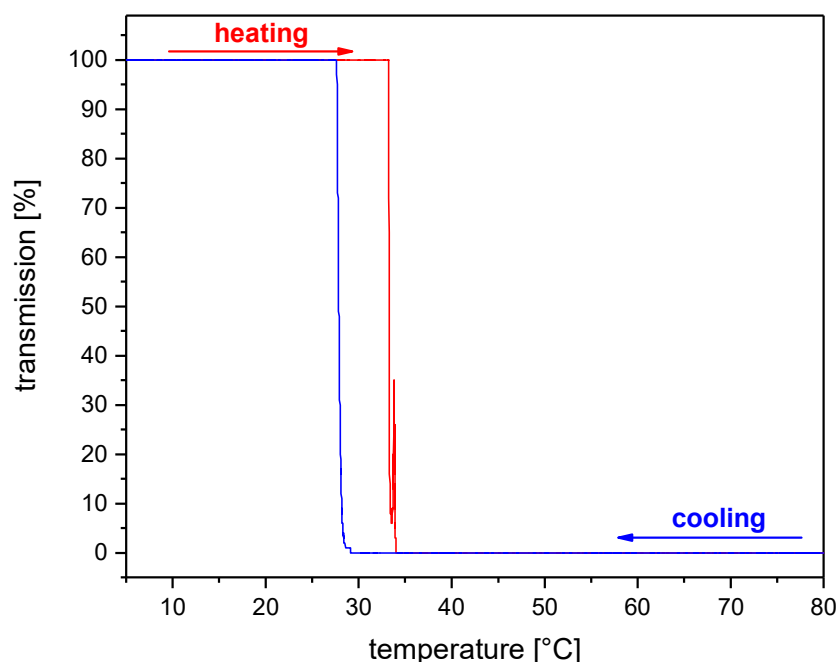
**Figure S5.2.** X-ray powder diffraction patterns of **2** in water with a concentration of 20 g L<sup>-1</sup> measured at room temperature before heating (A), measured at 40 °C featuring weak diffraction peaks indicated by arrows (B), and at room temperature after cooling (C). X-ray powder diffraction pattern of **2** as obtained from synthesis as reference (D).



**S6: Cloud and clearing point determination of 1,3,5-benzenetricarboxamide 2 in water**

The cloud and clearing points of **2** were determined optically for 16 concentrations in parallel using the crystallization system Crystal16 (Technobis Crystallization Systems). Concentrations of 1, 2, 3, 4, 5, 10, 15, 20, 30, 40, 50, 60, 70, 80, 90 and 100 g L<sup>-1</sup> of **2** in water were prepared at room temperature. The samples were stirred at 600 rpm and the transmission of each sample was recorded for two cycles in the range of 5 °C to 80 °C. Each cycle consists of a heating step with a rate of 0.5 K min<sup>-1</sup>, an isothermal hold at 80 °C for 5 min, a subsequent cooling step with a rate of 0.5 K min<sup>-1</sup>, and an isothermal hold at 5 °C for 30 min.

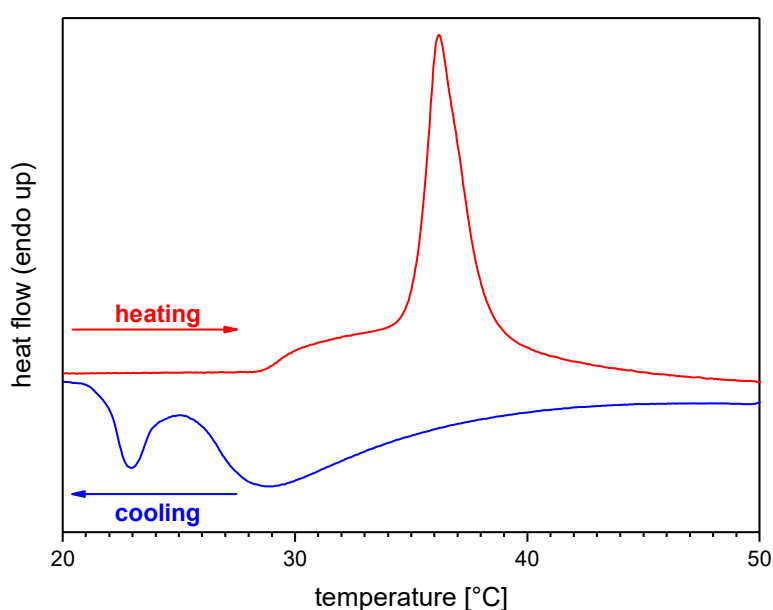
Here, we define transmission at 0 % as cloud point and at 100 % as clearing point. Exemplarily, the 1<sup>st</sup> heating and 1<sup>st</sup> cooling cycle and the recorded transmission for the sample **2** with a concentration 20 g L<sup>-1</sup> are shown in **Figure S6**. During heating, clouding of the sample occurs at around 33 °C and leads to a rapid change in the transmission from 100 % to 0 %. Upon subsequent cooling, a clear solution is obtained at around 27 °C, indicated by the rapid change of the transmission from 0 % to 100 %.



**Figure S6.** Cloud and clearing point determination. The 1<sup>st</sup> heating and 1<sup>st</sup> cooling cycle and the recorded transmission for **2** with a concentration 20 g L<sup>-1</sup> is shown. Upon heating, the cloud point of the sample was determined at around 33 °C (change of transmission from 100 % to 0 %). Upon cooling, the clearing point was indicated at around 27 °C (change of transmission from 0 % to 100 %).

**S7: Micro-differential scanning calorimetry of 1,3,5-benzenetricarboxamide **2** in water**

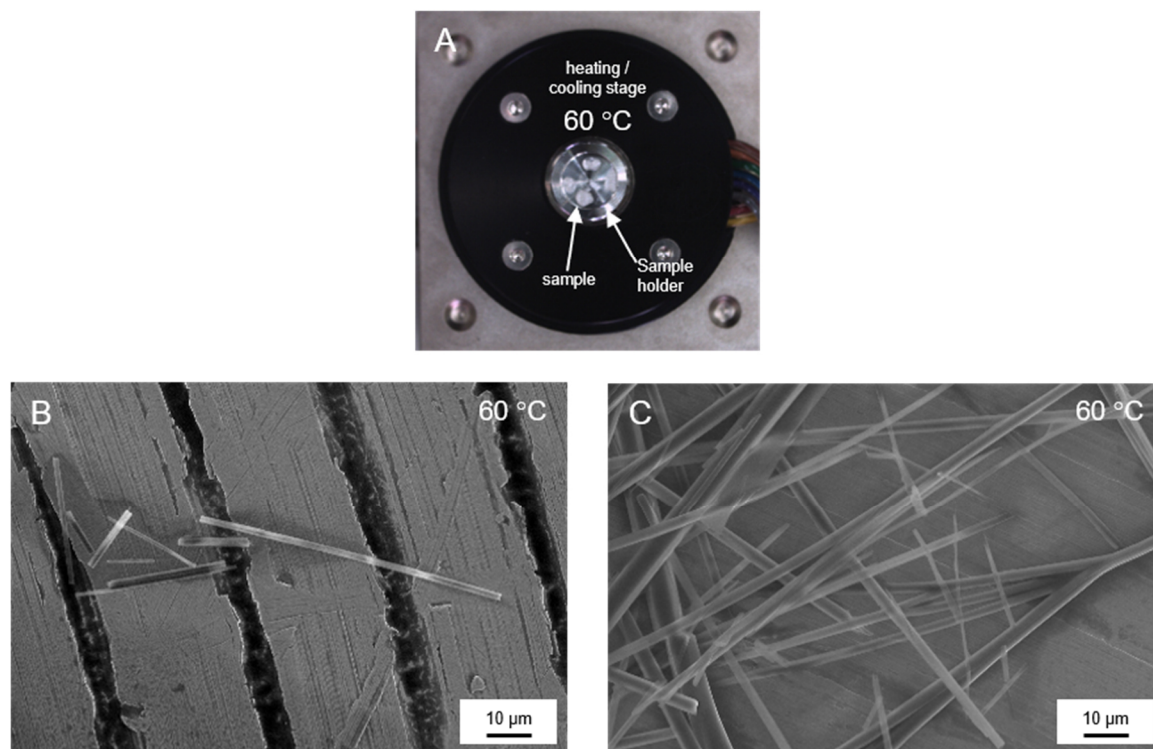
Micro-differential scanning calorimetry ( $\mu$ DSC) measurement was performed on a Setaram MicroDSC III. A solution of the compound under investigation (about 0.7 mL) was filled into a Hastelloy C276 sample cell which was immediately sealed to avoid evaporation. The reference cell was filled with an equal amount of water and sealed. Prior to measurement, the cells were kept at the desired starting temperature for at least 1 h to ensure thermal equilibration. The measurement was carried out applying a heating and cooling rate of  $0.1 \text{ K min}^{-1}$ .



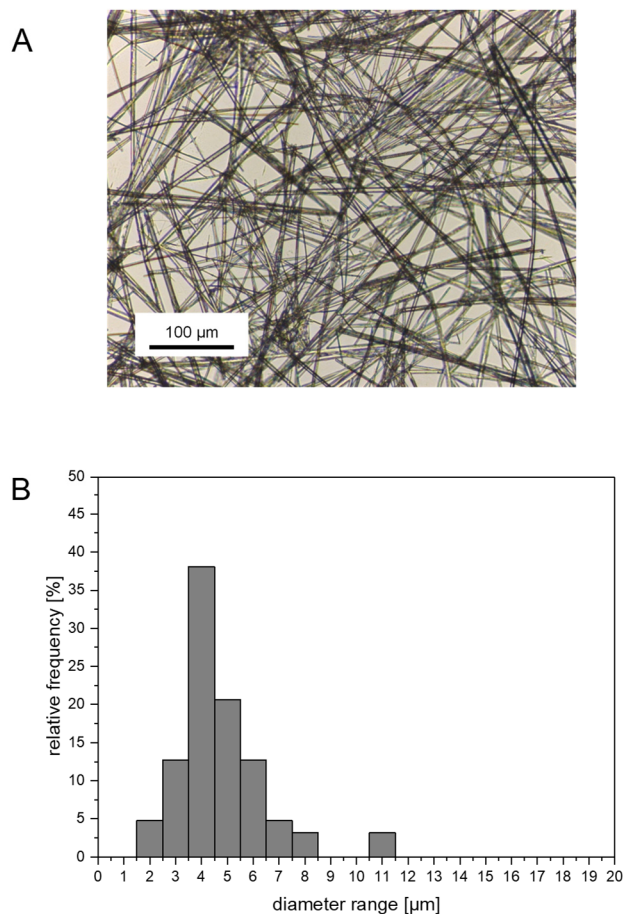
**Figure S7.** Micro-differential scanning calorimetry curves of **2** in water with a concentration of  $20 \text{ g L}^{-1}$  at a heating and cooling rate of  $0.1 \text{ K min}^{-1}$ . Upon heating, a smaller peak with an onset at about  $29 \text{ °C}$  followed by a stronger peak with a maximum at  $36 \text{ °C}$  is observed. Upon cooling, two peaks are visible demonstrating the reversibility of the process.

**S8: Scanning electron microscopy of 1,3,5-benzenetricarboxamide 2**

Measurements were conducted on different scanning electron microscopes, namely, Ultra plus (Zeiss), Dual-Beam FIB-SEM, 1540XB-CrossBeam (Zeiss) and FEI Quanta FEG 250 (Thermo Fisher Scientific). For the measurement on the Ultra plus microscope, the samples were mounted on a sample holder using an adhesion graphite pad and sputtered with platinum (1.3 – 2 nm) to ensure sufficient conductivity. Furthermore, the supramolecular microtubes were investigated with the focused ion beam FIB-SEM with a Ga-focused ion source. Here, the samples were attached on a sample holder using an adhesive conductive graphite pad. Cross-sections were produced with cutting lengths between 5  $\mu\text{m}$  and 20  $\mu\text{m}$ . The cutting line width was up to 30  $\mu\text{m}$ . The used FIB current was between 200 pA and 500 pA, and a step size of 20  $\text{nm min}^{-1}$  was applied. The FEI Quanta FEG 250 was conducted in the environmental scanning electron microscopy (ESEM) mode. 2  $\mu\text{L}$  of a clear solution of **2** in water with a concentration of 20  $\text{g L}^{-1}$  was placed at 60  $^{\circ}\text{C}$  in the sample holder (**Figure S8A**). At 60  $^{\circ}\text{C}$ , the solution turned turbid and supramolecular fiber-like structures were formed (**B** and **C**). **Figure S8B** and **S8C** show the supramolecular structures at different positions of the sample.

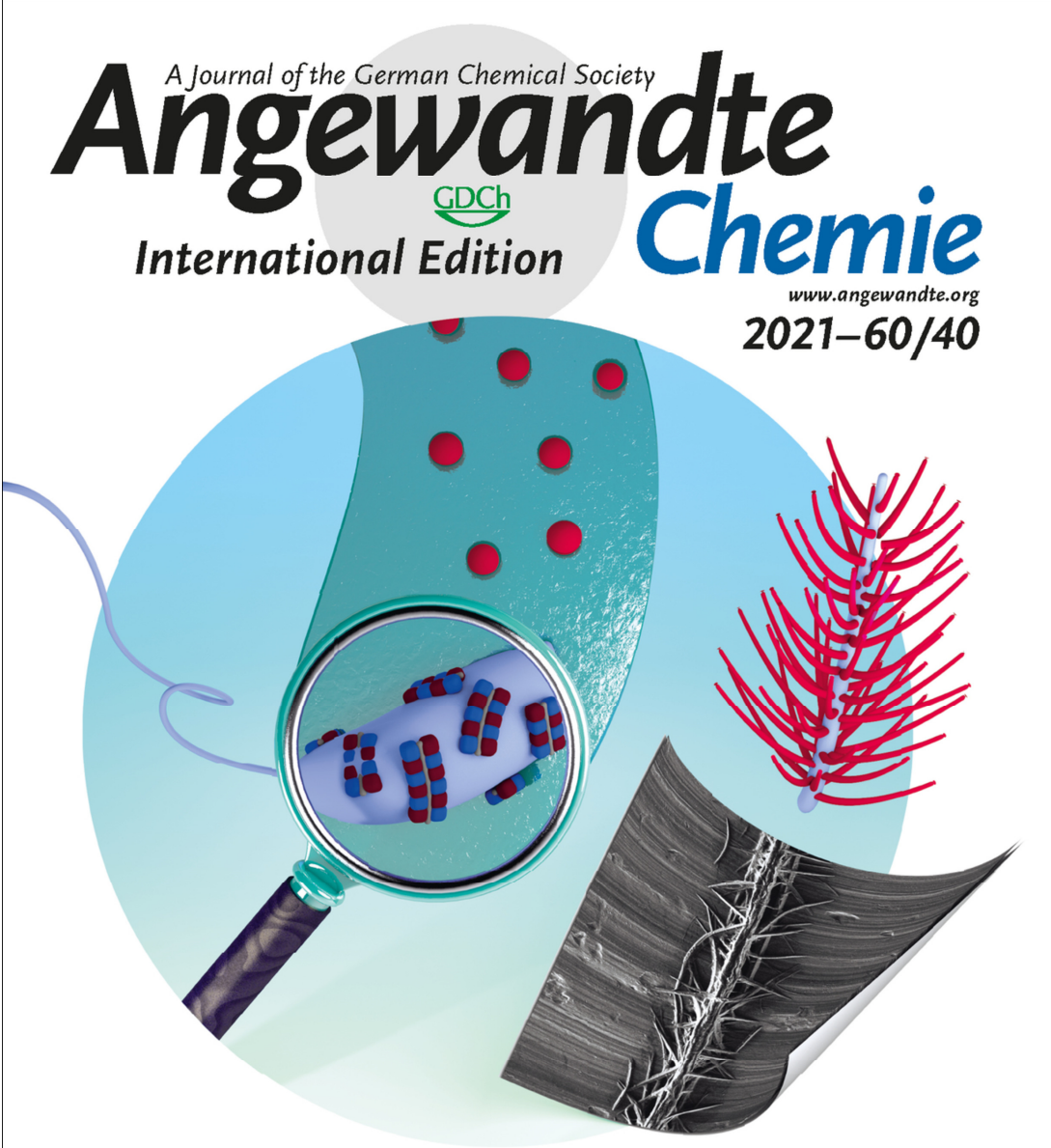


**Figure S8.** A: Optical micrograph of the cooling / heating stage in the environmental scanning electron microscope. B – C: Scanning electron micrographs of supramolecular microtubes at different positions of the sample.

**S9: Optical micrograph and fiber diameter histogram of supramolecular microtubes of 1,3,5-benzenetricarboxamide 2**

**Figure S9.** A: Optical micrograph of isolated supramolecular structures of **2** prepared by dropping a small amount of an aqueous solution of **2** with a concentration of  $10 \text{ g L}^{-1}$  onto a glass surface preheated to  $80 \text{ }^\circ\text{C}$  and subsequently evaporation of water at this temperature. Hollow supramolecular microtubes with lengths of several hundreds of  $\mu\text{m}$  are visible. B: Histogram of the diameters of supramolecular microtubes based on at least 60 individual microtubes from micrograph A. The mean diameter was determined to be  $4.7 \pm 1.6 \mu\text{m}$ .

### 4.3. Hierarchical superstructures by combining crystallization-driven and molecular self-assembly



A Journal of the German Chemical Society  
**Angewandte**  
GDCh  
**International Edition** **Chemie**  
www.angewandte.org  
2021–60/40

**Hierarchical fir-tree-like superstructures ...**

... have been realized by Holger Schmalz, Hans-Werner Schmidt, and co-workers in the Communication on page 21767, by utilizing the unique corona structure of patchy worm-like micelles for the directed molecular self-assembly of a 1,3,5-benzenetricarboxamide. The combination of crystallization-driven and molecular self-assembly concepts can give access to a large variety of fibrillar superstructures with potential applications in filtration or catalysis.

WILEY-VCH

***Hierarchical Superstructures by Combining Crystallization-Driven and Molecular Self-Assembly***

Andreas Frank,<sup>[a]+</sup> Christian Hils,<sup>[b]+</sup> Melina Weber,<sup>[a]</sup> Klaus Kreger,<sup>[a]</sup> Holger Schmalz,<sup>[b]\*</sup> and Hans-Werner Schmidt<sup>[a]\*</sup>

[a] Macromolecular Chemistry I, University of Bayreuth and Bavarian Polymer Institute, Universitätsstrasse 30, 95447 Bayreuth (Germany)

[b] Macromolecular Chemistry II, University of Bayreuth and Bavarian Polymer Institute, Keylab Synthesis and Molecular Characterization, Universitätsstrasse 30, 95447 Bayreuth (Germany)

[\*] These authors contributed equally to this work.

\*E-mail corresponding authors:

[hans-werner.schmidt@uni-bayreuth.de](mailto:hans-werner.schmidt@uni-bayreuth.de) and [holger.schmalz@uni-bayreuth.de](mailto:holger.schmalz@uni-bayreuth.de)

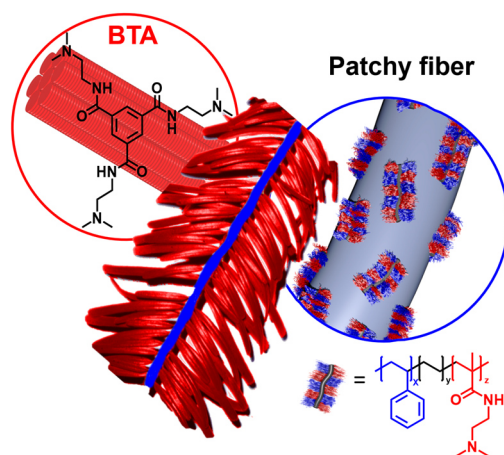
The results of this chapter have been published as a communication article in *Angew. Chem. Int. Ed.* **2021**, 60, 21767–21771. DOI: 10.1002/anie.202105787.

Published by Wiley-VCH GmbH. This is an open access article under the terms of the Creative Commons Attribution 4.0 International License, which permits use, distribution and reproduction in any medium, provided the original work is properly cited (© 2021 The Authors).

Supporting information and the ORCID identification number(s) for the author(s) of this article can be found under: <https://doi.org/10.1002/anie.202105787>.

(German edition: *Angew. Chem.* **2021**, 133, 21935–21939. DOI: 10.1002/ange.202105787.)

## Graphical abstract



Hierarchical fir-tree-like superstructures are accessible by utilizing the unique corona structure of patchy worm-like micelles immobilized on electrospun polymer fibers and the molecular self-assembly of a 1,3,5-benzenetricarboxamide. The used combination of crystallization-driven and molecular self-assembly concepts can give access to a large variety of fibrillar superstructures with potential applications in filtration or catalysis.



**Abstract:**

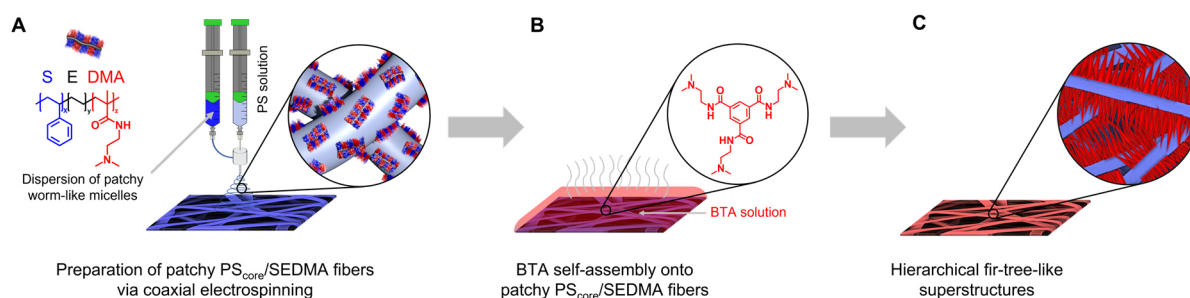
Combining the unique corona structure of worm-like patchy micelles immobilized on a polymer fiber with the molecular self-assembly of 1,3,5-benzenetricarboxamides (BTAs) leads to hierarchical superstructures with a fir-tree-like morphology. For this purpose, worm-like patchy micelles bearing pendant, functional tertiary amino groups in one of the corona patches were prepared by crystallization-driven self-assembly and immobilized on a supporting polystyrene fiber by coaxial electrospinning. The obtained patchy fibers were then immersed in an aqueous solution of a tertiary amino-functionalized BTA to induce patch-mediated molecular self-assembly to well-defined fir-tree-like superstructures upon solvent evaporation. Interestingly, defined superstructures are obtained only if the pendant functional groups in the surface patches match with the peripheral substituents of the BTA, which is attributed to a local increase in BTA concentration at the polymer fibers' surface.

Hierarchical self-assembly represents an intriguing approach to realizing complex superstructures at the nano- and mesoscale in nature. Although artificial molecular and macromolecular self-assembly concepts have already proven to pave the way to more complex assemblies, the outstanding control over shape, dimension, and functionality found in nature is still far from being achieved. The guided hierarchical self-assembly of amorphous block copolymers in solution has been shown to represent a facile way to tailor-made multicompartment structures.<sup>[1]</sup> However, particularly for one- (1D) and two-dimensional (2D) structures, the precise control over size and size distribution is difficult to achieve. Herein, the introduction of a crystallizable block, which adds an additional and strong driving force for micelle formation, can be harnessed to solve these issues in a process termed crystallization-driven self-assembly (CDSA). Especially the discovery of living CDSA,<sup>[2]</sup> which closely resembles the features of living polymerization processes with respect to control over size and size distribution, has given access to a multitude of complex and hierarchical micellar assemblies of controlled shape and size, like, for example, patchy and block co-micelles, branched and scarf-like micelles, colloidosomes and multidimensional superstructures.<sup>[3]</sup> A concept closely related to CDSA is supramolecular polymerization, that is, the self-assembly of small molecules via directed and reversible secondary interactions, which we denote as molecular self-assembly in the following.<sup>[4]</sup> Similarly, molecular self-assembly processes allow the fabrication of defined nanostructures and superstructures.<sup>[5]</sup> In particular, control over the



self-assembly process and, in turn, on the objects' dimensions can be achieved with living supramolecular polymerization,<sup>[6]</sup> which can be realized for instance by a seed-initiated growth approach. The combination of a precise top-down coating technique, such as coaxial electrospinning,<sup>[7]</sup> with CDSA, a typical bottom-up approach, was recently employed in our group to construct patchy hybrid nonwovens with excellent performance in heterogeneous catalysis.<sup>[8]</sup> Utilizing a similar strategy for the immobilization of 1,3,5-benzenetricarboxamide (BTA) seeds onto electrospun fibers yielded mesostructured nonwovens with a penguin downy-feather-like morphology by an in situ growth of supramolecular BTA fibers from the electrospun seed fibers.<sup>[9]</sup> However, with this approach the control over the seed density on the electrospun fibers is limited.

Herein, we show that hierarchical fir-tree-like superstructures can be generated by the combination of two self-assembly concepts, that is, crystallization-driven self-assembly and molecular self-assembly (**Scheme 1**). Our conceptual approach to these defined superstructures comprises A) the preparation of patchy PS<sub>core</sub>/SEDMA fibers by coaxial electrospinning of polystyrene (PS) and patchy worm-like polystyrene-*block*-polyethylene-*block*-poly(*N,N*-dimethylaminoethyl methacrylamide) (SEDMA) triblock terpolymer micelles, B) the immersion of this patchy fibers into an aqueous *N*<sup>1</sup>,*N*<sup>3</sup>,*N*<sup>5</sup>-tris[2-(dimethylamino)ethyl]-1,3,5-benzenetricarboxamide (BTA-Methyl) solution and C) the controlled molecular self-assembly of BTA-Methyl to highly defined hierarchical superstructures upon solvent evaporation. In the resulting fir-tree-like superstructures the PS<sub>core</sub>/SEDMA fibers form the core, from which supramolecular BTA-Methyl fibers ("needles") have grown away from the surface in a well-controlled fashion.



**Scheme 1.** Formation of hierarchical fir-tree-like superstructures. A) Coaxial electrospinning of a polystyrene (PS) solution and a dispersion of patchy worm-like polystyrene-*block*-polyethylene-*block*-poly(*N,N*-dimethylaminoethyl methacrylamide) (SEDMA) triblock terpolymer micelles to prepare patchy PS<sub>core</sub>/SEDMA fibers. B) Immersion of the patchy PS<sub>core</sub>/SEDMA fibers into an aqueous *N*<sup>1</sup>,*N*<sup>3</sup>,*N*<sup>5</sup>-tris[2-(dimethylamino)ethyl]-1,3,5-benzenetricarboxamide (BTA-Methyl) solution and subsequent evaporation induced molecular self-assembly of BTA-Methyl onto the patchy fibers. C) Final hierarchical fir-tree-like superstructures after complete solvent evaporation.

The PS<sub>core</sub>/SEDMA fibers with functional surface patches were prepared by immobilizing patchy worm-like SEDMA micelles on top of PS fibers by coaxial electrospinning, employing a PS solution (7 wt. % in DMF;  $M_n = 1.8 \times 10^6 \text{ g mol}^{-1}$ ) as core and a dispersion of patchy worm-like SEDMA micelles ( $c = 10 \text{ g L}^{-1}$  in THF) as shell, respectively (**Scheme 1 A**). The dispersion of the patchy worm-like SEDMA micelles was prepared via CDSA, as previously reported, whereby the PS patches provide compatibility with the supporting PS fiber and the PDMA patches provide the functionality.<sup>[10]</sup> Experimental details and the molecular characteristics of the employed triblock terpolymers are described in the Supporting Information. Exemplarily, a TEM image of the patchy worm-like SEDMA micelles is depicted in **Figure S1**. Here, the semi-crystalline PE block forms the core and the micellar corona consists of alternating, nanometer-sized PS ( $18 \pm 5 \text{ nm}$ ) and PDMA ( $17 \pm 5 \text{ nm}$ ) patches (**Table S1**). **Figure 1 A** shows a scanning electron microscope image of a patchy PS<sub>core</sub>/SEDMA polymer fiber, where the worm-like SEDMA micelles on top of the supporting PS fiber can be clearly distinguished.

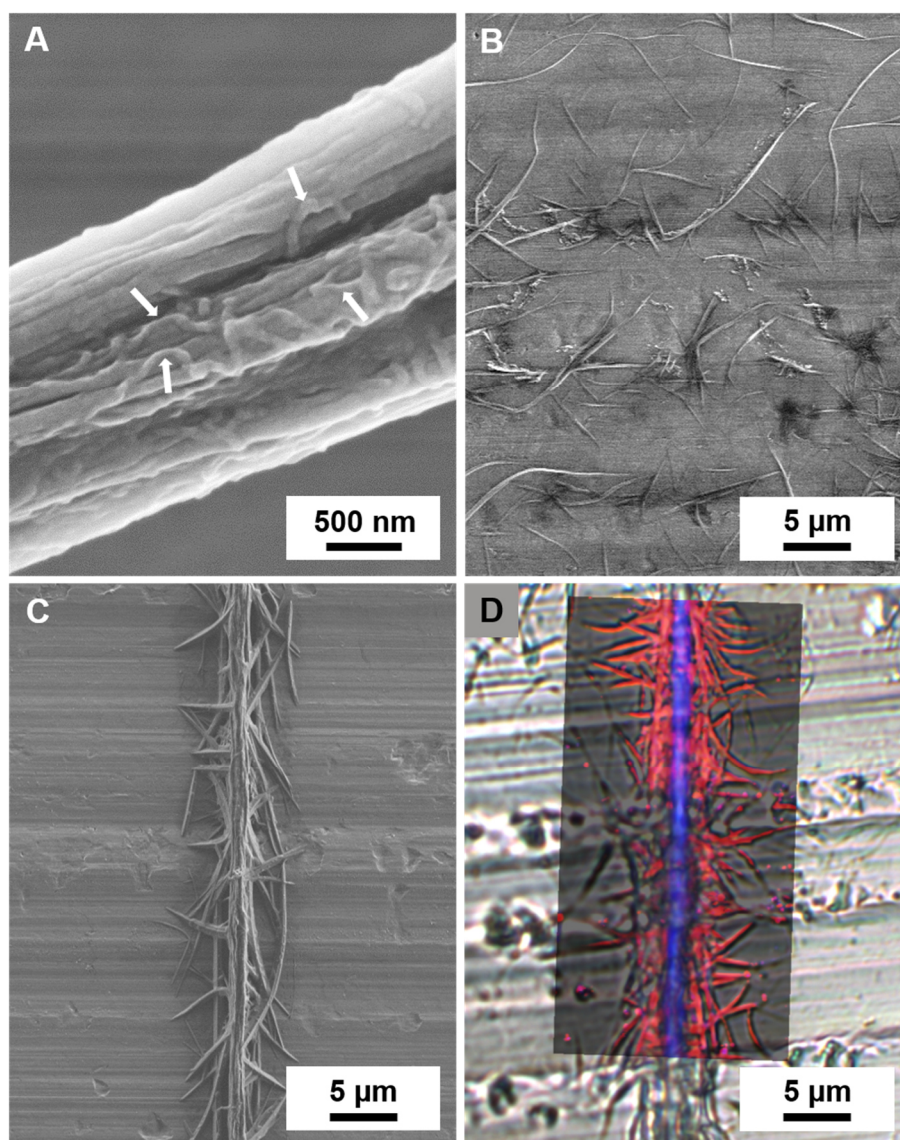


**Figure 1.** Scanning electron micrographs of A) a patchy PS<sub>core</sub>/SEDMA fiber (the arrows indicate the patchy worm-like micelles on top of the supporting PS<sub>core</sub> fiber); B) uncontrolled supramolecular BTA assemblies prepared upon solvent evaporation from a 0.050 wt. % aqueous solution on aluminum foil; C) a hierarchical fir-tree-like superstructure prepared by molecular self-assembly of a 0.050 wt. % aqueous BTA-Methyl solution onto patchy PS<sub>core</sub>/SEDMA fibers after solvent evaporation. D) Overlay of the spatially resolved component distribution from Raman imaging (PS-rich regions are colored in blue and BTA-Methyl rich in red, respectively) with the optical microscopy image of the fir-tree-like superstructure.

As building block for the molecular self-assembly (**Scheme 1 B**) BTA-Methyl was selected featuring peripheral tertiary *N,N*-dimethylaminoethyl substituents<sup>[11]</sup> which match the pendant functional groups in the PDMA patches of the SEDMA micelles. BTA-Methyl is highly water soluble up to a concentration of 15 wt. %<sup>[11]</sup> and exhibits no temperature induced formation of supramolecular structures at a concentration of 2 wt. %, as demonstrated by temperature-dependent turbidity measurements and micro-differential scanning calorimetry

(**Figure S2, S3**). Only upon solvent evaporation a threshold concentration is apparently reached where homogeneous nucleation results in the formation of randomly distributed supramolecular BTA-Methyl fibers with a broad length distribution (**Figure 1 B**). The final deposited fiber density correlates with the initially used concentration of BTA-Methyl (**Figure S4**). In an analogous manner, also the PDMA block of the SEDMA triblock terpolymer shows complete solubility in water over a broad temperature range.<sup>[12]</sup>

Remarkably, immersion of the patchy PS<sub>core</sub>/SEDMA fibers into a BTA-Methyl solution of only 0.05 wt. % followed by solvent evaporation (**Scheme 1 B, C**) resulted in highly defined hierarchical fir-tree-like superstructures as shown in **Figure 1 C**. Moreover, the BTA-Methyl fibers grow away from the patchy polymer fiber in an oriented manner and can be observed at different positions, which indicates different starting points owing to the randomly distributed worm-like micelles at the surface of the PS<sub>core</sub>/SEDMA fiber. This is confirmed by Raman imaging, which allows to distinguish between the patchy PS<sub>core</sub>/SEDMA fiber and the BTA fibers. The Raman spectra of the corresponding neat compounds can be found in **Figure S5**. **Figure 1D** shows an overlay of the optical microscopy image of the fir-tree-like superstructure and the spatially resolved component distribution from Raman imaging (PS is depicted in blue and BTA-Methyl in red), clearly demonstrating that the BTA-Methyl fibers are directly attached onto the patchy PS<sub>core</sub>/SEDMA fiber. Furthermore, Raman imaging allows to probe the alignment of the BTA-Methyl units, since the spectra differ depending on their orientation with respect to the polarization of the laser (horizontally polarized). Most of the BTA-Methyl units show a perpendicular stacking to the PS fiber (**Figure S6**).

These results indicate that the patchy surface of the fibers is able to initiate the molecular self-assembly of BTA-Methyl. As PDMA is amorphous and well soluble in water, the PDMA patches are highly swollen and, accordingly, the pendant tertiary *N,N*-dimethylaminoethyl groups are not expected to show any structural order. This makes a heterogeneous nucleation of BTA-Methyl due to an epitaxial match highly unlikely. Hence, the nucleation effect might be attributed to an accumulation (local increase in concentration) of BTA-Methyl in the PDMA patches at the fibers' surface promoted by the chemical match of peripheral groups of BTA-Methyl and pendant tertiary amino groups in the PDMA patches.

To get a closer insight into the superstructure formation via molecular self-assembly of BTA-Methyl mediated by the functional PDMA patches at the surface of PS<sub>core</sub>/SEDMA fibers, electrospun polymer fibers with immobilized, nonfunctional patchy micelles (PS<sub>core</sub>/SEM) and neat PS fibers were prepared and used as reference (**Figure 2**). Here, SEM denotes patchy worm-like micelles prepared by CDSA of a polystyrene-*block*-polyethylene-*block*-poly(methyl methacrylate) triblock terpolymer. Replacing the functional hydrophilic PDMA patches by hydrophobic poly(methyl methacrylate) (PMMA) patches in the micellar corona led predominantly to an accumulation of unstructured BTA-Methyl assemblies near the polymer fiber, which is attributed to a drying effect (**Figure 2 A**). In a similar manner, neat PS fibers also resulted in non-defined BTA structures near the polymer fibers, however to a slightly lesser extent (**Figure 2 B**).

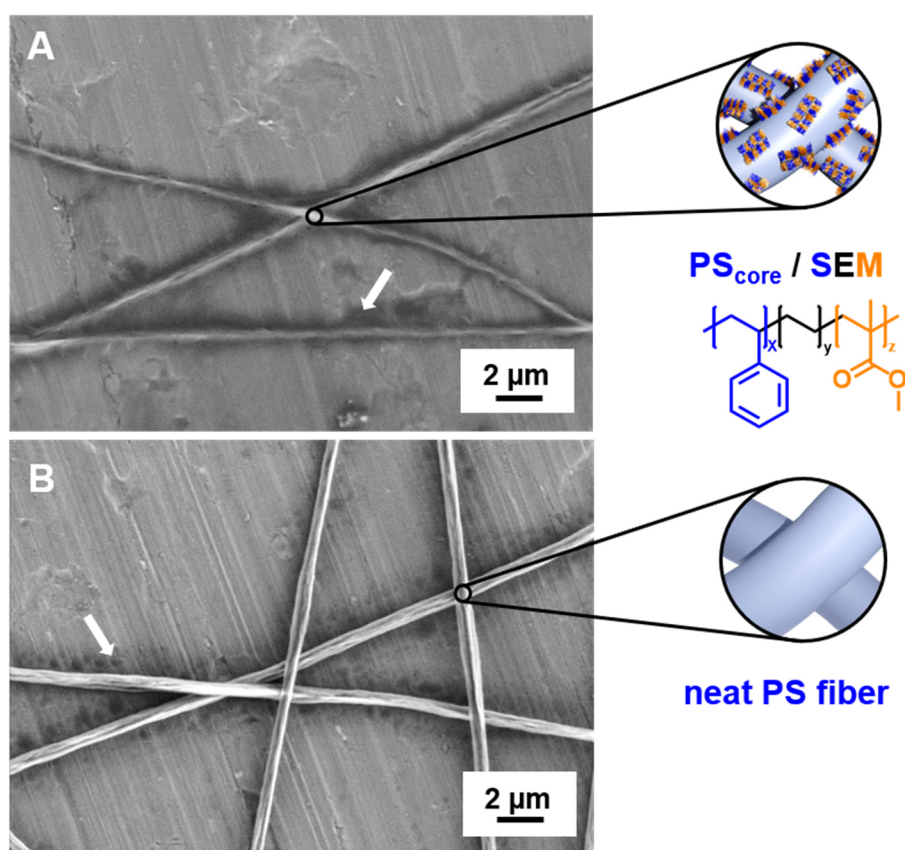


**Figure 2.** Scanning electron micrographs showing the absence of hierarchical superstructures for reference experiments employing A) PS fibers with patchy worm-like micelles of polystyrene-*block*-polyethylene-*block*-poly(methyl methacrylate) (PS<sub>core</sub>/SEM) and B) neat PS fibers without patches in the molecular self-assembly of BTA-Methyl. The arrows indicate unstructured BTA-Methyl assemblies formed upon drying.

This clearly demonstrates that neither a neat PS fiber nor patchy SEM micelles on top of the supporting PS fiber are sufficient to initiate the molecular self-assembly of BTA-Methyl, underlining the necessity of a chemical match of the pendant tertiary amino groups in the micellar patches and the peripheral groups of BTA-Methyl. Consequently, two decisive factors might be extracted from these observations: i) The patches need to be soluble in the solvent (here water) used for the molecular self-assembly of BTA-Methyl as, otherwise, they would not be accessible; and ii) hydrogen-bonding and dipole interactions between the pendant tertiary amino groups in the functional PDMA patches and the peripheral substituents of BTA-Methyl most likely result in a local increase of the BTA-Methyl concentration within the PDMA patches. The latter might in turn facilitate the formation of nuclei and, thus, a patch-mediated molecular self-assembly of BTA-Methyl from the surface of the patchy PS<sub>core</sub>/SEDMA fibers.

To support our assumption that the PDMA patches locally increase the concentration of BTA-Methyl and, thus, induce controlled self-assembly, the concentration of the BTA-Methyl solution was systematically varied (**Figure 3**). For a low BTA-Methyl concentration of only  $c = 0.025$  wt. % in water, no molecular self-assembly at the patchy PS<sub>core</sub>/SEDMA fibers was observed (**Figure 3 A**). Up to an initial concentration of  $c = 0.100$  wt. %, highly defined superstructures by patch-mediated molecular self-assembly were obtained (**Figure 3 B, C**). However, a further increase in concentration to  $c = 0.250$  wt. % led to very dense, less ordered supramolecular BTA-Methyl fibers instead of well-defined hierarchical superstructures (**Figure 3 D**). For the self-assembly of neat BTA-Methyl upon solvent evaporation, the formation of ordered structures was only observed from aqueous solutions with a concentration higher than  $c = 0.250$  wt. % (**Figure S4**). At this concentration, homogeneous nucleation is favored, resulting in star-shaped assemblies where several fibers emanate from one central starting point. Consequently, there is a competition between the patch-mediated molecular self-assembly and homogeneous BTA-Methyl nucleation. At low concentrations, that is, well below the concentration where self-assembly is observed for neat BTA-Methyl solutions, the patch-mediated self-assembly dominates and is driven by the local increase in BTA-Methyl concentration in the PDMA patches allowing the formation of BTA-Methyl nuclei. In contrast, at higher concentrations the homogeneous nucleation of BTA-Methyl to randomly distributed supramolecular fibers is favored and control over the formed superstructure is lost.

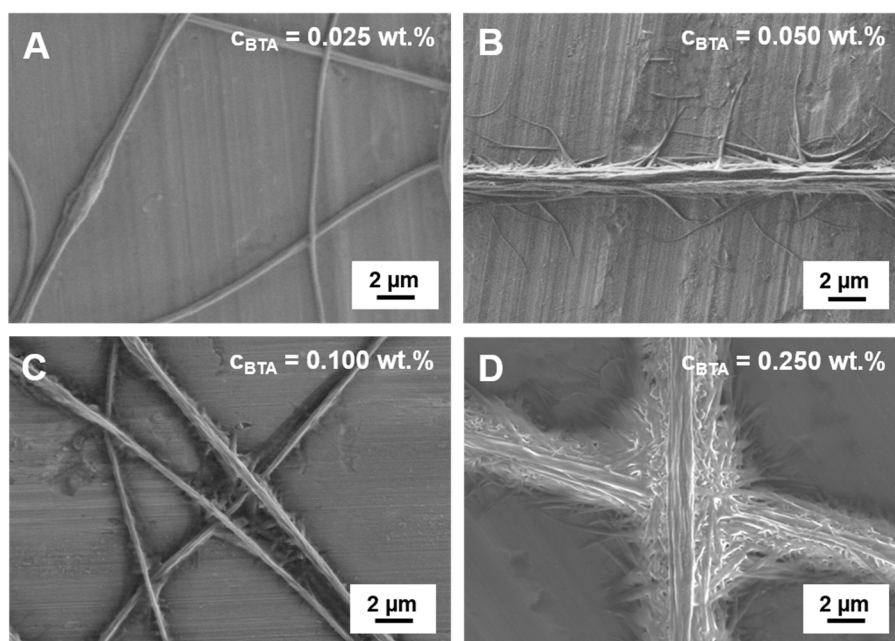


**Figure 3.** Scanning electron micrographs of hierarchical superstructures prepared by employing a A) 0.025 wt. %, B) 0.050 wt. %, C) 0.100 wt. % and D) 0.250 wt. % aqueous BTA-Methyl solution for molecular self-assembly onto patchy PS<sub>core</sub>/SEDMA fibers.

In conclusion, this work shows that polymer fibers with tailored functional surface patches can induce the molecular self-assembly of a designed 1,3,5-benzenetricarboxamide (BTA) into well-defined hierarchical fir-tree-like superstructures. The key for the patch-mediated molecular self-assembly of the BTA from the polymer fibers is the chemical match of the functional groups in the surface patches and the BTA peripheral groups that in turn controls the solubility and accessibility of the patch for the BTA. In particular, a close chemical match between the patches and the periphery of the molecular building blocks and their concentration can be regarded as design criteria for such hierarchical superstructures. These results open the opportunity to construct a large variety of complex hierarchical superstructures, as the chemistry of the polymer patches and the BTA peripheral groups can be easily tuned to transfer this concept to other functional components and solvent systems. This might stimulate further research on the fabrication of functional hierarchical superstructures for (nano)particle separation and immobilization with potential applications in filtration and heterogeneous catalysis.



### **Acknowledgements**

This work was supported by the German Research Foundation (DFG) in the framework of the Collaborative Research Centre SFB 840, projects A2 and B8. We thank Prof. Andreas Greiner for help with coaxial electrospinning. We acknowledge the Keylab Electron and Optical Microscopy of the Bavarian Polymer Institute (University of Bayreuth) for providing access to the electron microscopy facilities and for support during measurements. A.F. thanks the Elite Study Program Macromolecular Science within the Elite Network of Bavaria (ENB) for support. A.F. and C.H. acknowledge support by the University of Bayreuth Graduate School. Open access funding enabled and organized by Projekt DEAL.

### **Conflict of Interest**

The authors declare no conflict of interest.

### **Keywords**

crystallization-driven self-assembly · hierarchical superstructures · molecular self-assembly · patchy polymer fibers · supramolecular structures



## References\*

- [1] a) F. H. Schacher, P. A. Rugar, I. Manners.  
*Functional Block Copolymers: Nanostructured Materials with Emerging Applications*,  
Angew. Chem. Int. Ed. **2012**, 51, 7898–7921; Angew. Chem. **2012**, 124, 8020–8044.
- b) A. H. Gröschel, A. Walther, T. I. Löbbling, F. H. Schacher, H. Schmalz, A. H. E. Müller.  
*Guided hierarchical co-assembly of soft patchy nanoparticles*,  
Nature **2013**, 503, 247–251.
- c) J. C. Brendel, F. H. Schacher.  
*Block Copolymer Self-Assembly in Solution-Quo Vadis?*,  
Chem. Asian J. **2018**, 13, 230–239.
- d) A. H. Gröschel, A. H. E. Müller.  
*Self-assembly concepts for multicompartment nanostructures*,  
Nanoscale **2015**, 7, 11841–11876.
- e) D. J. Lunn, J. R. Finnegan, I. Manners.  
*Self-assembly of “patchy” nanoparticles: a versatile approach to functional hierarchical materials*,  
Chem. Sci. **2015**, 6, 3663–3673.
- f) U. Tritschler, S. Pearce, J. Gwyther, G. R. Whittell, I. Manners.  
*50th Anniversary Perspective: Functional Nanoparticles from the Solution Self-Assembly of Block Copolymers*,  
Macromolecules **2017**, 50, 3439–3463.
- g) A. O. Moughton, M. A. Hillmyer, T. P. Lodge.  
*Multicompartment Block Polymer Micelles*,  
Macromolecules **2012**, 45, 2–19.
- [2] a) X. Wang, G. Guerin, H. Wang, Y. Wang, I. Manners, M. A. Winnik.  
*Cylindrical Block Copolymer Micelles and Co-Micelles of Controlled Length and Architecture*,  
Science **2007**, 317, 644–647.

---

\*The titles of the publications are included in this list of references.

b) J. B. Gilroy, T. Gädt, G. R. Whittell, L. Chabanne, J. M. Mitchels, R. M. Richardson, M. A. Winnik, I. Manners.

*Monodisperse cylindrical micelles by crystallization-driven living self-assembly,*  
Nat. Chem. **2010**, 2, 566–570.

c) S. Ganda, M. H. Stenzel.

*Concepts, fabrication methods and applications of living crystallization-driven self-assembly of block copolymers,*  
Prog. Polym. Sci. **2020**, 101, 101195.

[3] a) L. MacFarlane, C. Zhao, J. Cai, H. Qiu, I. Manners.

*Emerging applications for living crystallization-driven self-assembly,*  
Chem. Sci. **2021**, 12, 4661–4682.

b) J. Schmelz, M. Karg, T. Hellweg, H. Schmalz.

*General pathway toward crystalline-core micelles with tunable morphology and corona segregation,*  
ACS Nano **2011**, 5, 9523–9534.

c) J. Schmelz, A. E. Schedl, C. Steinlein, I. Manners, H. Schmalz.

*Length Control and Block-Type Architectures in Worm-Like Micelles with Polyethylene Cores,*  
J. Am. Chem. Soc. **2012**, 134, 14217–14225.

d) H. Qiu, Z. M. Hudson, M. A. Winnik, I. Manners.

*Multidimensional hierarchical self-assembly of amphiphilic cylindrical block comicelles,*  
Science **2015**, 347, 1329–1332.

e) T. Gädt, N. S. Jeong, G. Cambridge, M. A. Winnik, I. Manners.

*Complex and hierarchical micelle architectures from diblock copolymers using living, crystallization-driven polymerizations,*  
Nat. Mater. **2009**, 8, 144–150.

- f) H. Dou, M. Li, Y. Qiao, R. Harniman, X. Li, C. E. Boott, S. Mann, I. Manners.  
*Higher-order assembly of crystalline cylindrical micelles into membrane-extendable colloidosomes,*  
Nat. Commun. **2017**, 8, 426.
- g) O. E. C. Gould, H. Qiu, D. J. Lunn, J. Rowden, R. L. Harniman, Z. M. Hudson, M. A. Winnik, M. J. Miles, I. Manners.  
*Transformation and patterning of supermicelles using dynamic holographic assembly,*  
Nat. Commun. **2015**, 6, 10009.
- [4] a) L. Brunsveld, B. J. Folmer, E. W. Meijer, R. P. Sijbesma.  
*Supramolecular polymers,*  
Chem. Rev. **2001**, 101, 4071–4097.
- b) T. F. A. de Greef, M. M. J. Smulders, M. Wolffs, A. P. H. J. Schenning, R. P. Sijbesma, E. W. Meijer.  
*Supramolecular Polymerization,*  
Chem. Rev. **2009**, 109, 5687–5754.
- [5] a) T. Aida, E. W. Meijer, S. I. Stupp.  
*Functional Supramolecular Polymers,*  
Science **2012**, 335, 813–817.
- b) T. Aida, E. W. Meijer.  
*Supramolecular Polymers – we’ve Come Full Circle,*  
Isr. J. Chem. **2020**, 60, 33–47.
- c) F. V. Gruschwitz, T. Klein, S. Catrouillet, J. C. Brendel.  
*Supramolecular polymer bottlebrushes,*  
Chem. Commun. **2020**, 56, 5079–5110.
- d) K. Liu, Y. Kang, Z. Wang, X. Zhang.  
*25th Anniversary Article: Reversible and Adaptive Functional Supramolecular Materials: “Noncovalent Interaction” Matters,*  
Adv. Mater. **2013**, 25, 5530–5548.

e) D. Spitzer, L. L. Rodrigues, D. Straßburger, M. Mezger, P. Besenius.

*Tunable Transient Thermogels Mediated by a pH- and Redox-Regulated Supramolecular Polymerization,*

Angew. Chem. Int. Ed. **2017**, 56, 15461–15465;

Angew. Chem. **2017**, 129, 15664–15669.

f) B. N. S. Thota, X. Lou, D. Bochicchio, T. F. E. Paffen, R. P. M. Lafleur,

J. L. J. van Dongen, S. Ehrmann, R. Haag, G. M. Pavan, A. R. A. Palmans, E. W. Meijer.

*Supramolecular Copolymerization as a Strategy to Control the Stability of Self-Assembled Nanofibers,*

Angew. Chem. Int. Ed. **2018**, 57, 6843–6847;

Angew. Chem. **2018**, 130, 6959–6963.

g) S.-P. Wang, W. Lin, X. Wang, T.-Y. Cen, H. Xie, J. Huang, B.-Y. Zhu, Z. Zhang, A. Song, J. Hao, J. Wu, S. Li.

*Controllable hierarchical self-assembly of porphyrin-derived supra-amphiphiles,*

Nat. Commun. **2019**, 10, 1399.

[6] a) J. Matern, Y. Dorca, L. Sánchez, G. Fernández.

*Revising Complex Supramolecular Polymerization under Kinetic and Thermodynamic Control,*

Angew. Chem. Int. Ed. **2019**, 58, 16730–16740;

Angew. Chem. **2019**, 131, 16884–16895.

b) M. Wehner, F. Würthner.

*Supramolecular polymerization through kinetic pathway control and living chain growth,*

Nat. Rev. Chem. **2020**, 4, 38–53.

c) E. Weyandt, M. F. J. Mabesoone, L. N. J. de Windt, E. W. Meijer, A. R. A. Palmans, G. Vantomme.

*How to Determine the Role of an Additive on the Length of Supramolecular Polymers?,*

Org. Mater. **2020**, 2, 129–142.

- d) S. Ogi, K. Sugiyasu, S. Manna, S. Samitsu, M. Takeuchi.  
*Living supramolecular polymerization realized through a biomimetic approach,*  
Nat. Chem. **2014**, 6, 188–195.
- e) K. Zhang, M. C.-L. Yeung, S. Y.-L. Leung, V. W.-W. Yam.  
*Living supramolecular polymerization achieved by collaborative assembly of platinum(II) complexes and block copolymers,*  
Proc. Natl. Acad. Sci. USA **2017**, 114, 11844–11849.
- f) A. Singh, J. P. Joseph, D. Gupta, I. Sarkar, A. Pal.  
*Pathway driven self-assembly and living supramolecular polymerization in an amyloid-inspired peptide amphiphile,*  
Chem. Commun. **2018**, 54, 10730–10733.
- [7] a) S. Agarwal, A. Greiner, J. H. Wendorff.  
Functional materials by electrospinning of polymers,  
Prog. Polym. Sci. **2013**, 38, 963–991.
- b) A. Greiner, J. H. Wendorff.  
*Electrospinning: A Fascinating Method for the Preparation of Ultrathin Fibers,*  
Angew. Chem. Int. Ed. **2007**, 46, 5670–5703; Angew. Chem. **2007**, 119, 5770–5805.
- [8] a) J. Schöbel, M. Burgard, C. Hils, R. Dersch, M. Dulle, K. Volk, M. Karg, A. Greiner, H. Schmalz.  
*Bottom-Up Meets Top-Down: Patchy Hybrid Nonwovens as an Efficient Catalysis Platform,*  
Angew. Chem. Int. Ed. **2017**, 56, 405–408; Angew. Chem. **2017**, 129, 416–419.
- b) C. Hils, M. Dulle, G. Sitaru, S. Gekle, J. Schöbel, A. Frank, M. Drechsler, A. Greiner, H. Schmalz.  
*Influence of patch size and chemistry on the catalytic activity of patchy hybrid nonwovens,*  
Nanoscale Adv. **2020**, 2, 438–452.

- [9] M. Burgard, D. Weiss, K. Kreger, H. Schmalz, S. Agarwal, H.-W. Schmidt, A. Greiner.  
*Mesostructured Nonwovens with Penguin Downy Feather-Like Morphology—  
Top-Down Combined with Bottom-Up,*  
Adv. Funct. Mater. **2019**, 29, 1903166.
- [10] J. Schöbel, C. Hils, A. Weckwerth, M. Schlenk, C. Bojer, M. C. A. Stuart, J. Brey,  
S. Förster, A. Greiner, M. Karg, H. Schmalz.  
*Strategies for the selective loading of patchy worm-like micelles with functional  
nanoparticles,*  
Nanoscale **2018**, 10, 18257–18268.
- [11] A. Frank, A. Bernet, K. Kreger, H.-W. Schmidt.  
*Supramolecular microtubes based on 1,3,5-benzenetricarboxamides prepared by  
self-assembly upon heating,*  
Soft Matter **2020**, 16, 4564–4568.
- [12] C. Hils, E. Fuchs, F. Eger, J. Schöbel, H. Schmalz.  
*Converting Poly(Methyl Methacrylate) into a Triple-Responsive Polymer,*  
Chem. Eur. J. **2020**, 26, 5611-5614.

## Supporting Information

### *Hierarchical Superstructures by Combining Crystallization-Driven and Molecular Self-Assembly*

Andreas Frank<sup>+</sup>, Christian Hils<sup>+</sup>, Melina Weber, Klaus Kreger, Holger Schmalz,<sup>\*</sup> and Hans-Werner Schmidt<sup>\*</sup>

## Table of Contents

### 1. Experimental Procedures and Methods

### 2. Supporting Figures

- S1:** Transmission electron micrograph of patchy worm-like SEDMA triblock terpolymer micelles
- S2:** Temperature-dependent turbidity measurements of aqueous BTA-Methyl solutions
- S3:** Micro-differential scanning calorimetry measurements of aqueous BTA-Methyl solutions
- S4:** Self-assembly of aqueous BTA-Methyl solutions upon solvent evaporation onto aluminium foil
- S5:** Raman measurements
- S6:** Spatially resolved component distribution from Raman imaging

### 3. References

## Experimental Procedures

### **Materials.**

All chemicals were used as received unless otherwise noted. *N,N*-dimethylformamide (DMF, 99%, Acros Organics), tetrahydrofuran (THF,  $\geq 99.9\%$ , VWR). Polystyrene (PS) was synthesized by anionic polymerization in THF at  $-80\text{ }^{\circ}\text{C}$  using *sec*-butyllithium as initiator ( $M_n = 1.8 \cdot 10^6\text{ g}\cdot\text{mol}^{-1}$ ,  $\text{Đ} = 1.08$ ).

### **Synthesis of $N^1, N^3, N^5$ -tris[2-(dimethylamino)-ethyl]-1,3,5-benzenetricarboxamide (BTA-Methyl).**

BTA-Methyl was synthesized as described previously.<sup>[1]</sup> Briefly, trimesic acid trimethyl ester was dispersed in *N,N*-dimethylethylenediamine under an argon atmosphere. The mixture was heated to  $125\text{ }^{\circ}\text{C}$ , stirred overnight and subsequently allowed to cool down to room temperature. The resulting mixture was dispersed in acetone and heated until an almost clear solution was obtained. The hot solution was filtrated using a sintered glass funnel filter. The solvent was removed and the product was dried in a vacuum oven at  $50\text{ }^{\circ}\text{C}$  over night, yielding a white powder.

### **Synthesis of triblock terpolymers.**

Polystyrene-*block*-polyethylene-*block*-poly(methyl methacrylate) ( $S_{40}E_{21}M_{39}^{108}$ ) was synthesized by a combination of living anionic polymerization and catalytic hydrogenation, as described elsewhere.<sup>[2]</sup> Polystyrene-*block*-polyethylene-*block*-poly(*N,N*-dimethylaminoethyl methacrylamide) ( $S_{33}E_{17}DMA_{50}^{132}$ ) was prepared *via* post-polymerization functionalization of the poly(methyl methacrylate) (PMMA) block of  $S_{40}E_{21}M_{39}^{108}$ .<sup>[3,4]</sup> In the used triblock terpolymer notation the subscripts describe the mass fraction of the corresponding block in wt.% and the superscript denotes the overall number average molecular weight ( $M_n$ ) in  $\text{kg}\cdot\text{mol}^{-1}$ .  $M_n$  was determined by a combination of MALDI-ToF MS (matrix-assisted laser desorption/ionization – time of flight mass spectrometry) and  $^1\text{H}$  NMR (nuclear magnetic resonance) spectroscopy, employing the absolute  $M_n$  of the polystyrene precursor from MALDI-ToF for  $^1\text{H}$  NMR signal calibration.



**Formation of patchy worm-like triblock terpolymer micelles.**

The patchy worm-like micelles were prepared by crystallization-driven self-assembly (CDSA) of the triblock terpolymers  $S_{40}E_{21}M_{39}^{108}$  and  $S_{33}E_{17}DMA_{50}^{132}$  in THF according to our previous work.<sup>[2,3]</sup> The polymers were dissolved in THF ( $c = 10 \text{ g}\cdot\text{L}^{-1}$ ) at  $65 \text{ }^\circ\text{C}$  for 0.5 h using a thermostated shaker unit (HCL-MKR 13, Ditabis). The self-assembly process occurred by subsequently cooling to the crystallization temperature ( $T_c$ ) of the polyethylene middle block (**Table S1**). The process was allowed to proceed for 24 h with 200 rpm resulting in the respective patchy worm-like micelle dispersions.

**Table S1:** Properties of the used patchy worm-like micelles.

Triblock terpolymer <sup>[a]</sup>	$T_c$ [ $^\circ\text{C}$ ] <sup>[b]</sup>	patch size [nm] <sup>[c]</sup>		length of micelles [nm] <sup>[c]</sup>	Ref.
		S	M / DMA		
$S_{40}E_{21}M_{39}^{108}$	20	$13 \pm 4$	$13 \pm 4$	$520 \pm 140$	[2,5]
$S_{33}E_{17}DMA_{50}^{132}$	21	$18 \pm 5$	$17 \pm 5$	$510 \pm 310$	[3]

<sup>[a]</sup> Subscripts describe the mass fraction of the corresponding block in wt.% and the superscript denotes the overall molecular weight in  $\text{kg}\cdot\text{mol}^{-1}$ .

<sup>[b]</sup> crystallization temperature of the PE block,  $c = 10 \text{ g}\cdot\text{L}^{-1}$  in THF.

<sup>[c]</sup> Average sizes  $\pm$  standard deviation as determined by TEM image analysis of at least 100 micelles/patches.

***Electrospinning.***

*Preparation of patchy polymer fibres PS<sub>core</sub> / SEM and PS<sub>core</sub> / SEDMA.* Patchy polymer fibres were produced by coaxial electrospinning, according to our previous work.<sup>[3,6]</sup> To this end, a 7 wt.% polystyrene (PS<sub>core</sub>) ( $M_n = 1.8 \cdot 10^6 \text{ g} \cdot \text{mol}^{-1}$ ) solution in DMF was used as core and for the shell dispersions of patchy worm-like SEM or SEDMA micelles in THF ( $c = 10 \text{ g} \cdot \text{L}^{-1}$ ) were employed. The fibres were spun on a collector placed at a distance of 20 cm from the coaxial needle (COAX\_2DISP sealed coaxial needles, LINARI NanoTech,  $d_{\text{core}} = 0.51 \text{ mm}$  and  $d_{\text{shell}} = 1.37 \text{ mm}$ ) at a temperature of 20.8 °C and a relative humidity of ca. 30%. For electrospinning, a high voltage of 11.4 kV at the needle and -1.0 kV at the collector were applied. The feed rate of the PS<sub>core</sub> solution was 1.2 mL·h<sup>-1</sup> and for the micellar dispersions 1.0 mL·h<sup>-1</sup>. Neat polystyrene fibres were prepared as reference material in the same manner but without using the micellar dispersions.

***Self-assembly of aqueous BTA-Methyl solutions upon solvent evaporation onto aluminium foil.***

25 µL of an aqueous BTA-Methyl solution with concentrations ranging from 0.025 to 1.000 wt.% were dropped onto aluminium foil and the solvent was allowed to evaporate at ambient conditions. After solvent evaporation, turbid films were obtained and investigated by scanning electron microscopy.

***Self-assembly of aqueous BTA-Methyl solutions onto patchy polymer fibres.***

The PS<sub>core</sub> / SEDMA and PS<sub>core</sub> / SEM fibres as well as the neat PS fibres on aluminium foil were immersed into BTA-Methyl solutions (varying in concentration ranging from 0.025 wt.% to 0.250 wt.% with a pH value from 7 to 11, respectively) for a fixed time of 30 s and allowed to dry at ambient conditions for complete solvent evaporation.

## Methods

### *Scanning electron microscopy.*

For scanning electron microscopy measurements, a FEI Quanta FEG 250 scanning electron microscope (Thermo Fisher Scientific) equipped with a field emission gun was used. The untreated samples, i.e. without applying a sputter coating, were measured in the beam deceleration mode (only **Figure 1A, 1C and 3B**) or in the low vacuum mode. Measurements in the beam deceleration mode were conducted under high vacuum at an acceleration voltage of 6 kV. This mode was used to image surfaces at high magnification with a concentric back scattered (CBS) electron detector, which is insensitive to sample charging. Here, an additional negative voltage (bias, -4 kV) was applied to the stage. In this way, the primary electrons were decelerated to 2 kV when reaching the sample and interacted electrons were accelerated toward the CBS detector. The samples measured in the low vacuum mode (water pressure of 40 Pa in the sample chamber) were mounted on a sample holder using an adhesive graphite pad and were investigated with an acceleration voltage of 3 kV with a large-field (gaseous secondary electron) detector (LFD) for topographical details.

### *Transmission electron microscopy.*

The morphology of triblock terpolymer worm-like micelles were analysed by elastic bright-field transmission electron microscopy (TEM) on a Zeiss 922 Omega EFTEM (Zeiss NTS GmbH, Oberkochen, Germany). Zero-loss filtered images were recorded digitally on a bottom mounted CCD camera system (Ultrascan 1000, Gatan) at an acceleration voltage of 200 kV. The micrographs were processed with the digital imaging processing system of Gatan (Digital Micrograph 3.9 for GMS 1.4). The samples were diluted to  $c = 0.1 \text{ g}\cdot\text{L}^{-1}$  and a droplet was placed onto a carbon coated copper grid. The residual solvent was immediately blotted by filter paper, dried in a vacuum oven (20 mbar, room temperature) and stained with  $\text{RuO}_4$  vapor (selective staining of PS). The average length and patch size were determined by measuring at least 100 micelles/patches using the software ImageJ.<sup>[7]</sup>

***Raman imaging.***

A WITec alpha 300 RA+ imaging system, equipped with a UHTS 300 spectrometer and a back-illuminated Andor Newton 970 EMCCD camera, was employed for confocal Raman imaging. The measurements were conducted at an excitation wavelength of  $\lambda = 532$  nm, using a laser power of 4 mW and an integration time of  $0.6 \text{ s}\cdot\text{pixel}^{-1}$  (100x objective, NA = 0.9, step size  $100 \text{ nm}\cdot\text{pixel}^{-1}$ , software WITec Control FIVE 5.3). All spectra were subjected to a cosmic ray removal routine and baseline correction. The spatial distribution of PS and BTA-Methyl was determined using the tool “true component analysis” in the WITec Project FIVE 5.3 software.

***Crystallization system Crystal16.***

Temperature-dependent turbidity measurements of aqueous BTA-Methyl solutions were determined optically for eight concentrations in parallel at a wavelength of  $\lambda = 645$  nm using the crystallization system Crystal16 (Technobis Crystallization Systems). Concentrations of 0.05, 0.10, 0.25, 0.50, 0.75, 1.00, 1.50 and 2.00 wt.% of BTA-Methyl in water were prepared at room temperature. The transmittance at  $\lambda = 645$  nm of each sample was recorded for two cycles in the range of 5 to 90 °C. Each cycle consists of a heating and cooling step with a scanning rate of  $0.5 \text{ K}\cdot\text{min}^{-1}$ .

***Micro-differential scanning calorimetry.***

Micro-differential scanning calorimetry measurements were performed on a SETARAM Micro DSC III using sealed measuring cells (“batch cells”,  $V = 1 \text{ mL}$ , stainless steel) filled with about 0.7 mL of aqueous solution of the BTA-Methyl at a concentration of  $c = 0.05$  or 2.00 wt.%. The measurements were carried out applying a heating and cooling rate of  $0.5 \text{ K}\cdot\text{min}^{-1}$ . The reference cell was filled with an equal amount of water.

## Supporting Figures

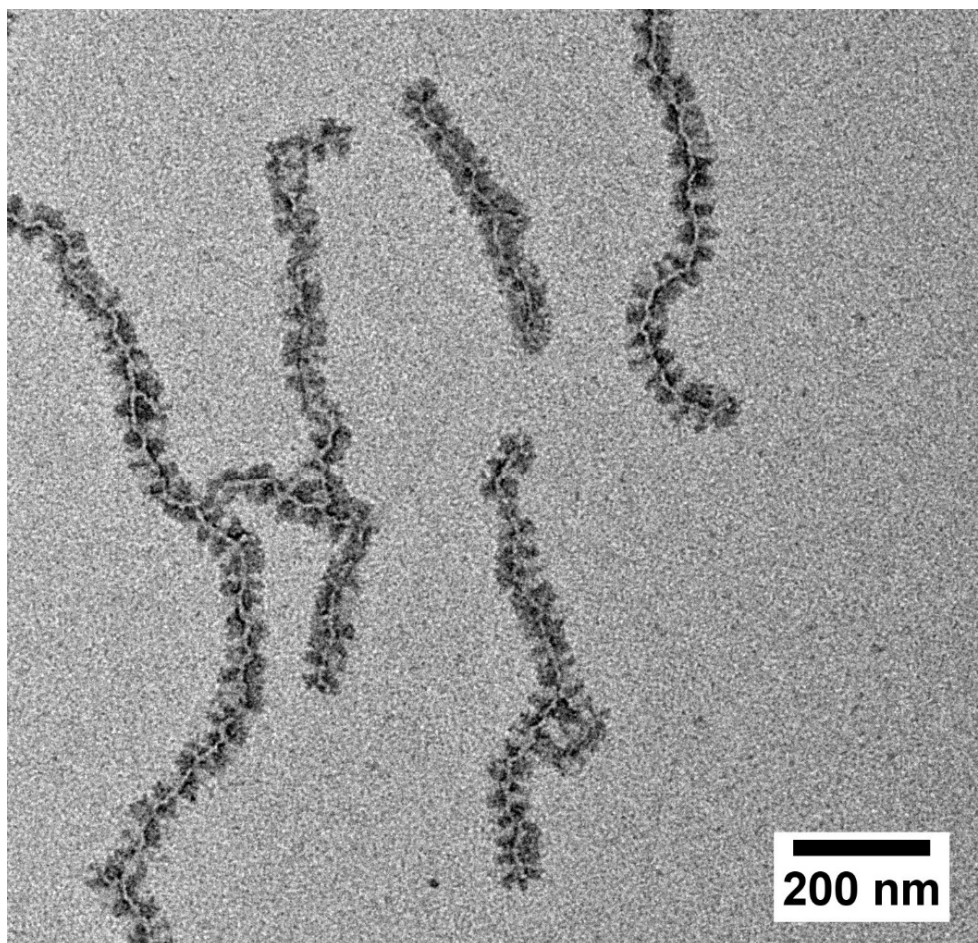


**Figure S1.** TEM micrograph of patchy worm-like  $S_{33}E_{17}DMA_{50}^{132}$  micelles ( $c = 0.1 \text{ g}\cdot\text{L}^{-1}$  in THF). The micelles are composed of polyethylene (PE) as crystalline core and almost alternating corona patches of polystyrene (PS) and poly(*N,N*-dimethylaminoethyl methacrylamide) (PDMA). The polystyrene block was selectively stained with  $\text{RuO}_4$  and appears dark.

Temperature-dependent turbidity measurement of aqueous BTA-Methyl solution. Exemplarily, both heating and cooling cycles and the recorded transmittance for BTA-Methyl with a concentration of  $c = 2.0$  wt.% are shown in **Figure S2**. During heating and cooling all measured samples show a constant transmittance of 100% indicating that the BTA-Methyl remains dissolved during the measurements.

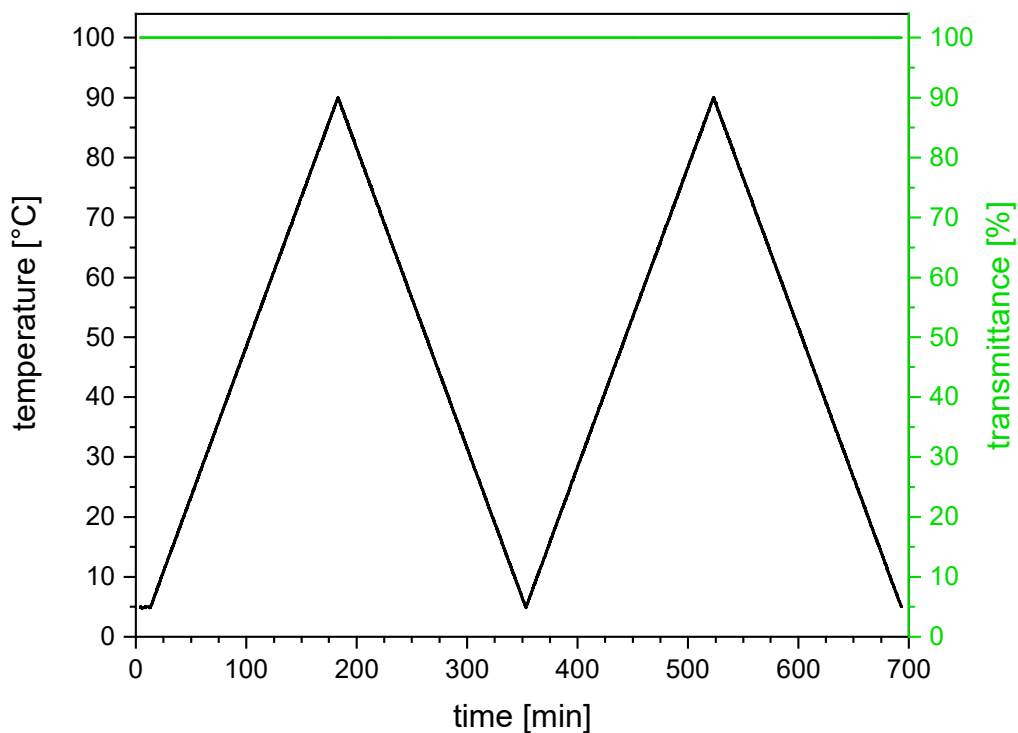


**Figure S2.** Temperature-dependent transmittance of a 2.00 wt.% aqueous BTA-Methyl solution upon subsequent heating and cooling cycles at a scanning rate of  $0.5 \text{ K}\cdot\text{min}^{-1}$ .

Exemplarily, the 2<sup>nd</sup> heating and 2<sup>nd</sup> cooling traces for the aqueous BTA-Methyl solution with a concentration of  $c = 2.00$  wt.% is shown in **Figure S3**. The same behaviour is observed for the 0.05 wt.% BTA-Methyl solution.

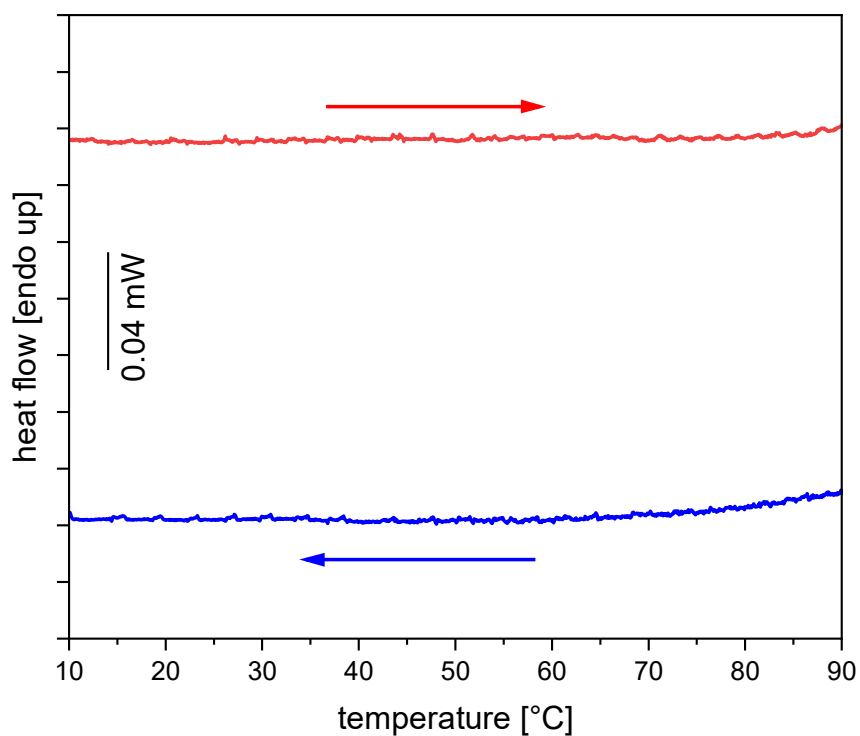


**Figure S3.** Micro-differential scanning calorimetry measurement of BTA-Methyl in water with a concentration of 2.00 wt.% at a scanning rate of  $0.5 \text{ K}\cdot\text{min}^{-1}$ .



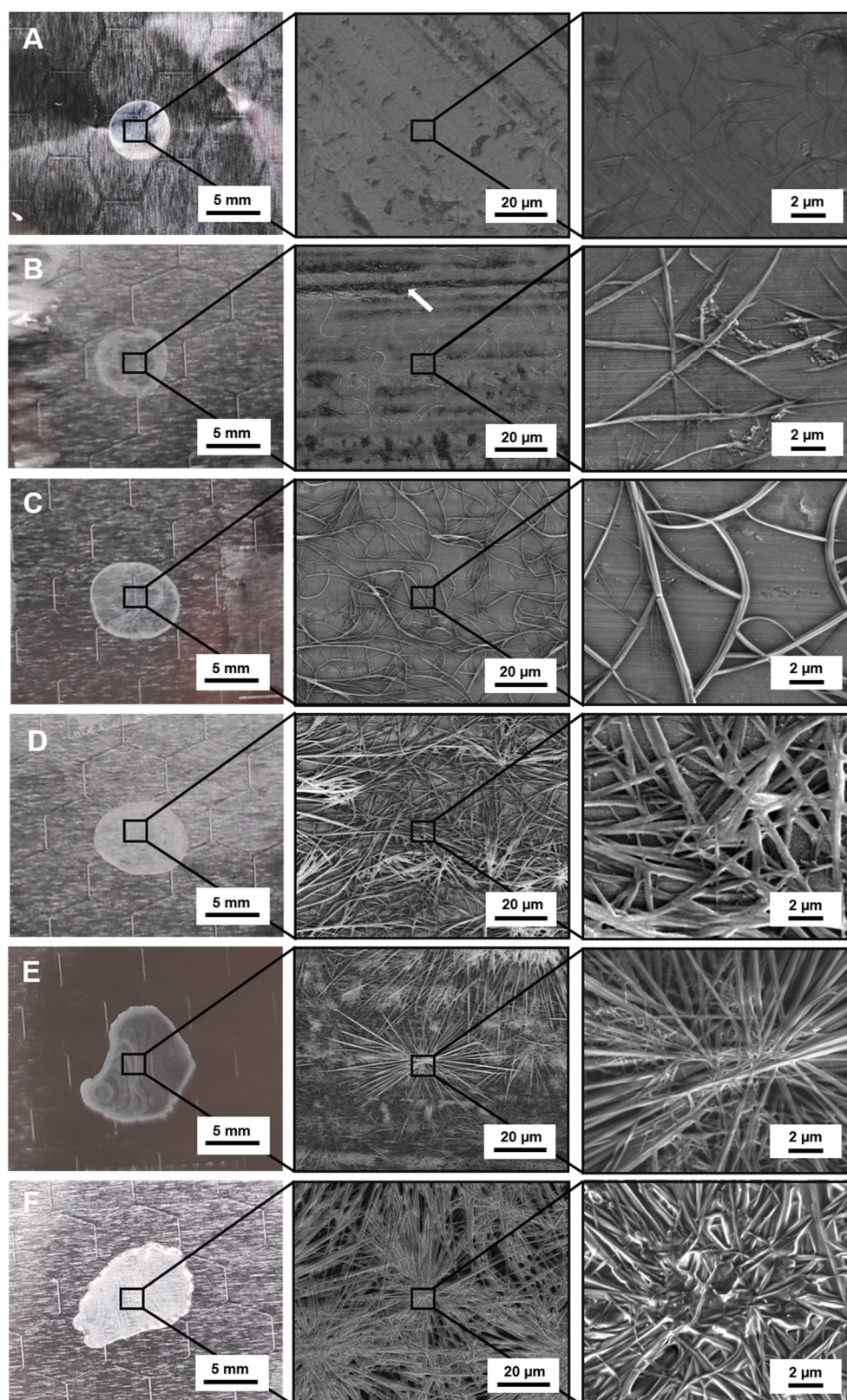


**Figure S4.** Optical (left) and scanning electron (middle and right with higher magnification) micrographs of the supramolecular fibres of BTA-Methyl prepared upon solvent evaporation from an A) 0.025 wt.% B) 0.050 wt.%, C) 0.100 wt.%, D) 0.250 wt.%, E) 0.500 wt.% and F) 1.000 wt.% aqueous solution onto aluminium foil.



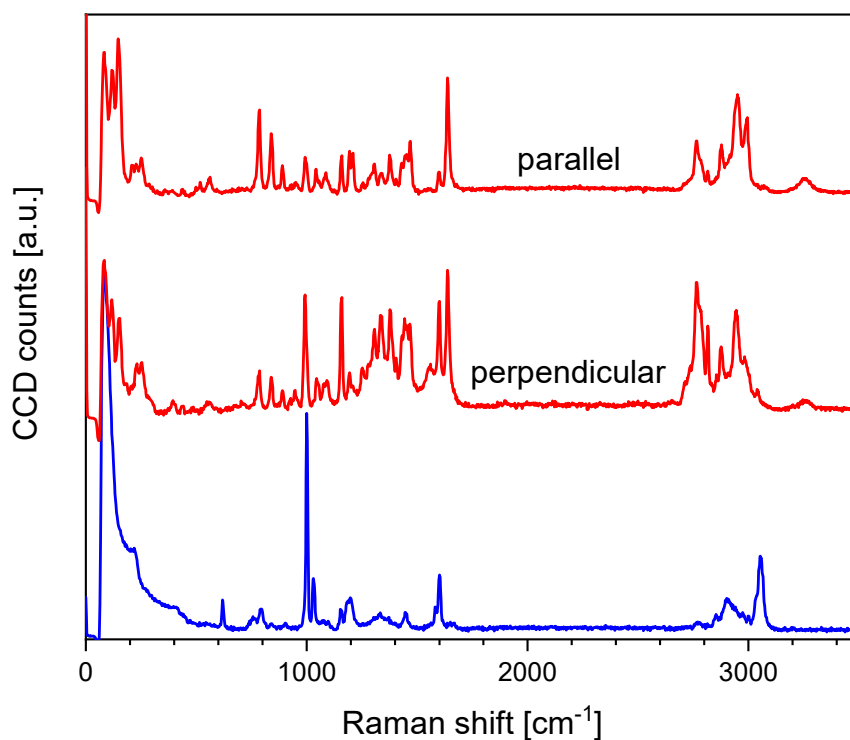


**Figure S5.** Raman measurements of polystyrene (blue) and a BTA-Methyl fibre (red) for polarization of the laser parallel and perpendicular to the self-assembled BTA-Methyl fibre long axis.

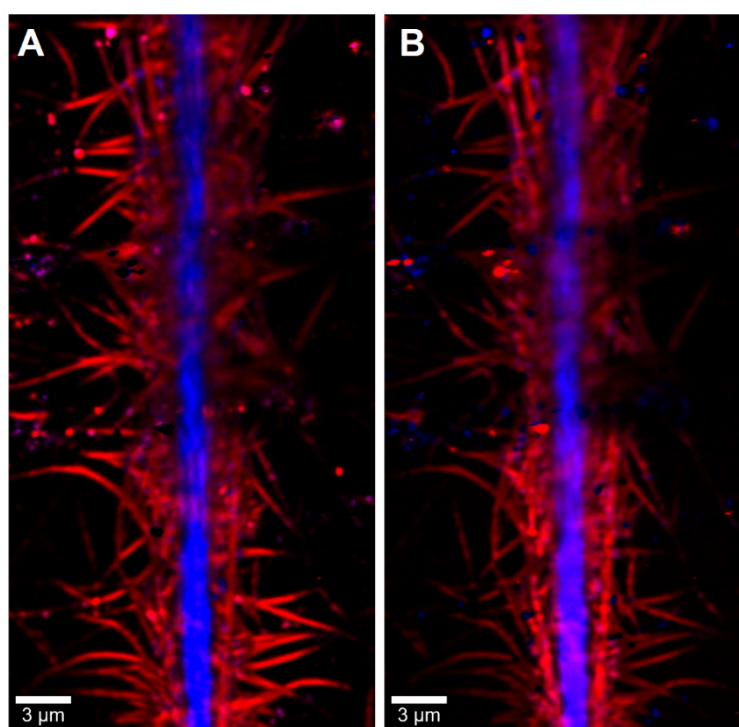


**Figure S6.** Spatially resolved component distribution from Raman imaging (horizontal polarization of the laser, PS rich regions are coloured in blue and BTA-Methyl rich in red), employing the Raman spectra of PS and BTA-Methyl for parallel and perpendicular orientation with respect to the laser polarization (**Figure S5**) in the true component analysis. As the Raman spectra of BTA-Methyl fibres depend on their orientation with respect to the laser polarization it is possible to extract the fraction of BTA-Methyl fibres being oriented parallel (A) and perpendicular (B) with respect to the laser, thus appearing more intense in the respective image.

**References\***

- [1] A. Frank, A. Bernet, K. Kreger, H.-W. Schmidt.  
*Supramolecular microtubes based on 1,3,5-benzenetricarboxamides prepared by self-assembly upon heating,*  
Soft Matter **2020**, 16, 4564–4568.
- [2] J. Schmelz, M. Karg, T. Hellweg, H. Schmalz.  
*General Pathway toward Crystalline-Core Micelles with Tunable Morphology and Corona Segregation,*  
ACS Nano **2011**, 5, 9523–9534.
- [3] C. Hils, M. Dulle, G. Sitaru, S. Gekle, J. Schöbel, A. Frank, M. Drechsler, A. Greiner, H. Schmalz.  
*Influence of patch size and chemistry on the catalytic activity of patchy hybrid nonwovens,*  
Nanoscale Adv. **2020**, 2, 438–452.
- [4] J. Schöbel, C. Hils, A. Weckwerth, M. Schlenk, C. Bojer, M. C. A. Stuart, J. Brey, S. Förster, A. Greiner, M. Karg, H. Schmalz.  
*Strategies for the selective loading of patchy worm-like micelles with functional nanoparticles,*  
Nanoscale **2018**, 10, 18257–18268.
- [5] J. Schmelz, D. Pirner, M. Krekhova, T. M. Ruhland, H. Schmalz.  
*Interfacial activity of patchy worm-like micelles,*  
Soft Matter **2013**, 9, 11173–11177.
- [6] J. Schöbel, M. Burgard, C. Hils, R. Dersch, M. Dulle, K. Volk, M. Karg, A. Greiner, H. Schmalz.  
*Bottom-Up Meets Top-Down: Patchy Hybrid Nonwovens as an Efficient Catalysis Platform,*  
Angew. Chem. Int. Ed. **2017**, 56, 405–408; Angew. Chem. **2017**, 129, 416–419.
- [7] W.S., Rasband, ImageJ, U. S. National Institutes of Health, Bethesda, Maryland, USA, “<https://imagej.nih.gov/ij/>, 1997-2018”.

---

\*The titles of the publications are included in this list of references.

#### 4.4. Functional mesostructured electrospun polymer nonwovens with supramolecular nanofibers

Andreas Frank,<sup>[a]</sup> Melina Weber,<sup>[a]</sup> Christian Hils,<sup>[b]</sup> Ulrich Mansfeld,<sup>[c]</sup> Klaus Kreger,<sup>[a]</sup> Holger Schmalz,<sup>[b]\*</sup> and Hans-Werner Schmidt<sup>[a]\*</sup>

*Dedicated to Professor Rudolf Zentel*

[a] Macromolecular Chemistry I and Bavarian Polymer Institute (BPI)  
University of Bayreuth, Universitätsstraße 30, Bayreuth 95447, Germany

[b] Macromolecular Chemistry II and Bavarian Polymer Institute (BPI)  
University of Bayreuth, Universitätsstraße 30, Bayreuth 95447, Germany

[c] Bavarian Polymer Institute (BPI)  
University of Bayreuth, Universitätsstraße 30, Bayreuth 95447, Germany

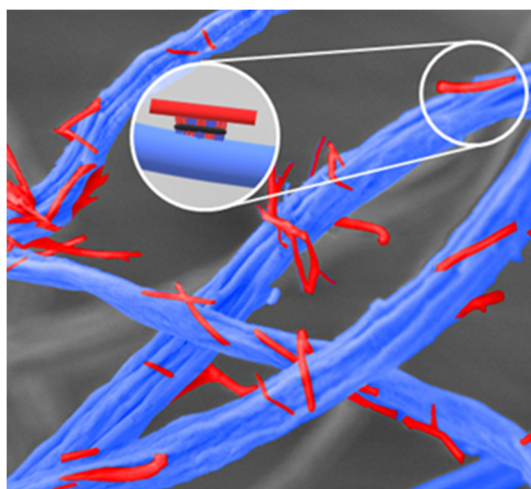
\*E-mail corresponding authors:

[hans-werner.schmidt@uni-bayreuth.de](mailto:hans-werner.schmidt@uni-bayreuth.de) and [holger.schmalz@uni-bayreuth.de](mailto:holger.schmalz@uni-bayreuth.de)

The results of this chapter have been published as a research article in  
*Macromol. Rapid Commun.* **2022**, 43, 2200052, 1–8. DOI: 10.1002/marc.202200052.

Published by Wiley-VCH GmbH. This is an open access article under the terms of the Creative Commons Attribution 4.0 International License, which permits use, distribution and reproduction in any medium, provided the original work is properly cited (© 2022 The Authors).

The ORCID identification number(s) for the author(s) of this article can be found under <https://doi.org/10.1002/marc.202200052>.

**Graphical abstract**

Mesostructured nonwovens with barbed wire-like morphologies are realized by combining electrospun polystyrene fibers, decorated with patchy worm-like micelles, with short supramolecular nanofibers of an amino-functionalized 1,3,5-benzenetricarboxamide. The patchy micelles promote the directed self-assembly and result in a fixation of both fiber types. The functional supramolecular nanofibers allow the immobilization of metal nanoparticles opening applications in separation or catalysis.

**Abstract**

Functional, hierarchically mesostructured nonwovens are of fundamental importance because complex fiber morphologies increase the active surface area and functionality allowing for the effective immobilization of metal nanoparticles. Such complex functional fiber morphologies clearly widen the property profile and enable the preparation of more efficient and selective filter media. Here, the realization of hierarchically mesostructured nonwovens with barbed wire-like morphology is demonstrated by combining electrospun polystyrene fibers, decorated with patchy worm-like micelles, with solution-processed supramolecular short fibers composed of 1,3,5-benzenetricarboxamides with peripheral *N,N*-diisopropylaminoethyl substituents. The worm-like micelles with a patchy microphase-separated corona are prepared by crystallization-driven self-assembly of a polyethylene based triblock terpolymer and deposited on top of the polystyrene fibers by coaxial electrospinning. The micelles are designed in a way that their patches promote the directed self-assembly of the 1,3,5-benzenetricarboxamide and the fixation of the supramolecular nanofibers on the supporting polystyrene fibers. Functionality of the mesostructured nonwoven is provided by the peripheral *N,N*-diisopropylaminoethyl substituents of the 1,3,5-benzenetricarboxamide and proven by the effective immobilization of individual palladium nanoparticles on the supramolecular nanofibers. The preparation of hierarchically mesostructured nonwovens and their shown functionality demonstrate that such systems are attractive candidates to be used for example in filtration, selective separation and heterogenous catalysis.

## 1. Introduction

Multifunctional hierarchical and mesostructured fibrous materials are expected to play a key role for the preparation of a new generation of filter media and membranes in life science and materials science. This includes for example personal protective equipment such as face masks with improved moisture permeability, antiviral and antibacterial properties as well as fibrous membranes with self-sustained long-range electrostatic adhesion for energy generation and compact composite sheets for catalysis.<sup>[1-4]</sup>

Conventional polymer micro- and nanofibers are achieved by top-down methods such as melt blowing,<sup>[5]</sup> centrifugal spinning,<sup>[6-8]</sup> and electrospinning.<sup>[9-11]</sup> These spinning processes are well-established and typically allows to create free-standing nonwovens or nonwovens deposited on top of a support. Improvement in this field is expected to fabricate nonwovens with different hierarchical levels in the fiber morphology.<sup>[12,13]</sup> Consequently, hierarchy is described by the combination of two or more fiber types with different fiber diameters of the entire nonwoven. This may also result in hierarchal levels with respect to the pore size distribution. For example, Zhang et al. prepared composites with different fiber diameters and pore sizes via sequential or multijet electrospinning of different polymers which shows improved filtration efficiency.<sup>[14,15]</sup> Another example of a hierarchical double layer structured composite was described by Wang et al. consisting of micro- and nanosized porous fibers and nanosized fibers of polylactic acid.<sup>[16]</sup>

Furthermore, Su et al. reviewed the combination of polymer fibers with carbon nanotubes (CNTs), demonstrating that CNTs are important for reinforcement and enhanced properties like mechanical strength and electrical conductivity.<sup>[17]</sup>

Another promising approach to achieve composites with different hierarchical fiber levels is the combination of polymer fibers and supramolecular fibers. In general, the preparation of supramolecular fibers is realized by self-assembly of molecular building blocks via directed secondary interactions. The unique feature of such a bottom-up approach is the in situ formation of the supramolecular fibers from solution, which enables the realization of composite fibers in an existing scaffold. In this context, we have demonstrated the preparation of microfiber/nanofiber composites using a commercial viscose polyester-based microfiber nonwoven and selected 1,3,5-benzenetricarboxamides (BTAs) as building blocks. These composites were found to be highly suitable for air filtration applications.<sup>[18,19]</sup> Hu et al. and Wang et al. have shown that selected small molecular sorbitol derivatives enable the formation

of supramolecular nanofiber webs within solution-blown polyacrylonitrile (PAN) nanofibers.<sup>[2,20]</sup> Such fiber composites can be used as air filter media with an improved moisture permeation due to the loading with the hydrophilic sorbitol nanofibers.<sup>[2]</sup>

Apart from these hierarchical supramolecular/polymer fiber composites, we have recently reported on mesoscale nonwovens, in those the supramolecular nanofibers feature a dedicated functionality enabling the efficient immobilization of gold nanoparticles. For this, we employed the wet-laid technique using a mixture of short electrospun PAN and supramolecular nanofibers based on BTAs with functional terpyridine side groups in the periphery resulting in compact functional nonwoven sheets.<sup>[4]</sup>

Besides these kinds of nonwovens, whose morphologies are a result of the combination of different fiber types, nature uses an intriguing approach based on hierarchically mesostructured fibers as present in plants like thistles and animal feathers. Such hierarchically mesostructured fibers comprise a middle strand with off-standing thinner branches and feature a superior property profile. In this context, we have demonstrated the preparation of hierarchically mesostructured nonwovens comprising an electrospun supporting polymer fiber with off-standing branches of nonfunctional supramolecular BTA fibers. Consequently, the hierarchical level refers to a fibrous superstructure, which we refer here as hierarchical mesostructured fibers. This morphology was realized by depositing BTA seeds on the electrospun fibers followed by an in situ growth of the BTA nanofibers from solution leading to a penguin downy feather-like morphology.<sup>[21]</sup> Such nonwovens enable the removal of particulate matter from air with improved efficiency while at the same time a low pressure drop is maintained.<sup>[21]</sup>

In a proof-of-concept we have also realized hierarchical superstructures composed of electrospun patchy polymer fibers with off-standing functional supramolecular fibers, utilizing a combination of crystallization-driven self-assembly (CDSA)<sup>[22–25]</sup> and molecular self-assembly.<sup>[26]</sup> The patchy polymer fibers consist of supporting polystyrene (PS) fibers that were decorated with patchy worm-like micelles (prepared by CDSA) via coaxial electrospinning. The functional patches on the polymer fiber's surface locally increase the BTA concentration driven by the chemical match of the peripheral amino groups of the BTA with the respective amino groups in the surface patches. This in turn promotes the patch-mediated molecular self-assembly of the BTA from the polymer fiber surface, resulting in a fir-tree like superstructure.<sup>[26]</sup>

Here, we report on hierarchically mesostructured nonwovens with a barbed wire-like morphology combining electrospun PS fibers, decorated with patchy worm-like micelles, and supramolecular nanofibers based on BTAs with functional tertiary amino substituents (**Figure 1**). The molecular self-assembly process is induced by a local enrichment of the BTA close to the patches due to the chemical similarity of one block of the patches and the periphery of the molecular building block. The chemical similarity between both also promotes the fixation of the supramolecular nanofibers on the supporting PS fiber. These hierarchical mesostructured fibers can be regarded as a fibrous superstructure, where in particular the off-standing branches feature an additional functionality. Here, the amino functionality in the periphery of the BTA can be harnessed for the immobilization of metal nanoparticles on the surface of the supramolecular nanofibers.

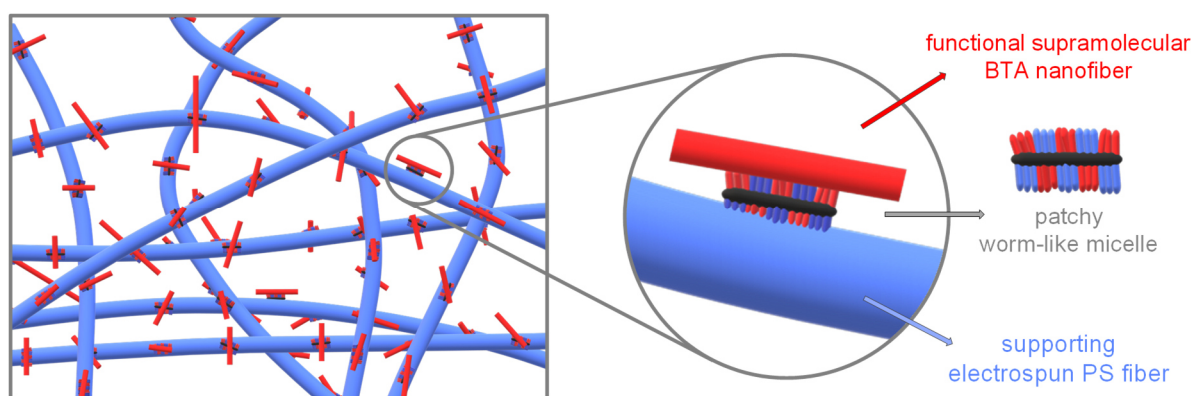


**Figure 1.** Schematic representation of a section of the hierarchically mesostructured electrospun PS nonwoven (blue) with functional supramolecular BTA nanofibers (red), with the magnification on the right showing the individual components. The mesostructured nonwoven comprises electrospun PS fibers as support with deposited patchy worm-like micelles on their surface. The patchy micelles promote the BTA self-assembly due to the chemical similarity of the patches, which results in a local enrichment of the BTA building blocks, as well as the fixation of the BTA nanofibers on the supporting electrospun PS fibers.



## 2. Results and Discussion

### 2.1. Solubility and Self-Assembly Behavior of the Functional 1,3,5-Benzenetricarboxamide

An important aspect of our functional, hierarchically mesostructured nonwovens is the preparation of supramolecular nanofibers with a high surface to volume area and a high functionality on the fibers' surface. Ready access to the functional groups of the supramolecular fibers allows for an effective immobilization of metal nanoparticles from aqueous media. As supramolecular motif for the structure formation, we focused on the well-known material class of BTAs. Under proper conditions, BTAs are known to self-assemble into fibrous nano-objects with a columnar structure created by the formation of three directed hydrogen bonds.<sup>[27]</sup> Functionality was introduced in the periphery using *N,N*-diisopropylaminoethyl substituents. These groups were selected since block copolymers featuring tertiary amino side groups were demonstrated to efficiently immobilize metal nanoparticles.<sup>[28–32]</sup> In contrast to BTAs with *N,N*-dimethylaminoethyl or *N,N*-diethylaminoethyl side groups,<sup>[33]</sup> BTAs with bulkier tertiary amino groups are not water-soluble. Thus, their structures are expected to be stable in aqueous media without disintegration. A similar behavior in view of water solubility was found for poly(*N,N*-dialkylaminoethyl methacrylamides) and poly(*N,N*-dialkylaminoethyl methacrylates) with pendant tertiary amino groups, i.e., water solubility decreases with increasing length of the alkyl substituents at the amino group.<sup>[34–36]</sup> For this purpose, *N*<sup>1</sup>,*N*<sup>3</sup>,*N*<sup>5</sup>-tris[2-(diisopropylamino)-ethyl]-1,3,5-benzenetricarboxamide (*iPr*-BTA, see **Figure 2A** inset) was synthesized in a similar manner as described previously.<sup>[33]</sup> Detailed information on the synthesis and molecular characterization is given in the Experimental Section. Fourier transformation infrared (FT-IR) spectroscopy was used to provide evidence for the formation of strong hydrogen bonds of *iPr*-BTA in bulk. In particular the N–H stretch vibrations at  $\tilde{\nu} = 3240 \text{ cm}^{-1}$  and the N–H bend and C–N stretch vibrations at  $\tilde{\nu} = 1560 \text{ cm}^{-1}$  indicate a columnar stacking<sup>[37]</sup> (**Figure S1**, Supporting Information) and is expected to promote nanofiber formation. This also indicates that the surfaces of supramolecular columns consist of densely packed functional tertiary amino groups.

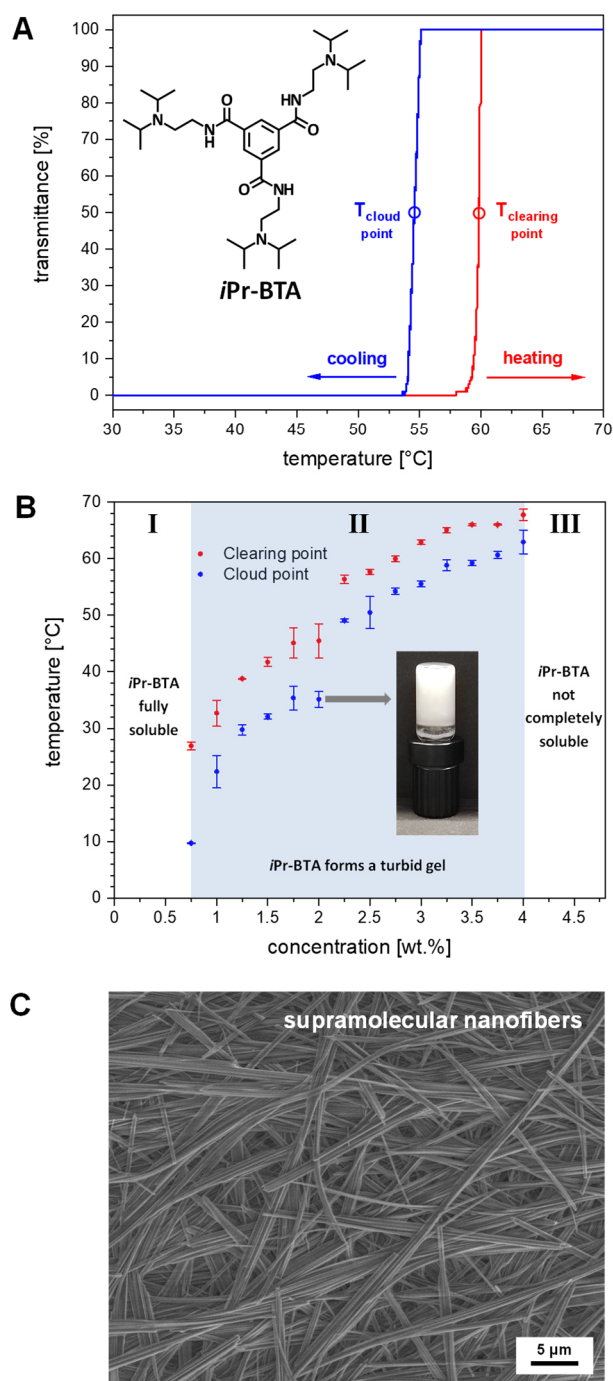


**Figure 2.** Self-assembly behavior of  $N^1,N^3,N^5$ -tris[2-(diisopropylamino)-ethyl]-1,3,5-benzenetricarboxamide (*iPr*-BTA). A) Temperature-dependent transmittance of *iPr*-BTA in isopropanol at a concentration of  $c = 2.75$  wt% at a heating/cooling rate of  $0.1 \text{ K min}^{-1}$ . Upon cooling the *iPr*-BTA solution, clouding of the sample occurs at  $T_{\text{cloud point}} = 55 \text{ °C}$  and a gel is obtained. Upon heating, the gel dissolves again at  $T_{\text{clearing point}} = 60 \text{ °C}$  resulting in a clear solution. This process is fully reversible. B) Concentration-dependent evolution of the cloud and clearing points of *iPr*-BTA in isopropanol. Indicated are three regimes (I-III). At low concentrations, the *iPr*-BTA remains dissolved in the investigated temperature range (regime I). With increasing concentration, the *iPr*-BTA forms a gel upon cooling and fully dissolves upon heating (regime II). At very high concentrations *iPr*-BTA is not completely soluble (regime III). C) SEM micrograph of a dried gel from a 2.00 wt% solution of *iPr*-BTA showing long uniform supramolecular nanofibers with a diameter of around 320 nm of the single fibers.

Prior to the nanofiber formation, we have investigated the solubility behavior of *iPr*-BTA. Indeed, we found that *iPr*-BTA features a solubility of less than 0.001 wt% in water at room temperature and at elevated temperatures. In contrast, polar organic solvents such as alcohols and in particular isopropanol were identified as suitable solvents. In general, alcohols allow the preparation of clear solutions with *iPr*-BTA concentrations up to  $c \approx 4.00$  wt% at elevated temperatures. To get a more detailed picture, we have performed temperature-dependent solubility and self-assembly studies of *iPr*-BTA in isopropanol in the concentration range from  $c = 0.25$  to 4.25 wt%. Initially, *iPr*-BTA was dispersed in isopropanol at room temperature. With the exception of concentrations above  $c = 4.00$  wt%, *iPr*-BTA can be molecularly dissolved at 70 °C. These samples were subsequently used to determine the temperature-dependent transmittance and, thus, the cloud and clearing points upon cooling and heating in the range of  $-5$  and 70 °C at a rate of  $0.1 \text{ K min}^{-1}$ . Cloud and clearing points were determined at 50% of transmittance. Exemplarily, the temperature-dependent transmittance upon cooling and subsequent heating of the sample with a concentration of  $c = 2.75$  wt% is shown in **Figure 2A**. Upon cooling, a rapid change in transmittance from 100% to 0% is observed resulting in clouding of the solution and the cloud point ( $T_{\text{cloud point}}$ ) was determined to 55 °C. This process is fully reversible upon heating as it can be observed again by a rapid change in transmittance from 0% to 100%. The clearing point ( $T_{\text{clearing point}}$ ) was found to be 60 °C, reflecting a small hysteresis of about 5 °C between the cloud and clearing point.

Based on all cloud and clearing points, we established a phase diagram of *iPr*-BTA in isopropanol from 0 to 70 °C as shown in **Figure 2B**. Three regimes can be identified: up to a concentration of  $c = 0.50$  wt%, the *iPr*-BTA is completely soluble in the investigated temperature range (regime I). Fully reversible self-assembly behavior was observed in the concentration range of  $c = 0.75 - 4.00$  wt% (regime II), followed by regime III, in which *iPr*-BTA cannot be completely dissolved anymore at elevated temperatures. In regime II, with increasing concentration of the *iPr*-BTA, the cloud points increase from 10 to 63 °C and the clearing points from 27 to 68 °C. At higher concentrations of more than 3.00 wt%, the cloud and clearing points seem to level off. This process is highly reproducible as indicated by the small error bars of the mean values for the cloud and clearing temperatures in **Figure 2B**. Upon cooling below the respective cloud point, the solution forms a turbid gel as exemplarily shown for a sample containing  $c = 2.00$  wt% of the *iPr*-BTA as depicted in the inset of **Figure 2B**. The presence of thermo-reversible organogels based on BTAs is very often indicative for the

formation of supramolecular (nano)fibers.<sup>[38–41]</sup> Thus, we have selected the 2.00 wt% gel sample, removed the solvent at ambient conditions and investigated the morphology by scanning electron microscopy (SEM). The SEM image revealed a dense network of supramolecular nanofibers as well as larger bundled aggregates of those. After evaluating the diameter of  $\approx 50$  individual supramolecular nanofibers, we found a mean fiber diameter of around  $320 \pm 130$  nm (**Figure 2C**).

## 2.2 Preparation of Hierarchically Mesostructured Nonwovens

Following our concept described in **Figure 1**, hierarchically mesostructured nonwovens were prepared employing a PS nonwoven decorated with patchy worm-like micelles for the directed molecular self-assembly of *iPr*-BTA nanofibers from the nonwovens' surface. The patchy nonwoven was produced by coaxial electrospinning, using a PS solution as the core and a dispersion of patchy worm-like micelles based on a polystyrene-*block*-polyethylene-*block*-poly(*N,N*-diisopropylaminoethyl methacrylamide) (SED*i*PA) triblock terpolymer as shell (**Figure S2**, Supporting Information), similar to the procedure described previously.<sup>[26,30]</sup> Accordingly, the nonwovens will be termed patchy PS<sub>core</sub>/SED*i*PA nonwovens in the following. The patchy, worm-like SED*i*PA micelles (average length:  $260 \pm 100$  nm) were prepared by CDSA in THF and are composed of a semi-crystalline polyethylene core and a patch-like microphase-separated corona with nanometer-sized PS ( $12 \pm 2$  nm) and poly(*N,N*-diisopropylaminoethyl methacrylamide) (PD*i*PA;  $10 \pm 3$  nm) patches in the corona (**Figure S3**, Supporting Information).<sup>[30,42]</sup> Here, the PS patches guarantee a good adhesion to the supporting PS nonwoven and the PD*i*PA patches bear pendant *N,N*-diisopropylaminoethyl groups matching the peripheral groups of *iPr*-BTA. We note, that the well-defined nanophase-separated patchy worm-like micelles are essential to promote the local increase of the *iPr*-BTA concentration close to the patches and thus the molecular self-assembly of *iPr*-BTA. Coating the supporting PS fiber with the corresponding di- or triblock copolymer do not lead to the formation of defined superstructures demonstrating the beneficial role of the patchy micelles prepared by CDSA.

Details on the coaxial electrospinning process, molecular characteristics of SED*i*PA and employed CDSA conditions can be found in the Experimental Section.

For the directed molecular self-assembly of *iPr*-BTA from the surface of the patchy nonwoven, isopropanol solutions with concentrations at which *iPr*-BTA is molecularly dissolved at elevated temperatures as well as at room temperature were selected. This ensures that molecular self-assembly of *iPr*-BTA does not take place prior to solvent evaporation and consequently allows solution uptake within the entire patchy PS<sub>core</sub>/SEDiPA nonwoven. Therefore, solutions within regime I (see **Figure 2B**) were chosen with concentrations up to  $c = 0.50$  wt% of *iPr*-BTA in isopropanol. Under these conditions, supramolecular nanofiber formation can only be initiated by solvent evaporation leading to an increase in concentration and consequently self-assembly after reaching a threshold concentration (**Figure S4**, Supporting Information).

To validate the molecular self-assembly of *iPr*-BTA from solution initiated close to the patches on the polymer fibers, we have separately deposited patchy PS<sub>core</sub>/SEDiPA fibers as well as neat electrospun PS fibers as reference on aluminum foil and subsequently immersed both samples in a solution of 0.10 wt% *iPr*-BTA in isopropanol. SEM images of the neat PS and the patchy PS<sub>core</sub>/SEDiPA fibers before the immersion are shown in **Figure S5A, B** in the Supporting Information. On the surface of the patchy PS<sub>core</sub>/SEDiPA fiber the worm-like micelles can be clearly recognized. After immersion and solvent evaporation at ambient conditions, the resulting morphologies were investigated by SEM. No supramolecular *iPr*-BTA fibers were observed on the electrospun PS reference fibers (**Figure S5C**, Supporting Information). In contrast, mesostructured fibers were found with the patchy PS<sub>core</sub>/SEDiPA fibers (**Figure S5D**, Supporting Information). In this sample, many short supramolecular nanofibers were predominantly formed on the polymer fibers' surface. This confirms that the patchy worm-like SEDiPA micelles initiate the self-assembly and promote the fixation of the supramolecular nanofibers on the supporting PS fibers.

To transfer and make use of our concept, we used a free-standing, electrospun patchy PS<sub>core</sub>/SEDiPA nonwoven in order to create a 3D hierarchically mesostructured nonwoven of sufficient size and stability. **Figure S6** in the Supporting Information shows an optical image of the free-standing nonwoven as well as a SEM image. In a similar manner as described above, hierarchically mesostructured nonwovens were prepared by immersing the patchy PS<sub>core</sub>/SEDiPA nonwovens in an *iPr*-BTA solution and subsequent drying at ambient conditions. Representative morphologies of hierarchically mesostructured nonwovens when a 0.10 wt% or a 0.50 wt% *iPr*-BTA solution in isopropanol was used for the immersion process are depicted

in **Figure 3**. Both nonwoven composites show short supramolecular nanofibers, which are either off-standing or on top of the PS<sub>core</sub>/SED*i*PA fibers, resembling a barbed wire-like morphology. The higher *i*Pr-BTA concentration of the immersion solution leads to supramolecular nanofibers with a predominantly increased fiber length (**Figure 3B**). We note that much shorter supramolecular nanofibers were found within the hierarchically mesostructured nonwovens compared to the supramolecular nanofibers, which were formed by the molecular self-assembly of neat *i*Pr-BTA upon solvent evaporation for the same concentrations (**Figure S4**, Supporting Information). Moreover, electrospun nonwovens with a higher fiber density have also an influence on the morphology depending on the concentration of *i*Pr-BTA. For instance, the use of the 0.10 wt% solution resulted in a similar barbed wire-like morphology (**Figure S7A**, Supporting Information). The immersion of such a dense nonwoven into a 0.50 wt% *i*Pr-BTA solution led to a mesostructured nonwoven with a significantly denser network of supramolecular nanofibers (**Figure S7B**, Supporting Information). This might be attributed to the higher density of the polymer fibers within the electrospun nonwoven together with the complex drying process in nonwovens.

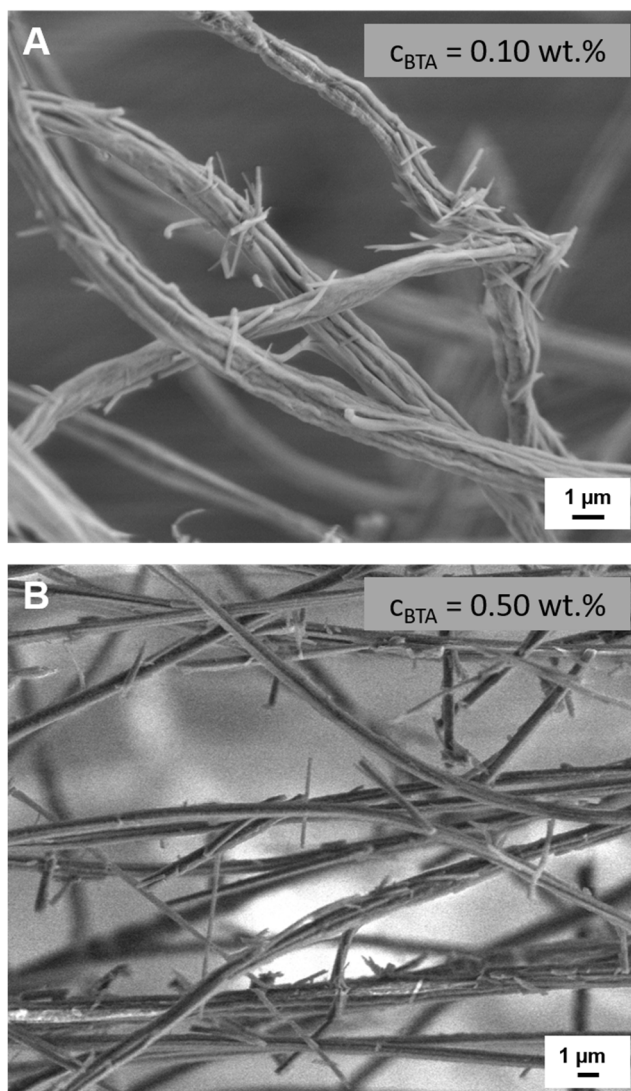


**Figure 3.** SEM images of hierarchically mesostructured nonwovens with functional supramolecular *iPr*-BTA nanofibers. The mesostructured nonwovens were prepared by immersion of electrospun patchy  $\text{PS}_{\text{core}}/\text{SED}/\text{PA}$  nonwovens in isopropanol solutions with a *iPr*-BTA concentration of A) 0.10 wt% and B) 0.50 wt% and subsequent drying at ambient conditions.

### 2.3 Functionalization of Hierarchically Mesostuctured Nonwovens with Palladium Nanoparticles

Fibrous supramolecular composites featuring a high surface area with distinct functional groups on the surface are highly suitable for metal nanoparticle capture from solution,<sup>[4,43]</sup> rendering our mesostructured nonwovens with a barbed wire-like morphology and functional *N,N*-diisopropylaminoethyl groups promising candidates.

To demonstrate the proof-of-concept, we have used palladium nanoparticles (PdNPs) which can be conveniently synthesized and dispersed in aqueous media (see the Experimental Section). The size distribution of the PdNPs was investigated by transmission electron microscopy (TEM) and evaluation of at least 150 particles yielded an average particle diameter of  $d_{\text{TEM}} = 2.7 \pm 0.4$  nm (**Figure S8**, Supporting Information).

For immobilization of the PdNPs a functional mesostructured nonwoven, prepared as described before by immersing a patchy  $\text{PS}_{\text{core}}/\text{SEDiPA}$  nonwoven in a 0.50 wt% *iPr*-BTA solution, was employed. PdNPs were immobilized by dipping the mesostructured nonwoven into the PdNP dispersion for 3 h at room temperature and subsequent drying at ambient conditions. Notably, after dipping of the hierarchical mesostructured nonwoven into the aqueous nanoparticle dispersion and drying, the shape of the nonwoven and the morphology is largely maintained under these conditions (**Figure S9**, Supporting Information). SEM images reveal no significant changes with respect to the  $\text{PS}_{\text{core}}/\text{SEDiPA}$  nonwoven shape in general after immersion in *iPr*-BTA isopropanol solution (**Figure S9A**, Supporting Information) or into the aqueous PdNP dispersion (**Figure S9B**, Supporting Information). The appearance of the supramolecular nanofibers of the mesostructured nonwoven also do not change after the immersion process. The SEM images show that PdNPs or agglomerates can be detected since they appear bright as they have a higher scattering intensity than the polymer fibers and the supramolecular fibers. To provide evidence on the particle size and particle distribution of single PdNPs on the BTA surface, TEM measurements of the functionalized nonwoven were conducted. As shown in **Figure 4**, only single PdNPs were deposited on the supramolecular short BTA nanofibers. By evaluation of 50 particles, we found a PdNP diameter of  $d_{\text{TEM}} = 2.7 \pm 0.4$  nm. This particle size corresponds well to the size of the synthesized PdNPs, indicating a predominantly single, nonagglomerated nanoparticle uptake from solution rather than during the drying process. These findings demonstrate that the fiber composites with a barbed wire-like morphology comprising functional supramolecular nanofibers are highly



stable in aqueous media and allow for the efficient immobilization of individual PdNPs without agglomeration.

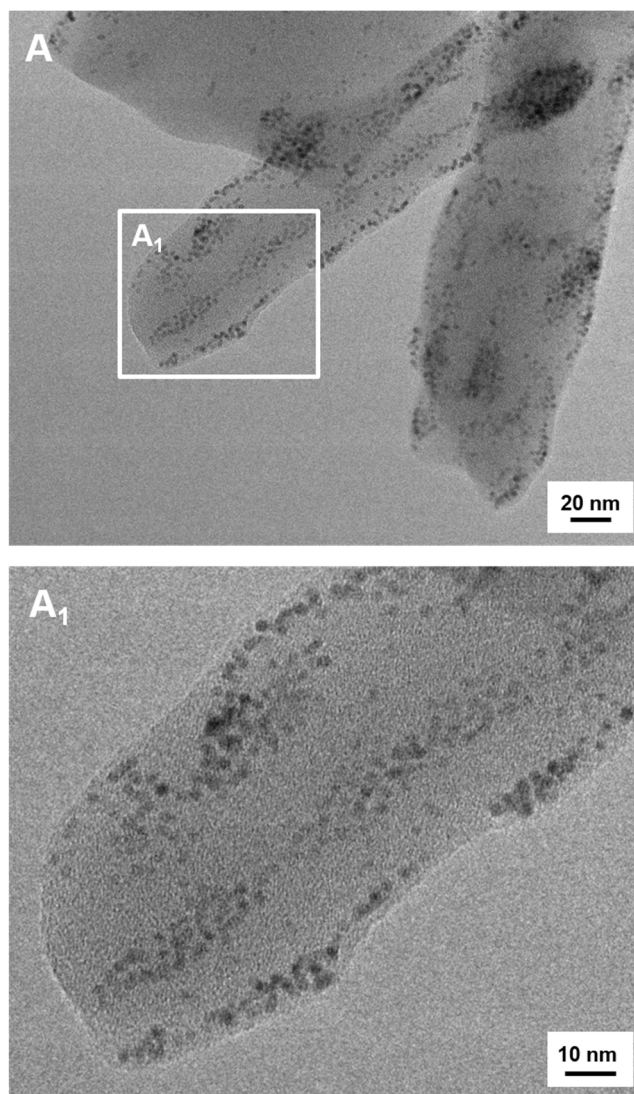


**Figure 4.** A) TEM images and magnification A<sub>1</sub>) of a supramolecular *iPr*-BTA nanofiber with immobilized palladium nanoparticles (PdNPs). For TEM sample preparation, a PdNP-loaded, hierarchically mesostructured nonwoven was mechanically broken.

### 3. Conclusion

We have demonstrated the preparation of functional, hierarchically mesostructured nonwovens with a barbed wire-like fiber morphology which are suitable to immobilize metal nanoparticles. These mesostructured nonwovens were realized by combining electrospun polystyrene fibers, decorated with patchy worm-like micelles, with supramolecular nanofibers based on a 1,3,5-benzotricarboxamide with functional peripheral *N,N*-diisopropylaminoethyl groups (*iPr*-BTA). Mediation and initiation of the supramolecular nanofiber growth from the surface of the supporting electrospun polymer fibers was accomplished by the functional patches on top of the electrospun fibers, featuring on one hand pendant *N,N*-diisopropylaminoethyl groups matching the peripheral groups of *iPr*-BTA. On the other hand, the polystyrene patches of the worm-like micelles ensure a proper fixation of the supramolecular *iPr*-BTA nanofibers on the supporting polystyrene fibers. These hierarchically mesostructured nonwovens were shown to be highly suitable for the immobilization of palladium nanoparticles from aqueous media which are deposited on the surface of the functional supramolecular nanofibers. We anticipate that the combination of a complex mesoscale morphology with a specific functionalization of such nonwovens are attractive candidates to be used in filtration and separation and for heterogeneous catalysis with metal nanoparticles.

#### 4. Experimental Section

##### *Materials:*

*N,N*-Diisopropylethylenediamine (ABCR), *n*-butyllithium (2.5 mol L<sup>-1</sup> in hexane, Acros Organics), *N,N*-dimethylformamide (DMF, 99%, Acros Organics), tetrahydrofuran (THF, ≥ 99.9%, VWR), sodium tetrachloropalladate(II) (Na<sub>2</sub>PdCl<sub>4</sub>, ≈36% Pd, Acros Organics), 4-dimethylaminopyridine (DMAP, ReagentPlus, ≥99%, Sigma-Aldrich), sodium borohydride (NaBH<sub>4</sub>, ≥ 96%, Fluka) were used as received. Isopropanol and pentane (technical grade) were distilled prior to use. THF used for the post-polymerization amidation was dried by successive distillation over calcium hydride and potassium prior to use. Deionized water with a conductivity of 18.2 MΩ cm was obtained by filtration through a Millipore Milli-Q Plus system (QPAK two purification cartridge). Polystyrene (PS) with a  $M_n = 1.8 \times 10^6$  g mol<sup>-1</sup> and  $\mathcal{D} = 1.08$  was prepared according to standard anionic polymerization procedures.

##### *Synthesis and Preparation:*

*N*<sup>1</sup>,*N*<sup>3</sup>,*N*<sup>5</sup>-tris[2-(diisopropylamino)-ethyl]-1,3,5-benzenetricarboxamide (*iPr*-BTA) was synthesized in a two-step reaction route accordingly to our previous work.<sup>[33]</sup> Briefly, 7.17 g (0.028 mol) of trimesic acid trimethyl ester were dispersed in 25.0 mL (20.5 g, 0.142 mol) of *N,N*-diisopropylethylenediamine under argon atmosphere. The mixture was heated to 125 °C, stirred for 17 h and subsequently allowed to cool down to room temperature. The crude product was boiled two times in around 400 mL acetic acid ethyl ester and filtered. The product was dried under high vacuum overnight resulting in 12.2 g (72%) of *iPr*-BTA as a white powder. <sup>1</sup>H NMR(300 MHz, CDCl<sub>3</sub>, δ): 1.06 (d, 36H), 2.71 (t, 6H), 3.07 (m, 6H), 3.45 (quartett, 6H), 7.24 (t(br), 3H), 8.41 (s, 3H) ppm; <sup>13</sup>C NMR (75 MHz, CDCl<sub>3</sub>, δ): 20.9, 38.5, 42.8, 47.8, 127.8, 135.3, 165.2 ppm; EIMS *m/z* (%): 588 (7) [M<sup>+</sup>], 115 (96), 114 (100), 72 (97), 43 (35); MALDI-ToF MS *m/z* 589 [M+H]<sup>+</sup>; Anal. calcd. for C<sub>33</sub>H<sub>60</sub>N<sub>6</sub>O<sub>3</sub>: C 67.3, H 10.3, N 14.3; found: C 67.3, H 9.8, N 14.0%.

The polystyrene-*block*-polyethylene-*block*-poly(*N,N*-diisopropylaminoethyl methacrylamide) triblock terpolymer (S<sub>28</sub>E<sub>15</sub>DiPA<sub>58</sub><sup>156</sup>, subscripts denote the mass fraction of the corresponding block in wt% and the superscript gives the overall number average molecular weight ( $M_n$ ) in kg mol<sup>-1</sup>) was prepared by post-polymerization functionalization of the poly(methyl

methacrylate) block of the respective polystyrene-*block*-polyethylene-*block*-poly(methyl methacrylate) ( $S_{40}E_{21}M_{39}^{108}$ ) triblock terpolymer precursor, according to our previous work.<sup>[29]</sup> In brief, *N,N*-diisopropylethylenediamine was first activated by deprotonation of the primary amino group with *n*-butyllithium in THF at  $-78$  °C followed by heating to room temperature. Subsequently, the activated amine solution (twofold excess of amine with respect to methyl ester units) was added to a THF solution of  $S_{40}E_{21}M_{39}^{108}$  ( $c = 10$  g L<sup>-1</sup>) at  $40$  °C allowing the reaction to proceed for 24 h. The amidated polymer ( $S_{28}E_{15}DiPA_{58}^{156}$ ) was isolated by precipitation from pentane. The employed  $S_{40}E_{21}M_{39}^{108}$  triblock terpolymer was synthesized by a combination of sequential living anionic polymerization and catalytic hydrogenation, as described elsewhere.<sup>[42,44]</sup>

Patchy, worm-like SEDiPA micelles were prepared by crystallization-driven self-assembly in THF. To this end, the  $S_{28}E_{15}DiPA_{58}^{156}$  triblock terpolymer was first molecularly dissolved in THF ( $c = 10$  g L<sup>-1</sup>) at  $65$  °C for 30 min using a temperature-controllable shaker unit (HCL-MKR 13, Ditabis), followed by cooling to the crystallization temperature of the polyethylene (PE) middle block ( $T_c = 15$  °C) to induce PE crystallization. The self-assembly process was allowed to proceed for 24 h at 200 rpm resulting in a dispersion of patchy worm-like micelles (average length:  $l = 260 \pm 100$  nm; patch sizes:  $12 \pm 2$  nm (PS),  $10 \pm 3$  nm (PDiPA)); determined by TEM image analysis of at least 100 micelles by the software ImageJ.<sup>[45]</sup>

PS fibers and nonwovens decorated with patchy, worm-like SEDiPA micelles were produced by coaxial electrospinning, in a similar manner as described previously.<sup>[30]</sup> A 7 wt% PS ( $M_n = 1.8 \times 10^6$  g mol<sup>-1</sup>) solution in DMF was used as core to yield the supporting PS fiber, and a dispersion of patchy worm-like SEDiPA micelles at a concentration of  $c = 10$  g L<sup>-1</sup> in THF was employed as shell (**Figure S2**, Supporting Information). Thin layers of patchy PS<sub>core</sub>/SEDiPA fibers were spun on aluminum foil placed at a distance of 20 cm from the coaxial needle (COAX\_2DISP sealed coaxial needles, LINARI NanoTech,  $d_{core} = 0.51$  mm and  $d_{shell} = 1.37$  mm) at a temperature of  $20.8$  °C and a relative humidity of around 30% (feed rates:  $1.2$  mL h<sup>-1</sup> (PS solution, core),  $1.0$  mL h<sup>-1</sup> (micelle dispersion, shell)). Corresponding free-standing nonwovens were spun on a rotating disk collector ( $D = 20$  cm, 800 rpm) placed at a distance of 5 cm of the coaxial needle. For electrospinning, a voltage of 11.4 kV at the needle and

–1.0 kV at the collector were applied. Neat PS fibers were prepared as reference material in the same manner but without using the micellar dispersions.

Hierarchically mesostructured fibers/nonwovens were prepared by immersion of the electrospun PS<sub>core</sub>/SEDiPA fibers/nonwovens in a BTA solution in isopropanol at a concentration of  $c = 0.10$  or  $0.50$  wt%. The immersion time was varied from 30 s to 5 h to 12 h at room temperature. We noted that the immersion time does not play a significant role on the resulting morphology because at already short immersion times the nonwoven is completely filled with the solution. Subsequently, the solvent was evaporated at ambient conditions by fixing the nonwoven in a vertical position.

DMAP-stabilized palladium nanoparticles (PdNPs) were synthesized according to literature procedure.<sup>[46]</sup> Therefore, 40.0 mg Na<sub>2</sub>PdCl<sub>4</sub> were dissolved in 3.23 g deionized water. 9.65 g of a  $75.8 \times 10^{-3}$  m aqueous DMAP solution was added and stirred for 20 min. Afterwards, 1.1 mL of a 1% w/v aqueous NaBH<sub>4</sub> solution was added.

PdNPs were immobilized by immersion of a hierarchical mesostructured nonwoven in an aqueous dispersion of PdNPs ( $c = 0.0258$  g L<sup>-1</sup>) for 3 h at room temperature and subsequent solvent evaporation in a vertical position at ambient conditions.

#### *Molecular Characterization:*

<sup>1</sup>H NMR (300 MHz) and <sup>13</sup>C NMR (75 MHz) measurements were carried out on a Bruker Avance AC 300 spectrometer at room temperature. Mass spectra were recorded on a Finnigan MAT 8500 spectrometer (EI, 70 eV) using direct injection mode. Elemental analysis (C, H, N) was carried out with a Unicube from Elementar Analysen-Systeme with sulfanilamide as standard. The theoretical amount of all elements was calculated using Chemicalize. Values are given in wt%. Matrix-assisted laser desorption/ionization time-of-flight mass spectroscopy (MALDI-ToF MS) measurements were performed using a Bruker AutoFlex Max mass spectrometer equipped with a Smartbeam II laser. The analyte was embedded in the matrix material trans-2-[3-(4-tert-butylphenyl)-2-methyl-2-propenylidene]malononitrile (DCTB) in

the matrix:analyte mass ratio 10:1. FT-IR spectra was recorded with a Perkin-Elmer Spectrum 100 FT-IR spectrometer using the attenuated total reflectance unit.

*Methods:*

Temperature-dependent transmittance of BTA solutions were determined at a wavelength of  $\lambda = 645$  nm using the crystallization system Crystal16 (Technobis Crystallization Systems). Solutions or dispersions of the BTA in isopropanol were prepared in a concentration range between 0.25 and 4.25 wt% in 0.25 wt% steps at room temperature and stirred at 600 rpm with a stirring bar. The samples were heated to 70 °C with 10 K min<sup>-1</sup> and hold isothermally for 30 min within the crystallization system. After that, the transmittance at  $\lambda = 645$  nm of the samples was recorded for three cycles from 70 to -5 °C. Each cycle comprises a cooling step with 0.1 K min<sup>-1</sup>, an isothermal at -5 °C for 10 min, a subsequent heating step with a rate of 0.1 K min<sup>-1</sup>, and an isothermal at 70 °C for 10 min. The cloud and clearing points were determined at a transmission of 50% upon cooling and heating, respectively. The given cloud and clearing points, as depicted in **Figure 2B**, are the mean values from three cooling and heating cycles, respectively.

SEM measurements were conducted with a FEI Quanta FEG 250 scanning electron microscope (Thermo Fisher Scientific) equipped with a field emission gun. For SEM, all samples were used without applying sputter coating. For **Figure S5A, B, D** (Supporting Information) measurements were conducted in the beam deceleration mode under high vacuum at an acceleration voltage of 6 kV. Here, an additional negative voltage of -4 kV was applied to the stage to decelerate the primary electrons to 2 kV. The electrons interacting with the sample were accelerated towards the concentric back scattered (CBS) detector. The samples measured in the beam deceleration mode were placed on the sample table and fixed with a conductive tape. All other SEM images were recorded in the low vacuum mode (water pressure of 40 Pa in the sample chamber) with an acceleration voltage of 3 or 5 kV with a large-field (gaseous secondary electron) detector for topographical details or CBS detector to visualize the PdNPs. The samples measured in the low vacuum mode were mounted on a sample holder using a double-sided adhesive graphite pad.

TEM measurements were performed with a JEOL JEM-2200FS equipped with a Gatan OneView CMOS camera using the Digital Micrograph Software. For the investigation of the size distribution of the nanoparticles, a small drop of the suspension with the PdNPs was placed onto a carbon-coated copper grid (S160, Plano EM, Germany) and excess solution was removed by a filter paper. For the investigation of the PdNPs distribution on the supramolecular fibers, a lacey carbon-coated copper grid (S166, Plano EM, Germany) was wiped over the surface of the functional, hierarchically mesostructured nonwoven to prepare the TEM sample. All specimens were investigated at room temperature using the bright-field mode at an acceleration voltage of 200 kV.

### Supporting Information

Supporting Information is available from the Wiley Online Library or from the author.

### Acknowledgements

This work was supported by the German Research Foundation (DFG) in the framework of the Collaborative Research Centre SFB840, projects A2 and B8. The authors thank Prof. Andreas Greiner for helpful discussions and his support with the coaxial electrospinning facility. The authors thank Sandra Ganzleben (Macromolecular Chemistry I, University of Bayreuth) for the support with the synthesis. The authors also thank Andreas Erhardt (Macromolecular Chemistry I, University of Bayreuth) for conducting the MALDI-ToF MS measurement. Hannah Kurz (Inorganic Chemistry IV, University of Bayreuth) is acknowledged for carrying out the elemental analysis. The authors acknowledge the support of the Keylabs Electron and Optical Microscopy and Synthesis and Molecular Characterization of the Bavarian Polymer Institute at the University of Bayreuth. A.F. thanks the Elite Study Program *Macromolecular Science* within the Elite Network of Bavaria (ENB) for support.

Open access funding enabled and organized by Projekt DEAL.

### **Conflict of Interest**

The authors declare no conflict of interest.

### **Data Availability Statement**

The data that support the findings of this study are available from the corresponding author upon reasonable request.

### **Keywords**

1,3,5-benzenetricarboxamides, mesostructured nonwovens, molecular and crystallization-driven self-assembly, patchy worm-like micelles, supramolecular nanofibers



## References\*

- [1] L. de Sio, B. Ding, M. Focsan, K. Kogermann, P. Pascoal-Faria, F. Petronela, G. Mitchell, E. Zussman, F. Pierini.  
*Personalized Reusable Face Masks with Smart Nano-Assisted Destruction of Pathogens for COVID-19: A Visionary Road,*  
Chemistry **2021**, 27, 6112–6130.
- [2] M. Hu, Y. Wang, Z. Yan, G. Zhao, Y. Zhao, L. Xia, B. Cheng, Y. Di, X. Zhuang.  
*Hierarchical dual-nanonet of polymer nanofibers and supramolecular nanofibrils for air filtration with a high filtration efficiency, low air resistance and high moisture permeation,*  
J. Mater. Chem. A **2021**, 9, 14093–14100.
- [3] S. Zhang, H. Liu, N. Tang, S. Zhou, J. Yu, B. Ding.  
*Spider-Web-Inspired PM<sub>0.3</sub> Filters Based on Self-Sustained Electrostatic Nanostructured Networks,*  
Adv. Mater. **2020**, 32, 2002361.
- [4] M. Drummer, C. Liang, K. Kreger, S. Rosenfeldt, A. Greiner, H.-W. Schmidt.  
*Stable Mesoscale Nonwovens of Electrospun Polyacrylonitrile and Interpenetrating Supramolecular 1,3,5-Benzenetrisamide Fibers as Efficient Carriers for Gold Nanoparticles,*  
ACS Appl. Mater. Interfaces **2021**, 13, 34818–34828.
- [5] A. Anstey, E. Chang, E. S. Kim, A. Rizvi, A. R. Kakroodi, C. B. Park, P. C. Lee.  
*Nanofibrillated polymer systems: Design, application, and current state of the art,*  
Prog. Polym. Sci. **2021**, 113, 101346.
- [6] X. Zhang, Y. Lu.  
*Centrifugal Spinning: An Alternative Approach to Fabricate Nanofibers at High Speed and Low Cost,*  
Polym. Rev. **2014**, 54, 677–701.

---

\*The titles of the publications are included in this list of references.

- [7] Z.-M. Zhang, Y.-S. Duan, Q. Xu, B. Zhang.  
*A review on nanofiber fabrication with the effect of high-speed centrifugal force field,*  
J. Eng. Fibers Fabr. **2019**, 14, 155892501986751.
- [8] B. Atıcı, C. H. Ünlü, M. Yanılmaz.  
*A Review on Centrifugally Spun Fibers and Their Applications,*  
Polym. Rev. **2021**, 62, 1-64.
- [9] D. Li, Y. Xia.  
*Electrospinning of Nanofibers: Reinventing the Wheel?,*  
Adv. Mater. **2004**, 16, 1151–1170.
- [10] A. Greiner, J. H. Wendorff.  
*Electrospinning: A Fascinating Method for the Preparation of Ultrathin Fibers,*  
Angew. Chem., Int. Ed. **2007**, 46, 5670–5703.
- [11] S. Agarwal, A. Greiner, J. H. Wendorff.  
*Electrospinning of Manmade and Biopolymer Nanofibers-Progress in Techniques,*  
*Materials, and Applications,*  
Adv. Funct. Mater. **2009**, 19, 2863–2879.
- [12] S. Jung, J. Kim.  
*Advanced Design of Fiber-Based Particulate Filters: Materials, Morphology, and*  
*Construction of Fibrous Assembly,*  
Polymers **2020**, 12, 1714.
- [13] Y. Li, X. Yin, J. Yu, B. Ding.  
*Electrospun nanofibers for high-performance air filtration,*  
Compos. Commun. **2019**, 15, 6–19.
- [14] S. Zhang, H. Liu, X. Yin, J. Yu, B. Ding.  
*Anti-deformed Polyacrylonitrile/Polysulfone Composite Membrane with Binary*  
*Structures for Effective Air Filtration,*  
ACS Appl. Mater. Interfaces **2016**, 8, 8086–8095.

- [15] S. Zhang, N. Tang, L. Cao, X. Yin, J. Yu, B. Ding.  
*Highly Integrated Polysulfone/Polyacrylonitrile/Polyamide-6 Air Filter for Multilevel Physical Sieving Airborne Particles,*  
ACS Appl. Mater. Interfaces **2016**, 8, 29062–29072.
- [16] Z. Wang, Z. Pan.  
*Preparation of hierarchical structured nano-sized/porous poly(lactic acid) composite fibrous membranes for air filtration,*  
Appl. Surf. Sci. **2015**, 356, 1168–1179.
- [17] Z. Su, J. Ding, G. Wei.  
*Electrospinning: a facile technique for fabricating polymeric nanofibers doped with carbon nanotubes and metallic nanoparticles for sensor applications,*  
RSC Adv. **2014**, 4, 52598–52610.
- [18] H. Misslitz, K. Kreger, H.-W. Schmidt.  
*Supramolecular Nanofiber Webs in Nonwoven Scaffolds as Potential Filter Media,*  
Small **2013**, 9, 2053–2058.
- [19] D. Weiss, D. Skrybeck, H. Misslitz, D. Nardini, A. Kern, K. Kreger, H.-W. Schmidt.  
*Tailoring Supramolecular Nanofibers for Air Filtration Applications,*  
ACS Appl. Mater. Interfaces **2016**, 8, 14885–14892.
- [20] Y. Wang, G. Chao, X. Li, F. Dong, X. Zhuang, L. Shi, B. Cheng, X. Xu.  
*Hierarchical fibrous microfiltration membranes by self-assembling DBS nanofibrils in solution-blown nanofibers,*  
Soft Matter **2018**, 14, 8879–8882.
- [21] M. Burgard, D. Weiss, K. Kreger, H. Schmalz, S. Agarwal, H.-W. Schmidt, A. Greiner.  
*Mesostructured Nonwovens with Penguin Downy Feather-Like Morphology – Top-Down Combined with Bottom-Up,*  
Adv. Funct. Mater. **2019**, 29, 1903166.
- [22] A. M. Oliver, J. Gwyther, C. E. Boott, S. Davis, S. Pearce, I. Manners.  
*Scalable Fiber-like Micelles and Block Co-micelles by Polymerization-Induced Crystallization-Driven Self-Assembly,*  
J. Am. Chem. Soc. **2018**, 140, 18104–18114.

- [23] S. Ganda, M. H. Stenzel.  
*Concepts, fabrication methods and applications of living crystallization-driven self-assembly of block copolymers,*  
Prog. Polym. Sci. **2020**, 101, 101195.
- [24] L. MacFarlane, C. Zhao, J. Cai, H. Qiu, I. Manners.  
*Emerging applications for living crystallization-driven self-assembly,*  
Chem. Sci. **2021**, 12, 4661–4682.
- [25] C. Hils, I. Manners, J. Schöbel, H. Schmalz.  
*Patchy Micelles with a Crystalline Core: Self-Assembly Concepts, Properties, and Applications,*  
Polymers **2021**, 13, 1481.
- [26] A. Frank, C. Hils, M. Weber, K. Kreger, H. Schmalz, H.-W. Schmidt.  
*Hierarchical Superstructures by Combining Crystallization-Driven and Molecular Self-Assembly,*  
Angew. Chem., Int. Ed. **2021**, 60, 21767–21771.
- [27] S. Cantekin, T. F. A. de Greef, A. R. A. Palmans.  
*Benzene-1,3,5-tricarboxamide: a versatile ordering moiety for supramolecular chemistry,*  
Chem. Soc. Rev. **2012**, 41, 6125–6137.
- [28] J. Schöbel, M. Burgard, C. Hils, R. Dersch, M. Dulle, K. Volk, M. Karg, A. Greiner, H. Schmalz.  
*Bottom-Up Meets Top-Down: Patchy Hybrid Nonwovens as an Efficient Catalysis Platform,*  
Angew. Chem., Int. Ed. **2017**, 56, 405–408.
- [29] J. Schöbel, C. Hils, A. Weckwerth, M. Schlenk, C. Bojer, M. C. A. Stuart, J. Breu, S. Förster, A. Greiner, M. Karg, H. Schmalz.  
*Strategies for the selective loading of patchy worm-like micelles with functional nanoparticles,*  
Nanoscale **2018**, 10, 18257–18268.

- [30] C. Hils, M. Dulle, G. Sitaru, S. Gekle, J. Schöbel, A. Frank, M. Drechsler, A. Greiner, H. Schmalz.  
*Influence of patch size and chemistry on the catalytic activity of patchy hybrid nonwovens,*  
Nanoscale Adv. **2020**, 2, 438–452.
- [31] D. Besold, S. Risse, Y. Lu, J. Dzubiella, M. Ballauff.  
*Kinetics of the Reduction of 4-Nitrophenol by Silver Nanoparticles Immobilized in Thermoresponsive Core-Shell Nanoreactors,*  
Ind. Eng. Chem. Res. **2021**, 60, 3922–3935.
- [32] P. Hervés, M. Pérez-Lorenzo, L. M. Liz-Marzán, J. Dzubiella, Y. Lu, M. Ballauff.  
*Catalysis by metallic nanoparticles in aqueous solution: model reactions,*  
Chem. Soc. Rev. **2012**, 41, 5577–5587.
- [33] A. Frank, A. Bernet, K. Kreger, H.-W. Schmidt.  
*Supramolecular microtubes based on 1,3,5-benzenetricarboxamides prepared by self-assembly upon heating,*  
Soft Matter **2020**, 16, 4564–4568.
- [34] C. Hils, E. Fuchs, F. Eger, J. Schöbel, H. Schmalz.  
*Converting Poly(Methyl Methacrylate) into a Triple-Responsive Polymer,*  
Chem. – Eur. J. **2020**, 26, 5611–5614.
- [35] B. Pang, Y. Yu, W. Zhang.  
*Thermoresponsive Polymers Based on Tertiary Amine Moieties,*  
Macromol. Rapid Commun. **2021**, 42, 2100504.
- [36] T. Thavanesan, C. Herbert, F. A. Plamper.  
*Insight in the Phase Separation Peculiarities of Poly(dialkylaminoethyl methacrylate)s,*  
Langmuir **2014**, 30, 5609–5619.
- [37] P. J. M. Stals, M. M. J. Smulders, R. Martín-Rapún, A. R. A. Palmans, E. W. Meijer.  
*Asymmetrically Substituted Benzene-1,3,5-tricarboxamides: Self-Assembly and Odd-Even Effects in the Solid State and in Dilute Solution,*  
Chem. – Eur. J. **2009**, 15, 2071–2080.

- [38] X.-J. Kuang, A. Wajahat, W.-T. Gong, M. K. Dhinakaran, X.-H. Li, G.-L. Ning.  
*Supramolecular gel from self-assembly of a C<sub>3</sub>-symmetrical discotic molecular bearing pillar[5]arene,*  
Soft Matter **2017**, 13, 4074–4079.
- [39] A. Paikar, A. Pramanik, D. Haldar.  
*Influence of side-chain interactions on the self-assembly of discotic tricarboxyamides: a crystallographic insight,*  
RSC Adv. **2015**, 5, 31845–31851.
- [40] V. Nagarajan, V. R. Pedireddi.  
*Gelation and Structural Transformation Study of Some 1,3,5-Benzenetricarboxamide Derivatives,*  
Cryst. Growth Des. **2014**, 14, 1895–1901.
- [41] S. Kumar, S. Bera, S. K. Nandi, D. Haldar.  
*The effect of amide bond orientation and symmetry on the self-assembly and gelation of discotic tripeptides,*  
Soft Matter **2021**, 17, 113–119.
- [42] J. Schmelz, M. Karg, T. Hellweg, H. Schmalz.  
*General Pathway toward Crystalline-Core Micelles with Tunable Morphology and Corona Segregation,*  
ACS Nano **2011**, 5, 9523–9534.
- [43] E. Krieg, H. Weissman, E. Shirman, E. Shimoni, B. Rybtchinski.  
*A recyclable supramolecular membrane for size-selective separation of nanoparticles,*  
Nat. Nanotechnol. **2011**, 6, 141–146.
- [44] H. Ruckdäschel, J. K. W. Sandler, V. Altstädt, C. Rettig, H. Schmalz, V. Abetz, A. H. Müller.  
*Compatibilisation of PPE/SAN blends by triblock terpolymers: Correlation between block terpolymer composition, morphology and properties,*  
Polymer **2006**, 47, 2772–2790.
- [45] W. S. Rasband, U. S. ImageJ, National Institutes of Health, Bethesda, Maryland, USA,  
<https://imagej.nih.gov/ij/> (accessed: 2022).

- [46] K. A. Flanagan, J. A. Sullivan, H. Müller-Bunz.  
*Preparation and Characterization of 4-Dimethylaminopyridine-Stabilized Palladium Nanoparticles,*  
Langmuir **2007**, 23, 12508–12520.

## Supporting Information

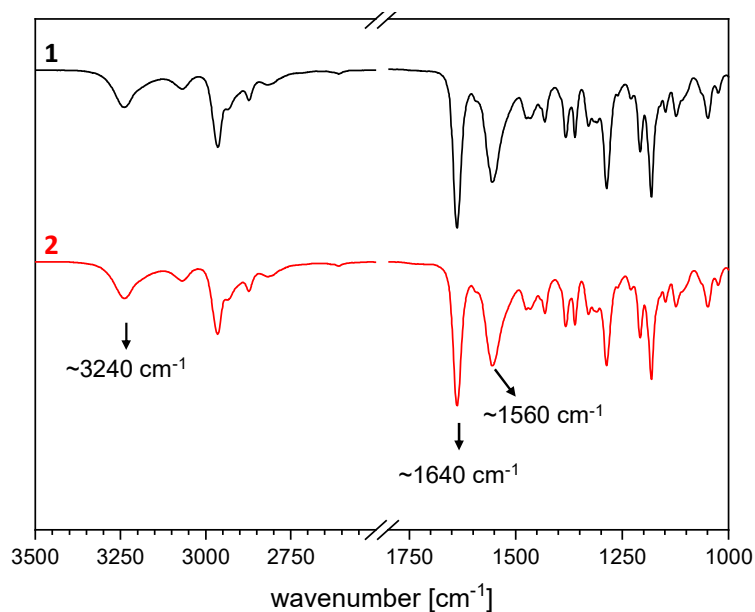
### ***Functional Mesostructured Electrospun Polymer Nonwovens with Supramolecular Nanofibers***

Andreas Frank, Melina Weber, Christian Hils, Ulrich Mansfeld, Klaus Kreger, Holger Schmalz\* and Hans-Werner Schmidt\*

#### **Content:**

FT-IR spectra of $N^1, N^3, N^5$ -tris[2-(diisopropylamino)-ethyl]-1,3,5-benzenetricarboxamide.....	S-1
Coaxial electrospinning.....	S-2
Transmission electron micrograph of patchy worm-like micelles.....	S-3
Self-assembly of $N^1, N^3, N^5$ -tris[2-(diisopropylamino)-ethyl]-1,3,5-benzenetricarboxamide.....	S-4
Scanning electron micrographs of electrospun polymer fibers without and with patchy worm-like micelles in the presence of $N^1, N^3, N^5$ -tris[2-(diisopropylamino)-ethyl]-1,3,5-benzenetricarboxamide.....	S-5
Optical image and scanning electron micrograph of coaxially electrospun polystyrene nonwovens with patchy worm-like micelles.....	S-6
Hierarchically mesostructured polymer nonwovens with supramolecular nanofibers.....	S-7
Transmission electron micrograph and size distribution of the palladium nanoparticles.....	S-8
Hierarchically mesostructured polymer nonwovens before and after immersion in palladium nanoparticle dispersion.....	S-9

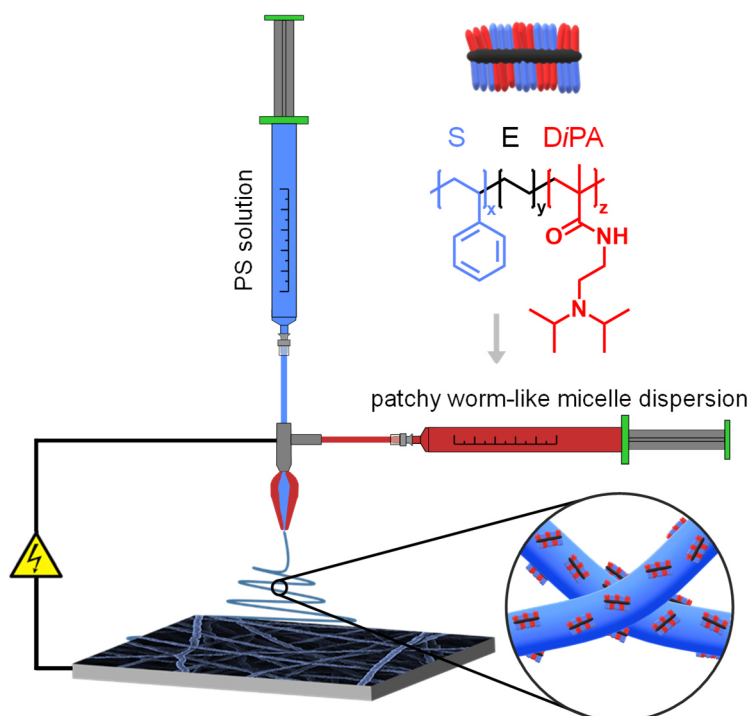


FT-IR spectra of  $N^1, N^3, N^5$ -tris[2-(diisopropylamino)-ethyl]-1,3,5-benzenetricarboxamide

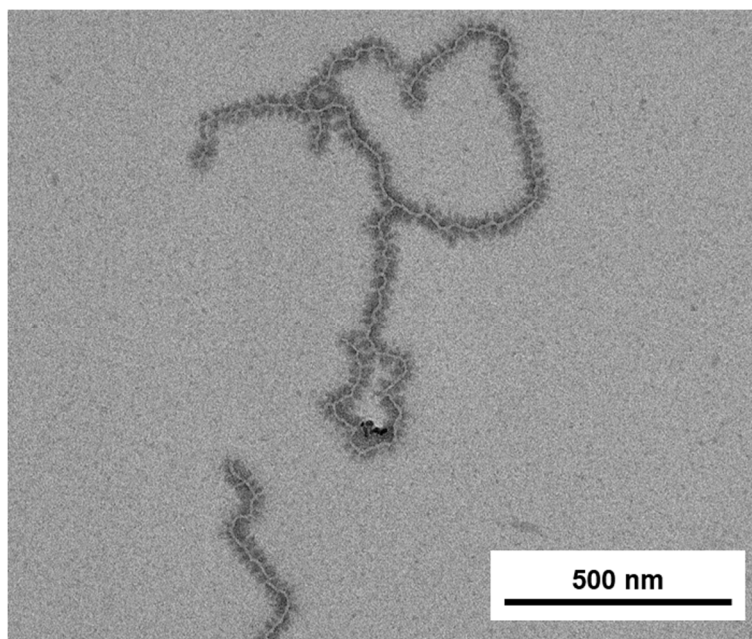
**Figure S1.** FT-IR spectra of  $N^1, N^3, N^5$ -tris[2-(diisopropylamino)-ethyl]-1,3,5-benzenetricarboxamide as obtained from synthesis (1) and after self-assembly from isopropanol (2). Both spectra are almost identical. The most relevant amide vibrations (amide A, amide I and II) are indicated and can be found at around  $3240\text{ cm}^{-1}$  (amide A, N-H stretch vibrations), at around  $1640\text{ cm}^{-1}$  (amide I, C=O stretch vibrations) and at around  $1560\text{ cm}^{-1}$  (amide II; superposition of N-H bend and C-N stretch vibrations). The location of these vibrations is indicative for a columnar stacking of the BTA molecules.<sup>[1]</sup>

[1] P. J. M. Stals, M. M. J. Smulders, R. Martín-Rapún, A. R. A. Palmans and E. W. Meijer. Asymmetrically substituted benzene-1,3,5-tricarboxamides: Self-assembly and odd-even effects in the solid state and in dilute solution, *Chem. - Eur. J.* **2009**, 15, 2071.

## Coaxial electrospinning



**Figure S2.** Preparation of patchy PS<sub>core</sub>/SEDiPA nonwovens by coaxial electrospinning using a polystyrene (PS) solution ( $M_n = 1.8 \cdot 10^6 \text{ g} \cdot \text{mol}^{-1}$ , 7 wt.% in DMF) as core and a dispersion of patchy worm-like S<sub>28</sub>E<sub>15</sub>DiPA<sub>58</sub><sup>156</sup> micelles ( $c = 10 \text{ g} \cdot \text{L}^{-1}$  in THF) as shell.

**Transmission electron micrograph of patchy worm-like micelles**

**Figure S3.** TEM micrograph of patchy worm-like  $S_{28}E_{15}DiPA_{58}^{156}$  micelles prepared by crystallization-driven self-assembly (CDSA) in THF ( $c = 10 \text{ g}\cdot\text{L}^{-1}$ ). The polystyrene (PS) patches were selectively stained with  $\text{RuO}_4$ . Accordingly, the semi-crystalline polyethylene (PE) core and the poly(*N,N*-diisopropylaminoethyl methacrylamide) (PDiPA) patches in the corona appear bright and the PS corona patches dark.

Self-assembly of  $N^1, N^3, N^5$ -tris[2-(diisopropylamino)-ethyl]-1,3,5-benzenetricarboxamide

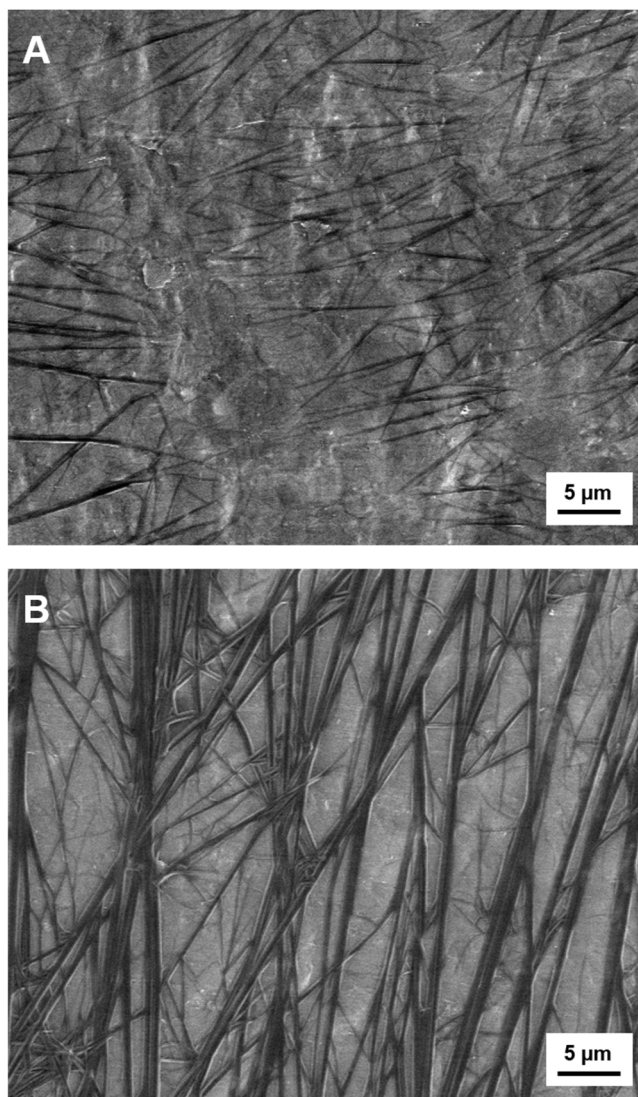


**Figure S4.** SEM micrographs of supramolecular *t*Pr-BTA assemblies prepared upon solvent evaporation of 5 μL from a A) 0.10 wt.% and B) 0.50 wt.% isopropanol solution onto aluminum foil.

Scanning electron micrographs of electrospun polymer fibers without and with patchy worm-like micelles in the presence of  $N^1,N^3,N^5$ -tris[2-(diisopropylamino)-ethyl]-1,3,5-benzenetricarboxamide

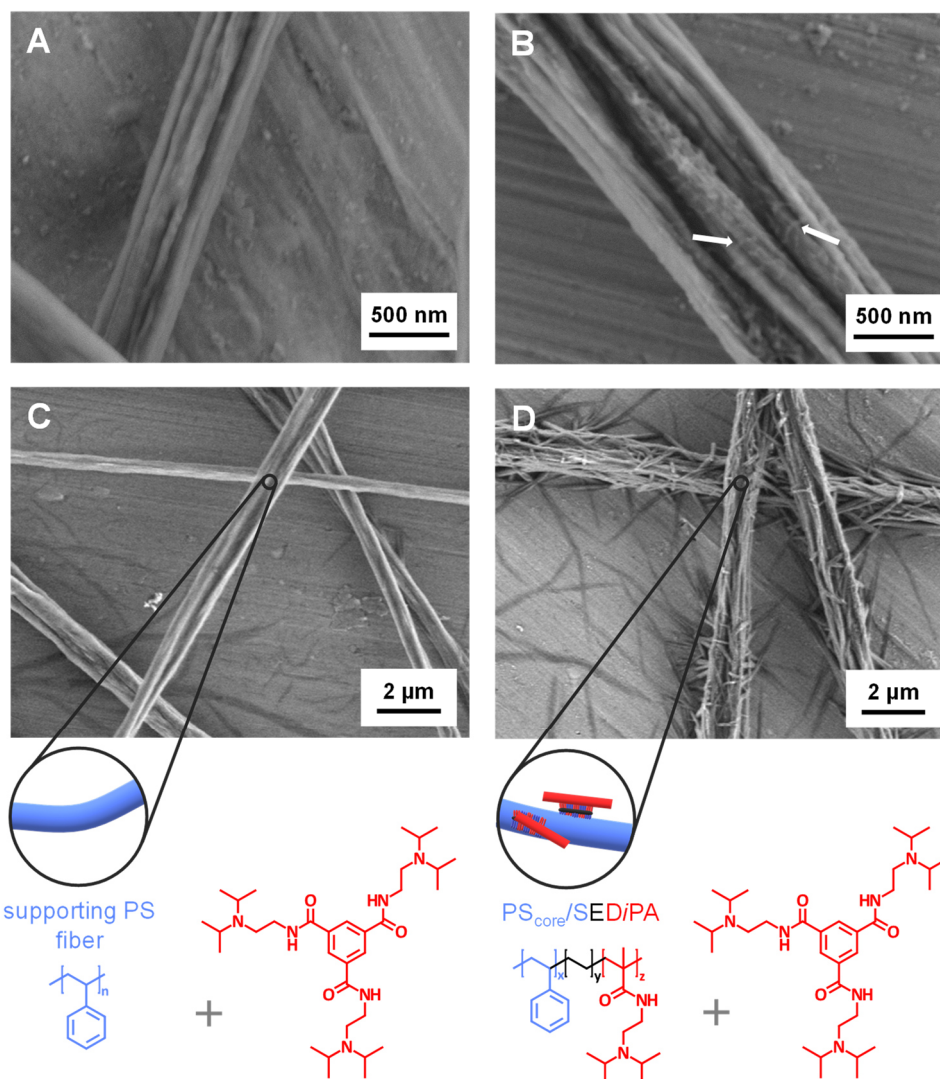


**Figure S5.** SEM micrographs of the neat supporting PS fibers and patchy PS<sub>core</sub>/SEDiPA fibers on aluminum foil before (A and B) and after immersion in a 0.10 wt.% *iPr*-BTA isopropanol solution and subsequent drying at ambient conditions (C and D). A) shows the neat electrospun PS fiber. B) shows the coaxially electrospun PS fiber decorated with patchy worm-like SEDiPA micelles (indicated by the arrows). C) By using neat PS fibers without patchy worm-like micelles, no supramolecular BTA structures were found on the PS fibers. D) Using coaxially electrospun PS fibers decorated with patchy worm-like SEDiPA micelles results in a hierarchical structure with short supramolecular BTA nanofibers formed from the polymer fibers.

**Optical image and scanning electron micrograph of coaxially electrospun polystyrene nonwovens decorated with patchy worm-like micelles**

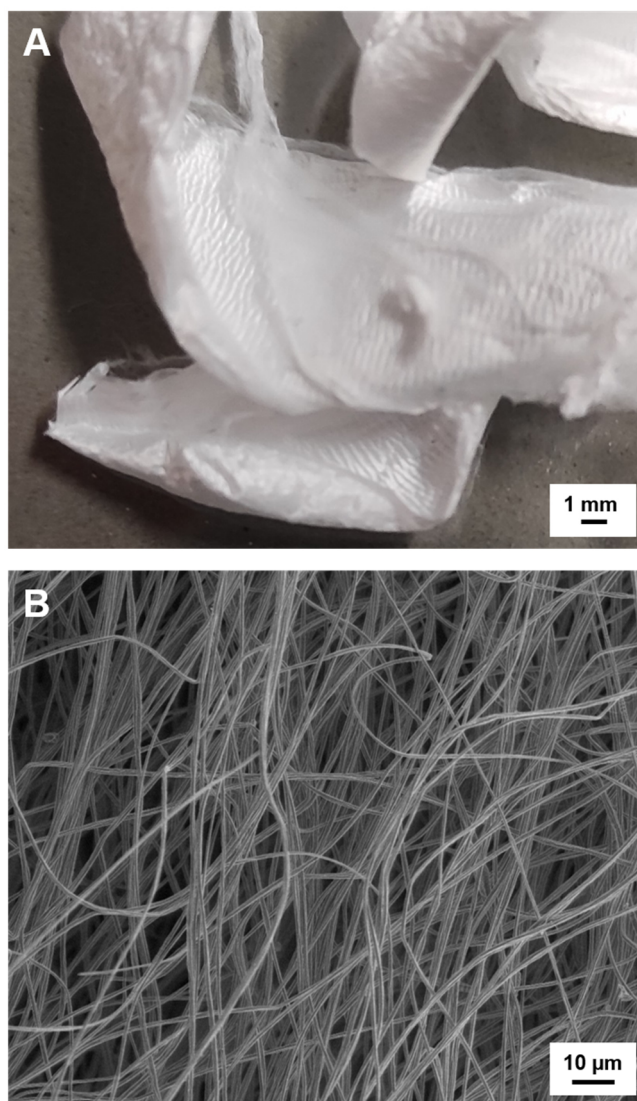


**Figure S6.** A) Optical image of a patchy PS<sub>core</sub>/SEDiPA nonwoven prepared by coaxial electrospinning of polystyrene (PS) (core) and a dispersion of patchy worm-like SEDiPA micelles (shell) and B) corresponding SEM micrograph.

## Hierarchically mesostructured polymer nonwovens with supramolecular nanofibers

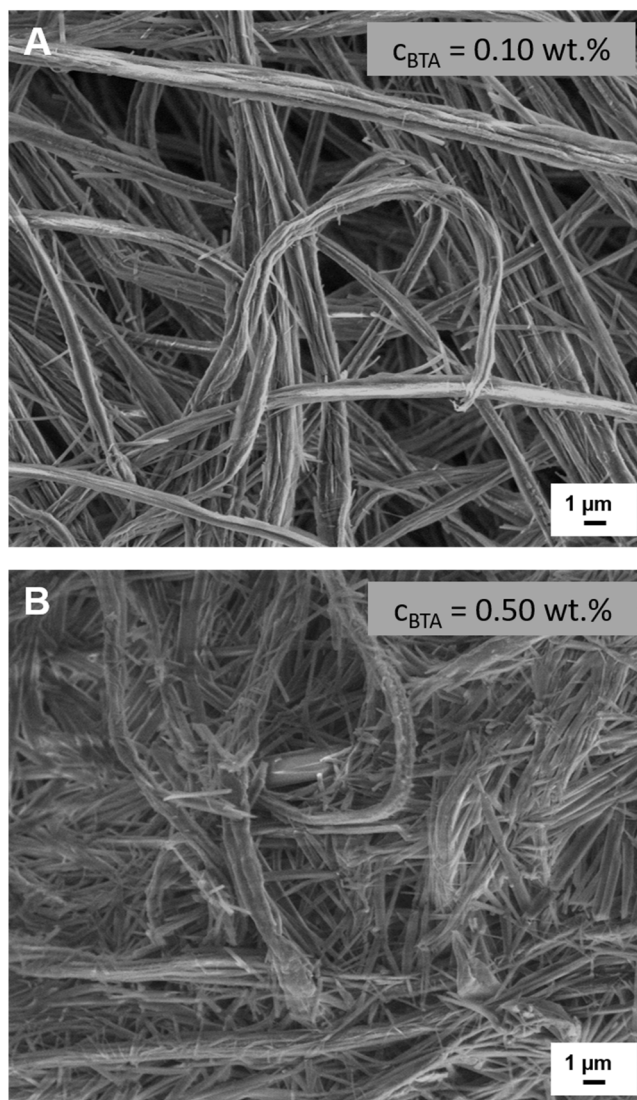


**Figure S7.** SEM micrographs of hierarchically mesostructured nonwovens with functional supramolecular *iPr*-BTA nanofibers. The mesostructured nonwovens were prepared by immersion of dense, electrospun patchy PS<sub>core</sub>/SED/PA nonwovens in an isopropanol solution with a *iPr*-BTA concentration of A) 0.10 wt.% and B) 0.50 wt.% and subsequent drying at ambient conditions.

## Transmission electron micrograph and size distribution of the palladium nanoparticles

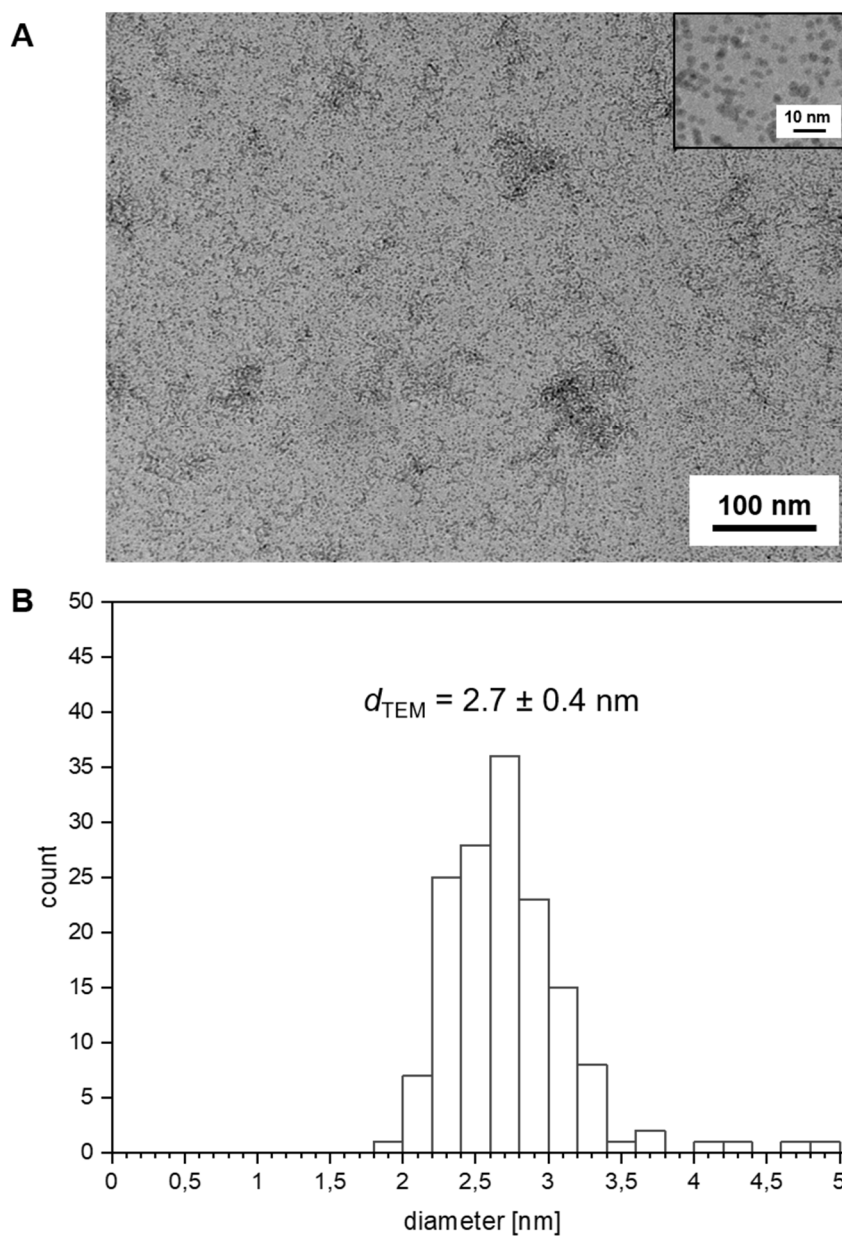


**Figure S8.** A) TEM micrograph and B) size distribution of the synthesized palladium nanoparticles (PdNPs). To determine the average diameter ( $d_{\text{TEM}}$ ), 150 individual PdNPs were evaluated from the TEM micrograph by *ImageJ*, yielding a  $d_{\text{TEM}}$  of  $2.7 \pm 0.4$  nm.



### Hierarchically mesostructured polymer nonwovens before and after immersion in palladium nanoparticle dispersion

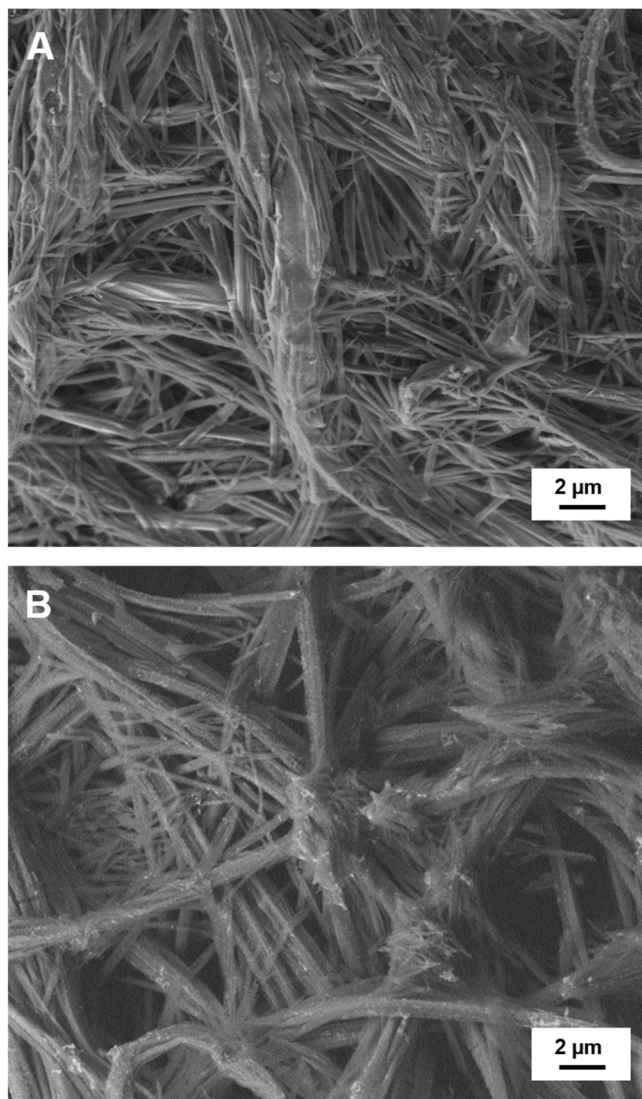


**Figure S9.** SEM micrographs of hierarchically mesostructured nonwovens A) before and B) after immersion into aqueous PdNP dispersion. A) The mesostructured nonwoven was prepared by immersion electrospun patchy PS<sub>core</sub>/SED/PA nonwovens in an isopropanol solution with a *i*Pr-BTA concentration of 0.50 wt.% and subsequent drying at ambient conditions. B) PdNPs were immobilized by dipping the mesostructured nonwoven into the PdNP dispersion for 3 h at room temperature and subsequent drying at ambient conditions.



## 5. Extended summary

1,3,5-benzenetricarboxamides (BTAs) are one of the best-known and well-studied classes of molecular building blocks in supramolecular chemistry. Whereas the self-assembly behavior in organic solvents for common BTAs without functional groups is widely explored, less is known about the role and influence of functional groups in the periphery of BTAs. In this thesis, *a new class of BTAs with functional tertiary amino substituents* was synthesized and investigated with respect to the solubility and self-assembly behavior, mainly in aqueous media and alcohols. In particular, the formation and reproducible preparation of *supramolecular fibers* and complex *hierarchical superstructures* are explored. The functional supramolecular BTA fiber surface allows for the immobilization of metal nanoparticles. The beneficial role and functionality of the supramolecular BTA fibers were demonstrated by preparing *hierarchically mesostructured nonwovens* allowing, for example, the fixation of palladium nanoparticles.

One focus of this thesis is the synthesis, characterization and self-assembly of *1,3,5-benzenetricarboxamides with functional tertiary amino substituents*. To investigate structure-property relations, BTAs with an aliphatic ethyl spacer and tertiary amino substituents with different alkyl groups were synthesized (see **Figure 5.1**). By these structural modifications, the hydrophilicity of the molecule is systematically varied.

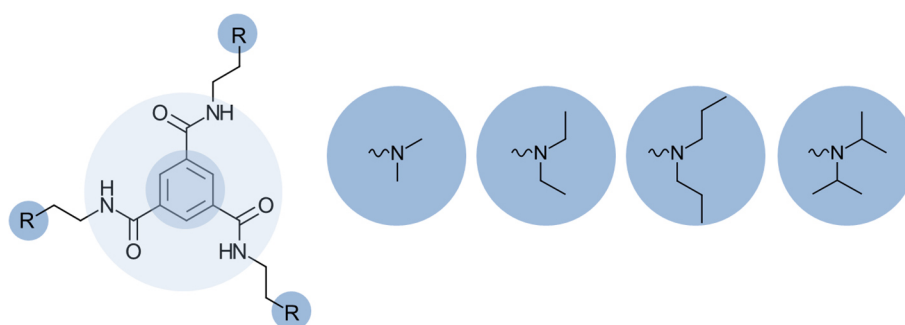


**Figure 5.1.** Chemical structures of 1,3,5-benzenetricarboxamides with an aliphatic ethyl spacer and peripheral tertiary amino groups. The BTAs periphery varies systematically in the alkyl groups ranging from *N,N*-dimethyl, *N,N*-diethyl, *N,N*-di-*n*-propyl to *N,N*-di-isopropyl.

Typically, BTAs are synthesized using trimesic acid trichloride. During such type of reaction, hydrochloric acid is formed, which leads to a salt formation with the tertiary amino groups and thus requires elaborated work up. To avoid this, a *straightforward two-step route* was developed for the synthesis of BTAs with tertiary amino substituents, also in larger quantities. The first step is the esterification of trimesic acid to trimesic trimethyl ester. Subsequent conversion of the trimesic trimethyl ester with *N,N*-alkylamine in bulk resulted in the respective BTA with peripheral *N,N*-dimethyl, *N,N*-diethyl, *N,N*-di-*n*-propyl and *N,N*-di-isopropyl groups.

The bulk thermal properties of the synthesized BTAs were investigated by differential scanning calorimetry. For all investigated BTAs, one pronounced phase transition occurs upon heating and cooling. Upon heating, the phase transition was found at 212 °C, 206 °C, 207 °C and 291 °C for the BTA with *N,N*-dimethyl, *N,N*-diethyl, *N,N*-di-*n*-propyl and *N,N*-di-isopropyl groups. To further investigate the nature of the phase transitions in bulk, temperature-dependent polarizing optical microscopy investigations were conducted. The BTA with *N,N*-dimethyl groups shows a brittle behavior confirming a crystalline phase, while the other three BTAs show deformable structures, which are indicative for a mesophase.

*Supramolecular microtubes based on 1,3,5-benzenetricarboxamides prepared by self-assembly upon heating<sup>[1]</sup>*

Only a few BTAs are known that self-assemble from aqueous media. The most common method to initiate the self-assembly of BTAs to supramolecular fibers is upon cooling a molecularly dissolved solution at an elevated temperature at a given concentration.

From the synthesized BTAs with tertiary amino substituents, the BTAs with *N,N*-dimethyl and *N,N*-diethyl groups allow the preparation of molecularly dissolved aqueous solutions at ambient conditions with high concentrations. The BTA with *N,N*-dimethyl groups shows an extremely high water solubility of more than 150 g L<sup>-1</sup>. The BTA with *N,N*-diethyl groups shows a water solubility of up to 100 g L<sup>-1</sup> at room temperature. For both BTAs, such a high solubility in water is uncommon for BTAs. In contrast, the BTA with *N,N*-di-*n*-propyl groups possess in water a solubility of less than 0.01 g L<sup>-1</sup> at ambient conditions. This demonstrates that

---

<sup>[1]</sup> A. Frank, A. Berner, K. Kreger, H.-W. Schmidt. *Supramolecular microtubes based on 1,3,5-benzenetricarboxamides prepared by self-assembly upon heating*, *Soft Matter* **2020**, 16, 4564–4568.

moderate variations of the length of the alkyl groups at the tertiary amino substituents have a strong effect on the solubility of the BTAs.

Interestingly, the solubility of the BTA with *N,N*-diethyl groups can be even increased upon cooling. Therefore, the common method to initiate the self-assembly upon cooling from a solution at an elevated temperature is not possible. Surprisingly, this BTA shows a reversible, unique two-step self-assembly behavior upon heating aqueous solutions. This two-step process can be clearly seen by temperature-dependent polarizing optical microscopy studies. At room temperature, a clear aqueous solution of the BTA with *N,N*-diethyl groups with a concentration of 20 g L<sup>-1</sup> is present. Upon heating, a liquid-liquid phase separation occurs. Increasing the temperature, the phase separation becomes clearly visible. In the second step, the self-assembly to fiber-like structures is initiated. A further increase in temperature leads to supramolecular fibers with increasing length by the consumption of the phase-separated BTA-rich droplets. This two-step self-assembly process of the BTA with *N,N*-diethyl groups occurs at slightly different temperatures, depending on the BTA concentration. The supramolecular fibers disassemble upon cooling and a clear solution is obtained, demonstrating that this process is fully reversible. However, it is possible to isolate these supramolecular structures by evaporation of the solvent at elevated temperatures. Microscopic studies reveal that these supramolecular structures feature a *microtubular morphology*. These microtubes are several hundred micrometers long and show a mean outer diameter of around 4.7 μm (Figure 5.2).

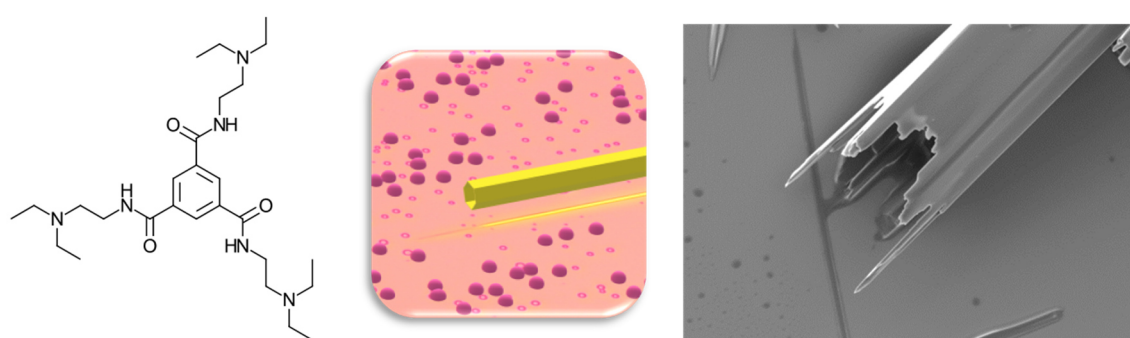


**Figure 5.2.** Chemical structure of *N*<sup>1</sup>,*N*<sup>3</sup>,*N*<sup>5</sup>-tris[2-(diethylamino)-ethyl]-1,3,5-benzenetricarboxamide. The sketch shows the phase separated BTA-rich droplets followed by the self-assembly towards supramolecular fiber-like structures with a microtubular morphology by the consumption of the droplets upon heating aqueous solutions. Scanning electron micrograph of the isolated supramolecular microtube.<sup>[1]</sup>

*Hierarchical Superstructures by Combining Crystallization-Driven and Molecular Self-Assembly<sup>[1]</sup>*

The preparation of defined *hierarchical superstructures* from aqueous solutions was investigated for the first time by the combination of two self-assembly concepts, namely the *molecular self-assembly* of functional BTAs to fiber-like structures and the *crystallization-driven self-assembly* of triblock terpolymers to patchy worm-like micelles.

To initiate the molecular self-assembly of BTAs from a functional polymer fiber surface and ultimately to create *hierarchical superstructures*, patchy worm-like micelles were immobilized on the surface of a supporting polystyrene fiber by coaxial electrospinning. The patchy worm-like micelles, composed of the triblock terpolymer polystyrene-*block*-polyethylene-*block*-poly(*N,N*-dimethylaminoethyl methacrylamide), were prepared by crystallization-driven self-assembly. The patchy worm-like micelles have a crystalline polyethylene core with pendant alternating nanometer-sized polystyrene patches and patches containing tertiary amino groups in the corona. The polystyrene patches guarantee adhesion to the supporting polystyrene fibers and the functional amino patches enable the initiation of supramolecular BTA fiber growth. A chemical matching of the tertiary amino groups in the methacrylamide patches and the periphery of the BTA was found to be important. This ensures the swelling of the functional amino patches in water and thus the accessibility for the water-soluble BTA with *N,N*-dimethyl groups. These patchy worm-like micelles allow the immersion of the polystyrene fibers decorated with these micelles into an aqueous solution containing the molecularly dissolved BTA. The self-assembly of the BTA is promoted by the patchy worm-like micelles. The patch-mediated molecular self-assembly is attributed to the local increase in the concentration of the BTA after reaching a threshold concentration. After solvent evaporation, defined *hierarchical superstructures* are observed (**Figure 5.3**). The complex structure resembles a *fir-tree-like morphology* where defined short supramolecular functional BTA fibers are grown away from the polystyrene fibers in a controlled manner.

---

<sup>[1]</sup> A. Frank, C. Hils, M. Weber, K. Kreger, H. Schmalz, H.-W. Schmidt. *Hierarchical Superstructures by Combining Crystallization-Driven and Molecular Self-Assembly*, *Angew. Chem. Int. Ed.* **2021**, 60, 21767–21771.

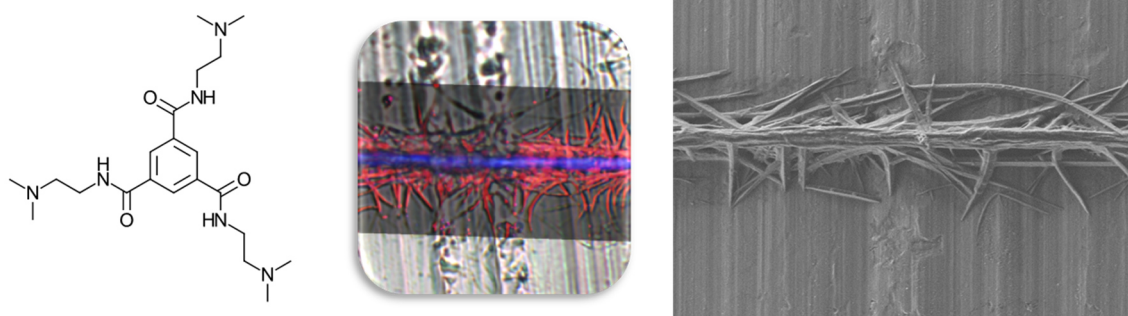


**Figure 5.3.** Chemical structure of  $N^1,N^3,N^5$ -tris[2-(dimethylamino)-ethyl]-1,3,5-benzenetricarboxamide. The sketch shows the hierarchical superstructure with the supporting polystyrene fiber colored in blue and the defined supramolecular fibers colored in red from Raman imaging. Scanning electron micrograph of the hierarchical superstructure prepared by combining crystallization-driven and molecular self-assembly.<sup>[11]</sup>

Further evidence for the necessity of the chemical matching of the tertiary amino groups between the patchy worm-like micelles and the periphery of the BTAs was provided by a series of reference experiments. This included the use of polystyrene fibers decorated with non-functional patchy worm-like micelles, which do not result in such complex structures.

#### *Functional Mesostructured Electrospun Polymer Nonwovens with Supramolecular Nanofibers<sup>[11]</sup>*

Complex hierarchical fiber morphologies which contain supramolecular BTA fibers with a functional surface are promising carriers, for example, for catalysts. To create and utilize such a *complex hierarchical superstructure* with functional supramolecular BTA fibers, the use of *electrospun polystyrene nonwovens as support* is beneficial. Furthermore, for applications in water, the stability of the supramolecular BTA fibers in water is an additional requirement. The concept of patch-mediated molecular self-assembly was investigated by different combinations of BTAs with tertiary amino substituents and electrospun polystyrene nonwovens decorated with suitable patchy worm-like micelles. By this, *functional mesostructured nonwovens with supramolecular BTA fibers* could be prepared. The BTA with  $N,N$ -di-isopropyl groups was identified from the solubility studies and self-assembly investigations for this purpose also due to its negligible water solubility.

<sup>[11]</sup> A. Frank, M. Weber, C. Hils, U. Mansfeld, K. Kreger, H. Schmalz, H.-W. Schmidt. *Functional Mesostructured Electrospun Polymer Nonwovens with Supramolecular Nanofibers*, Macromol. Rapid Commun. **2022**, 43, 2200052, 1–8.

Temperature-dependent solubility studies revealed molecularly dissolved BTA solutions at room temperature for concentration below 0.75 wt.% in isopropanol. This allows the immersion of the electrospun polystyrene nonwoven at room temperature in isopropanol solutions containing the molecularly dissolved BTA with *N,N*-di-isopropyl groups and a BTA uptake within the nonwoven without dissolving the supporting polymer nonwoven. The supporting polystyrene nonwoven decorated with patchy worm-like micelles of the triblock terpolymer polystyrene-*block*-polyethylene-*block*-poly(*N,N*-diisopropylaminoethyl methacrylamide) was immersed in a BTA solution to prepare *hierarchically mesostructured nonwovens*. The patchy worm-like micelles are chemically matched with the tertiary amino groups in the methacrylamide patches with the peripheral groups of the BTA. This leads to the initiation of the self-assembly of the BTA into supramolecular nanofibers due to local enrichment of the molecular BTA building blocks and fixation on the surface of the nonwoven fibers. The resulting *hierarchically mesostructured nonwovens* are stable in water and feature defined off-standing short supramolecular BTA nanofibers on top of the supporting polystyrene fibers of the nonwoven, resembling a *barbed wire-like morphology* (**Figure 5.4**).

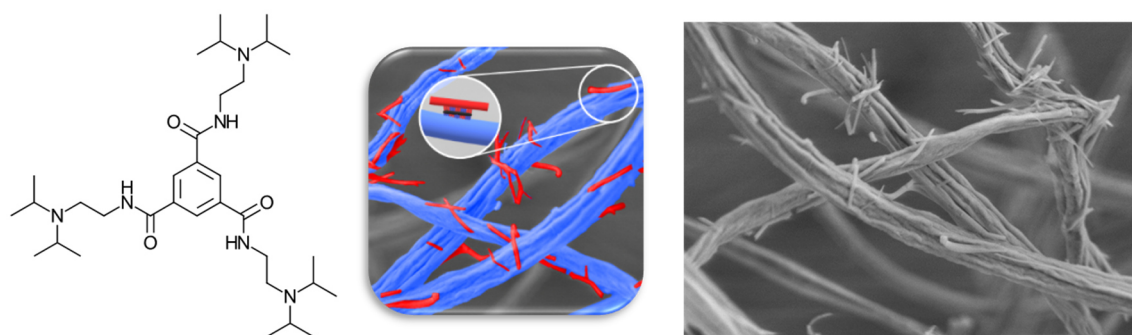


**Figure 5.4.** Chemical structure of  $N^1,N^3,N^5$ -tris[2-(diisopropylamino)-ethyl]-1,3,5-benzenetricarboxamide. The sketch shows the hierarchical mesostructured nonwoven with the supporting polystyrene fibers colored in blue and the off-standing short supramolecular BTA nanofibers colored in red. The patchy worm-like micelles promote the directed self-assembly and guarantee the fixation between the fiber types. Scanning electron micrograph of the resulting functional mesostructured nonwoven with supramolecular nanofibers.<sup>[111]</sup>

The *mesostructured nonwovens* allow the selective adsorption of single palladium nanoparticles on the surface of the *functional supramolecular nanofibers* from aqueous media. The complex morphology of the composite stays intact. This composite shows different levels of hierarchy as well as complexity which makes the mesostructured nonwovens attractive candidates, for example, in catalytic applications.



## 6. Danksagung

An dieser Stelle möchte ich mich bei allen bedanken, die irgendeiner Art und Weise zum Erfolg dieser Arbeit beigetragen haben, auch wenn nicht alle namentlich erwähnt sind.

Allen voran gilt mein herzlichstes Dankeschön meinem Doktorvater Prof. Dr. Hans-Werner Schmidt für das äußerst interessante, vielseitige und interdisziplinäre Forschungsthema meiner Doktorarbeit. Darüber hinaus bin ich besonders dankbar für das entgegengebrachte Vertrauen, die permanente Unterstützung durch zahlreiche wissenschaftliche Diskussionen, Inspiration durch Ideen, die gewährte Freiheit in der Forschung sowie die Bereitstellung eines erstklassig ausgestatteten Labor- und Arbeitsplatzes. Ich wurde stets gefordert, aber somit stark gefördert und durch Ihre hervorragende Betreuung bin ich persönlich gewachsen. Durch Herausforderungen außerhalb des Kernforschungsgebiet konnte ich meinen Erfahrungs- und Wissensschatz deutlich erweitern, was ich sehr zu schätzen gelernt habe.

Für die finanzielle Unterstützung bedanke ich mich bei der Deutschen Forschungsgemeinschaft (DFG) im Rahmen der Sonderforschungsbereiche SFB840 und SFB-TRR225.

Ebenfalls bedanke ich mich für die individuelle Förderung und Unterstützung durch den Elitestudiengang *Macromolecular Science* im Rahmen des Elitenetzwerks Bayern.

Ein besonderer Dank gilt Dr. Klaus Kreger für die vielseitige Unterstützung, sei es die Hilfestellung im Labor, die zahlreichen Diskussionen und die Weitergabe der fachlich umfangreichen Expertise.

Bei meinem Vorgänger Dr. Andreas Bernet bedanke ich mich für die geleisteten Vorarbeiten auf diesem Themengebiet.

Ein großer Dank gilt Melina Weber für die sehr gute und erfolgreiche Zusammenarbeit im Rahmen der Forschung über das Selbstassemblierungsverhalten von Benzoltricarboxamiden. Durch die Unterstützung und unzähligen Diskussionen sind wertvolle Elemente dieser Arbeit entstanden.

Für die erfolgreiche Zusammenarbeit möchte ich Dr. Christian Hils und Dr. Holger Schmalz vom Lehrstuhl Makromolekulare Chemie II danken.

Herzlich bedanken möchte ich mich bei den technischen Angestellten Jutta Failner und Sandra Opel für die Unterstützung bei Synthesen und das Teilen eures Erfahrungsschatzes im Labor.

Ebenfalls möchte ich mich bei Dr. Beate Förster, Dr. Ulrich Mansfeld und Martina Heider für die Hilfestellungen bei Fragen zur Elektronenmikroskopie bedanken.

Ein weiteres Dankeschön gilt Dr. Reiner Giesa und Dr. Christian Neuber für die Unterstützung bei wissenschaftlichen Fragestellungen und für die hilfreichen Diskussionen.

Ganz besonders danke ich meinen Laborkollegen Andreas Schedl, Eva Fürsattel und Lisa Weber für die freundschaftliche Atmosphäre im Labor und Unterstützung jeglicher Art sowie meinen Praktikanten für die gute Zusammenarbeit.

Vielen Dank an den gesamten Lehrstuhl MCI für die großartige Atmosphäre, tolle Zusammenarbeit und schöne Zeit während meiner Promotion. Ich werde diese Momente in guter Erinnerung behalten. Herzlichen Dank an Petra Weiss und Christina Wunderlich für die Unterstützung bei administrativen Anliegen und sämtlichen Belangen. Alexander Kern danke ich für die Unterstützung bei IT-Problemen.

Für die angenehme Abwechslung zum Laboralltag möchte ich mich bei meinen Freunden aus der Heimat und den neu gewonnenen Freundschaften, die während der Promotionszeit entstanden sind, bedanken.

Ebenfalls möchte ich meiner Familie und meinen Geschwistern Natalia, Johannes und Karl mit Familien danken, die mir während meines gesamten Studiums und der Doktorarbeit stets Halt gegeben und mich motiviert haben. Diese Arbeit wurde durch den Mut meiner Eltern, einen großen Schritt ins Ungewisse zu gehen ermöglicht, um uns eine Zukunft mit Perspektive zu geben. Meine größte Kraft beziehe ich durch euch.

Meine liebe Christina, du und Johann erfüllt mich mit Glück und macht das Leben lebenswert. Ich danke dir für alles und freue mich auf unseren gemeinsamen Lebensweg.

---

## **(Eidesstattliche) Versicherungen und Erklärungen**

### **(§ 9 Satz 2 Nr. 3 PromO BayNAT)**

Hiermit versichere ich eidesstattlich, dass ich die Arbeit selbstständig verfasst und keine anderen als die von mir angegebenen Quellen und Hilfsmittel benutzt habe (vgl. Art. 97 Abs. 1 Satz 8 BayHIG).

### **(§ 9 Satz 2 Nr. 3 PromO BayNAT)**

Hiermit erkläre ich, dass ich die Dissertation nicht bereits zur Erlangung eines akademischen Grades eingereicht habe und dass ich nicht bereits diese oder eine gleichartige Doktorprüfung endgültig nicht bestanden habe.

### **(§ 9 Satz 2 Nr. 4 PromO BayNAT)**

Hiermit erkläre ich, dass ich Hilfe von gewerblichen Promotionsberatern bzw. -vermittlern oder ähnlichen Dienstleistern weder bisher in Anspruch genommen habe noch künftig in Anspruch nehmen werde.

### **(§ 9 Satz 2 Nr. 7 PromO BayNAT)**

Hiermit erkläre ich mein Einverständnis, dass die elektronische Fassung meiner Dissertation unter Wahrung meiner Urheberrechte und des Datenschutzes einer gesonderten Überprüfung unterzogen werden kann.

### **(§ 9 Satz 2 Nr. 8 PromO BayNAT)**

Hiermit erkläre ich mein Einverständnis, dass bei Verdacht wissenschaftlichen Fehlverhaltens Ermittlungen durch universitätsinterne Organe der wissenschaftlichen Selbstkontrolle stattfinden können.



